

# **Reprogramming to Pluripotency Facilitates the Study of Genotype- Phenotype Relationships in Glioma**

**Ryan Koshy Mathew**

Submitted in accordance with the requirements for the degree of  
Doctor of Philosophy

The University of Leeds  
School of Medicine  
Faculty of Medicine and Health

October 2018

The candidate confirms that the work submitted is his own and that appropriate credit has been given where reference has been made to the work of others.

This copy has been supplied on the understanding that it is copyright material and that no quotation from the thesis may be published without proper acknowledgement.

The right of Ryan Koshy Mathew to be identified as Author of this work has been asserted by him in accordance with the Copyright, Designs and Patents Act 1988.

© 2018 The University of Leeds and Ryan Koshy Mathew

## **Acknowledgements**

Firstly, I would like to express my sincere thanks to my supervisor Dr Heiko Wurdak for my scientific education during my PhD. His passion for science, unerring standards for output of the highest quality and integrity, and encouragement to develop my independent scientific thinking have been invaluable and inspirational.

I would like to thank my co-supervisor Mr Paul Chumas, who encouraged and supported my academic ambitions, helped keep my parallel research and neurosurgical careers moving forward, and always believed everything would end well.

I am thankful to my other co-supervisor Professor Susan Short for her support and words of wisdom.

I would like to thank Dr Mihaela Lorgier, Dr Laurence Daheron (Harvard Stem Cell Institute), Professor James Rutka (Labatt Brain Tumour Research Centre, Toronto) for their scientific support and advice, Ms Angela Bennett (Leeds General Infirmary) for her clinical support, and Ms Lynette Steele for her administrative support.

I am especially thankful for the contributions of Dr Euan Polson (extracellular flux analysis), Dr Bárbara da Silva (stem cell and organoid culture), Miss Jenny Williams (immunocytochemistry, histology, qRT-PCR), Mr Gary Short (technical support for intracranial injections *in vivo*), Dr Claire Taylor (gDNA preparation, STR profiling, bulk qRT-PCR), Dr Daniel Tams (differentiation RNA) and Dr Orla O'Shea (induced pluripotent stem cell marker flow cytometry, tri-germinal layer differentiation and qRT-PCR, karyotyping). I want to say thanks to Dr Stephane Ballereau and Dr Florian Markowitz at the CRUK Cambridge Institute for computational analysis of the whole genome sequencing and gene expression analysis of the differentiation. I wish to acknowledge the contribution of my summer student Dr Praveena Deekonda during the initial stages of reprogramming. The scientific expertise and invaluable input of those mentioned herein helped keep this project moving forward.

I would like to thank all past and present members of the Wurdak group, the Leeds Institute of Medical Research at St James's and the Department of Neurosurgery at Leeds General Infirmary.

I am thankful to my parents and sister, who always believe in me and have supported me in all my endeavours throughout life.

Lastly, I want to say a special thank you to my loving family – my wife Bryony and my children Noah and Raphael – who never complain about yet more prolonged studentship and yet another day when I must work. I am forever indebted and grateful for their unconditional love and support.

## **Abstract**

### **Background**

Dysregulated, stem cell-like self-renewal has been implicated in glioma treatment resistance and tumour recurrence. Drugs that eliminate tumour cells possessing this malignant characteristic are urgently needed. It remains, however, an experimental challenge to link heterogeneous glioma genotypes to cell phenotypes that can indicate positive and negative drug responses. To this end, we successfully derived patient-specific induced pluripotent stem cell (iPSC) models from both low- (LGG) and high-grade gliomas (HGG) and developed an initial drug discovery application, based on the characterisation of a HGG iPSC differentiation blockade.

### **Methods**

Brain tumour tissue, acquired at surgery, was reprogrammed. Derived iPSC models were characterised using pluripotency markers, tri-germinal layer differentiation, gene expression, karyology and deep whole genome sequencing (WGS, iPSC versus parental tumour). Glioma iPSC differentiation in 2-dimensional (adherent, optically clear 96-well imaging plates) and 3-dimensional (organoid) culture was carried out. Gene expression of neural induction and neuronal differentiation was analysed using mRNA-seq. Neural cancer stem cells from each of the three glioma iPSC lines were orthotopically implanted *in vivo*.

### **Results**

Reprogrammed cells were confirmed as fully-reprogrammed/stable iPSCs, with preserved mutational variants (CNVs, total copy number) as compared to the parental tumours. Glioma iPSC maturation and quantification of TUJ1 staining indicated a 'differentiation block' in the HGG iPSC models. This phenotype was concordant in HGG iPSC-derived tumour organoids which displayed SOX2-positive neural rosettes. Consistently, mice developed xenograft tumours. Expression profiling during neuronal differentiation (from iPSC to neural stem cells to neurons) has revealed candidate genes that may be responsible for the phenotypic differences between HGG and control/LGG iPSC models.

## **Conclusions**

Our adherent, organoid and *in vivo* iPSC models may uncover genetic mutations and regulatory networks underlying glioma stem cell self-renewal and cellular differentiation capability and provide a basis for linking glioma genotypes and phenotypes in drug discovery applications. Here, we have successfully implemented the first stages towards this development (in a 96-well assay format). Ultimately, our patient-derived iPSC-based approach may enable personalised precision medicine strategies against glioma.

# Contents

<b>Acknowledgements</b>	iii
<b>Abstract</b>	v
<b>Table of Contents</b>	vii
<b>List of Tables</b>	xi
<b>List of Figures</b>	xii
<b>1 Introduction</b>	1
1.1 Glioma	2
1.1.1 Classification, incidence and prognosis	2
1.1.2 Current treatment and challenges	4
1.2 Glioma stem cells (GSCs)	9
1.2.1 Evidence and Characteristics of GSCs	9
1.2.2 Isolation of GSCs	11
1.3 Current models of glioma	13
1.3.1 In vitro models of glioma	13
1.3.2 In vivo models of glioma	16
1.4 induced pluripotent stem cells (iPSCs)	20
1.4.1 Reprogramming somatic cells to iPSCs	20
1.4.2 iPSCs in cancer and glioma	23
1.5 Cerebral organoids	25
1.5.1 Development of cerebral organoids	25
1.5.2 Cerebral organoids in glioma	26
1.6 Aims and objectives	29
<b>2 Reprogramming of patient-derived brain tumour tissue results in stable iPSCs with tumorigenic capacity</b>	31
2.1 Results	31
2.1.1 Stable iPSCs can be derived from primary glioma tissue	31

2.1.1.1	Characterisation of primary glioma tissue and cells	31
2.1.1.2	Glioma iPSCs show stem cell morphology	46
2.1.1.3	Glioma iPSCs express markers of pluripotency	53
2.1.1.4	Glioma iPSCs can differentiate into all 3 germinal layers	56
2.1.1.5	Glioma iPSCs express pluripotency-driving genes	58
2.1.1.6	Glioma iPSCs show genomic stability through unaltered karyotype	60
2.1.1.7	Patient-derived glioma iPSCs retain no residual reprogramming vectors	62
2.1.2	Glioma iPSCs show tumorigenic capacity <i>in vivo</i>	63
2.1.3	Patient-derived glioma iPSCs retain genetic mutations of parental tissue	66
2.2	Discussion	70
<b>3</b>	<b>Cerebral organoids can incorporate primary brain tumour tissue by co-culturing with mouse embryonic stem cells</b>	<b>78</b>
3.1	Results	78
3.1.1	mESC organoids demonstrate incorporation of primary low-grade glioma brain tumour tissue	78
3.2	Discussion	85
<b>4</b>	<b>Tumour organoid models demonstrating phenotypic and genotypic differences can be derived from patient-derived glioma iPSCs</b>	<b>87</b>
4.1	Results	87
4.1.1	Tumour organoids derived from glioma iPSCs exhibit a 'differentiation block' phenotype	87
4.1.2	Gene expression analyses of glioma iPSC organoids demonstrate an undifferentiated gene expression signature	94
4.2	Discussion	97

<b>5</b>	<b>Glioma iPSCs can be used to develop reproducible stem cell differentiation assays in chemically-defined culture conditions</b>	101
5.1	Results	101
5.1.1	Glioma iPSCs fail to differentiate into neurons and provide proof of principle for the development of drug discovery assays	101
5.1.2	mRNA-seq analysis of the undifferentiated, partially differentiated and terminally differentiated neurons demonstrate differential gene expression between normal and glioma iPSCs	104
5.2	Discussion	106
<b>6</b>	<b>Conclusion and Future Work</b>	110
<b>7</b>	<b>Materials and methods</b>	114
7.1	Surgical procedure, tissue transfer and cell culture	114
7.2	Extracellular flux analysis – quantification of metabolic phenotyping	115
7.3	Sendai virus feasibility in primary cells	115
7.4	Reprogramming glioma cells to iPSCs	116
7.4.1	Plating mouse embryonic feeders (MEFs)	117
7.4.2	Transfer onto feeder-culture	117
7.4.3	Picking iPSC colonies	118
7.4.4	Live stain immunocytochemistry	118
7.4.5	Maintenance, passage and freezing of iPSCs	119
7.4.6	Mycoplasma testing	120
7.4.7	Sendai virus clearance testing	120
7.4.8	Transfer onto feeder-free culture	120
7.4.9	Characterisation of glioma iPSCs	122
7.5	Maintenance, passage and freezing of R1 mouse embryonic stem cells (mESCs)	122
7.6	Cerebral and tumour organoid derivation	122
7.6.1	Preparing organoids for immunocytochemistry	125

7.7	iPSC differentiation to neural stem cells (NSCs) and neurons	125
7.8	Immunocytochemistry	126
7.9	Illumina gene expression analysis	127
	7.9.1 qRT-PCR	127
	7.9.2 Whole genome sequencing	129
	7.9.3 mRNA sequencing	130
7.10	Computational mRNA-seq gene expression analysis	130
7.11	Computational whole genome sequencing analysis	130
7.12	Animal experiments	130
7.13	Histology	131
7.14	Image analysis	132
7.15	Statistical analysis	132
	<b>List of abbreviations</b>	<b>133</b>
	<b>References</b>	<b>138</b>

## List of Tables

<b>Table 1:</b> Summary of commonly used reprogramming methods	22
<b>Table 2:</b> Patient characteristics (including post-operative adjuvant therapy and survival) for the samples obtained at surgery	33
<b>Table 3:</b> Issues, solutions and appropriate testing methods proposed in order to improve the quality of iPSCs derived (adapted from Yaffe <i>et al.</i> (1))	47
<b>Table 4:</b> EmGFP reporter calculations	116
<b>Table 5:</b> CytoTune-iPS 2.0 Sendai reprogramming calculations	117
<b>Table 6:</b> Numbers of reprogrammed Sendai virus reprogrammed cells seeded onto feeder-culture (mouse embryonic fibroblasts, MEFS)	118
<b>Table 7:</b> List of TaqMan probes used for qRT-PCR	128

## List of Figures

<b>Figure 2.1:</b> Magnetic Resonance Imaging (MRI) of WHO Grade IV GBM and sampling regions	32
<b>Figure 2.2:</b> Inverted light microscopy (x10 magnification) of cultured cell lines	34
<b>Figure 2.3:</b> Immunofluorescence staining of primary cell lines for stemness and central nervous system (CNS) markers	36
<b>Figure 2.4:</b> qRT-PCR analyses of the successfully reprogrammed HGG (non-contrast-enhancing tumour margin – HGm, contrast-enhancing tumour bulk – HGb) and LGG lines	40
<b>Figure 2.5:</b> Metabolic analysis (Seahorse Bioanalyzer) of oxygen consumption rate (OCR) between HGG contrast enhancing tumour bulk (HGb and HGb2) and non-contrast-enhancing tumour margin cell lines (HGm and HGm2)	42
<b>Figure 2.6:</b> Metabolic analysis (Seahorse Bioanalyzer) of extracellular acidification rate (ECAR) between HGG contrast enhancing tumour bulk (HGb and HGb2) and non-contrast-enhancing tumour margin cell lines (HGm and HGm2)	43
<b>Figure 2.7:</b> HGb (p3) EmGFP at time of transduction (0 h), 24 hours and 72 hours post-transduction (x10 magnification)	44
<b>Figure 2.8:</b> LGG (p0) EmGFP at time of transduction (0 h), 24 hours and 72 hours post-transduction (x10 magnification)	45
<b>Figure 2.9:</b> HGm (p3) EmGFP at time of transduction (0 h), 24 hours and 72 hours post-transduction (x10 magnification)	46
<b>Figure 2.10:</b> induced pluripotent stem cells (iPSCs) derived from reprogrammed low-grade glioma (LGG) cells transduced with SeV, passage 6, on mouse embryonic feeder (MEF) culture.	48
<b>Figure 2.11:</b> induced pluripotent stem cells (iPSCs) derived from reprogrammed non-contrast-enhancing HGG tumour margin (HGm) cells transduced with SeV, passage 3, on mouse embryonic feeder (MEF) culture	49
<b>Figure 2.12:</b> induced pluripotent stem cells (iPSCs) derived from contrast-enhancing HGG tumour bulk (HGb) cells transduced with SeV, passage 3, on mouse embryonic feeder (MEF) culture	50
<b>Figure 2.13:</b> induced pluripotent stem cells (iPSCs) derived from	

non-contrast enhancing HGG tumour margin (HGm2) cells transduced with SeV, passage 5, on mouse embryonic feeder (MEF) culture	51
<b>Figure 2.14:</b> induced pluripotent stem cells (iPSCs) derived from contrast-enhancing HGG tumour bulk (HGb2) cells transduced with SeV, passage 4, on mouse embryonic feeder (MEF) culture	52
<b>Figure 2.15:</b> Non-contrast-enhancing HGG tumour margin (HGm) colonies undergoing reprogramming, live cell immunostained for Tra-1-60	53
<b>Figure 2.16:</b> Contrast-enhancing HGG tumour bulk (HGb2) colonies undergoing reprogramming, live cell immunostained for Tra-1-60	54
<b>Figure 2.17:</b> LGG tumour (LGG) colonies undergoing reprogramming, live cell immunostained for Tra-1-60	54
<b>Figure 2.18:</b> Brightfield representative images of HGm, HGb and LGG primary culture, and derived iPSC colonies on mouse embryonic feeder (MEF) culture	55
<b>Figure 2.19:</b> Flow cytometry conducted in all 3 iPSC lines derived from HGm, HGb and LGG cells	56
<b>Figure 2.20:</b> Tri-germinal layer marker expression of iPSC lines derived from HGm, HGb and LGG	57
<b>Figure 2.21:</b> Heatmap and hierarchical clustering of relative gene expression of study and reference stem cells	59
<b>Figure 2.22:</b> Representative comparative genomic hybridisation (CGH) array karyotyping report from the analysis of the iPSC line derived from LGG primary cells	61
<b>Figure 2.23:</b> qRT-PCR analysis of residual Sendai virus expression	62
<b>Figure 2.24:</b> Representative magnetic resonance (MRI) and confocal microscopy images after orthotopic xenotransplantation neural stem cells derived from HGb iPSCs	64
<b>Figure 2.25:</b> Representative magnetic resonance (MRI) and confocal microscopy images after orthotopic xenotransplantation neural stem cells derived from HGm iPSCs	65
<b>Figure 2.26:</b> Representative magnetic resonance (MRI) and confocal microscopy images after orthotopic xenotransplantation neural stem cells derived from LGG iPSCs	66
<b>Figure 2.27:</b> Deep (90X) whole genome sequencing analysis	

comparing total number of copies between each primary (P) tissue sample and its respective derived iPSC line	67
<b>Figure 2.28:</b> Deep (90X) whole genome sequencing analysis comparing number of copy number variants (CNVs) and gains:loss status ratios between each primary (P) tissue sample and its respective derived iPSC line	68
<b>Figure 2.29:</b> Deep (90X) whole genome sequencing analysis comparing specific 'hallmark' gene abnormalities between each primary (P) tissue sample and its respective derived iPSC line.	69
<b>Figure 3.1:</b> Cerebral organoids	79
<b>Figure 3.2:</b> H&E stains at serial magnifications of cerebral organoids generated from mESCs co-cultured with primary human LGG tissue	81
<b>Figure 3.3:</b> Digital inverted fluorescence microscope images of organoids formed from mESCs and primary LGG tissue in co-culture	83
<b>Figure 3.4:</b> Z-stack confocal microscope images of a permeabilised whole cerebral organoid formed from mESC co-cultured with primary LGG tissue	84
<b>Figure 4.1:</b> Representative stereoscopic microscopy images of day 15 organoids	88
<b>Figure 4.2:</b> Representative light microscopy images of haematoxylin and eosin (H&E) stained control and glioma iPSC tumour organoids	91
<b>Figure 4.3:</b> Representative confocal images of immunofluorescence stained day 15 control and tumour organoids	92
<b>Figure 4.4:</b> Quantification of number of rosettes within organoids formed from control and glioma iPSCs	93
<b>Figure 4.5:</b> Representative 'stitched' inverted fluorescent microscopy images of immunofluorescence stained day 32 control cerebral organoid	94
<b>Figure 4.6:</b> Radar plots depicting model-specific gene expression signatures obtained by bulk qRT-PCR performed in day 15 tumour and control organoids	96
<b>Figure 5.1:</b> Immunofluorescence staining of fixed neural stem cells (NSCs) differentiated from control and glioma iPSCs	101
<b>Figure 5.2:</b> Immunofluorescence staining of fixed neurons differentiated from control and glioma iPSCs	102
<b>Figure 5.3:</b> Quantification of percentage of TUJ1 positive cells in	

neuronal differentiation assays	103
<b>Figure 5.4:</b> Principal components analysis of gene expression signatures (by mRNAseq) during stages of differentiation	104
<b>Figure 5.5:</b> Volcano plot showing individual gene expression values with fold change > 1 at iPSC, NSC and neuronal stages of differentiation	105
<b>Figure 7.1:</b> Workflow for feeder-dependent Sendai virus iPSC reprogramming	116
<b>Figure 7.2:</b> Reaction mixture compositions and qRT-PCR conditions	127

## 1. Introduction

This thesis describes work undertaken to develop new (predominantly *in vitro*) models of glioma that complement existing published work. I approached the work from the viewpoint of my skills as a practicing neurosurgeon caring for patients wanting and able to donate fresh brain tumour tissue for use in research, and two new complementary technologies that emerged during my period of study – namely the reprogramming of somatic cells into induced pluripotent stem cells (iPSCs) (2) and the development of cerebral organoid methodology (3). The development of models with human micro-environmental context that have an ability to incorporate individual patient's brain tumour tissue would, in theory, provide a personalised model of glioma tumour biology. It follows, and has been argued, that such personalised 'human-human' models would bring the possibility of precision medicine tailored to the individual closer to clinical translation (4). In addition to the personalised aspect of my model development work presented here, I also aim to address an unmet clinical need for models that represent low-grade gliomas. Such models are scarce *in vivo* and are not available *in vitro*. The result is that a significant proportion of brain tumour patients therefore have inadequate basic and translational research activity aligned to their disease outcomes, and invaluable research into the transformation of low- to high-grade gliomas is currently limited in the laboratory setting.

The thesis begins with an overview of glioma, the current treatments available, their limitations and the biological challenges that result in such a poor prognosis from this devastating disease. I then describe the brain tumour/glioma stem cell hypothesis, and its implications and challenges for brain tumour treatment resistance and tumour regrowth. I then provide an overview of the strengths and limitations of current *in vitro* and *in vivo* glioma models. My work has sought to address some of the challenges in representing the population of stem-like cells in the tumour bulk by utilising cellular reprogramming. Following a review of reprogramming methodologies, I will outline the use of iPSCs to study cancer. Another approach to modelling I have used is in utilising and modifying cerebral organoid methodology, and therefore I introduce this technology and its recent (limited) use in glioma modelling. Lastly, I outline the aims and objectives of my PhD work.

## 1.1. Glioma

### 1.1.2. Classification, incidence and prognosis

It is estimated that there are 10,000 new primary brain tumour cases per year in the UK, with gliomas making up approximately 60-80% (5,6). Gliomas are malignant brain tumours that predominantly contain cells that share morphological characteristics with glial lineage cells (astrocytes, oligodendrocytes and ependymal cells). They are subclassified according to their presumed predominant cell of origin type i.e. astrocytomas, oligodendrogliomas, oligoastrocytomas and ependymomas (7).

The latest World Health Organisation (WHO) 2016 classification (8) of central nervous system (CNS) tumours continues to follow previous precedence in grading tumours I-IV according to histological features. Grade I tumours are predominantly seen in children and generally considered a separate entity to Grade II-IV tumours as they behave in a non-malignant fashion and are frequently curable with complete surgical resection (overall survival is >99% at 10 years) (9,10). Grade II tumours are termed low-grade gliomas (LGGs) whilst Grade III-IV tumours are termed high-grade gliomas (HGGs). In order to satisfy the criteria for a WHO Grade III high-grade glioma, tumours must exhibit hypercellularity, nuclear atypia, and mitotic activity (11). In addition, to be graded as a WHO Grade IV glioma (glioblastoma multiforme, GBM), tumours must demonstrate microvascular proliferation and/or necrosis. This latest WHO version is the first to integrate molecular and morphological criteria in the diagnostic nomenclature. In addition to the morphological similarity of the predominant cell type in the analysed tumour sample, pathologists also consider the presence or absence of a mutation in the isocitrate dehydrogenase 1 (*IDH1*) gene, and the preservation or co-deletion of the short (p) arm of chromosome 1 and the long (q) arm of chromosome 19 (so called '1p/19q co-deletion') in the classification of gliomas. *IDH1* mutation status is particularly important as it has been shown to delineate "primary" or "*de novo*" GBM (approximately 90% of GBMs, *IDH1*-wild type) from "secondary" GBM (approximately 10% of GBMs, *IDH1*-mutant) (12). When diagnosed at presentation, secondary GBMs are thought to arise from previously (clinically undetected) LGGs (12). Primary and secondary GBMs vary in their age of presentation (younger in secondary) and also in their prognosis (better for secondary) (12,13). A third group, "not otherwise specified" (NOS) exists for

patients in whom *IDH1* is not tested (including historical cases prior to the current WHO 2016 classification) or in whom *IDH1* testing is inconclusive (14). The latest published National Institute for Health and Care Excellence (NICE) guidelines on primary brain tumours in adults (5,15) clearly recommends the use of molecular markers to determine prognosis and guide treatment for glioma. In addition to reporting all gliomas in accordance with the WHO 2016 classification, this latest set of guidelines also recommends including the following: *IDH1* and *IDH2*, *ATRX* mutations to identify *IDH* mutant astrocytomas and GBM, 1p/19q co-deletion to identify oligodendrogliomas, histone H3.3 K27M mutations in midline gliomas, and *BRAF* fusion and gene mutation to identify pilocytic astrocytoma (WHO Grade I glioma).

GBMs are both the most common single type of primary malignant brain tumour, and the most common (45%) of all the gliomas (6). In England, the overall age-standardised incidence of GBM is 4.64 per 100,000 per year, and increases with age (16). For gliomas overall, annual global incidence is estimated to be between 4-6 per 100,000 (6).

For GBM in England, overall survival is 28.4% at 1-year, 11.5% at 2-years and 3.4% at 5-years with median overall survival 6.1 months – these figures significantly decrease with increasing age cohorts (16). In patients aged up to 69 years, median survival is 14.9 months with maximal treatment (debulking neurosurgery, radio- and chemotherapy) (16). However, patients aged over 60 years are less likely to receive maximal treatment. These figures align with those globally with progression free survival of 7-8 months (17), 5-year overall survival of <5% and median overall survival with maximal treatment of 14-16 months (6,18). Patients with LGGs fare significantly better with median overall survival 7 years (10).

Aside from the challenges of improving outcomes for people with gliomas, there is also a societal impact of gliomas. Significant demands are placed on emergency departments (60% of patients present via this route), general practitioners and other specialist referral services by patients presenting with primary brain tumours. Furthermore, although these patients only represent 3% of all cancers, they result in the most life-years loss of any cancer (5). Taking into

consideration a peak age incidence of 41 years in LGGs (10) and 55-60 years in GBMs (18,19), this also represents a significant loss of working-age economic cost to the national productivity (7).

### **1.1.2. Current treatment and challenges**

Improving survival in patients with World Health Organisation Grade IV Glioblastoma Multiforme (WHO IV GBM) remains one of the most challenging unmet needs in oncology (20). In the field of neurosurgery, advances in imaging, neuro-navigation and awake surgery have enabled more targeted debulking of tumours, identification of eloquent brain, and preservation of cognitive function (21–23). Combined with better tolerated anaesthetic agents, improved post-operative nursing care and rehabilitation, patients recover faster, with reduced procedure-related morbidity and mortality. This improved functional outcome from surgery, with a smaller tumour burden, allows for more patients to be eligible for a key component of improving overall survival – adjuvant chemoradiotherapy (24). However, gliomas are infiltrative and diffuse by nature, disseminating along white matter tracts, expanding in eloquent regions and frequently crossing the corpus callosum (25). Such factors mean that not all tumours are surgically amenable to gross total debulking and microscopic residual is present even after maximal debulking surgery. Technological advances have enabled more focused radiation with multi-modal delivery options that minimise off-target effects (26). Successful clinical trials have introduced new chemotherapeutic agents (Temozolomide) taking into account molecular characteristics, leading to treatment algorithms such as the ‘Stupp regimen’ (27), which has improved overall survival by 2.5 months, and progression-free survival by 1.9 months (7,28).

However, despite all the above therapeutic approaches, tumours recur, patients deteriorate and median overall survival from GBM remains dismal, as described earlier. Although, low grade glioma (LGG) patients (WHO grade II) fare better, they pose significant challenges by exhibiting a variable disease time course, and most (approximately 90%) will undergo high grade transformation and the resultant poor prognosis of secondary GBM (21,29). Furthermore, LGGs have a preponderance for eloquent areas of the brain and this makes gross surgical resection (associated with better PFS) more difficult (10). Radiotherapy for LGGs

has been shown to improve PFS but not OS (30–32), and may be associated with significant cognitive deficits and poorer quality of life (33). While the overall survival benefit of concomitant temozolomide with radiotherapy in GBM is proven (27), the role of this alkylating agent in the treatment of LGGs remains fully unassessed and inconclusive (34–37). There are significant, and quite separate challenges in defining the best treatment regimen for LGGs. Neuro-oncology research has sought to understand glioma biology and find novel treatments that exploit vulnerabilities of these tumours. Developing models to understand the drivers of transformation from LGG to HGG remains another significant challenge in glioma research. It is hoped that one day, a biomarker of transformation will be identified and validated to help clinicians better inform patients with LGGs.

One of the key challenges in improving outcomes from glioma treatment is the wide cellular and molecular inter- and intra-tumoural heterogeneity (24,38). Distinct subpopulations or clones within tumours have been shown to possess their own biological and genetic profiles (39). The treatment response in these subclones has been shown to vary (40), with their presence proposed as a possible cause of treatment resistance/failure and subsequent tumour recurrence (41). An attempt has been made to help deal with the inter-tumour heterogeneity by subtyping histologically diagnosed GBM tumours according to *IDH1* mutation status into primary and secondary, as described earlier. Another way of stratifying patients and considering inter-tumoural heterogeneity is based on the activity of O<sup>6</sup>-methylguanine-DNA methyltransferase (*MGMT*). Hypermethylation of the promotor region of *MGMT* has been shown to improve the response to temozolomide as a result of gene silencing (42), which results in impaired DNA repair. Median overall survival in patients with hypermethylated *MGMT* is 22-26 months, compared to 12-15 months in non-hypermethylated *MGMT* tumours. Thus, *MGMT* methylation status has been shown to be a powerful predictor of difference in treatment response and related outcome.

Based on the work by Hanahan and Weinberg (43,44), the relevance of the six hallmark, and two emerging, mutations of cancer have also been studied in GBM by performing genome wide analysis and expression profiling (38,45,46). This has translated into so called ‘hallmark’ mutations of GBM – significant alterations to the RTK/RAS/PI3K pathway occur due to overexpression of epidermal growth

factor receptor (*EGFR*, most commonly vIII) and inactivation of phosphatase and tensin homologue (*PTEN*) (17). Other common mutations and genomic abnormalities include activation of platelet derived growth factor receptor A (*PDGFRA*), loss of chromosome 10q, mutations in *TP53* and loss of chromosome 19q (47,48).

Verhaak *et al.* (49) used data from The Cancer Genome Atlas (TCGA) to analyse gene expression signatures to molecularly classify GBM into subtypes. These subtypes are characterised by aberrations of *EGFR* (Classical), *NF1* (Mesenchymal) and *PDGFRA/IDH1* (Proneural). A fourth subtype – Neural – has been proposed but without attribution to a specific gene expression signature. These subtypes are clinically relevant because of their differing response to aggressive therapy – patients with a Classical subtype benefit the greatest and those with a Proneural subtype the least. This integration of transcriptomic and genomic data has helped other groups evaluate and demonstrate that their proposed targeted therapies can potentially work across the spectrum of GBM (50), at an early stage. Traditionally, significant amounts of time and money have been invested developing promising small molecules, which have only been tested and shown to work on a single subtype, only for these to fail in clinical trials when faced with the heterogeneity of GBM tumours seen in practice. Developing models that can incorporate this heterogeneity and/or at least cover the basic spectrum of subtypes will be equally important to make them useful. Unfortunately current clinical diagnostic techniques fail to capture the single cell intra-tumoural heterogeneity, which has been shown to be varied and significant (51).

As described earlier, GBMs inevitably recur. Limited options exist for the patient at that point and management is unclear (52). Many of them are too unwell from the effects of previous chemoradiotherapy (poor Karnofsky performance status (53)) to undergo further debulking surgery (54). There is a significant risk of toxicity with reirradiation (and the implication on all-important quality of life in all cancer patients), especially in view of the relatively high dose given as first line (2 Gy per day for 6 weeks, total 60 Gy). In a small cohort of patients (Karnofsky performance status > 60, a major lesion size < 40mm, and progression > 6 months after surgery), there may be a case for reirradiation (likely with

stereotactic radiosurgery) but the survival benefit outcome data for this is largely limited to case series (55). Therefore, second-line treatment relies almost entirely on chemotherapeutic agents (54). Despite trials with numerous agents (*EGFR* inhibitors, nitrosoureas, anti-angiogenics and re-treatment with TMZ), no standard therapy has emerged (54). There is a further layer of complexity to this challenge in that, although GBM recurrence most often occurs within 2-3cm of the original tumour border (56), the recurrent lesions have been shown (in the limited cases where repeat tissue samples have been amenable to biopsy and analysis) to have significant mutational differences (54). Some of these may arise *de novo* as part of cancer evolution but it is now well known that treatment with alkylating agents such as TMZ itself causes genomic mutational evolution – this latter effect is particularly pronounced in *IDH1* mutated GBMs (57,58). These changes can significantly mislead targeted therapies for recurrent tumours and, without repeat biopsy/molecular testing, many are treated ‘blind’ (59). Recurrences may have different mutational characteristics to the original tumour (60).

Mutational change is also relevant for LGGs as it is proposed that a slow accumulation in mutations causes the typical progression to HGGs termed malignant transformation (61,62). This transformation is characterised by rapid increase in tumour size, cellularity, vascular proliferation and contrast enhancement (CE) uptake on magnetic resonance imaging (MRI) (63). Depending on previously obtained treatment such as radiotherapy, the time to malignant transformation occurs on average between 2.1 to 10.1 years after LGG diagnosis (21,31). This highly variable PFS between patients makes predicting the exact time of histopathological change clinically impossible currently and relies on regular and relatively frequent MRI surveillance imaging with new appearance of CE indicative of malignant transformation (63). This has both an economic cost in terms of MRI resources use and a cost to the patient in poverty of prognostic information and anxiety surrounding the results of each scan at the subsequent clinic appointment. Unfortunately, even interval imaging with MRI is not always reliable since although CE is supposed to reflect the breakdown of the blood-brain barrier brought on by the more aggressive infiltration of malignancy (64,65), up to 20-30% of LGGs will exhibit CE without malignant transformation (66), and 30% lack CE in the presence of histologically-confirmed malignant

transformation (67,68). Furthermore, surgical debulking or chemoradiotherapy itself can cause CE (69), making it very difficult to judge the difference between pseudo-progression and true progression (70). Despite the development and study of MRI modalities such as diffusion-weighted imaging (DWI), perfusion-weighted imaging (PWI), magnetic resonance spectroscopy (MRSpec) in LGG malignant transformation, none have been proven to be reliable enough to make it into routine clinical practice (63). The ability to model LGG malignant transformation could address some of these challenges by revealing insights into the key mutations and inform more clinically useful surveillance strategies. This will only be possible once LGGs themselves can be modelled.

## **1.2. Glioma stem cells (GSCs)**

### **1.2.1. Evidence and Characteristics of GSCs**

A number of research groups have proposed that a subset of cells within the tumour mass have properties similar to stem cells. These so-called brain-tumour stem cells (BTSCs), brain tumour-initiating cells (BTICs) or glioma stem cells (GSCs) have been variably proposed as responsible for tumour initiation (gliomagenesis), progression and recurrence (71–73). This builds on the cancer stem cell hypothesis proposed across other cancer types. GSCs are purported to possess stem cell properties and ‘escape’ anti-tumour therapy, subsequently evolving and clonally expanding into new tumours (74,75). One mechanism by which they may evade therapy - that typically relies on rapidly dividing cells - is by acquiring the ability to remain quiescent, reactivating in favourable conditions (76). This relative quiescence and the ability to divide asymmetrically to give rise to transient progenitor-like pools of tumour cells has also been proposed as an explanation for drug resistance (76). Transcription factor networks have been constructed that propose the epigenetic mechanisms responsible for directing GSC fate (77).

Some of the evidence for the existence of GCSs and the retention of a normal tissue hierarchy by tumours comes from the analyses of malignant tumours developed by genetically engineered mouse models (GEMMs) (76). Utilising the principle of a marker to enrich for tumour-propagating cells, as first shown by Singh *et al.* (78) (CD133+ in that case), a transplant assay was studied in a hedgehog-driven medulloblastoma GEMM (79,80). This study showed that within the large fraction of highly proliferative cells (positive for the cell surface marker CD15+) enriched from the tumours developed in these mice, there was a subset of stem-like cells (SOX2 positive) that could initiate further tumours when transplanted (81). Further evidence comes from an approach using a tumour suppressor GEMM with a nestin promoter-enhancer-driven green fluorescence protein (GFP) reporter transgene (NesTK-GFP) (82). This transgene, designed to mark quiescent adult murine neural stem cells, elicited spontaneous GBM tumours. Several observations from the tumours studied in this preclinical model adds weight to the existence of GSCs. Firstly, all tumours contained populations of KI67-negative GFP-positive cells. Secondly, after treatment of these mice with TMZ (which would specifically target the proliferating bromo-deoxyuridine-

incorporating cells), recurrent tumours were attributed to the GFP-positive cells, with no evidence that a significant portion of the new tumour cells came from outside this subset (83). Lastly, ganciclovir administration, targeted to kill NesTK-GFP cells, caused prolonged survival in the tumour-bearing mice. In tumours developed by mouse glioma models, only a small percentage of the cells are GSCs (79,81,84). This information can be used to either support the CSC hypothesis in gliomas i.e. only a small proportion of cells need to retain stem-like abilities, or question the hypothesis i.e. how can such a small cell niche be responsible for all the morphologically, phenotypically and genetically diverse cells seen in one single tumour and are there more important subpopulations (possibly even smaller than the GSC niche) that remain undetected or undefined? One response to this is provided by studies into hierarchical, clonal evolutionary and fate mapping dynamics in glioma (85,86) that show single-cell derived clones within single tumours. This heterogeneous clonal and subclonal diversity may explain the different behaviours observed such as aggressive proliferation and drug resistance. The relationship between clonal evolution, heterogeneity and whether these cells, at some point or another, acquire or retain stem-like characteristics remains to be delineated. A further characteristic of stem-like cells is the ability to form spheres when cultured at low density (87). Human primary brain glioma cells, when isolated and cultured, readily form neurospheres (88).

Studies of both *IDH* mutant LGGs and oligodendrogliomas show that these tumours contain cells with glial properties but also a subpopulation that is most closely aligned to stem cells at the transcriptional level (89,90). Interestingly, in the *IDH*-mutant glioma single-cell work, the pool of undifferentiated glioma cells was shown to increase, as tumour grade increased.

It remains contested whether GSCs have a common cell of origin, such as a neural stem cell (quiescent or not) or arise from a somatic cell that dedifferentiates and acquires characteristics such as pluripotency and self-renewal capability (91)(72). Recent evidence from human GBM tissue has added weight to these cells being neural stem cells, arising from the subventricular zone, that contain the driver mutations of GBM (92). GSCs can and have, regardless of origin, been described as undifferentiated tumour cells that are characterised by their capacity to give rise to more differentiated progeny (neuronal and glial cells),

their ability to self-renew (divide indefinitely) and initiate tumour growth *in vivo* (93).

Given their ability to evade conventional chemoradiotherapy, either due to quiescence, an ability to activate DNA repair mechanisms or the existence of efflux drug transporters (94,95), the ability to target GSCs is an area of critical unmet need. Success has been very limited, partly due to the limitations outlined above (GSC identification, definition, enrichment). Forced differentiation strategies have been tested, using a number of compounds such as bone morphogenetic protein (BMP) (96,97), 2-hydroxyoleic acid (98), serum (99), curcumin (100) and retinoic acid (101), with limited success.

### **1.2.2. Isolation of GSCs**

Current methods of isolating GSCs *in vitro*, either for propagation in culture, or xenotransplantation, require a number of harsh mechanical and enzymatic treatments, followed by a variable period of incubation under artificial culture conditions (76). These protocols therefore inevitably subject the resulting assays to potential biases and artefacts. However, few better alternatives have emerged, and so these culture methods remain important. Moreover, they have revealed crucial insights into glioma biology. A commonly used isolation protocol involves putting dissociated primary human brain tumour tissue, taken directly at the time of surgery, into serum-free medium with defined growth factors (human basic fibroblast growth factor (bFGF) and epidermal growth factor (EGF)). (88). Cells isolated in this way have been shown to closely resemble the gene expression profile, phenotype and *in vivo* biology of their parental tumour (102) and represent the most basic cell model. The strengths and caveats of such an *in vitro* model are discussed later.

CD133 enrichment can be used to isolate populations of cells that exhibit characteristics consistent with those expected for GSCs, but the specificity of CD133 for GSCs remains under debate since studies have demonstrated that CD133 negative cells also have the potential to form tumours (76,103–105).

As discussed previously, the variability in methods for isolating cells that are universally termed GSCs/BTSCs/BTICs/CSCs mean that the findings from the

studies in which they are used may not relate to the same subpopulation within the tumour, and between research groups.

Despite, and perhaps because of, the debate surrounding the existence and importance of stem-like cells in gliomas, it is clear that any new model that aims to evaluate therapy, study gliomagenesis and investigate treatment resistance needs to represent this population, in a defined matter.

### **1.3. Current models of glioma**

This section provides an overview of the models that have been developed and used in glioma research. Such models have the potential to greatly add to our understanding of underlying glioma biology, identify biomarkers and facilitate the development and evaluation of new therapies. In addition to needing to represent genetic abnormalities, glioma models carry an added responsibility to also incorporate the unique brain microenvironment in which these tumours develop and grow. This is a very specific and strict combination to achieve and is unlike many other extra-cranial cancer models. It may, in part, explain the slow progress made with the development of new models, the poor translation of laboratory-based discoveries into clinical practice, and the subsequent failure to improve outcomes for patients with glioma.

The strengths and weaknesses of the models will be discussed with respect to their ability to represent glioma (epi)genetics, heterogeneity, immunocompetence, consider the brain micro-environment, possess a blood-brain barrier, stability and reproducibility.

#### **1.3.1. In vitro models of glioma**

Remarkable progress has been made in understanding gliomagenesis, invasion, progression and recurrence (106). Much of this owes to the development and study of glioma models. Adherent patient-derived primary cell culture frequently represents the most common and technically most-straightforward *in vitro* glioma model used in research. Such adherent monolayers can be derived from brain tumour tissue taken directly from patients, as described above, or from commercial sources using immortalised lines. The two most commonly used lines are U87 and U251, both of which were generated many decades ago from patients with GBM (107,108). Expansion and propagation of these cell lines has been successfully used in genetic and chemical screens (50,88,109). This model has been proven to be disease-relevant, but concerns have emerged regarding genetic mutational drift and clonal selection pressures exerted by long term culture (especially with foetal bovine serum) (110–113). Recent genomic sequencing of the U87 line showed massive numbers of copy number variations, translocations and indels, most of which have been proposed to have been acquired after decades of cell culture (114). Furthermore, analyses from different

laboratories purporting to be using U87 lines have questioned the provenance of these lines and resulted in journals requiring cell line authentication as prerequisite to publication using U87 (110,115). The U251 line underwent an early cross-contamination and now is known to have been incorrectly labelled as U-373 in numerous publications (111). Analysis of the common subclones from various laboratories using U251 show that only the original line, developed in the 1960s, maintains the DNA copy number variation typical of GBM. Long-term passaged subclones of U251 have been shown to have more aggressive growth *in vivo* and an increased growth *in vitro* (111). Accordingly, the predominant use of these lines in current practice is in the pre-screening of targeted therapies in a rapid and reproducible way, prior to further testing of promising candidates in appropriate preclinical models (116).

Neurosphere culture arose from work to develop a way to stably maintain and propagate neural stem cells (NSCs) in medium, and obviate the need for serum (117). Cells cultured in this way express many of the typical stem cell markers such as *SOX2*, *NESTIN*, *SSEA1* and *CD133* (88,118). When cells lose these markers (for example, when cultured under serum conditions), they have been shown to lose the ability to diffusely infiltrate into the brain parenchyma (102,119).

Tumour grade and *IDH* mutation status, however play a large part in the success of generating these cell lines (116). Very few examples of cell cultures generated from WHO Grade II and III gliomas with mutant *IDH1* exist. Jin *et al.* (120) were able to culture WHO Grade III anaplastic astrocytoma cells which underwent loss of the wild-type *IDH1* allele but preserved the *IDH1* mutant allele following progression to GBM. One proposed hypothesis for the difficulty to culture cells with an *IDH1* mutation – thought to exert its effects in gliomas partly through altered metabolism (121) – is the challenge of modelling the brain micro-environment and the influence this has on the metabolic phenotype of a cell (122). Rohle *et al.* (123) developed a WHO Grade III anaplastic oligodendroglioma cell line with an *IDH1* mutation and co-deletion of *1p19q*. To date, no group has published successful culture of WHO Grade II glioma cells with an *IDH1* mutation.

A move to serum-free cell culture media has been demonstrated to provide more genetically and transcriptionally stable lines (88,102,124) than traditional cell

culture methods but concerns have emerged that significant drift still occurs (125). A recent study looking at genomic stability of primary GBM cell culture during the first 20-30 passages showed that they undergo significant genomic and transcriptional changes (126). At a genomic level, the authors demonstrated variations in aneuploid cell content, subpopulation cell cycling time, and proportions of subchromosomal lesions resulting in sequential clonal takeovers. Several metabolic and signalling pathways were also shown to be altered temporally. These included telomere packaging, ribosomal synthesis, and signalling via the mammalian target of rapamycin, Wnt and interferon pathways. Much of this transcriptional drift was linked to the changes at a gene level. Cultured GBM cell lines also showed changes to the subtype over time, through transcriptional changes. Epigenetic changes such as DNA methylation, when compared to gene expression and chromosomal abnormalities, remained relatively stable. Some of these changes may be due to the use of growth factors such as basic fibroblast growth factor (bFGF) (127), which are important for maintaining stemness *in vitro* (102,128). Changes proposed to be caused by bFGF in culture include altered signalling pathways, modulation of apoptosis, mediation of DNA repair, increased proliferation and migration. Some research groups have therefore investigated the need to add growth factors to GSC cultures and found that primary cells could still be cultured with a subpopulation of GSCs (129), and that even neurospheres can proliferate without bFGF and epidermal growth factor (EGF), albeit at a lower rate of proliferation and at a smaller size (130). There does therefore appear to be a trade-off between *in vitro* proliferation, the use of growth factors and the phenotypic representation of cultured GSCs to original tumour cells.

In the context of drift, understanding which relevant genetic aberrations from the original tumour exist in the particular 'variant' of these lines being used can make them helpful in the study of certain oncogenic pathways. Failing to consider these drifts in functional biological experiments and biomarker studies may make the results less relevant (126). This principle can be extended to any new model developed.

Newer *in vitro* glioma models based on organoid methodology will be discussed in a separate section.

### 1.3.2. In vivo models of glioma

Despite ethical considerations and the lack of human context, *in vivo* models continue to be used extensively in all forms of cancer research, including glioma.

Subcutaneous grafting of glioma cell lines represents a relatively straightforward preclinical model and is frequently used in proof of concept studies testing the efficacy of targeted drugs (131). They have the simple advantage of being able to be tracked (and quantified) visually. They are particularly useful where there is a defined target within tumour cells and the activity of the drug does not rely on modulation or interaction with the micro-environment – the lack of which is this model's significant drawback (116). Previous studies that have failed to take this into account have overinterpreted the translation of their results (for example, the effects of angiogenesis inhibitors (132)).

Orthotopic patient-derived xenograft (PDX) models aim to overcome this lack of microenvironment and avoid the aforementioned cell culture problems by bypassing *in vitro* propagation at all. In PDX models, glioma samples taken at the time of surgery are injected directly into the brains of immunodeficient mice, with at most a brief period of *in vitro* mechanical dissociation for technical reasons (106,119,133–135). Intracranial injection might be done freehand or with a stereotactic frame device. Models such as these have been used successfully to evaluate the effects of small molecules on tumour burden (50).

Unlike the limited success in culturing cells *in vitro* with *IDH1* mutations, there has been some ability to model this *in vivo*. Examples include xenograft models of WHO Grade III human anaplastic oligodendrogliomas (one with mutations in *FUBP1*, *CIC*, and *IDH1*) (133,136) and an orthotopic xenograft model of a neurosphere cultured *IDH1*-mutant WHO grade III anaplastic oligoastrocytoma (134). The polymutational oligodendroglioma model is particularly interesting since it failed to grow *in vitro* after passage through a mouse. This can be considered to strengthen the argument for the importance of micro-environmental context in glioma modelling (133), although passaging in mice has been shown to exert a selection pressure that causes changes to genetic and epigenetic

signatures (137), and this drawback of animal models might be responsible for the failure to grow cells in which *IDH1* mutation is present.

Another significant drawback to xenografting, from cell lines derived in culture, or directly from fresh tissue samples, is that the host mice are immune-deficient. This creates several caveats within the model. This lack of immunocompetency means that it is challenging to: fully evaluate the effects of drugs that target or modulate the immune system, study the interactions of the immune system with other aspects of the microenvironment and achieve representative intratumoural heterogeneity due to the selection pressure for the fastest growing clones (116). Perhaps the most striking difference to the human immune context is the lack of peri-tumoural oedema seen on small-animal MRI of established *in vivo* brain tumours (138). Humanised mouse xenograft models (where the mouse Ig-locus is exchanged for the human Ig-locus) have been proposed as one way of addressing the problem of an immune system in these models (139,140).

One of the earliest developed *in vivo* models is based on carcinogen-induced gliomagenesis in rats (141). In this model, DNA-damaging intravenous N-ethyl-nitrosourea (ENU) was injected into pregnant animals with the resulting *in utero* exposure inducing predominantly brain tumours. This model has been used to strengthen the argument for the cell of origin of gliomas to be in NSCs as when ENU is injected into adult animals (relatively much fewer NSCs) they do not develop brain tumours (142). This model has enabled the temporal analysis of accumulation of mutations in brain tumours and helped identify key driver mutations such as *TP53*, *PDGFRA*, *CDKN2A* and *EGFR* (143). Recently, the ENU-induced preclinical model was used to demonstrate that the *BRAF* codon 545 mutation (V545E) is a frequent early event in rat glioma development (144). This mutation corresponds to the *BRAF*V600E mutation in humans and is usually seen in non-diffuse gliomas (pilocytic astrocytoma) but is observed in diffuse gliomas too. The ENU-model has a number of strengths – it has a more complete brain micro-environment, with an intact immune system and BBB, and also gives rise to genetically heterogenous tumours (145). Unfortunately, it is a poorly reproducible model with low rates of tumour formation, which results in significant investments of time, money and animals (116). This has, in turn, resulted in a number of ENU-induced rat glioma *in vitro* cell lines being established – C6, 9L,

RG2, F98, BT4C and RT-2 (146). Another line (GL261) has been created from a carcinogen induced glioma model (147,148) generated by intracranial injection of the alkylating agent 3-methylcholantrene into C57BL/6 mice. Murine gliomas created by these models (with the exception of C6) enable the study of glioma immunology and the evaluation of immunomodulatory therapies (149) as they can be isolated, cultured and then orthotopically xenografted into syngeneic, immunocompetent mice (146). One of the drawbacks of these models is that humanised antibodies can only be used for a limited number of times before an allogeneic reaction occurs (116).

Genetically engineered mouse models (GEMMs) of glioma build on the knowledge of specific driver mutations that are involved in human gliomas. These models often reflect many of the histopathological, aetiological and biological features of human gliomas (113). Current models can incorporate complex gain and loss of function mutations in specific cell types and at specific time points of development. This may be facilitated by introducing alleles of genes that can modulate expression by tet-regulation and cre-induction. The replication competent avian leukosis virus splice acceptor (RCAS/tv-a) system has also enabled the somatic introduction of multiple genes into a single mouse strain using retroviral or adenoviral vectors delivering cre-recombinase (150,151). Other GEMM models have been developed by disrupting signalling pathways known to be altered in gliomas, such as *PDGFRA*, *EGFR*, retinoblastoma (Rb), Ras and AKT (152–154). Models of murine HGG resembling human glioma phenotype and with a BBB (155), and *IDH1* mutation expression (156) have been developed using these techniques.

GEMMs have distinct strengths in being able to study specific molecular events responsible for glioma initiation and progression (113). They are also immune competent and have a BBB, allowing for studies of drug distribution to glioma cells in the brain (157,158). Disadvantages of these models include the lack of intratumoural heterogeneity that is observed in human gliomas. Also, therapeutic outcome is only translated into patients if the targeted drugs that are tested have similar activity against murine and human targets (116).

Other *in vivo* models that are emerging include zebrafish (*Danio rerio*) (159), which have been shown to share similar cancer-forming pathways with humans. Current zebrafish models either involve injection of day 3 post-fertilisation embryos or intracerebral implantation with glioma cells (116). The tumours formed in these systems, when using the same cells, have been shown to be similar to those grown in mouse, but at a much lower cost and in greater numbers. Adding compounds to their water supply allows for a semi-high throughput drug screening set-up (159). A major drawback of this system is that glioma cells must adapt to 32°C prior to implantation, which could adversely affect their metabolism and the activity of oncogenic pathways (160). Furthermore, the fish may die before the BBB has fully developed and/or the immune system fully matured (161,162). Another model that has emerged in glioma is one that has been used extensively in other aspects of neuroscience and cancer; the fruit fly (*Drosophila melanogaster*) (163). This organism has the advantage of being able to be genetically manipulated in a single cell fashion *in vivo* (164). Increased migration, and proliferation, by the manipulation of highly conserved molecular pathways such as the RTK signalling pathway, have been studied using fruit flies (165,166).

## **1.4. induced pluripotent stem cells (iPSCs)**

### **1.4.1. Reprogramming somatic cells to iPSCs**

Stem cells exhibit the fundamental hallmarks of self-renewal (unlimited proliferation in vitro) and pluripotency (differentiation into any cell type) (167). Embryonic stem cells (ESCs) have been isolated in both mice (1981) and humans (1998) but they require the destruction or manipulation of pre-implantation embryos and can therefore evoke strong ethical debates (168–170). Adult somatic cells can be reprogrammed to induced pluripotent stem cells (iPSCs) (171). These cells offer the potential of a limitless source of autologous cells that would not be rejected by the recipient's immune system. Potential benefits include replacement of damaged or diseased tissues, as well as personalised drug discovery and modelling of patient-specific diseases (172). iPSCs have been successfully derived from adult skin cells, liver, urinary tract cells, prostate cells, blood cells and gastric cells (171). The first clinical trial using iPSCs was approved in Japan in 2013 (173). The study aimed to treat patients with age-related macular degeneration with autologous transplantation of iPSCs derived from retinal pigment epithelium.

Reprogramming aims to reset the role that epigenetics play in the process of cellular decision-making during development, a concept first described by Waddington in 1957 (174). The first cellular reprogramming itself was undertaken by Gurdon in 1962 by nuclear transfer from a mature intestinal cell into a frog egg, which developed into a normal tadpole (175). His research showed that specialisation of cells is reversible, and that the DNA of the mature cell still retained embryonic developmental information. In 2006, the reprogramming field was revolutionised by Takahashi and Yamanaka who published a method of directly reprogramming mouse embryonic fibroblasts (MEFs) using retroviral infection (2). Investigating a panel of 24 factors that had been previously identified as important in ESCs, the MEFs were engineered (via antibiotic selection) to report the ESC-specific gene *Fbx15* upon successful activation. By removing one factor at a time from colonies that emerged with activated *Fbx15* reporter, the group eventually identified the 4 key 'Yamanaka factors' – Oct3/4, Sox2, Klf4 and cMyc. Refinement of the technique was achieved using *NANOG* as the reporter gene, eventually producing iPSCs with characteristics similar to ESCs (176). These iPSCs were crucially able to form all 3 germinal layers (ectoderm,

mesoderm, endoderm) and produce viable chimeras when injected into developing embryos. In 2007, both Thomson (177) and Yamanaka (178) produced human iPSCs from adult fibroblasts. Yamanaka *et al.* used the same 4 factors with a retroviral system, but Thomson *et al.* replaced cMyc and Klf4 with NANOG and Lin28 and used a lentiviral system. Yamanaka and Gurdon were jointly awarded the Nobel Prize in 2012 for their work on cellular reprogramming.

Oct3/4 (also known as POU5F1 (POU domain, class 5, transcription factor 1) is an octamer-binding transcription factor that maintains pluripotency and confers differentiation potential [35]. It is exclusively expressed in pluripotent stem cells. SOX2 (Sry-related high mobility group box) genes encode a family of transcription factors that also maintains pluripotency but is expressed in multipotent and unipotent stem cells (179). SOX genes are involved in sex determination and neuronal development. Klf4 is one of the Kruppel-like families of transcription factors that are a set of zinc finger DNA-binding proteins that regulate gene expression and induce pluripotency [39]. cMyc is a proto-oncogene that codes for a transcription factor and is involved in cell cycle progression, apoptosis and cellular transformation (180). In the context of reprogramming, it induces pluripotency.

Reprogramming has several disadvantages and challenges. Efficiencies are typically low, around 0.01-0.1% (171). Precise timing, concentration of each individual factor and cell type used for reprogramming all play a key role in determining success (172). Unpredictable genomic integration resulting from the reprogramming method was a major barrier to studying conditions linked to genetic changes (181). Non-integrative technologies have since been developed (182). cMyc and KLF4 are recognised oncogenes and therefore infer a risk of tumour formation in iPSCs (171). Incomplete reprogramming is always a possibility - techniques such as live cell staining for ESC surface markers aim to prevent colonies being expanded that may not have fully reprogrammed (167,183).

Currently available, validated reprogramming technologies broadly fall into categories – integrative systems, inducible systems, integration and excision systems, and integration-free systems. Each has distinct advantages and

disadvantages (Table 1). No single method is suitable for every scenario or research question. Although mRNA transfection carries the highest efficiency with the fastest colony formation, the workload is laborious and it has only been shown to work in fibroblasts so far (182). I have chosen to use the Sendai virus method as it has very good efficiency (blood cells ~0.1%, fibroblasts ~1%), high reliability, low workload and has been shown to work in a wider number of cell types (172,181). The virus vector contains transgenes that will express the 4 Yamanaka factors, causing the cell to express these genes after transduction.

Feature	mRNA (Stemgent)	SeV (Life Technologies)	Epi (Addgene)	Lenti (Mostoslavsky)
Efficiency (Fibroblasts)	High	Moderate	Low	High
Reliability (fibroblasts)	Moderate (mi+mRNA)	High	High	High
Reprogramming workload	High	Low	Low	Very High
Aneuploidy rate	2.3%	5.0%	10.2%	4.5%
Input cell requirement (fibroblasts)	Low	Moderate	High	Moderate
Time to colony emergence	Fast	Moderate	Moderate	Moderate
Number of colonies to pick	3	6	7	No data
Adoption: rejection rate	1.2	3.5	0.	0.3
Special equipment requirement	Hypoxia	None	Nucleofactor	None
Reprogramming agent cost	Moderate	Expensive	Cheap	No data
Scalability or automatability	High	Moderate	Low	Moderate
Lines free of reprogramming agents by passage 5	100%	0%	60%	N/A

Lines free of reprogramming agents by passage 9-11	100%	79%	67%	N/A
--	------	-----	-----	-----

**Table 1:** Comparison of commonly used reprogramming methods (modified from Schlaeger *et al.*) (184). RNA = Ribose nucleic acid, SeV = Sendai Virus, Epi = Episomal Vector, Lenti = Lentivirus.

Sendai virus (SeV) is a mouse and rat respiratory virus of the *Paramyxoviridae* family (185). Other viruses in this family include measles and parainfluenza. SeV was first isolated in Sendai, Japan in the early 1950s. Its genome is a negative-sense single-stranded RNA virus that contains 6 major genes and is non-pathogenic to humans. Once cells are infected, the fusion protein F is deleted and therefore no more infectious particles are produced. It can therefore be cleared relatively quickly (~5-10 passages) (186). Sendai will bind to a large range of targets and only requires one transduction (185). It is non-integrative to the host as it replicates in cytoplasm and so there is no nuclear/DNA phase (184).

#### 1.4.2. iPSCs in cancer and glioma

GEMMS have enabled the study of cancer progression by observing the effects of oncogene induction or tumour-suppressor inhibition in a time-dependent manner (60). It is hoped that the use of iPSC models in cancer research will enable the study of underlying dynamic networks, elucidate biomarkers of early malignancy and provide an evaluation of new therapeutics; all with the crucial human specific context that GEMMs lack (187). Recapitulating disease initiation and progression is difficult with tumour cell lines and xenografts of primary tumour cells since they represent the advanced tumour state. Reprogramming cancer cells to pluripotency is one approach that has been used to overcome this gap (188). Where this approach has been used, pluripotency has been shown to be transient over the cancer phenotype and that partial expression of the cancer genome may be enough for cells to exhibit early-stage cancer phenotypes (189). iPSC technology has been used to reprogram cancer cells in chronic myeloid leukaemia (190,191), gastrointestinal cancer (192) and human primary pancreatic ductal adenocarcinoma (193)

In the context of glioma, very few iPSC-based models have been described. Stricker *et al.* (2013) (194) derived iPSCs, using piggyBac transposon vectors expressing OCT4 and KLF4, from cultured neural stem cells enriched from GBM. Their aim was to invoke epigenetic resetting and study the effects of this on DNA methylation, changes to the transcriptome and malignancy. They discovered that widespread resetting of epigenetic methylation occurred after reprogramming, causing removal of repression of certain tumour suppressor genes (CDKN1C and TES) and the growth of non-infiltrative teratomas. Highly proliferative neural progenitors (NPs) were derived from these teratomas. Subsequent orthotopic xenotransplantation of NPs differentiated from the iPSC line resulted in aggressive GBMs, whereas non-neural mesodermal progenitors differentiated from the iPSC line conserved the TSG derepression and failed to form infiltrative tumours. These observations demonstrate that despite epigenetic resetting secondary to reprogramming, oncogenic mutations still persist that drive malignant phenotypes. There is no published literature outlining direct reprogramming of primary human LGG tissue.

All of the cancers described above that have been reprogrammed to pluripotency using iPSC technology have revealed a few key observations (60). Firstly, that the differentiation potential of the cancer cells can, at least in part, be restored. Secondly, a reduced aggressive cancer phenotype in teratoma assays is exhibited by the reprogrammed cells, potentially due to suppression of oncogenes from the original cancer and activation of tumour suppressor genes. Thirdly, epigenetic states are altered markedly during reprogramming. Fourthly, the cancer phenotype can be re-acquired during differentiation into the lineage from which the reprogrammed cancer cells were derived. Lastly, that this model has the potential to study cancer progression even though the cells being reprogrammed are taken from mature cancers (though this may represent selective/preferential reprogramming of more cancer-immature/stem-like cells among the parental cell source).

## **1.5. Cerebral organoids**

### **1.5.1. Development of cerebral organoids**

Reaggregation studies have demonstrated the brain's intrinsic self-organising capacity to form highly spatially organised, complex interconnected regions (195). This key property can be used to direct stem cells (iPSCs or ESCs) to form neural ectoderm that differentiates into a highly organised brain-like structure that exhibits multiple cell types; a cerebral organoid (3). Developmental biology studies have shown that cells self-organise and demonstrate two key events during organogenesis: cell sorting out and spatially restricted lineage commitment (196). Both processes are evident in organoid formation (197). Previous 3-dimensional brain modelling (using growth factors) has produced tissues with homogenous brain regions derived from neuroectoderm – forebrain, cerebellum and hypothalamus (198). Using concepts and techniques previously pioneered in Hans Clevers' group (197), Lancaster *et al.* (3) advanced this model by using Matrigel embedding to encourage buds to form from single embryoid bodies and develop into brain regions. Transferring these structures into spinning bioreactors improves nutrient and oxygen exchange to allow further growth. Self-assembly and a remarkable resemblance to a brain-like structure makes this technology promising for adaptation to glioma modelling.

Other in-vitro models exist such as neural stem cell (NSC), neurospheres and neural rosette systems, as discussed previously (117,199–201). NSC model systems allow the study of live cells as they progress through malignancy, which could elicit new information about transcriptional networks and underlying pathology (60). Aggregating NSCs or tumour cells to form neurospheres attempts to recreate the 3D properties of brains and tumour masses, respectively (87). Cerebral organoids aim to advance this model by creating multiple specific brain regions contained within the same 3D structure (202). Neural rosettes are 2D neural tube-like structures established from directed differentiation of ESCs or isolated neuroepithelium (200). They have the advantages of exhibiting apical-basal polarity, spontaneous radial organisation, production of intermediate progenitor types, and timed production of layer identities similar to *in vivo* development (201). However, neural rosettes are not 3-dimensional and so ultimately lack the overall organisation of the human brain (203).

Human iPSCs have been used to generate gastrointestinal, kidney, retinal, pancreatic, prostate, inner ear, brain and liver organoids (204–210). Limitations such as ultimate size, lack of immune system and vascularity exist but it would be hoped that these could be overcome in time.

In neuro-oncology, the reproducibility of brain organoids could be used for drug discovery and screening (potentially in a medium or high-throughput fashion), and contribute to the ‘replacement’ arm of the 3 R’s consideration in animal studies (211). If patient-derived iPSCs are used to form the organoid, as proposed here, such modelling and drug testing could be personalised.

### **1.5.2. Cerebral organoids in glioma**

Primary patient-derived organoids provide an alternative, complementary *in vitro* model for study of cancer phenotypes. It has been proposed that they may bridge the gap between simple cancer cell lines, that are well suited for high-throughput applications but lack physiological context, and xenografts that provide a micro-environment context but are complicated and expensive (212). Work primarily conducted in colorectal organoids shows that conferment of drug resistance to cancer stem cells can be modelled by the presence of differentiated cell within the same organoid, and additional heterogeneity can be achieved by co-culturing with patient-matched control healthy organoids (213,214). Furthermore, the methodology of organoid formation involves providing the conditions for progressive differentiation and cellular proliferation. Since cancers are thought to occur due to uncontrolled proliferation and loss of differentiation (43,44), the organoid model could lend itself well to studying these phenomena, potentially in real-time. However, it is not known whether the mutations seen in the advanced cancer of interest is replicated in developing organoids and/or whether additional genomic instability occurs due to selection pressure *in vitro* (212). Furthermore, organoids still do not have an immune system, lack vasculature (and therefore a BBB), remain expensive and labour-intensive to maintain (relative to simple cell lines) and exhibit batch to batch variability (215). Attempts have been made to address some of these drawbacks in cerebral organoids by the development of brain-region specific organoids (reduces batch-to-batch variability and more simplifies methodology) (216,217), by the use of stackable mini-bioreactors (to

aid throughput) (218) and by the use of microfluidics chips (to mimic vasculature and/or a BBB) (219).

There has been a limited application of cerebral organoid methodology in glioma modelling thus far.

Hubert *et al.* (220) were the first to describe a three-dimensional culture system that aimed to support the long-term growth and expansion of GBM organoids. Organoids were formed from cells from a variety of sources including patient-derived primary culture, xenografts and GEMMs. They also derived organoids from brain metastases secondary to oesophageal adenocarcinoma. Although the cerebral organoid methodology was based on the previously established protocol by Lancaster *et al.* (202), this group used cells directly from tumours (patient-derived or mouse), rather than using ESCs or iPSCs. They were able to culture the GBM organoids for months, observing regional heterogeneity. This included a highly proliferative outer region and a hypoxic core of non-stem-like cells and quiescent GSCs. The latter were radioresistant. The patient-derived organoids, when orthotopically transplanted, retained the features of the parental tumours (histology and single-cell invasiveness).

Da Silva *et al.* (221) co-cultured early cerebral organoids (eCOs), derived from mouse ESCs and prior to embedding in Matrigel, with GBM spheres pre-formed from patient-derived cell lines. They were able to show with time-lapse imaging that, compared to control spheres pre-formed from human neural progenitor cells, GBM spheres would spontaneously infiltrate and migrate within the eCOs. This model has the significant advantages of having a short organoid formation time (12 days), which has been associated with reduced batch variability (215), and being able to be conducted in a medium-throughput (96-well) fashion. The period of co-culture was also short (48 hours) and may therefore be suited to real-time assays for anti-GBM strategies using personalised samples. The model will be even more relevant when the eCOs are formed from human stem cells and could be used to study the molecular mechanisms underlying migration. The group also do not confirm the tumour-forming capability of the hybrid eCOs with orthotopic xenotransplantation.

Ogawa *et al.* (222) cultured cerebral organoids for 4 months and then injected plasmids close to their surface, using CRISPR/Cas9 technology to target an HRas<sup>G12V</sup>-IRES-tdTomato *TP53* locus. The resulting transformative mutation caused cells to become invasive and exhibit gene expression profiles consistent with the GBM mesenchymal subtype. Moreover, they overwhelmed the entire organoid and destroyed surrounding structures. They also showed that these cells, when orthotopically xenografted, exhibited an invasive phenotype. Furthermore, this group showed that GBM cells, either derived from primary patient samples or from GBM organoids, invade and proliferate within healthy cerebral organoids after co-culture.

All the above examples demonstrate the potential of using the cerebral organoid technology in glioma modelling. The ability to incorporate tumour cells/tissue and the possibility to alter the genome with gene editing make this potentially a very useful tool in drug discovery assays and studying tumour initiation events, respectively.

## 1.6. Aims and Objectives

Even with maximal medical treatment (debulking neurosurgery, full course radiotherapy and chemotherapy), the prognosis for the most malignant grade of glioma, WHO Grade IV glioblastoma remains poor, especially when compared to other cancers. Despite persistent and intensive research efforts, outcomes from glioma have not significantly changed for decades. One reason for this is the poverty of *in vitro* and *in vivo* models that faithfully recapitulate the biology of glioma initiation, resistance to therapy and recurrence. New models, especially those that use patient/human cells, are urgently required. To achieve this, I investigated whether primary glioma tissue, taken from patients directly at the time of neurosurgery, could be reprogrammed to induced pluripotent cells (iPSCs) and whether these iPSCs would retain genetic information relevant to the parental tissue. Furthermore, I sought to use these iPSCs in differentiation experiments, in both adherent and low-adherence 3-dimensional conditions to see if they could be developed into personalised models with a stem cell-like self-renewal phenotype.

1. The first objective was to use reprogramming methodology to revert tumour cells to a pluripotent state. In achieving this, I aimed to convert a resource (primary tissue) typically limited by quality and quantity, and prone to genetic drift in culture conditions (126), into a self-renewing cellular resource with retained genetic aberrations (glioma iPSCs). The iPSCs were subjected to state of the art pluripotency testing, and whole genome sequencing to characterise their stable iPSC status, and glioma-relevant genetic mutational burden. In order to link this new resource to existing models, *in vivo* orthotopic xenografting was undertaken to elucidate glioma iPSC tumorigenicity.
2. The second objective was to develop the newly-created glioma iPSCs into models that could be used to interrogate glioma biology and identify candidate genes for future modulation. To this end, I aimed to investigate the differentiation behaviour of glioma iPSCs, in comparison to normal iPSCs, in both adherent neuronal differentiation conditions, and in 3-dimensional cerebral organoid culture conditions. The adherent conditions used established protocols for neuronal differentiation whilst the organoid

methodology used relatively new techniques but one that is more faithful in recapitulating the architecture of a human brain and 3-dimensional nature of a tumour. I analysed gene expression in both these models comparing differences between glioma iPSC and normal iPSC differentiation.

## **2. Reprogramming of patient-derived brain tumour tissue results in stable iPSCs with tumorigenic capacity**

### **2.1. Results**

#### **2.1.1. Stable iPSCs can be derived from primary glioma tissue**

##### **2.1.1.1. Characterisation of primary glioma tissue and cells**

Patients were consented prior to neurosurgery for donation of surplus brain tumour tissue under the umbrella of the Health Research Authority ethically-approved Leeds Multi-Disciplinary Regional Tissue Bank. Two patient-matched WHO Grade IV GBM tissue samples were obtained – one each from the bulk of the contrast enhancing tumour (HGb and HGb2), and one each from the non-enhancing margin of the tumour (HGm and HGm2). Figure 2.1 shows an MRI image of a GBM tumour with superimposed schematic highlighting the contrast enhancing tumour (outlined in orange) representing the HGb and HGb2 samples, and the margin zone samples (outlined in yellow) representing the HGm and HGm2 samples. The margin zone samples are accessible en route to the GBM as part of the surgical corridor to access the tumour bulk. A WHO Grade II Diffuse Astrocytoma tissue sample was also obtained (LGG). Table 2 shows the details of the samples – basic patient demographics (age, sex and presenting symptoms), final confirmed histopathological diagnosis, post-op adjuvant therapy and overall survival. For the purposes of cell modelling, it is beneficial to have both sexes represented in models as there is an increased recognition that male and female cells may be differentially sensitive to malignant transformation due to cell-intrinsic gender differences (223). The patient from whom HGb2 and HGm2 samples were taken had short-course radiotherapy post-operatively and was enrolled in the hydroxychloroquine (HCQ) trial (Clinical Trials.gov ID NCT01602588), both of which are typical for patients diagnosed with GBM in this age group. Sampling tumours prior to chemoradiotherapy means that tissue is more representative of the clinical scenario when patients first present since mutational evolution has been shown to occur after adjuvant therapy (57). In time, the model itself can be used as comparator to study further genomic instability if the same patients undergo repeat surgery for recurrence (GBM) or malignant transformation (LGG) and are subsequently sampled again.

Molecular data shows MGMT methylation in HGb2/HGm2 and hypo-methylation in HGb/HGm. Neither GBM sample had *IDH1* or *IDH2* mutations. This infers that the samples represent primary GBM (*IDH* mutation is more commonly associated with secondary GBM that has transformed from LGG) (224). Since primary GBMs account for approximately 90% of all GBMs (225), this means the model represents the vast majority of patients with GBM. The LGG sample was *IDH1* mutated and *19q13* deleted alone, the latter of which is to be expected given the lack of an oligodendroglial component (11) (an oligodendroglioma would be defined by the WHO CNS 2016 classification to have 1p/19q co-deletion). The clinical significance of 19q deletion alone is unknown; co-deletion of 1p and 19q is known to be a strong prognostic factor and predictor of response to chemoradiotherapy in oligodendrogliomas and anaplastic oligoastrocytomas (226).

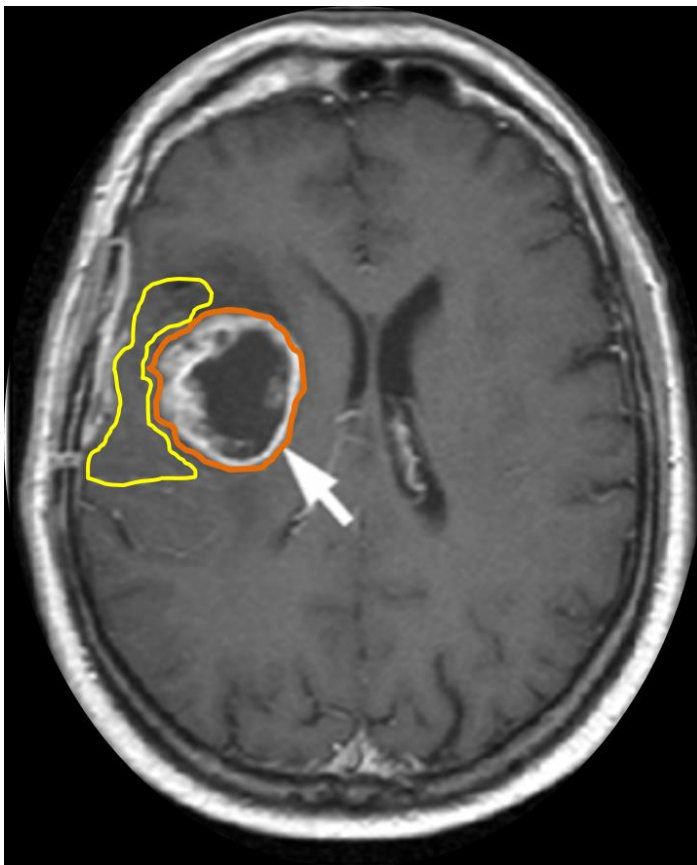


**Figure 2.1:** Magnetic resonance image (MRI) T1-weighted with gadolinium showing right temporal WHO Grade IV GBM with contrast enhancement (indicated by white arrow), central necrotic core, peri-tumoural oedema, and mass effect as evidenced by effacement of the right lateral ventricle. Area highlighted by orange shows representative sampling region for HGb and HGb2 tissue. Area highlighted by yellow shows representative sampling region for HGm and HGm2 tumour margin tissue, taken en route to tumour bulk via the surgical access corridor. Image adapted from (227).

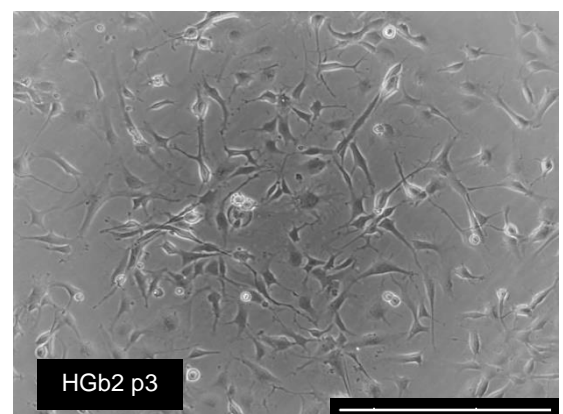
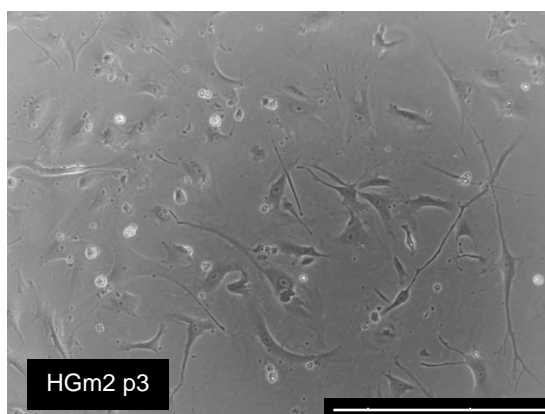
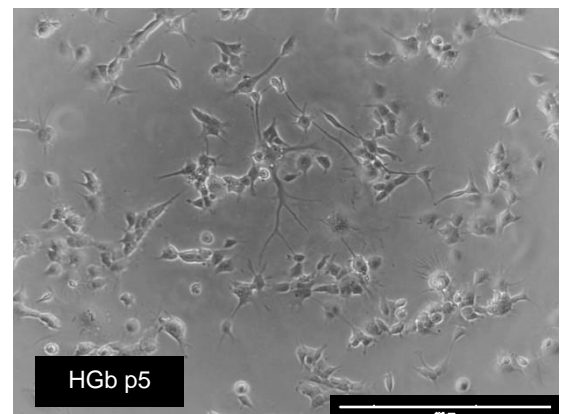
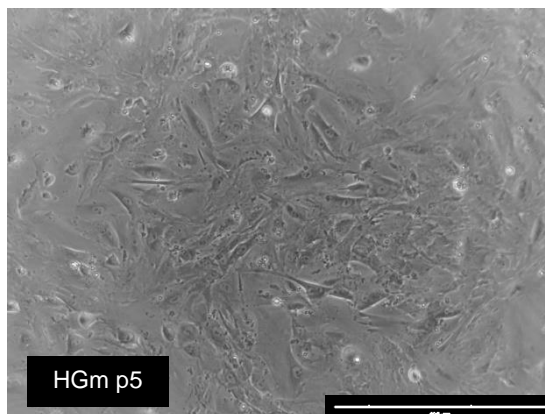
Line Alias	Sex	Age	Presentation	Diagnosis	Date of Surgery	Post-op Radiotherapy	Post-op Chemotherapy	Survival
HGm HGb	F	48	6 weeks headaches & olfactory hallucinations	WHO Grade IV GBM	27/03/15	54Gy in 30# over 6/52	TMZ, PCV at recurrence	PFS 3 months OS 11 months
HGm2 HGb2	M	74	2 weeks ataxia, impaired memory & vision, intermittent dull headaches	WHO Grade IV GBM	01/06/15	30Gy in 6# over 2/52	HCQ	PFS 2 months OS 9 months
LGG	F	30	Weekly complex partial seizures	WHO Grade II Diffuse Astrocytoma	14/07/15	54Gy in 30# over 6/52 at progression to HGG	PCV, TMZ at progression to HGG	PFS 9 months OS 3 years (radiological progression to HGG after 9 months)

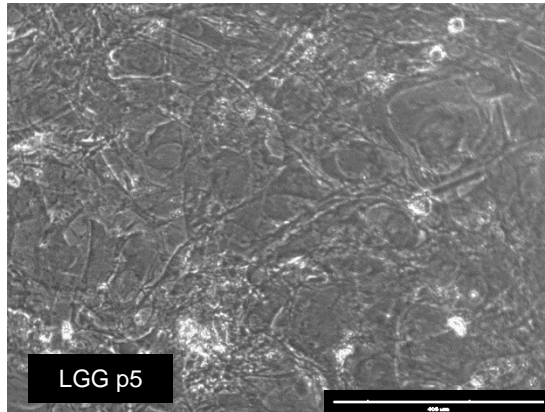
Line Alias	Molecular Data					
	IDH1	IDH2	MGMT	1p19q	PTEN	EGFR
HGm HGb	WT	WT	Unmethylated	Not co-deleted	Not tested	Not tested
HGm2 HGb2	WT	WT	Methylated	Not co-deleted	Not tested	Not tested
LGG	IDH1m	WT	Unmethylated	19q13 deletion alone	No loss	No amplification

Table 2: Patient characteristics (including post-operative adjuvant therapy and survival) for the samples obtained at surgery

LGG = Low Grade Glioma, HGG = High Grade Glioma, WT = Wild Type, PFS = Progression Free Survival, OS = Overall Survival, PCV = Procarbazine, Lomustine, Vincristine, TMZ = Temozolomide, IDH = Isocitrate Dehydrogenase, MGMT = O<sup>6</sup>-methylguanine-DNA methyltransferase, PTEN = Phosphatase and Tensin homolog, EGFR = Epidermal Growth Factor Receptor

All 5 samples (HGb, HGm, HGb2, HGm2, LGG) were dissociated, established in serum-free culture and passaged. Frozen vials at intermittent passages were stored. Light microscopy was used to confirm differences in morphology that were present, both between lines from the same patient, and between patients (Figure 2.2). In comparison to the HGm cells, HGb cells show a more rounded shape and appear to clump together. Contrastingly, HGb2 cells are morphologically more alike to HGm2 cells, showing similar shape and distribution. Single cell analysis and gene expression profiling may help with subtyping (49). If the cell lines were to be passaged further and used as a model in themselves, analysis of morphology and molecular subtyping would need repeating at intervals to observe any differences secondary to adaptation in culture (228). LGG cells exhibit morphology similar to both HGm and HGm2 cell lines. This may be expected given that WHO Grade II Diffuse Astrocytoma is closer in histological grade to normal tissue than contrast-enhancing GBM tumour bulk (HGb and HGb2). Cells were imaged at different degrees of confluency.





**Figure 2.2:** Inverted light microscopy (x10 magnification) of cultured cell lines. HGm and HGb cell lines are shown at passage 5, HGm2 and HGb2 cells at passage 3 and LGG cells at passage 5. HGb cells show a greater degree of difference to the matched HGm cells than HGb2 cells do to HGm2 cells. HGb cells show a more rounded shape with cells clumping together, whilst HGb2 cells appear more like their matched HGm2 cells. LGG cells appear more like the HGm and HGm2 cells – this may be expected given they are likely to be closer in histological grade to the non-contrast enhancing tumour margin cells than the contrast-enhancing tumour bulk cells.

Glioma cells have been shown to demonstrate stem-like features (72). Markers of stemness such as SOX2 and NESTIN, and markers of proliferation such as Ki67 can be used to characterise differences. Immunostaining of these markers, and those for astrocytic (GFAP) and neuronal (TUJ1, MAP2) expression are typically used in glioma cell culture (102).

Immunostaining of the markers mentioned above in the primary cell lines was performed and the results were analysed qualitatively (Figure 2.3). This was followed by quantification by qRT-PCR of gene expression of key markers (Figure 2.4). Stemness markers SOX2 and NESTIN, and the proliferation marker Ki67 appear to show increased staining in the lines derived from the contrast-enhancing tumour bulk (HGb and HGb2) when compared to the lines derived from the non-contrast-enhancing tumour margin (HGm and HGm2). This infers that the HGb and HGb2 lines exhibit a more stem-like phenotype, with increased proliferation. All lines staining positively for astrocytes (GFAP), neurons (TUJ1) and dendrites (MAP2), confirming that the samples were of central nervous system origin.

# HGm

**SOX2**

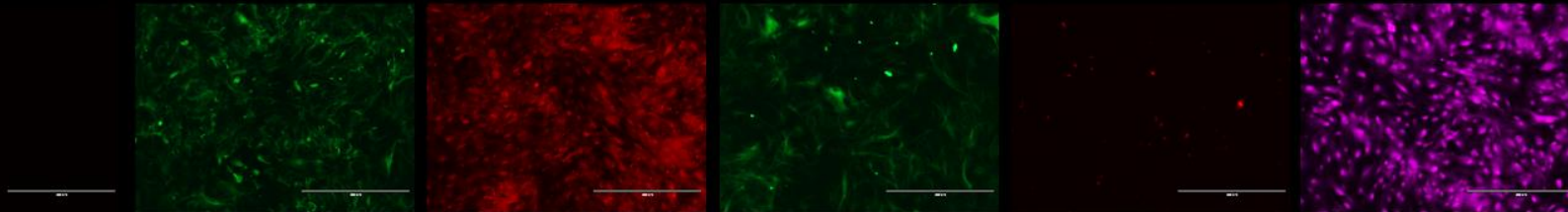
**NESTIN**

**GFAP**

**TUJ1**

**Ki67**

**MAP2**



**SOX2 + DAPI**

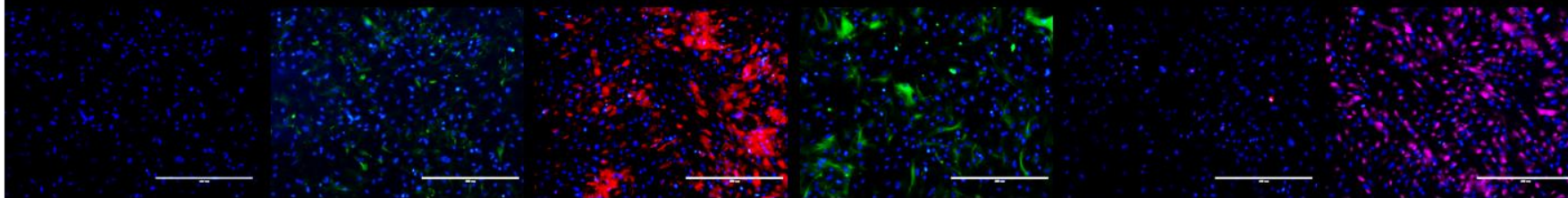
**NESTIN + DAPI**

**GFAP + DAPI**

**TUJ1 + DAPI**

**Ki67 + DAPI**

**MAP2 + DAPI**



# HGb

SOX2

NESTIN

GFAP

TUJ1

Ki67

MAP2

SOX2 + DAPI

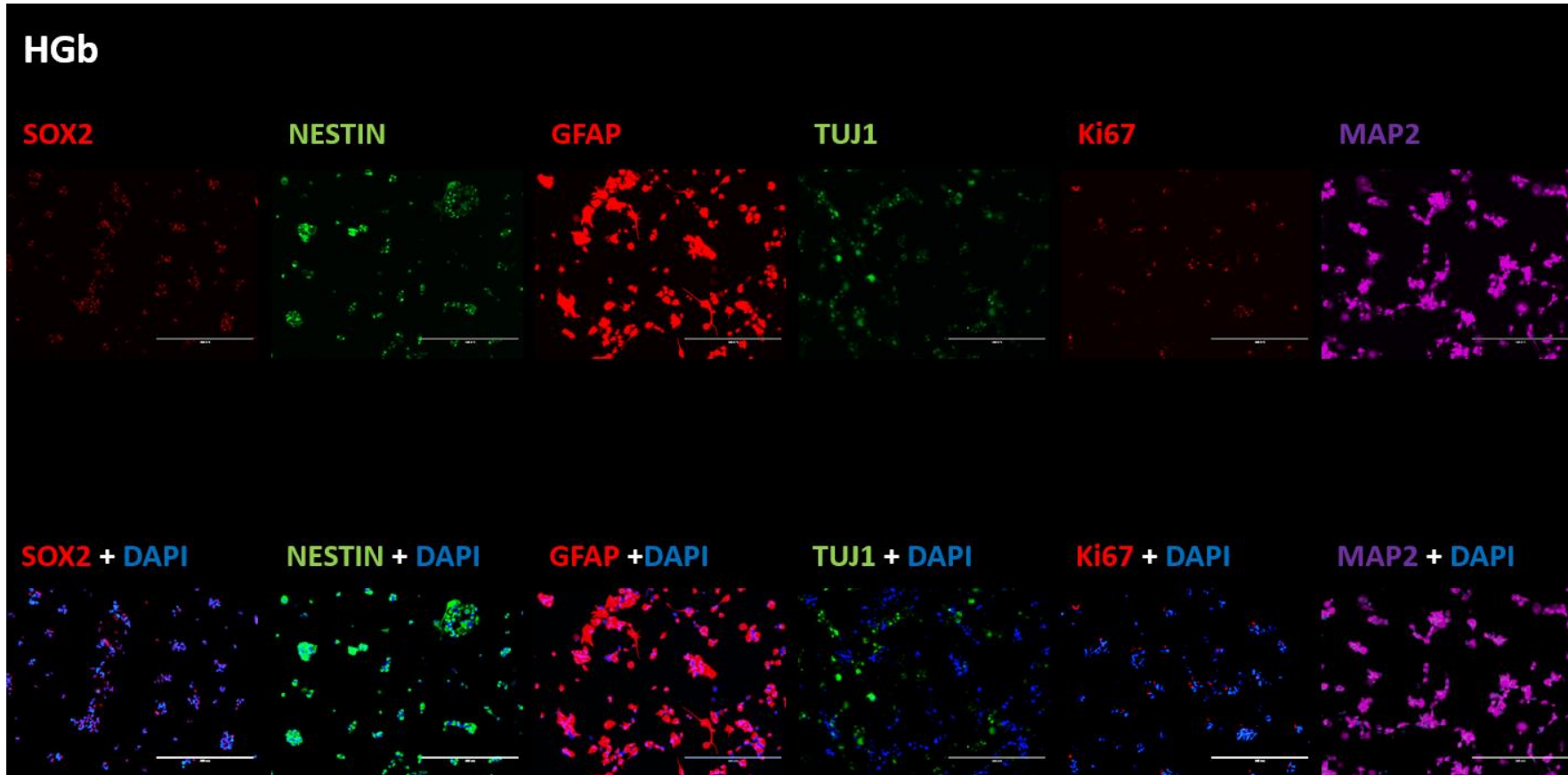
NESTIN + DAPI

GFAP + DAPI

TUJ1 + DAPI

Ki67 + DAPI

MAP2 + DAPI



# HGb2

SOX2

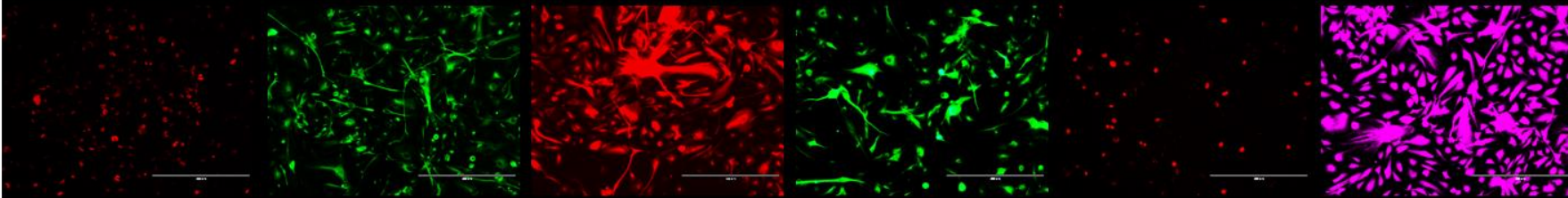
NESTIN

GFAP

TUJ1

Ki67

MAP2



SOX2 + DAPI

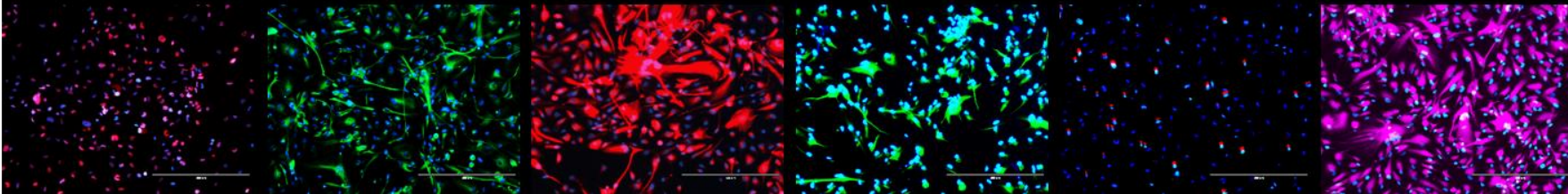
NESTIN + DAPI

GFAP + DAPI

TUJ1 + DAPI

Ki67 + DAPI

MAP2 + DAPI



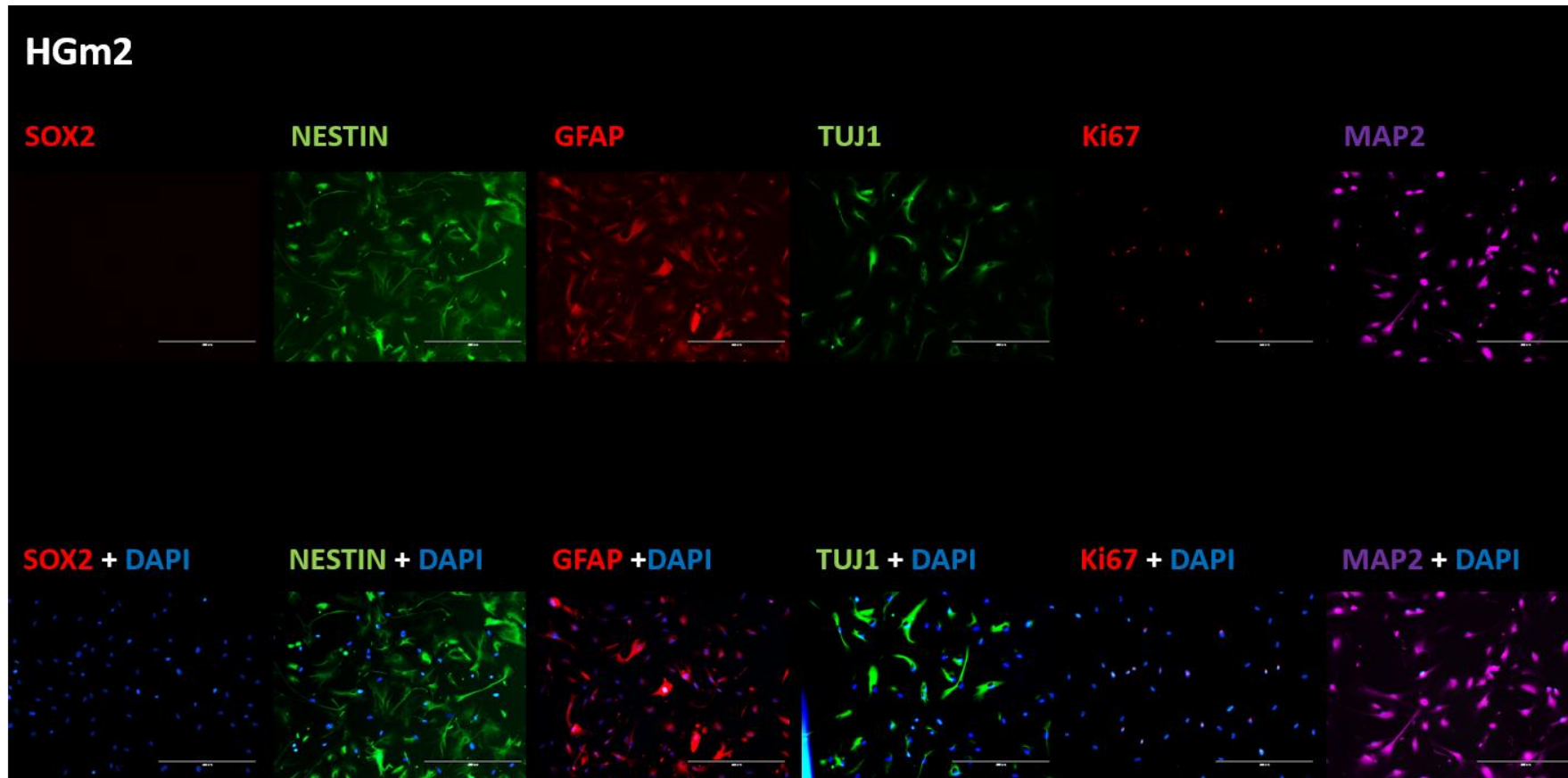
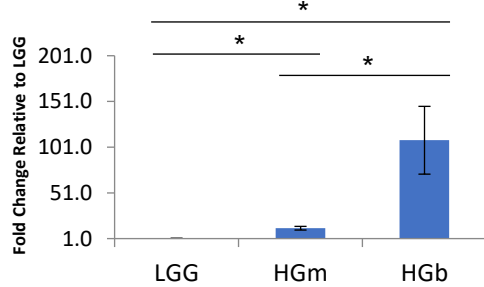


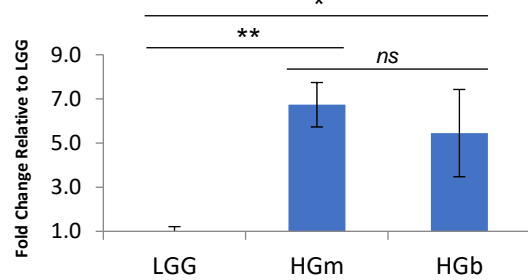
**Figure 2.3:** Immunofluorescence staining of primary cell lines for stemness and central nervous system (CNS) markers. Nuclei are co-stained with DAPI (x10 magnification). When compared to non-contrast-enhancing HGG tumour margin primary cell lines (HGm and HGm2), staining for stemness (SOX2, NESTIN), and proliferation (Ki67) markers appeared increased in the contrast-enhancing tumour bulk primary cell lines (HGb and HGb2). All primary cell lines stained positively for astrocytic (GFAP) and neuronal (TUJ1, MAP2) markers indicating that they are of CNS origin.

Gene expression analyses by qRT-PCR shows significantly higher expression of *SOX2* in HGm compared to LGG (FC > 12;  $p < 0.05$ ), HGb compared to LGG (FC > 108;  $p < 0.05$ ) and HGb compared to HGm  $p < 0.05$ ); significantly higher expression of *NESTIN* in HGm compared to LGG (FC > 6;  $p < 0.01$ ) and HGb compared to LGG (FC > 5;  $p < 0.05$ ); significantly higher expression of *Ki67* in HGb compared to LGG (FC > 58;  $p < 0.05$ ) and HGb compared to HGm  $p < 0.05$ ); significantly higher expression of *MAP2* in HGb compared to LGG (FC > 146;  $p < 0.05$ ) and HGb compared to HGm  $p < 0.05$ ); significantly higher expression of *TUJ1* in HGb compared to LGG (FC > 2;  $p < 0.05$ ) and HGb compared to HGm  $p < 0.05$ ). These analyses were done after reprogramming so only the successfully reprogrammed lines (as described later) have been characterised for gene expression.

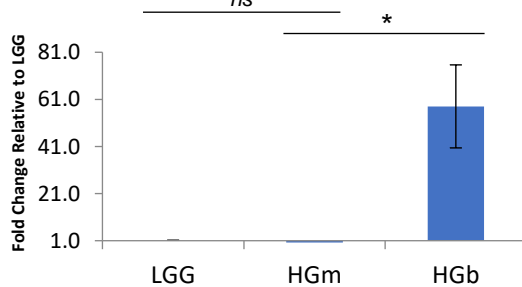
### SOX2



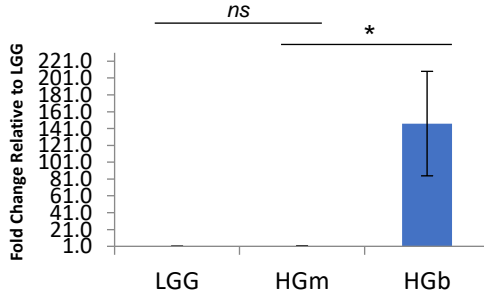
### NESTIN



### Ki67



### MAP2



### TUJ1

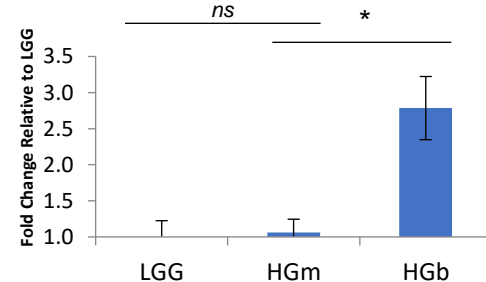
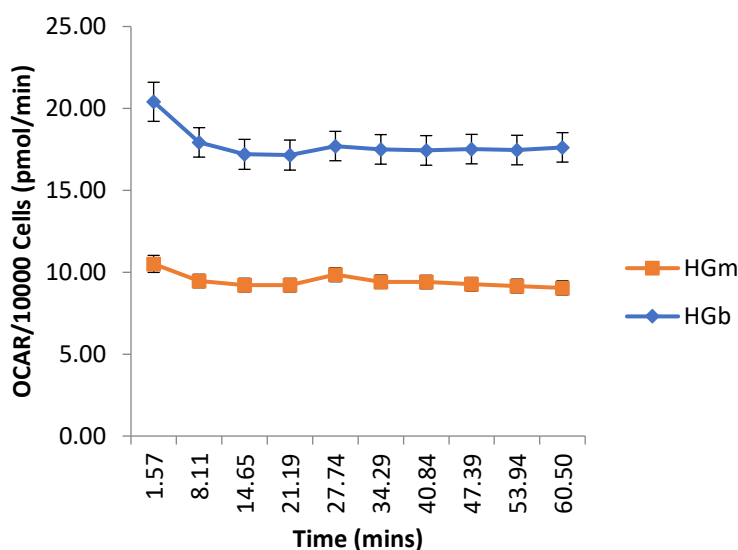


**Figure 2.4:** qRT-PCR analyses of the successfully reprogrammed HGG lines (non-contrast-enhancing tumour margin – HGm, contrast-enhancing tumour bulk – HGb) and LGG lines. Stemness markers *SOX2* and *NESTIN* showed significantly higher expression in lines derived from the HGG lines (HGb and HGm) compared to LGG. Proliferation marker *Ki67* and central nervous system markers *MAP2* and *TUJ1* all showed significantly higher expression in the HGb line compared to the LGG and HGm lines. (3 technical replicates per line; mean  $\pm$  SD; Student's t-test;  $P \leq 0.05$  were presented as \*;  $P \leq 0.01$  as \*\*,  $P \leq 0.001$  as \*\*\* and  $P \leq 0.0001$  as \*\*\*\*).

The Seahorse Bioanalyser detects rapid changes to the concentrations of dissolved oxygen and free protons caused by respiration and glycolysis, respectively. These are measured by solid state probes in a transient microchamber where cells are seeded. After the rate of change becomes linear, the slope is determined and OCR and ECAR calculated. Baseline metabolism is restored when the probe is lifted following a measurement and the larger volume media above the probe is allowed to mix with the media in the transient microchamber. Previous work from our group (Kuchler *et al.* (50)) performing similar analysis on neural progenitor cells and immortalised patient-derived GBM lines shows a difference in both OCR and ECAR between cell types. If the sampled lines are phenotypically different, it would be expected that the contrast-enhancing HGG tumour bulk lines (HGb and HGb2) would exhibit a higher rate of metabolism than non-contrast-enhancing tumour margin lines (HGm and HGm2). Results are presented as rate per  $1 \times 10^4$  cells in order to adjust for initial seeding numbers and growth rates during incubation. HGb lines show a 2-fold increase in the level of oxygen consumption when compared to HGm, whilst HGb2 lines show a near 3-fold increase in oxygen consumption when compared to HGm2, respectively (Figure 2.5). Lactate production is also increased in both tumour bulk lines (HGb and HGb2), when compared to tumour margin cell lines (HGm and HGm2) (Figure 2.6). In all analyses, the differences are preserved across 60 minutes. The differences in OCR and ECAR infer that the tumour bulk cells (HGb and HGb2) are more metabolically active than the tumour margin cells (HGm and HGm2).

## HGm v HGb OCR/10000 Cells



## HGm2 v HGb2 OCR/10000 Cells

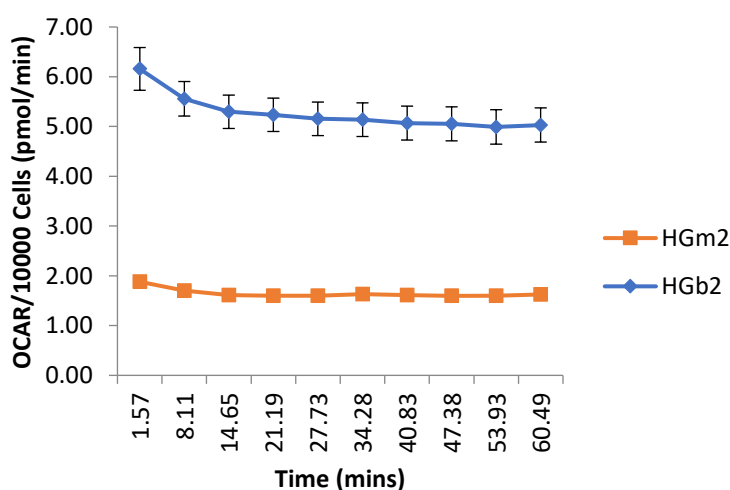
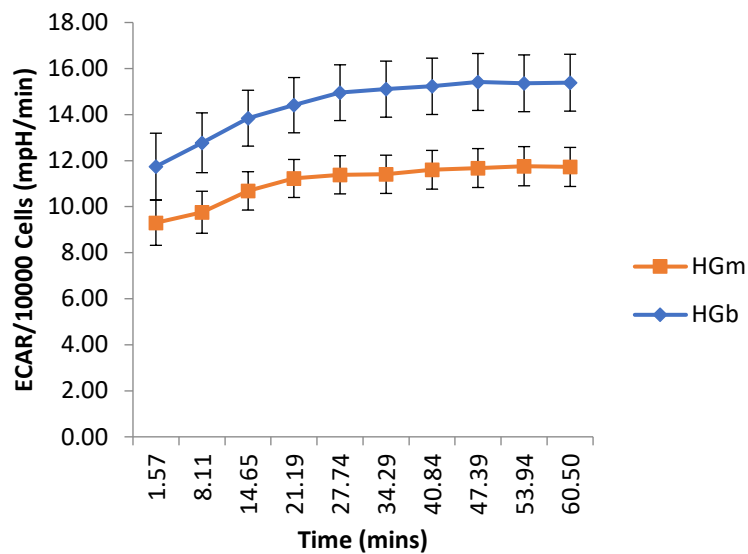


**Figure 2.5:** Metabolic analysis (Seahorse Bioanalyzer) of oxygen consumption rate (OCR) between HGG contrast-enhancing tumour bulk (HGb and HGb2) and non-contrast-enhancing tumour margin cell lines (HGm and HGm2). Cells were counted after the end of the analysis in order to calculate a final average rate per  $1 \times 10^4$  cells. A 2-fold increase in OCR is observed in HGb cells compared to HGm. A near 3-fold increase in OCR is observed in HGb2 cells compared to HGm2. In both analyses, differences are preserved over 60 minutes. These findings infer that metabolism is greater in tumour bulk cells (HGb and HGb2) compared to tumour margin cells (HGm and HGm2). Biological triplicates; mean  $\pm$  SD.

## HGm v HGb ECAR/10000 Cells



## HGm2 v HGb2 ECAR/10000 Cells

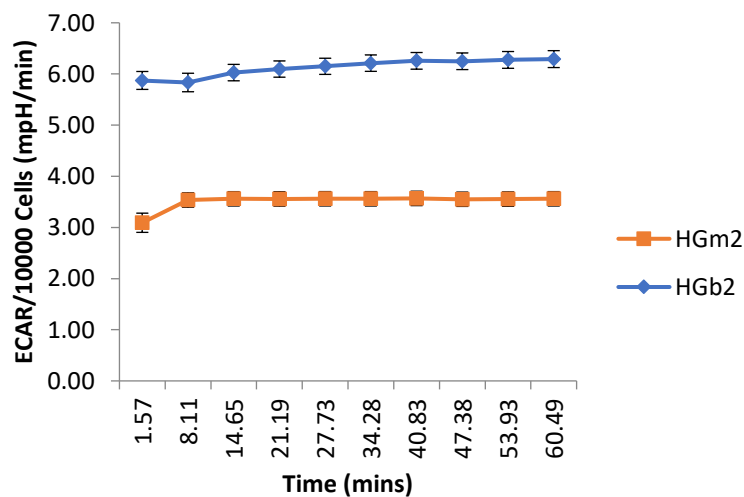


**Figure 2.6:** Metabolic analysis (Seahorse Bioanalyzer) of extracellular acidification rate (ECAR) between HGG contrast-enhancing tumour bulk (HGb and HGb2) and non-contrast-enhancing tumour margin cell lines (HGm and HGm2). Cells were counted after the end of the analysis in order to calculate a final average rate per  $1 \times 10^4$  cells. An increase in ECAR is observed in both tumour bulk lines (HGb and HGb2) compared to tumour margin lines (HGm and HGm2). In HGb2 cells, this increase is 2-fold. In both analyses, differences are preserved over 60 minutes. These findings infer that lactate production is greater in tumour bulk cells (HGb and HGb2) compared to tumour margin cells (HGm and HGm2), and therefore these cells are more metabolically active than tumour margin cells. Biological triplicates; mean  $\pm$  SD.

Sendai virus (SeV) has been used to reprogram many different cell types (185). However, there are no publications to date that describe reprogramming of primary glioma tissue using this method. In order to ensure the HGG and LGG samples were amenable to reprogramming by Sendai virus, a fluorescent control vector carrying the Emerald Green Fluorescent Protein (EmGFP) was transduced into the primary cells (Cytotune EmGFP Sendai Fluorescence Reporter, Life Technologies). EmGFP expression is detectable at 24 hours but reaches maximal levels at 48-72 hours post-transduction.

All lines transduced with EmGFP Sendai Virus Reporter showed positive staining at 72 hours (Figures 2.7-2. 9). Cell cytotoxicity, as demonstrated by cell rounding and detachment, was observed in all lines. This is to be expected with Sendai virus transduction and is a marker of successful transduction (229). These results suggested that the primary cell lines could be transduced successfully with SeV carrying reprogramming factors but do not infer any feasibility or efficiency of reprogramming itself.

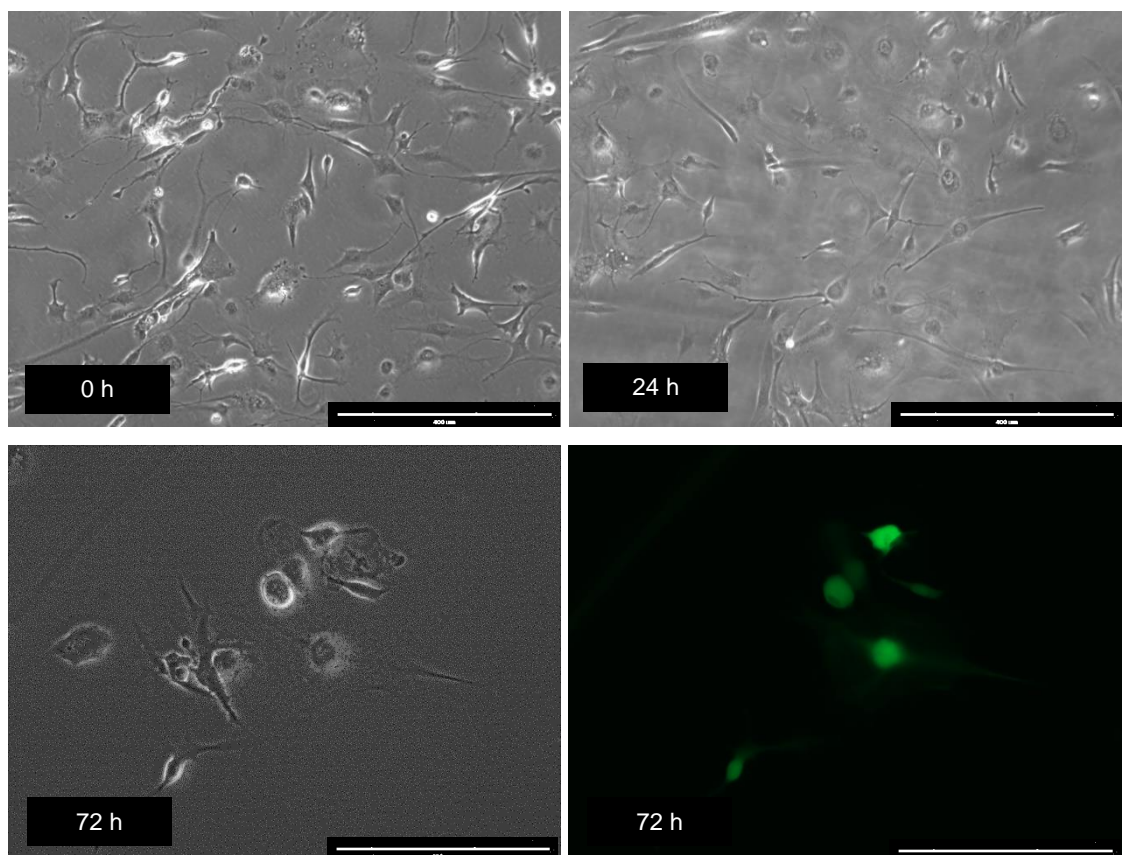


**Figure 2.7:** HGb (p3) EmGFP at time of transduction (0 h), 24 hours and 72 hours post-transduction (x10 magnification). Phase contrast images show cell cytotoxicity after 72

hours, which is to be expected. Immunofluorescence shows that all cells seen in the phase contrast image have been transduced with SeV.

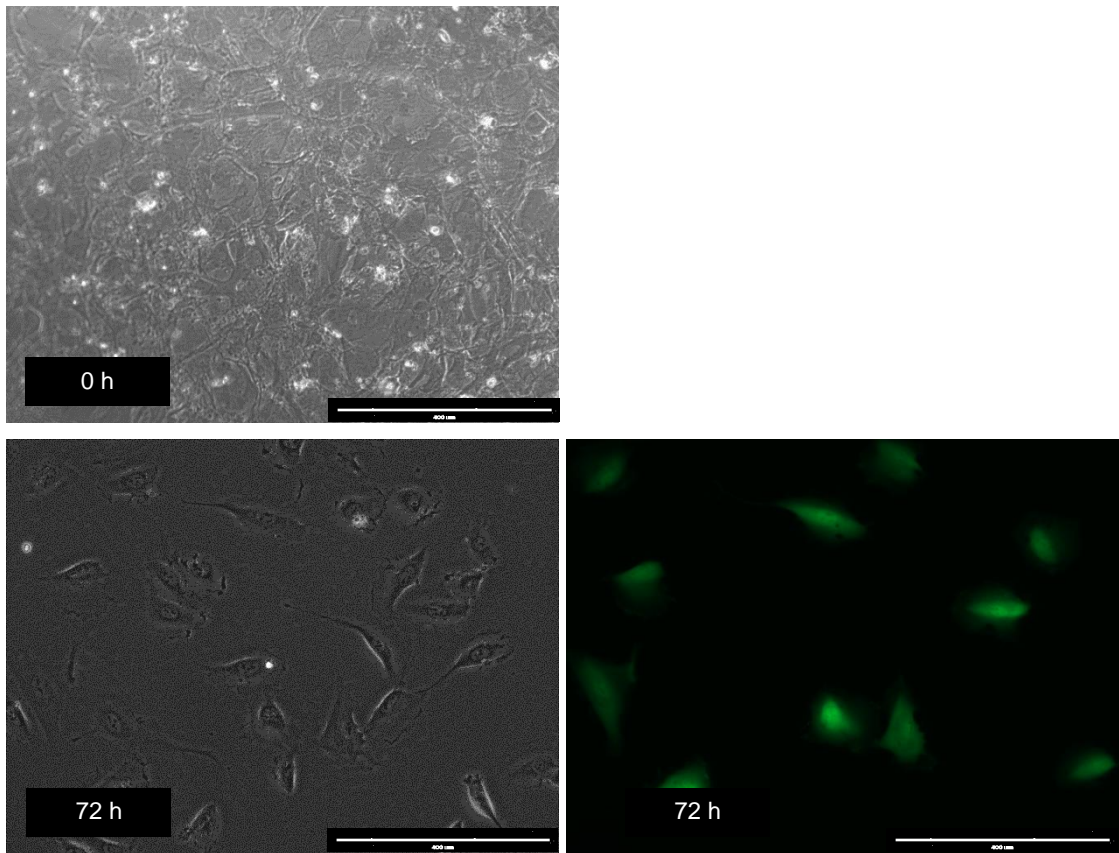


**Figure 2.8:** LGG (p0) EmGFP at time of transduction (0 h), 24 hours and 72 hours post-transduction (x10 magnification). Phase contrast images show cell cytotoxicity after 72 hours, which is to be expected. Immunofluorescence shows that all cells seen in the phase contrast image have been transduced with SeV.

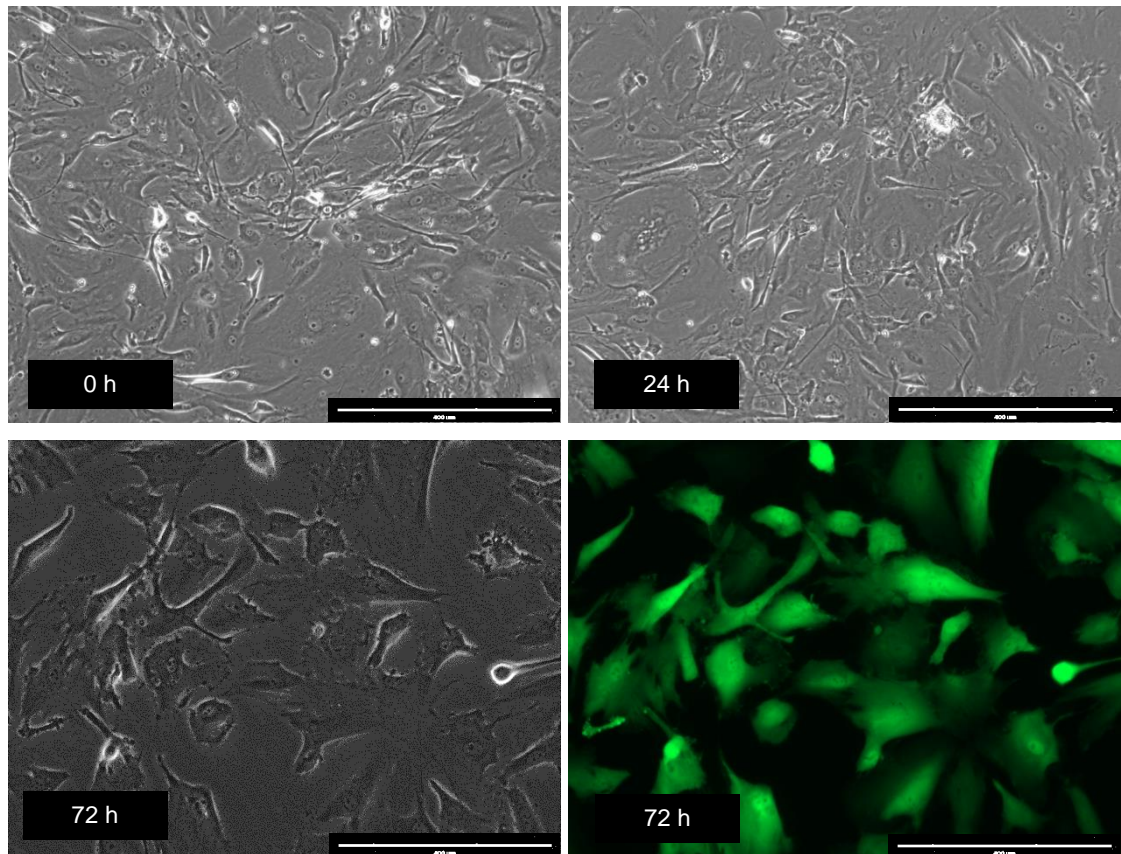


**Figure 2.9:** HGm (p3) EmGFP at time of transduction (0 h), 24 hours and 72 hours post-transduction (x10 magnification). Phase contrast images show cell cytotoxicity after 72 hours, which is to be expected. Immunofluorescence shows that all cells seen in the phase contrast image have been transduced with SeV.

#### **2.1.1.2. Glioma iPSCs show stem cell morphology**

Due to the relative technical ease of somatic cell reprogramming, and availability of reprogramming vectors (including in kit form), there has been a considerable increase in the number of iPSCs being derived and associated publications related to cellular reprogramming (230). There have been attempts therefore to come up with 'gold standard' criteria for newly derived iPSCs to adhere. These are outlined in Table 3 (adapted from (1)):

Issue	Potential Solution	Appropriate Testing Methods
<b>Cell line identity</b>	Early and frequent identity testing	STR analysis SNP analysis Genomic sequencing
<b>Genomic instability</b>	Karyotyping	G-banding Chromosomal microarray Nanostring technology
<b>Pluripotency</b>	Pluripotency testing	Marker expression analysis Embryoid body (EB) analysis Teratoma assays
<b>Residual reprogramming factors</b>	Rigorous molecular detection or alternative reprogramming approaches	PCR analysis RNA or chemical based reprogramming

**Table 3:** Issues, solutions and appropriate testing methods proposed in order to improve the quality of iPSCs derived (adapted from Yaffe *et al.* (1)).

The most basic characterisation of iPSCs is to observe morphological features that are seen in ESCs (231). Inverted light microscopy of iPSCs on mouse embryonic feeder (MEF)-culture derived from all primary cell lines reprogrammed with Sendai virus demonstrated classical morphology seen in ESCs (and so-called *bona fide* iPSCs) – round, densely packed colonies with tight borders, flat, cobblestone appearance, high nuclei/cytoplasm ratio and prominent nucleoli (232) (Figures 2.10-2.14). Multiple colonies demonstrating similar morphology have been observed for each reprogrammed line passaged thus far.

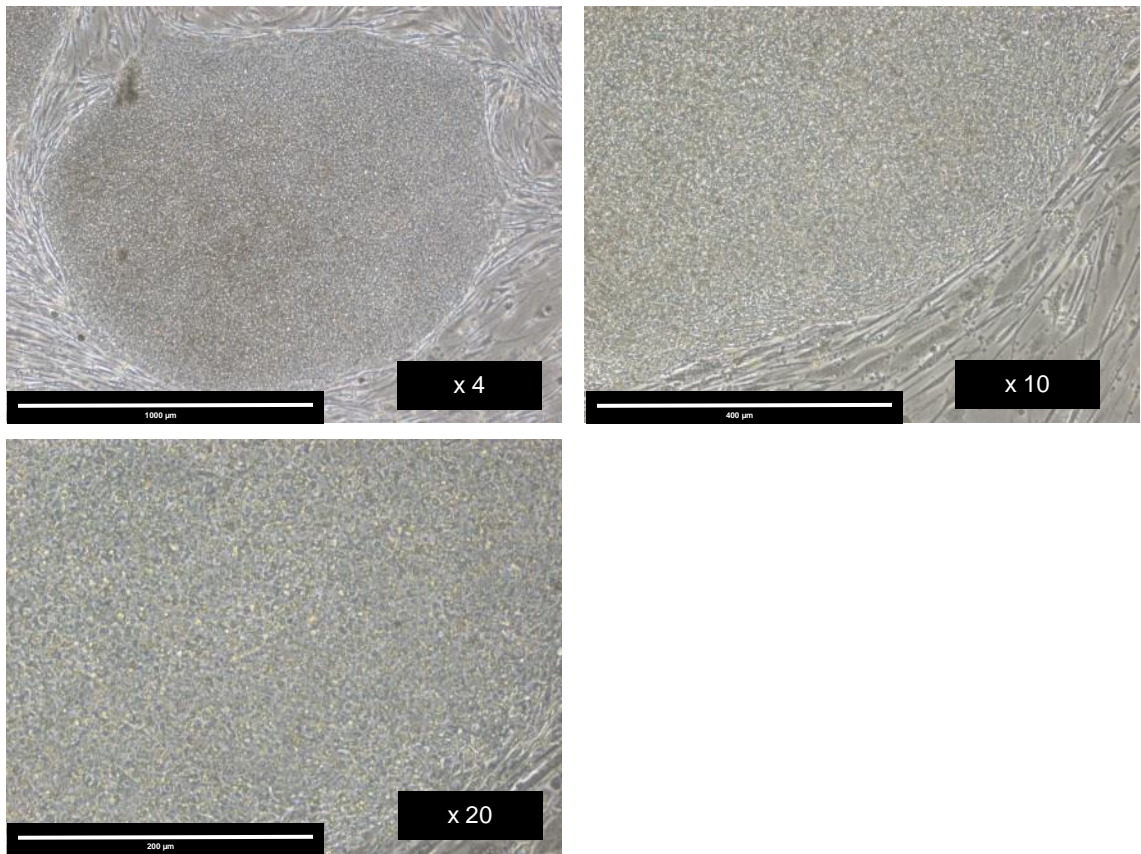


**Figure 2.10:** induced pluripotent stem cells (iPSCs) derived from reprogrammed low-grade glioma (LGG) cells transduced with SeV, passage 6, on mouse embryonic feeder (MEF) culture. Light microscopy shows classical embryonic stem cell (ESC) morphological features – round, densely packed colonies with tight borders, flat, cobblestone appearance, high nuclei/cytoplasm ratio and prominent nucleoli (x4, x10, x20 magnification).

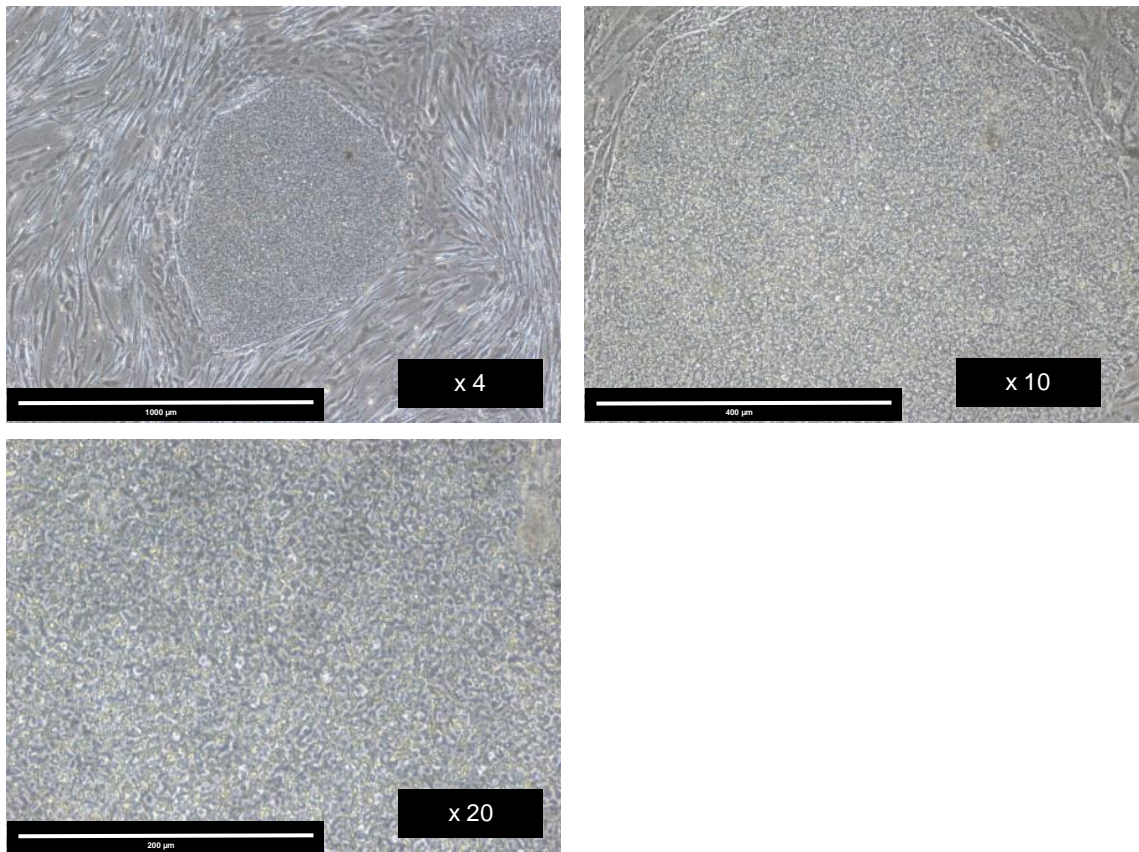


**Figure 2.11:** induced pluripotent stem cells (iPSCs) derived from reprogrammed non-contrast-enhancing HGG tumour margin (HGm) cells transduced with SeV, passage 3, on mouse embryonic feeder (MEF) culture. Light microscopy shows classical embryonic stem cell (ESC) morphological features – round, densely packed colonies with tight borders, flat, cobblestone appearance, high nuclei/cytoplasm ratio and prominent nucleoli (x4, x10, x20 magnification).

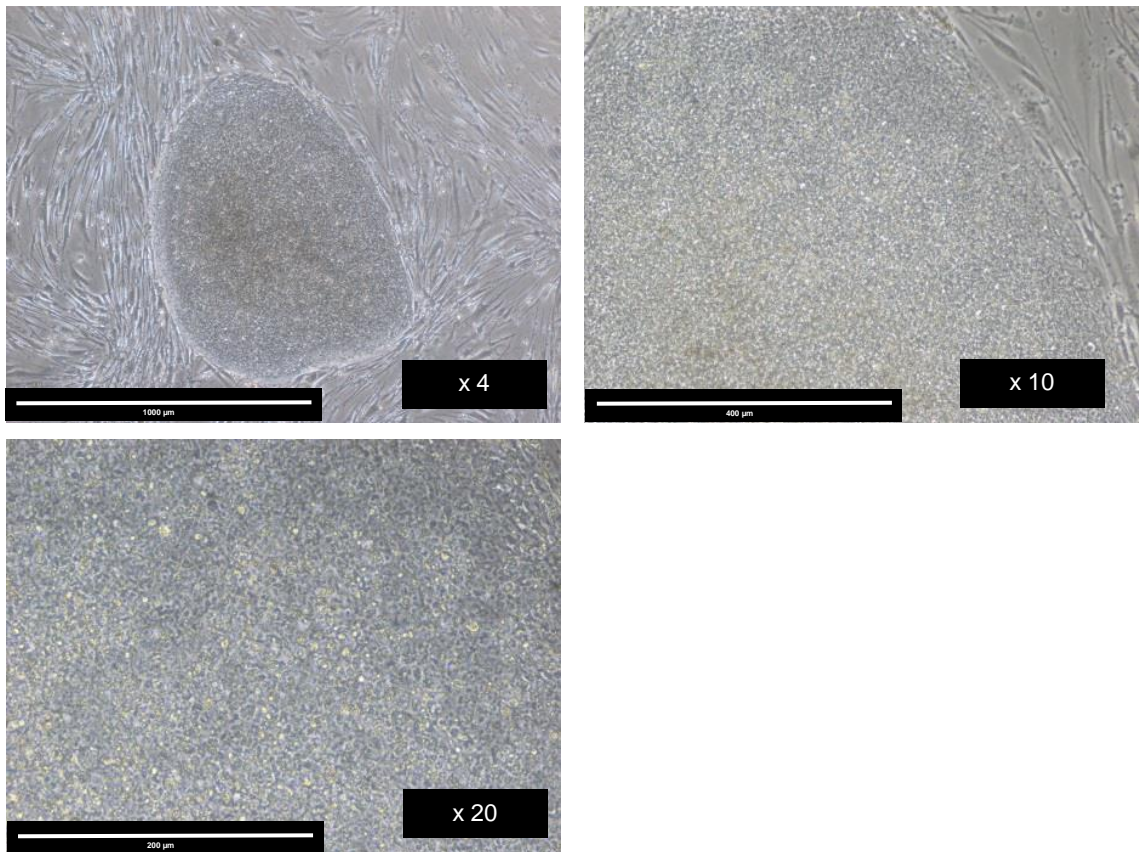


**Figure 2.12:** induced pluripotent stem cells (iPSCs) derived from contrast-enhancing HGG tumour bulk (HGb) cells transduced with SeV, passage 3, on mouse embryonic feeder (MEF) culture. Light microscopy shows classical embryonic stem cell (ESC) morphological features - round, densely packed colonies with tight borders, flat, cobblestone appearance, high nuclei/cytoplasm ratio and prominent nucleoli (x4, x10, x20 magnification).

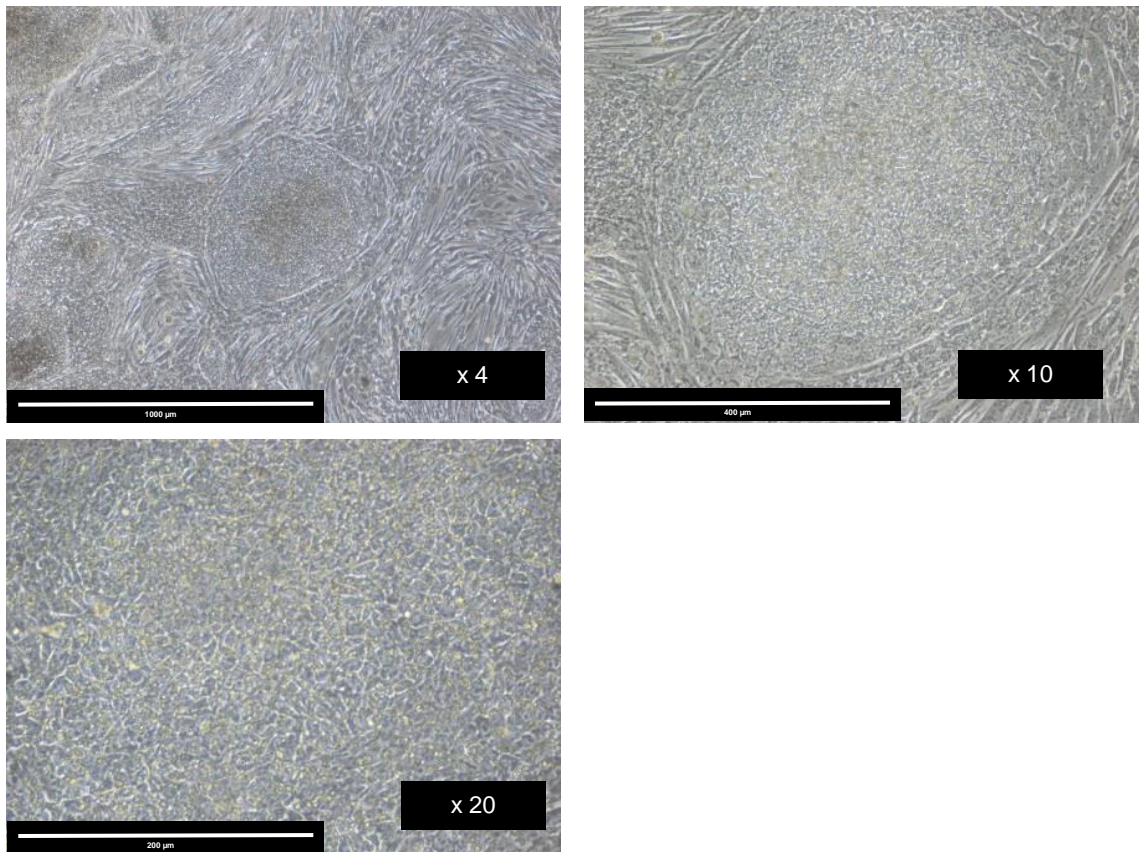


**Figure 2.13:** induced pluripotent stem cells (iPSCs) derived from non-contrast enhancing HGG tumour margin (HGm2) cells transduced with SeV, passage 5, on mouse embryonic feeder (MEF) culture. Light microscopy shows classical embryonic stem cell (ESC) morphological features - round, densely packed colonies with tight borders, flat, cobblestone appearance, high nuclei/cytoplasm ratio and prominent nucleoli (x4, x10, x20 magnification).

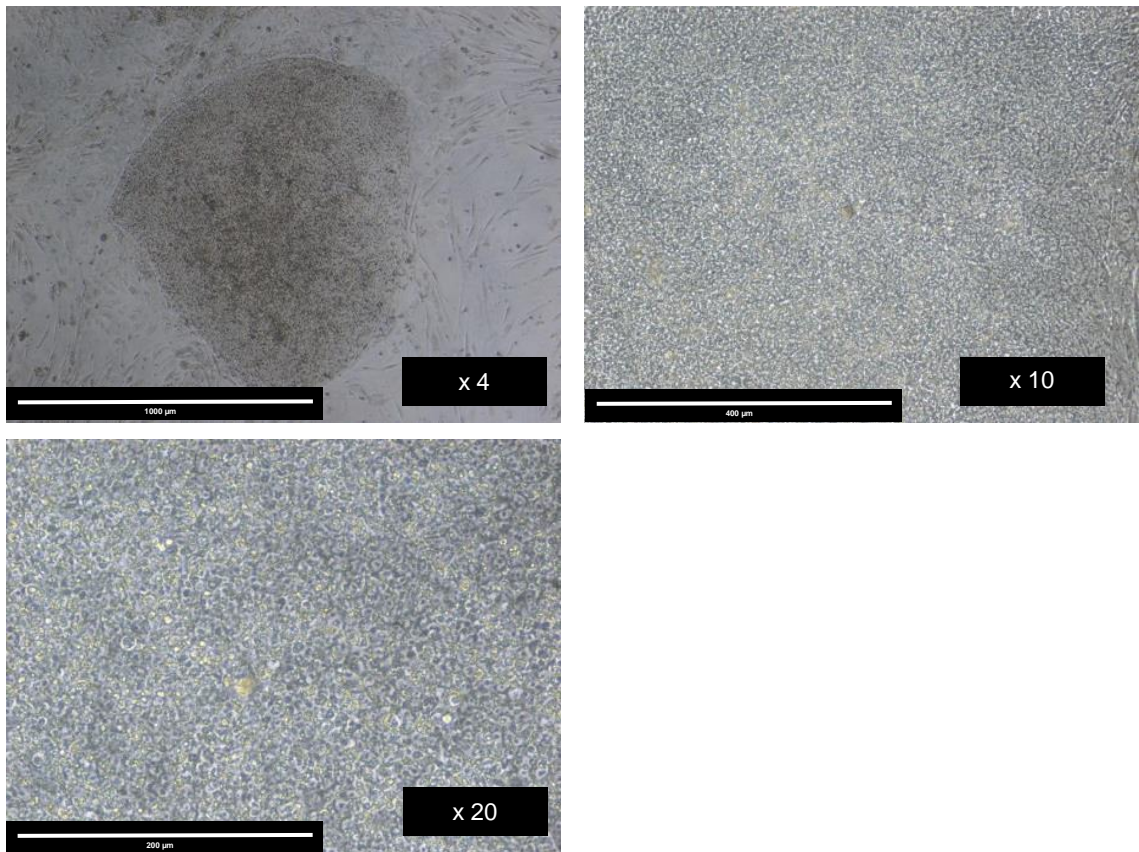


**Figure 2.14:** induced pluripotent stem cells (iPSCs) derived from contrast-enhancing HGG tumour bulk (HGb2) cells transduced with SeV, passage 4, on mouse embryonic feeder (MEF) culture. Light microscopy shows classical embryonic stem cell (ESC) morphological features - round, densely packed colonies with tight borders, flat, cobblestone appearance, high nuclei/cytoplasm ratio and prominent nucleoli (x4, x10, x20 magnification).

### 2.1.1.3. Glioma iPSCs express markers of pluripotency

Terato-related-antigen-1-60 (Tra-1-60) has been shown to be a stem cell specific surface marker (183). It has been mapped to carbohydrate epitopes found on the 200KDa form of podocalyxin, a surface glycoprotein found on stem cells and embryonic carcinomas. Live cell Tra-1-60 staining allows real-time assessment of cells undergoing reprogramming, without loss of viability (232). This means that colonies can be monitored and picked for expansion at the optimum time, when cells are observed to be fully reprogrammed and consequently should be at their most pluripotent. Other positive pluripotent stem cell markers that could be used in live culture are Tra-1-81 and stage-specific embryonic antigen 4 (SSEA4) (231). However, Tra-1-60 is thought to represent the most rigorous surface cell marker amenable to live cell staining as it is upregulated later on during reprogramming (232). Phase contrast microscopy showed multiple colonies in reprogrammed cell lines that demonstrated typical stem cell morphology (round, flat, cobblestone appearance with tightly packed cells). Live cell staining helped distinguish fully reprogrammed colonies from only partially reprogrammed colonies (Figures 2.15-2.17), enabling only the former to be picked and expanded. Partially reprogrammed colonies were left in culture and stained again after a few days.

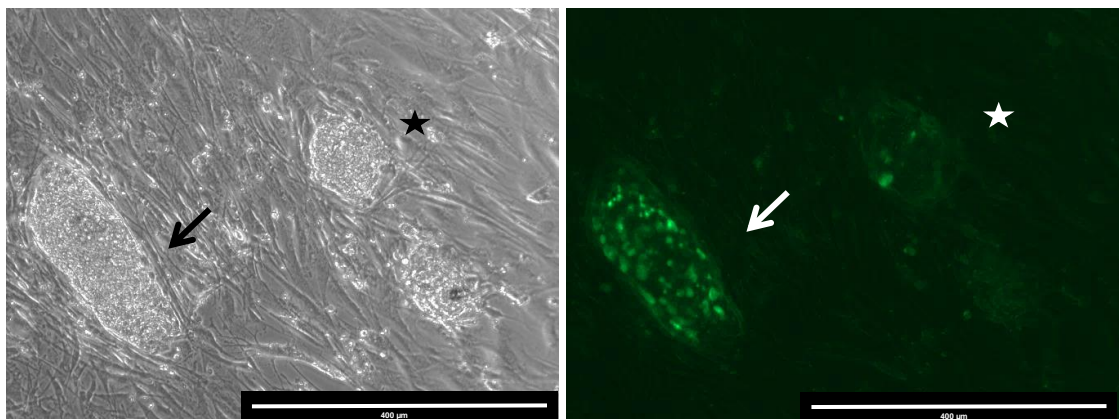


**Figure 2.15:** Non-contrast-enhancing HGG tumour margin (HGm) colonies undergoing reprogramming, live cell immunostained for Tra-1-60. Phase contrast imaging shows 2 colonies with morphological features representative of ESCs (round, flat, cobblestone appearance with tightly packed cells) but Tra-1-60 staining shows that only the colony on the left (marked with an arrow) is likely to be fully reprogrammed, whereas the one on the right (marked with a star) is likely to be only partially reprogrammed (x10 magnification).

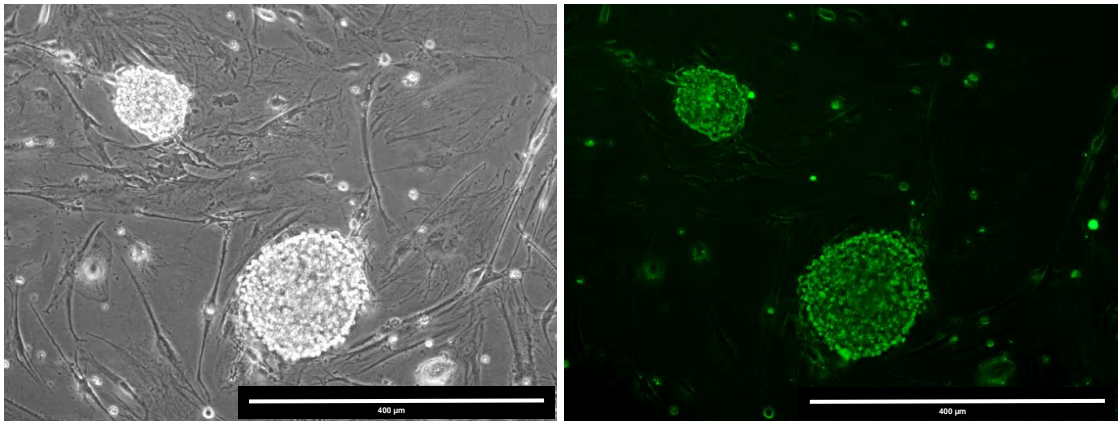


**Figure 2.16:** Contrast-enhancing HGG tumour bulk (HGb2) colonies undergoing reprogramming, live cell immunostained for Tra-1-60. Phase contrast imaging shows 2 colonies with distinct ESC morphology (round, flat, cobblestone appearance with tightly packed cells). Tra-1-60 positive staining in both colonies is consistent with full reprogramming (x10 magnification). These colonies were picked and expanded.

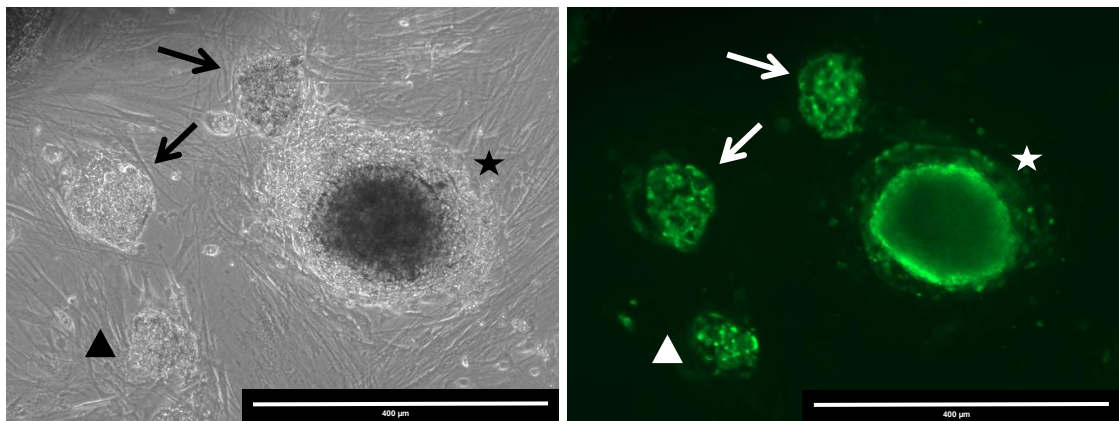


**Figure 2.17:** LGG tumour (LGG) colonies undergoing reprogramming, live cell immunostained for Tra-1-60. Phase contrast imaging shows 3 colonies (marked with two arrows and a triangle) with distinct ESC morphology (round, flat, cobblestone appearance with tightly packed cells). The largest colony (marked with a star shows signs of differentiation in the middle and was not expanded. This colony was scraped off under sterile conditions, to minimise the risk of differentiation of other neighbouring colonies. It is unclear if the colony marked with a triangle has fully reprogrammed and so was not picked and expanded at this stage. Tra-1-60 positive staining in both colonies marked with white arrows is consistent with full reprogramming (x10 magnification). These colonies were picked and expanded.

On expansion, HGb2 and HGM2 did not survive beyond passage 4 and passage 6, respectively. Therefore, only results for iPSCs derived from primary cells of

contrast-enhancing HGG tumour margin (HGm), contrast-enhancing HGG tumour bulk (HGb) and LGG cells will be presented and discussed from here forth.

The transcription factors OCT4 and SOX2 are well-established as key to maintaining pluripotency via self-renewal (177). These are both intracellular proteins and so require fixation and permeabilisation. SSEA4 is a cell surface marker found on pluripotent stem cells that usually represents lineage-restricted patterns of expression during development (233).

Fixed cell immunostaining of iPSCs derived from HGm, HGb and LGG on feeder-free culture using antibodies against SOX2, Tra-1-60, SSEA4 and OCT4 show consistent expression of all four pluripotent stem cell markers across all the iPSC lines (Figure 2.18).

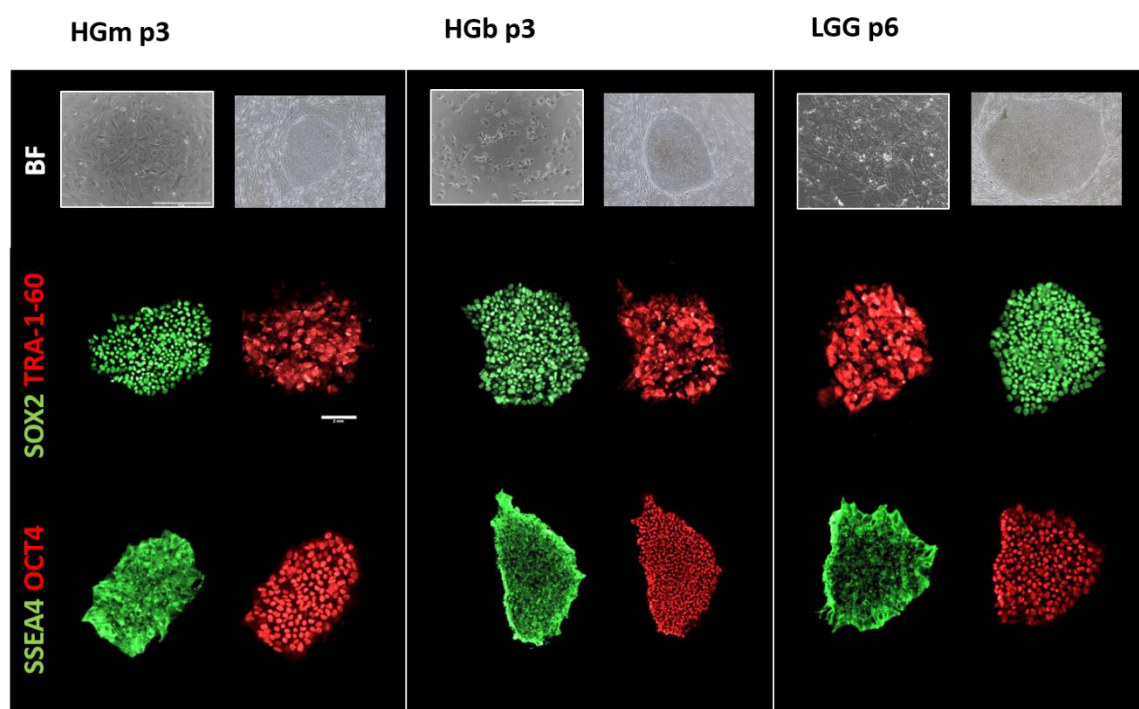


**Figure 2.18:** Brightfield representative images of HGm, HGb and LGG primary culture, and derived iPSC colonies on mouse embryonic feeder (MEF) culture. Confocal representative images of iPSCs derived from HGm, HGb and LGG on feeder-free culture after undergoing fixed cell immunostaining. Consistent expression of intracellular pluripotent stem cell markers OCT4 and SOX2, and surface markers of pluripotency Tra-

1-60 and SSEA4 (all false colours) are demonstrated across all glioma-derived iPSC lines.

Flow cytometry analysis of the iPSC lines derived from HGm, HGb and LGG showed a significantly larger fraction of cells were positive for pluripotency markers SSEA4 ( $P \leq 0.0001$  in all lines), EpCam ( $P \leq 0.0001$  in all lines), Tra-1-60 ( $P \leq 0.0001$  in HGb,  $P \leq 0.001$  in HGm and LGG), whereas only a very small percentage of cells were positive for SSEA1 (mean  $< 4\%$  in all lines), which is a marker that is usually absent from human iPSCs and indicates loss of pluripotency (118) (Figure 2.19).

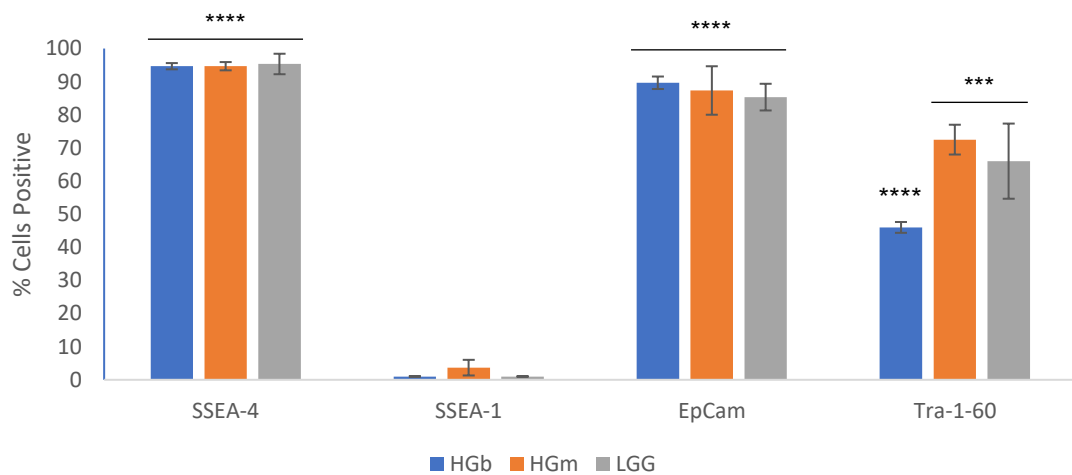
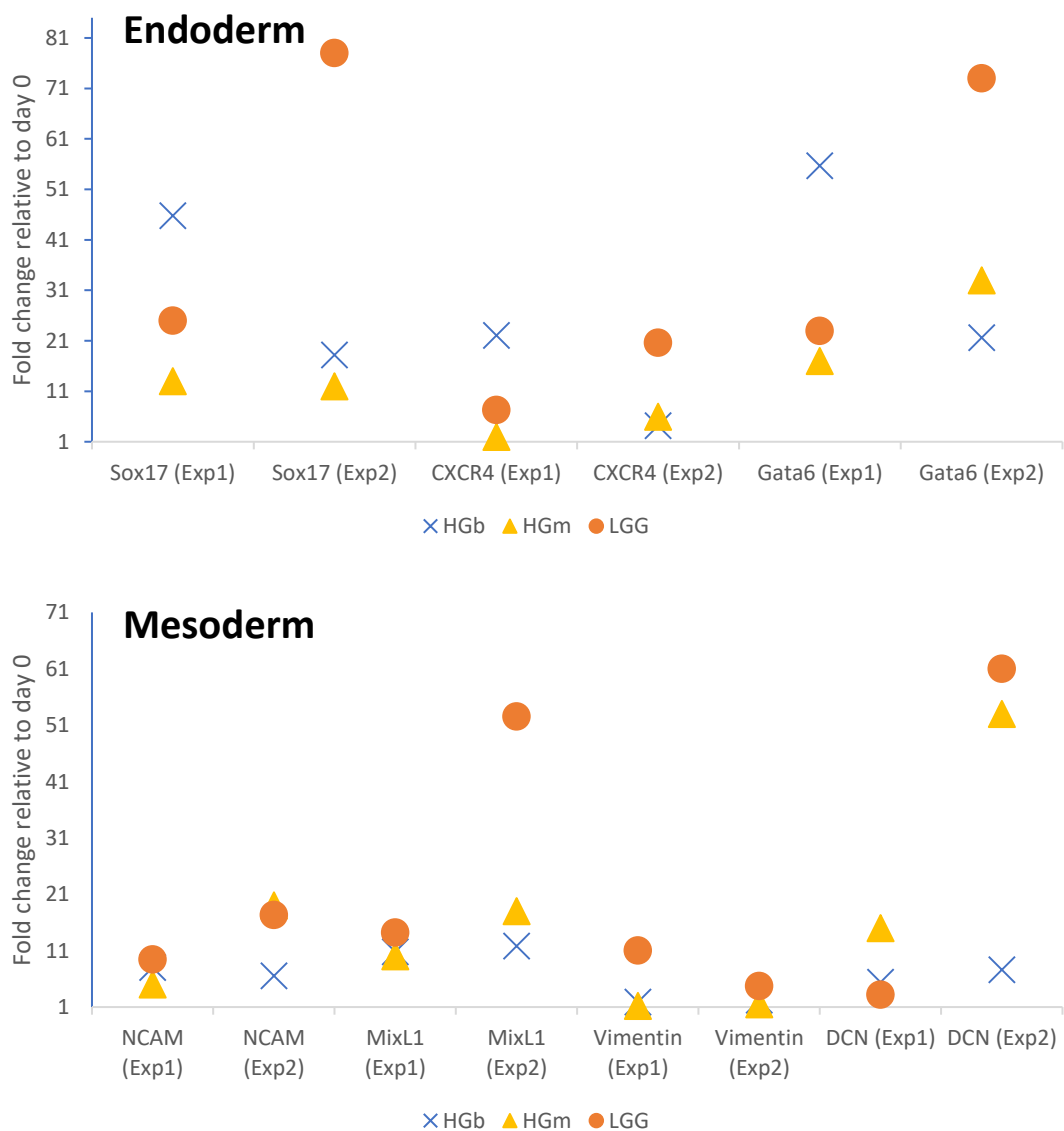


**Figure 2.19:** Flow cytometry conducted in all 3 iPSC lines derived from HGm, HGb and LGG cells showed a large fraction of cells positive for pluripotency markers SSEA4 ( $P \leq 0.0001$  in all lines), EpCam ( $P \leq 0.0001$  in all lines), Tra-1-60 ( $P \leq 0.0001$  in HGb,  $P \leq 0.001$  in HGm and LGG) whereas only a low percentage of cells were positive for SSEA-1 (mean  $< 4\%$  in all lines), a negative marker of pluripotency (3 independent experiments with at least a passage between each experiment; mean  $\pm$  SD; Student's t-test;  $P \leq 0.05$  were presented as \*,  $P \leq 0.01$  as \*\*,  $P \leq 0.001$  as \*\*\* and  $P \leq 0.0001$  as \*\*\*\*).

#### 2.1.1.4. Glioma iPSCs can differentiate into all 3 germinal layers

The glioma iPSCs derived from HGm, HGb and LGG underwent spontaneous embryoid body differentiation in ultra-low attachment U-bottom 96-well plates to investigate their ability to form all 3 germinal layers. Withdrawing bFGF from the human stem cell medium enables spontaneous differentiation (234). The resultant EBs were collected for RNA extraction. Gene expression analysis by

qRT-PCR showed that iPSCs derived from contrast-enhancing HGG tumour bulk (HGb), non-contrast-enhancing HGG tumour margin (HGm), and LGG tumour have the capacity to produce each germ layer (endoderm, mesoderm and ectoderm) as demonstrated by increased expression of germ layer specific markers (endoderm – *SOX17*, *CXCR4*, *GATA6*; mesoderm – *NCAM*, *MixL1*, *Vimentin*, *DCN*; ectoderm – *PAX6*, *NEUROD1*, *Hes5*) and concomitant reduced expression of pluripotency markers (*OCT4*, *NANOG*) (Figure 2.20). Pluripotency was further quantified by gene expression analysis by mRNA-seq as described later.



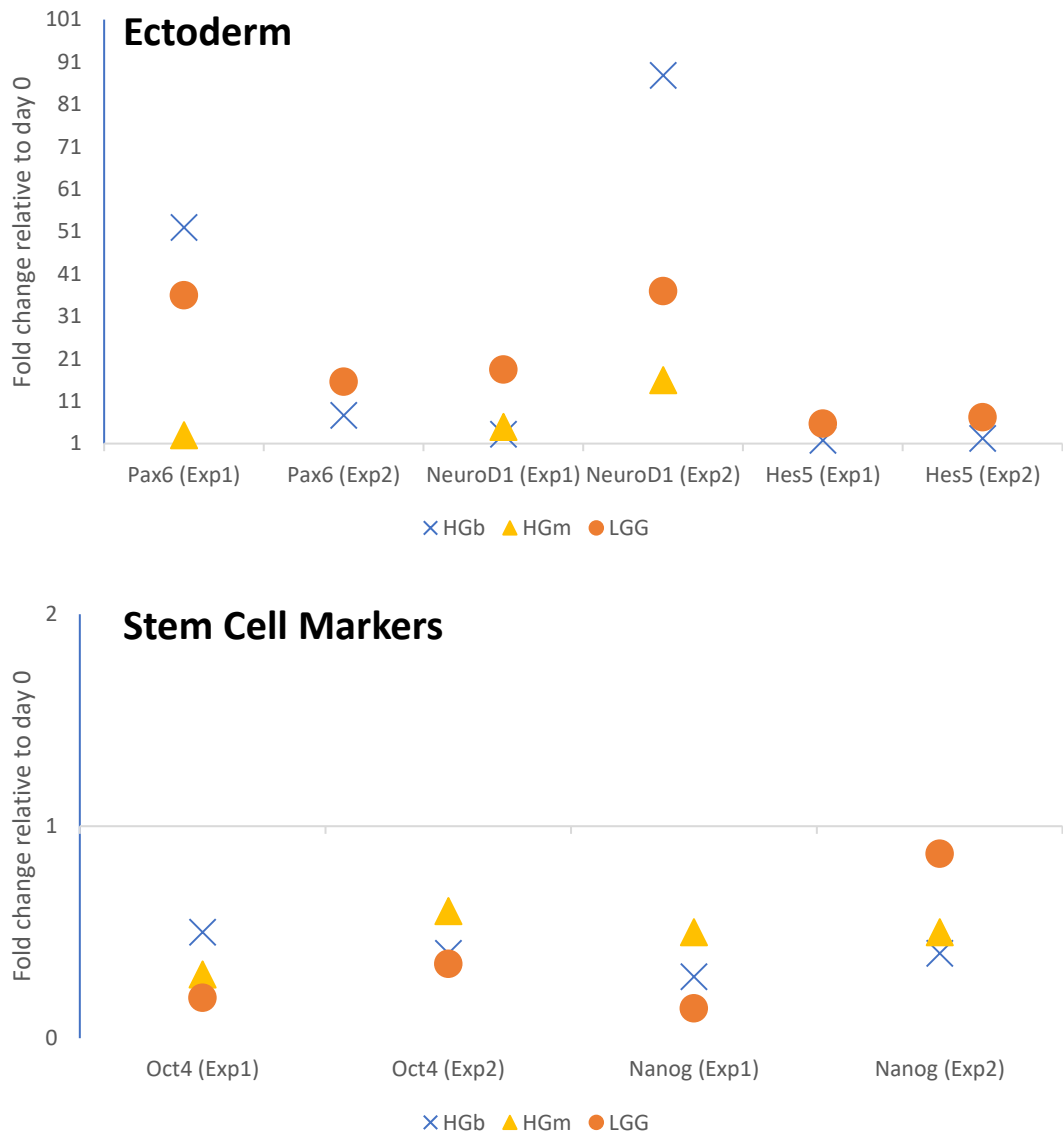


**Figure 2.20:** Spontaneous differentiation by embryoid body formation shows iPSC lines derived from HGm, HGb and LGG have the capacity to produce each germ layer (endoderm, mesoderm and ectoderm) as demonstrated by increased expression of germ layer specific markers and concomitant reduced expression of pluripotency markers (*OCT4*, *NANOG*) (each point (Exp1, Exp2) represents an independent experiment with at least a passage between each experiment).

#### 2.1.1.5. Glioma iPSCs express pluripotency-driving genes

A previous study, performed to test the equivalence between human ESCs and human iPSCs derived from fibroblasts donated by healthy donors, has generated a stem cell reference set (GSE73211), which also included the healthy fibroblasts (235). Using the same analysis methodology and reference set as that study and another similar study (236), the gene expression profiles of the glioma iPSCs derived herein (HGm, HGb, LGG) and a control iPSC (derived from fibroblasts

donated by a healthy individual and gifted by the UK Stem Cell Bank) were compared. This gene expression analysis showed that the glioma iPSCs in this study had higher overall expression of pluripotency markers, which compared favourably with the healthy iPSCs and ESCs, with which they clustered (Figure 2.21). Native fibroblasts (i.e. not reprogrammed) had higher overall expression of most mesoderm markers and lower expression of pluripotency markers. Gene expression profiles of the fibroblasts did not cluster with the glioma iPSCs, control iPSC and reference set stem cells (GSE73211).

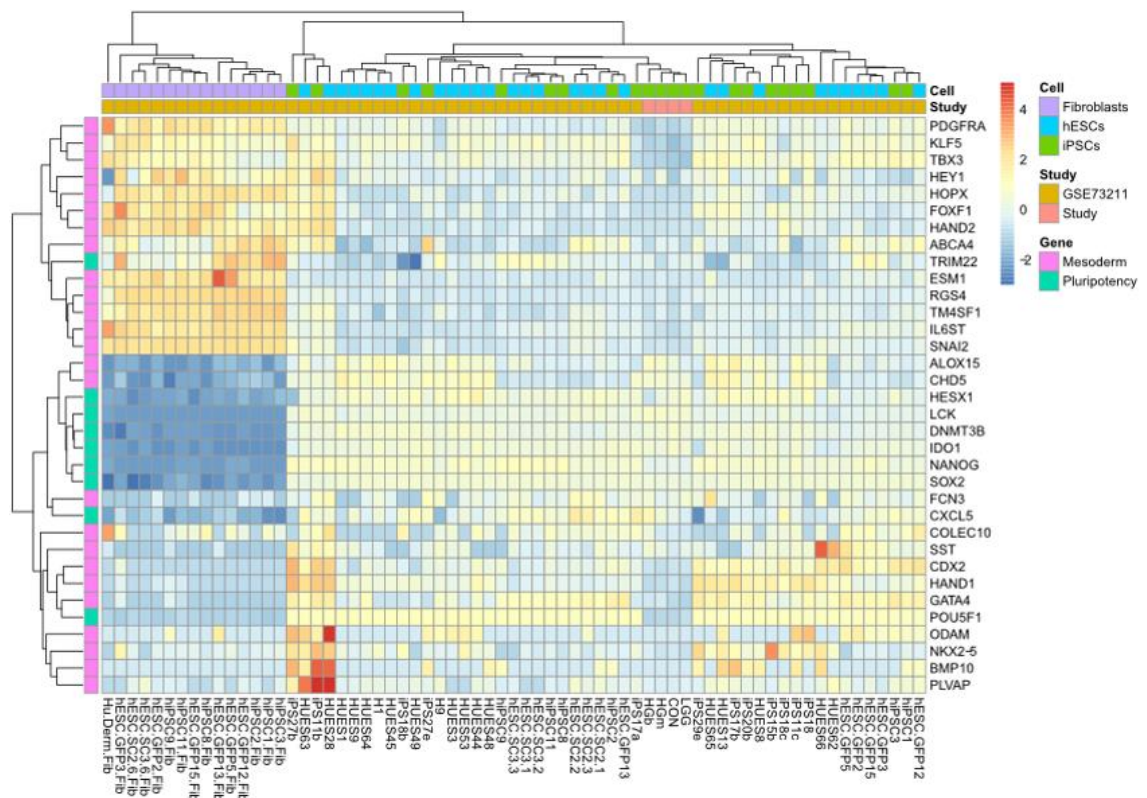


**Figure 2.21:** Heatmap and hierarchical clustering showing normalised expression levels (Z scores derived from VST expression levels) of nine pluripotency (blue) (237–239) and 25 mesoderm (pink) (240) marker genes in the 4 study iPSCs (3 glioma iPSCs HGm, HGb, LGG and 1 control iPSC derived from fibroblasts donated by a healthy individual, CON) and 62 human cell lines (15 fibroblasts, 17 iPSC, and 30 ESC) obtained from GEO: GSE73211 (241). Samples are colour coded to show whether they are glioma iPSCs (pink) or from GEO: GSE73211 (brown), and on the basis of line type (purple for fibroblasts, blue for hESCs and green for hiPSCs). The heatmap shows that glioma iPSCs cluster with the reference iPSCs and hESCs, which both show higher overall expression of pluripotency genes than fibroblasts, which show higher expression of most

mesoderm markers and lower expression of pluripotency markers than the hiPSC and hESC lines (including the glioma iPSC lines).

#### **2.1.1.6. Glioma iPSCs have confirmed cell identity and show genomic stability through unaltered karyotype**

In order to ensure there had been no mislabelling between the derived iPSCs during the reprogramming process and multiple passages, all the glioma iPSCs were tested by short tandem repeat (STR) analysis. This confirmed a match between the parent sample and its derived iPSC line, with the obvious caveat being that the HGm and HGb lines could not be distinguished (in iPSCs or primary cells) since they were from the same patient. However, WGS was performed at a later date, which confirmed a match between each iPSC line and the primary cells from which they were derived.

In order to ensure that reprogramming had not altered the chromosomal structural integrity of the derived iPSCs, the glioma iPSCs underwent karyotype analysis by comparative genomic hybridisation (CGH) array. Karyotype reports for all 3 glioma iPSC lines showed no gross structural abnormality. A representative example of a CGH array karyotyping report is shown in Figure 2.22.



**North East Thames Regional Genetics Laboratory**

Great Ormond Street Hospital for Children NHS Foundation Trust  
Levels 5 & 6 Barclay House, 37 Queen Square, London WC1N



Director: Lucy Jenkins FRCPATH  
Head of Service (Cytogenetics): Jonathan Waters PhD FRCPATH  
Head of Service (Molecular Genetics): Sam Loughlin DipRCPATH  
Telephone: 020 7829 8870; Fax: 020 7813 8578; Email: Genetics.Labs@gosh.nhs.uk

\*\*\*\* The following results have been amended \*\*\*\*

Dr O O'Shea	<b>Cell Pellet Identifier:</b>	LGG
UK Stem Cell Bank		
National Institute for Biological Standards and Control		
Blanche Lane		
Potters Bar	<b>Your reference:</b>	
	<b>Postcode:</b>	
EN6 3QG	<b>Request Date:</b>	12-May-2016
	<b>Sample Collected:</b>	Unknown
	<b>Sample Type:</b>	Cell Pellet

**GENETICS LABORATORY REPORT**

<b>Date of Report:</b>	17-June-2016	<b>Lab Number:</b>	16G07995
<b>Clinical Details (As stated on request form):</b>			
Cell Pellet from Stem Cell Culture: ?gross chromosomal changes			

**RESULT - NO SIGNIFICANT ABNORMALITY**

**Microarray Result**

Genome wide array analysis indicated that there was no evidence of any copy number change involving a chromosomal region greater than 3Mb in size.

**Authorised by:** Jonathan Waters PhD FRCPATH, Consultant Clinical Scientist

WLU: 2.25/RES/D/X

<p><b>Array used:</b> Affymetrix 750K (Oligonucleotide Positions based on HG19): Array resolution varies according to clinical importance of the chromosome region. Estimated average resolution 3Mb.</p> <p><b>Analysis Software used:</b> infoQuant Fusion v6</p> <p><b>Limitations:</b> Microarray analysis does not detect balanced rearrangements and may not detect mosaicism</p> <p>Note: The technique used to generate this result is not currently included in the laboratory ISO15189 schedule of accreditation.</p>
---

\*\*\*\* End of Amendment \*\*\*\*

Report Printed: 17/06/2016 1:55 Page 1 of 1

**Figure 2.22:** Representative comparative genomic hybridisation (CGH) array karyotyping report from the analysis of the iPSC line derived from LGG primary cells. The report confirms no significant structural abnormality in a chromosomal region greater than 3Mb in size.

Mycoplasma can affect the characteristics and function of iPSCs and can produce spurious experimental results through altered karyotype (242). It is therefore

important to check all cells in culture. All primary and iPSC cell lines tested were negative for mycoplasma.

#### 2.1.1.7. Patient-derived glioma iPSCs retain no residual reprogramming vectors

In order to confirm the clearance of the viral vectors that carry the reprogramming factors and thus confirm lack of residual exogenous factor expression, SeV vector clearance was confirmed by qRT-PCR using a primer (TaqMan Mr04269880\_mr) that binds to the common backbone of the SeV that is used to deliver all of the factors. It is expected that SeV will be cleared between 5-15 passages after reprogramming (185). Analysis of all the lines reprogrammed (HGb, HGm, LGG) showed no evidence of residual SeV at passage 13 (Figure 2.23).

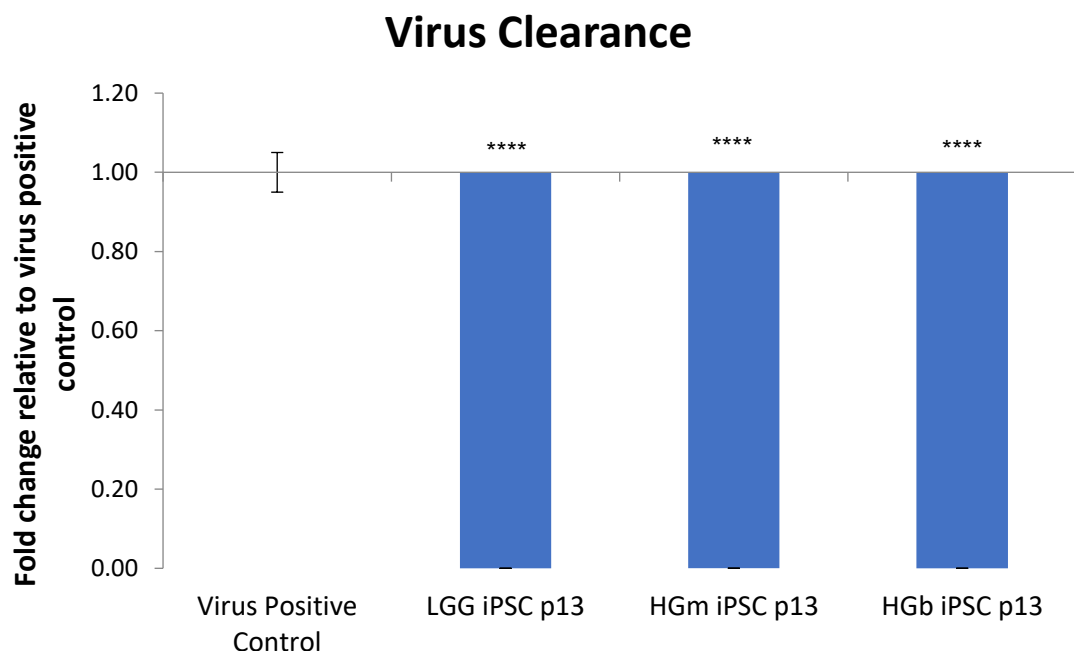


**Figure 2.23:** qRT-PCR analysis shows no evidence of residual Sendai virus polycistronic reprogramming vectors in any of the glioma-derived iPSCs at passage 13 (3 biological replicates per line; mean  $\pm$  SD; Student's t-test;  $P \leq 0.05$  were presented as \*,  $P \leq 0.01$  as \*\*,  $P \leq 0.001$  as \*\*\* and  $P \leq 0.0001$  as \*\*\*\*).

### **2.1.2. Glioma iPSCs show tumorigenic capacity *in vivo***

As outlined previously, the ability to form tumours *in vivo* has been considered a key characteristic of GSCs (93,243). It can be argued therefore that any new *in vitro* models developed to either replace or complement current *in vivo* models would be more useful if they could recapitulate this characteristic. However, these models are iPSCs and therefore likely to form teratomas *in vivo* if directly orthotopically xenografted into immunodeficient mice - as evidenced by their ability to form all 3 embryonic germ layers during spontaneous differentiation. Therefore, the iPSCs were differentiated using a proprietary neural stem cell (NSC) induction kit (Thermo Fisher Scientific). Immunocytochemistry was used to confirm marker expression consistent with NSCs – SOX2 positive, NESTIN positive and OCT4 negative. NSCs derived from each iPSC line (HGb, HGm and LGG) were orthotopically xenografted into the right striatum of 6- to 10-week old NSG mice ( $1 \times 10^5$  cells per line per mouse; 6 mice per line). Interim imaging by small animal magnetic resonance imaging (MRI) was performed. Mice were sacrificed at 16 weeks, brains harvested and analysed by immunocytochemistry.

MRI images showed tumours were formed from all the injected lines. Tumours formed from the HGb-derived NSCs were poorly demarcated, infiltrative and extended across the midline into the contralateral hemisphere (Figure 2.24a). Migration and invasion across the midline is considered a pathological hallmark of GBM (50). Tumours formed from the HGm-derived NSCs were well demarcated, infiltrative and interestingly, did not cross the midline into the contralateral hemisphere (Figure 2.25a). Perhaps even more interestingly, tumours formed from the LGG-derived NSCs (Figure 2.26a) were more similar in appearance to the HGb mice – poorly demarcated, infiltrative and crossed the midline into the contralateral hemisphere.

Sections through the tumours immunostained with antibodies to NESTIN and Ki67 showed diffuse infiltration in all lines. This was most extensive in the HGb mice (Figure 2.24b), extensive in the HGm mice (but less so than in the HGb mice) (Figure 2.25b) and more localised in the LGG mice (Figure 2.26b).

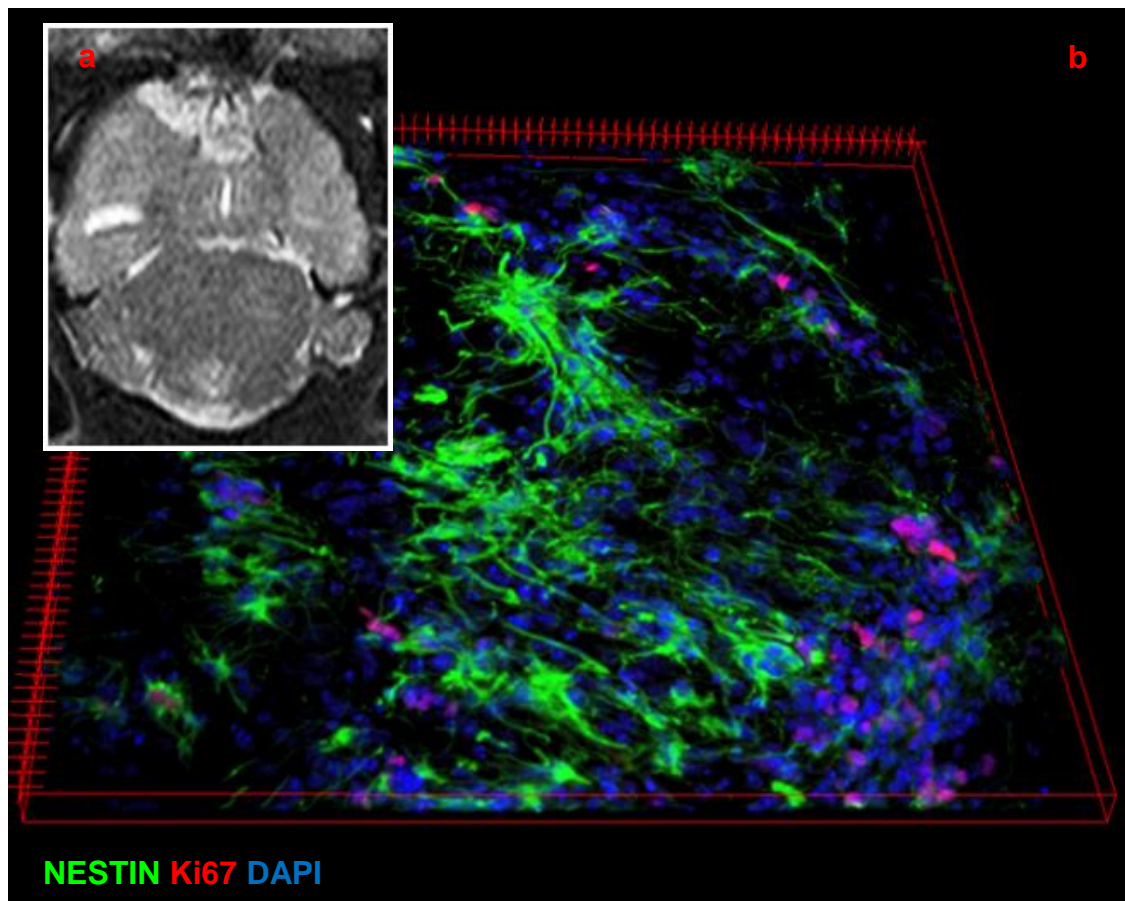


**Figure 2.24:** (a) Representative magnetic resonance image (MRI) 15 weeks after orthotopic xenotransplantation into immunodeficient NSG mice of  $1 \times 10^5$  neural stem cells (SOX2/NESTIN positive, OCT4 negative) derived from HGb iPSCs ( $n = 6$ ). T2-weighted image shows poorly demarcated, infiltrative right frontal tumour causing midline shift and extension across the midline into the contralateral hemisphere. (b) Representative confocal microscopy image of section through mouse brain with intracranial tumour immunostained with antibodies to NESTIN, Ki67 and DAPI nuclear counter-stain. Extensive, diffuse infiltration of tumour is seen throughout the mouse brain with evidence of increased proliferation.

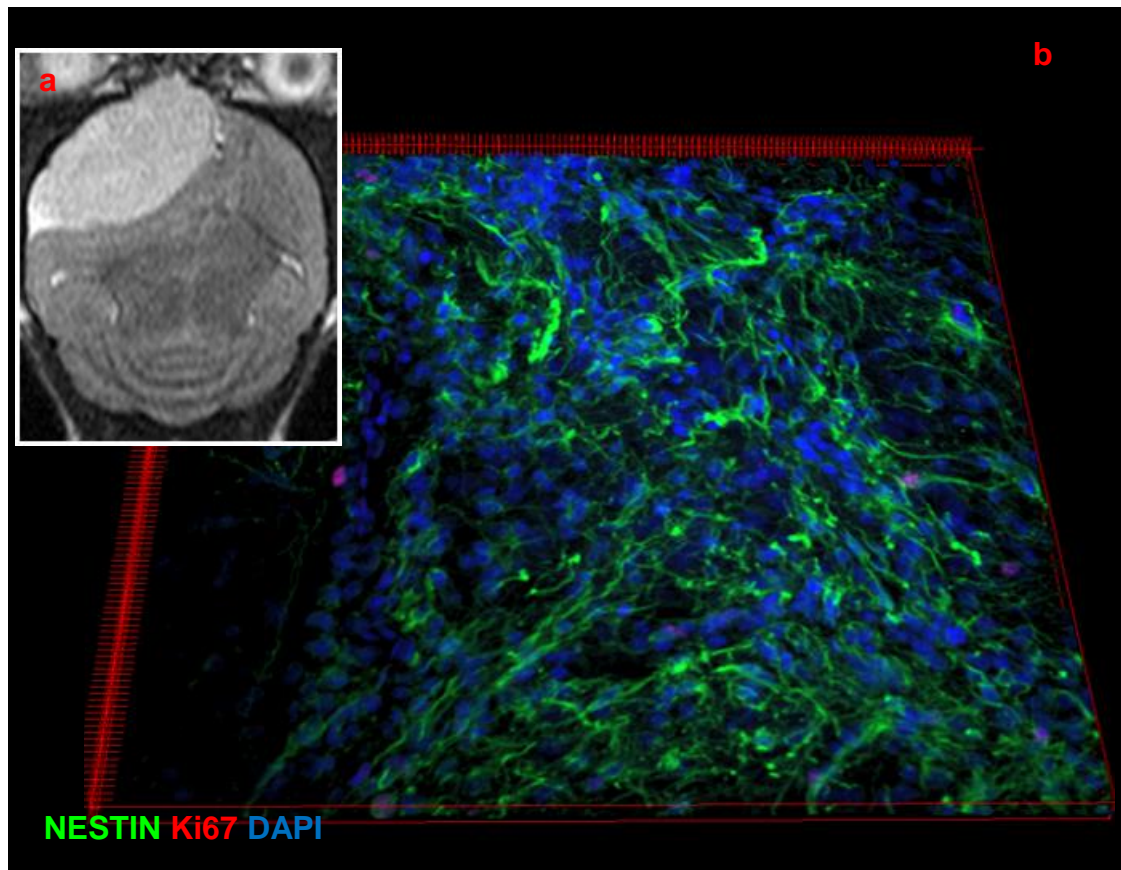


**Figure 2.25:** **(a)** Representative magnetic resonance image (MRI) 16 weeks after orthotopic xenotransplantation into immunodeficient NSG mice of  $1 \times 10^5$  neural stem cells (SOX2/NESTIN positive, OCT4 negative) derived from HGm iPSCs ( $n = 6$ ). T2-weighted image shows large right well demarcated right frontal tumour causing significant midline shift. There is no extension across the midline into the contralateral hemisphere. **(b)** Representative confocal microscopy image of section through mouse brain with intracranial tumour immunostained with antibodies to NESTIN, Ki67 and DAPI nuclear counter-stain. Diffuse infiltration of tumour is seen throughout the mouse brain with some minor evidence of increased proliferation.

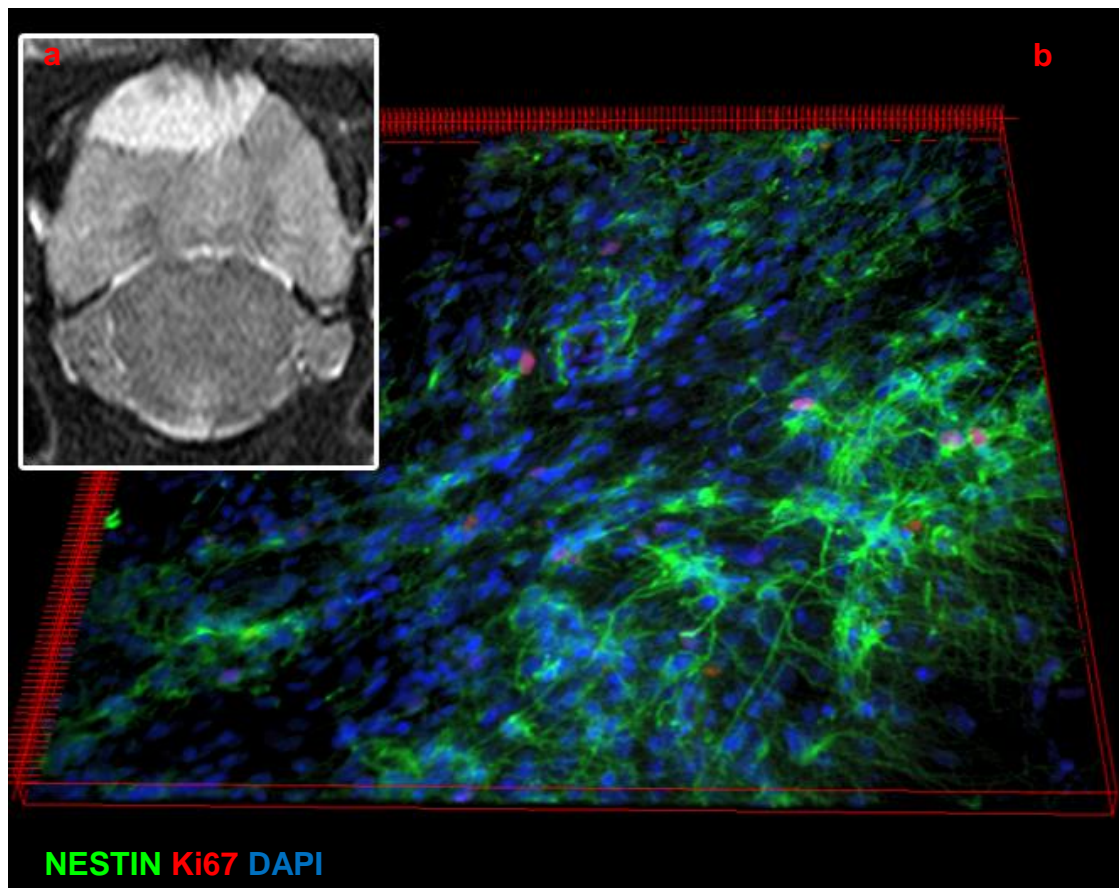


**Figure 2.26:** (a) Representative magnetic resonance image (MRI) 16 weeks after orthotopic xenotransplantation into immunodeficient NSG mice of  $1 \times 10^5$  neural stem cells (SOX2/NESTIN positive, OCT4 negative) derived from LGG iPSCs ( $n = 6$ ). T2-weighted image shows large right poorly demarcated right frontal tumour causing midline shift and extension across the midline into the contralateral hemisphere. (b) Representative confocal microscopy image of section through mouse brain with intracranial tumour immunostained with antibodies to NESTIN, Ki67 and DAPI nuclear counter-stain. More localised infiltration of tumour is seen throughout the mouse brain with some minor evidence of increased proliferation.

### 2.1.3. Patient-derived glioma iPSCs retain genetic mutations of parental tissue

Evaluation at karyotypic level has already been discussed earlier. Subkaryotypic genomic analysis consists of assessing total number of copies, copy number variation (CNV), single nucleotide polymorphisms (SNPs) and loss of heterozygosity (244). Accordingly, deep (90X) whole genome sequencing (WGS) was performed of the parental tumour lines (HGb, HGm, LGG) and the derived iPSCs. Comparative analysis between each primary line and its derived iPSC line

using mutational variant calling so far show that in the contrast-enhancing HGG tumour bulk (HGb) sample, 69% of the total number of copies has been preserved in the iPSC line with a change from 90:10 gains:loss ratio in the primary line to 95:5 gains:loss ratio in the derived iPSC line (Figure 2.27). In the non-contrast-enhancing HGG tumour margin (HGm) sample, 60% of the total number of copies has been preserved in the iPSC line with a change from 90:10 gains:loss ratio in the primary line to 94:6 gains:loss ratio in the derived iPSC line (Figure 2.27). In the LGG sample, 56% of the total number of copies has been preserved in the iPSC line with a change from 97:3 gains:loss ratio in the primary line to 93:7 gains:loss ratio in the derived iPSC line (Figure 2.27).

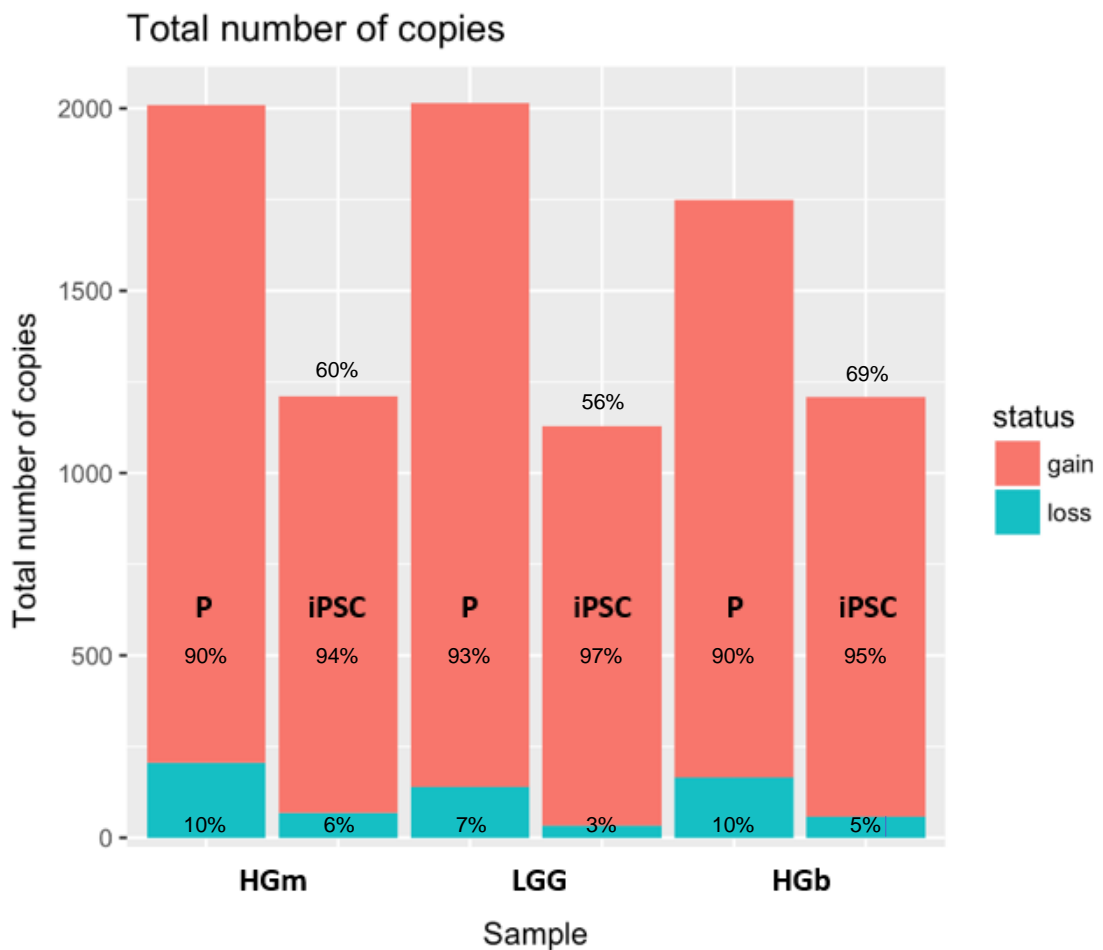


**Figure 2.27:** Deep (90X) whole genome sequencing analysis comparing total number of copies between each primary (P) tissue sample and its respective derived iPSC line. Each derived iPSC line shows a partial preservation of the total number of copies of its parental tumour sample (HGm 60%, LGG 56%, HGb 69%). Changes in the ratios of gains:loss status are also observed between the iPSC lines and their respective parental tumour sample.

With respect to number of CNVs comparative analysis, 52% of CNVs have been preserved in the HGb iPSC line compared to the parental sample with a change from 49:51 gains:loss ratio in the primary line to 56:44 gains:loss ratio in the derived iPSC line (Figure 2.28). In the HGm sample, 49% of CNVs has been preserved with a change from 43:57 gains:loss ratio in the primary line to 52:48 gains:loss ratio in the derived iPSC line (Figure 2.28). In the LGG sample, 44% of CNVs have been preserved with a change from 47:53 gains:loss ratio in the primary line to 59:41 gains:loss ratio in the derived iPSC line (Figure 2.28).

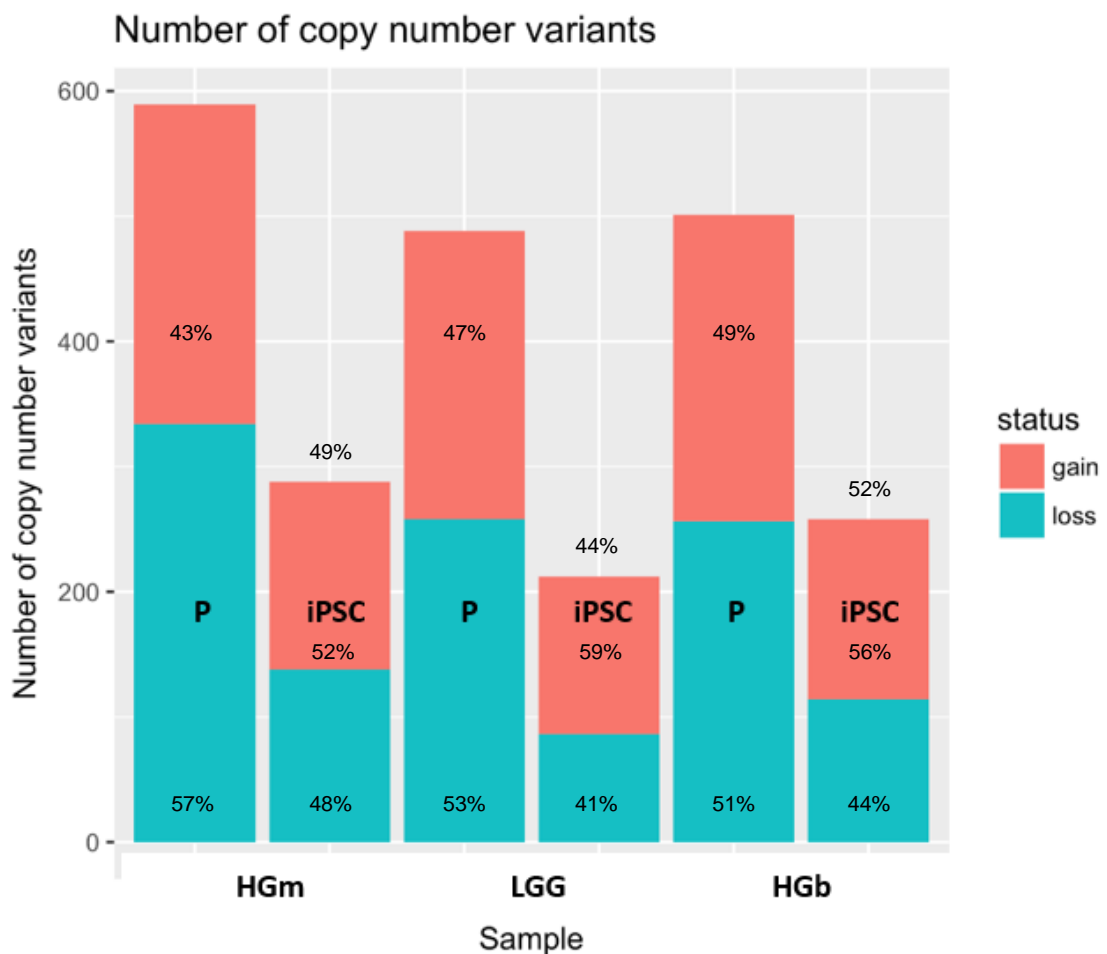


**Figure 2.28:** Deep (90X) whole genome sequencing analysis comparing number of copy number variants (CNVs) and gains:loss status ratios between each primary (P) tissue sample and its respective derived iPSC line. Each derived iPSC line shows a partial preservation of the number of CNVs of its parental tumour sample (HGm 49%, LGG 44%, HGb 52%). Changes in the ratios of gains:loss status are also observed between the iPSC lines and their respective parental tumour sample.

With respect to the so-called ‘hallmark’ mutations of GBM, WGS analysis shows that, when compared to the respective primary line, there has been a loss of mutation of *NF1* in the HGb and HGm derived iPSC lines, and losses of amplifications of *EGFR*, *ROS1*, *PTEN*, *BRAF*, *CDKN2A*, *MET*, *POU3F2* and *RB1* in the HGb iPSC line (Figure 2.29).

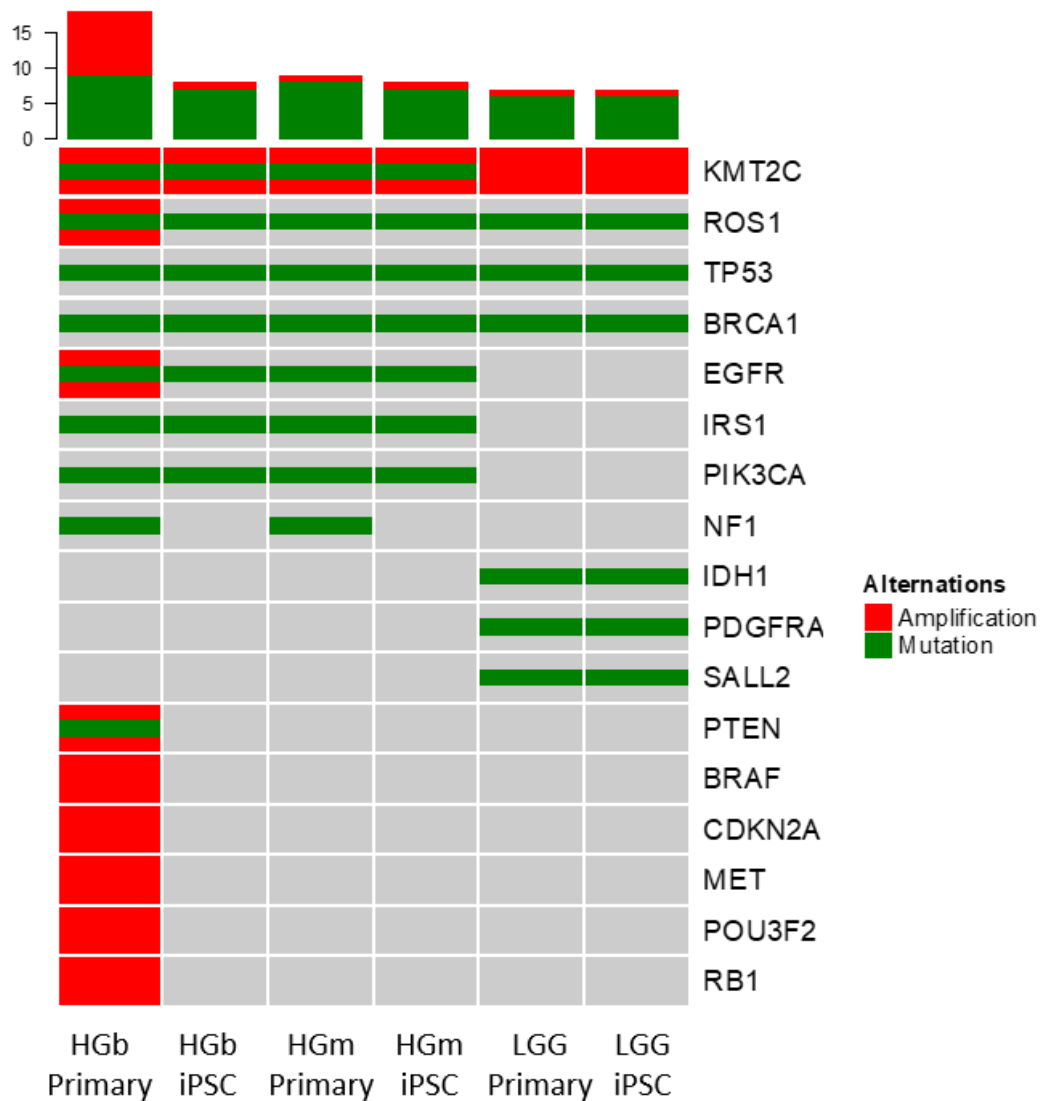


**Figure 2.29:** Deep (90X) whole genome sequencing analysis comparing specific ‘hallmark’ gene abnormalities between each primary (P) tissue sample and its respective derived iPSC line.

## 2.2. Discussion

Gliomas represent the most common malignant primary brain tumour (6). Even with maximal medical and surgical treatment, prognosis remains extremely poor (16). It is clearly a cancer of unmet need (245). New models that aim to study the proposed tumour-initiating subset of stem-like cells could be extremely valuable in understanding underlying drivers of gliomagenesis, resistance to treatment and tumour recurrence. There is much debate about whether brain tumours develop in a hierarchical fashion or not. This only heightens the importance of resolving this question. As outlined earlier, GEMMs have provided some of the best evidence of the CSC hypothesis, but it could be argued that ultimately it is only relevant if this is robustly confirmed in human tumours. Numerous studies using human primary tumour stem-like cells in culture and for xenotransplantation have added to the evidence, but current methodologies use different protocols and standards for enriching and identifying CSCs/GSCs, which means that results are not always comparable (116).

The iPSCs described in this study represent a new set of experimental models to study the stem-like subpopulation in gliomas. The approach that I have used aims to recapitulate the 'stemness' phenotype (selected out by brief serum-free culture) and take advantage of the preservation of genetic mutations after reprogramming that have been observed in numerous examples of disease-relevant iPSC derivation thus far (187); thus facilitating the study of genotype-phenotype relationships.

Characterisation of the primary tissue reveals typical GBM and LGG features such as presence of 'stemness' and higher rate of proliferation in the HGG models, and *IDH1* mutation in the LGG model. SOX2 is a nuclear marker of NSCs and PSCs that is a key transcription factor in maintaining self-renewal in these cell populations (246). Along with NESTIN, SOX2 is considered a key 'stemness' factor in GSCs (247,248). NESTIN is a cytoskeletal marker for NSCs which is expressed during the early development of the CNS that subsequently disappears upon differentiation of NSCs into mature neurons or glial cells (249). NESTIN expression is elevated in both HGG models, compared to the LGG model, inferring an increased 'stemness' phenotype in the HGG models. Ki67 is only expressed in cycling cells and is therefore used commonly as a marker of

proliferation (250). Along with the typical patient features such as age, PFS and OS, the characteristics of the primary cells would appear to make them representative of HGG and LGG tumours, and therefore appropriate to take forward in reprogramming to derive glioma iPSC models.

It is interesting to note the differences in metabolic phenotype between HGb and HGm primary cells inferred by the extracellular flux analysis (Seahorse). The cells from the bulk of the tumour appear more metabolically active than those on the periphery. This is expected as enhancing areas of tumour are considered a higher grade (thus more cancerous), and are therefore purported to acquire capabilities to become self-sufficient in growth, insensitive to anti-growth signals, and more metabolically active (44). Since the HGm cells are sampled from the non-enhancing margin of the tumour, they may be less aggressive than the contrast-enhancing tumour bulk cells (preservation of the BBB minimising contrast enhancement has been associated with lower grade (63)). This is also supported by the reduced expression of SOX2 and Ki67 in the HGm compared to the HGb cells. These findings support the development of these phenotypically different lines as separate cellular models.

It has been shown that primary tumour cells donated by patients pre-treated with radiation failed to reprogram into iPSCs (193). This could be a major disadvantage in many cancers where neo-adjuvant chemoradiation therapy may induce resistance to reprogramming and prevent the creation of iPSC lines, but this not a hurdle that has to be overcome in glioma as neo-adjuvant treatment is not current standard of care.

With respect to genomic and transcriptional drift in primary cell culture, this has only quantitatively been shown beyond passage 7 (126). Furthermore, glioma cells cultured under GSC conditions have been shown to maintain their overall genotype and gene expression profile upon propagation *in vitro* for up to 11-13 passages (102). All the iPSC models derived in this study were reprogrammed at or below passage 5. It is hoped that reprogramming at an early passage i.e. when the cells are closest in genotype and phenotype to the original tumour sample, should increase the chances of genotypic features of the primary tumours being preserved in the final iPSC model.

Since it became known that ESC-equivalent stem cells in the form of iPSCs could be derived from somatic cells, there has been a dramatic increase in the number of groups using this technology, in many different ways, to study development and disease (171). There have also been considerable efforts to agree on the acceptable standards that newly derived iPSCs must demonstrate in order to be considered valid and stable (251). The iPSCs derived in this study have been characterised for all of these features, ranging from exhibiting stem cell morphology, expressing markers of pluripotency, having the ability to differentiate into all 3 embryonic germ layers, stability of karyotypes and clearance of residual reprogramming factors. Furthermore, they have been tested for their ability to form tumours *in vivo* – which is considered a key characteristic of GSCs (84) – and their genetic mutational similarity to their parent tumour cells.

Evaluating the true pluripotency of a derived iPSC line also involves testing for the functional ability to differentiate into all three embryonic germ layers (endoderm, mesoderm and ectoderm) (1). This can be done *in vivo* by injecting iPSCs into various anatomical sites in immunocompromised mice (e.g. subcutaneous, intra-muscular, renal capsule, intra-testicular) and confirming the presence of all three germ layers (by histology, immunocytochemistry and/or gene expression profiling) in the resultant teratoma formed (252). This assay is considered the gold standard for pluripotency as it is differentiation under physiological conditions (253). However, the necessity for the teratoma assay has been questioned recently given how labour intensive it is (takes around 6-12 weeks to complete) and the associated animal welfare burden (254). Instead, it has been suggested that completing the other traditional pluripotent tests (morphology, markers of pluripotency) in addition to *in vitro* spontaneous embryoid body formation (EB) with evidence of all three germ layers, along with newer tests such as gene expression profiling – all done in this study for the glioma iPSCs – is sufficient to confirm pluripotency. Indeed, most commercially available iPSC lines in the UK such as those from the Human Induced Pluripotent Stem Cell Initiative (HipSci) e.g. HPSI1014i-quls\_2 and HPSI1013i-yemz\_3 no longer include teratoma assays as part of their certificate of validity/pluripotency (255).

Given the frequent manipulation of cell lines (primary and iPSC) during culture, passage and expansion, the potential for mistakes in identity and labelling are high (111). Short tandem repeat (STR) profiling is a genetic authenticity technique that has been proposed as mandatory in ensuring iPSCs are matched to the donor tissue from which they were derived, as part of their initial characterisation and also periodically during passaging (230). STR analysis uses PCR to evaluate regions of tandemly repeating DNA motifs 1 to 6 base pairs in length that occur in intergenic and intragenic regions (256). These STR microsatellites account for approximately 36% of the whole genome and the variations in length at specified regions can discriminate between individuals (257). Other techniques that can achieve the same include single nucleotide polymorphism (SNP) and human leukocyte antigen (HLA) profiling. The concern about the use of these techniques is in their vulnerability to identify the donor, if combined with other personal information (258,259). The results of STR and WGS analysis in this study confirmed a match between the primary tissue and the derived iPSC line.

Gross genomic abnormalities such as mosaicism, SNPs and structural aberrations (inversions, loss of heterozygosity) can be induced by cellular reprogramming (244). The most common abnormality in both human ESCs and iPSCs is amplification of chromosome 12 and 12p. In addition, other mutations common in iPSCs include recurrent amplifications of chromosome 8, mosaic isochromosome 20q10, and amplification of the X chromosome. It is therefore essential to check the karyotype of any derived iPSC. There are a number of methods which include G-banding, fluorescent in-situ hybridisation (FISH), spectral karyotyping (SKY), comparative genomic hybridisation (CGH) and SNP arrays, WGS and global gene expression meta-analysis (260). Genomic integrity following reprogramming is particularly important for disease-relevant iPSC models (244). Most human iPSC lines will remain karyotypically normal during maintenance and propagation in culture (261). This is particularly true where non-integrative methods of reprogramming have been used. However, human iPSCs can acquire chromosomal aberrations during prolonged culture, for example amplification of chromosome 12 (244). This is analogous to the trisomy 12 observed in human ESCs upon extended culture (262). Repeat interval karyotyping (for example, at every 10 passages) has therefore been suggested as good practice when using patient-derived disease-relevant iPSCs (230). Of

note is that the composition of culture media, feeder conditions (mouse embryonic feeder or feeder-free) and passaging technique were shown not to influence karyotypic stability and CNV (263,264). In this study, CGH array was used to check the karyotypes of the derived iPSCs. This has the advantage of a higher resolution (>3 Mb by the provider used in this study) but has the disadvantage of being unable to detect balanced translocations and possibly not detecting mosaicism, although these are likely to be picked up during WGS analysis comparing primary versus derived iPSC lines.

Reprogramming-associated subkaryotypic mutations can occur in low frequencies (265). These can either be present at early passages and be maintained during prolonged culture or be acquired because of extended culture. The usefulness of creating new glioma iPSC models relies on their genomic integrity and stability after reprogramming, and during long-term culture i.e. the ability of the glioma iPSCs to recapitulate all or part of the genome of their parental tumour. Many of the published reviews and analyses concentrate on understanding this from the perspective of the developmental and malignant potential of the derived iPSCs so as to assess the safety of their use in stem cell therapy (266). The glioma iPSCs described in this study are not intended for therapeutic use and so the most important aspect of their genome to characterise is their integrity with respect to their usefulness in modelling the genetic drivers of their glioma phenotype. Given the heterogeneity of gliomas, it is likely that certain clones have been preferentially or stochastically reprogrammed – given the limited previous research on this approach, there is no evidence to reference this reprogramming dynamic in gliomas – and so it is unlikely that all of the genomic heterogeneity will be recapitulated in its entirety in the derived iPSCs. Indeed, the comparative analysis of the so called ‘hallmark’ mutations of GBM show that there have been some losses of mutations and amplifications in the (predominantly HGb) iPSC lines. Along with the loss of total number of copies in each derived iPSC and the changes in gains:loss status ratios between the iPSC line and its parental sample, it is unclear what the significance of this is on subsequent differentiation programs. Again, it is unclear at this stage of the analysis what the significance of this loss of number of CNVs in each derived iPSC is, and the significance of the changes in gains:loss status ratios between the iPSC line and its parental sample. Perhaps most significantly and valuably,

the *IDH1* mutation present in the LGG primary lines has been preserved in the LGG iPSC line. If this could be shown to be preserved through serial passaging, then it would represent the first available *in vitro* WHO Grade II Diffuse Astrocytoma model with an *IDH1* mutation. This would potentially allow the study of the effect of mutated *IDH1* on oncometabolism in gliomas. This work has previously been unable to be conducted using patient-derived tissue due to the lack of a suitable model. It is hoped that further WGS analyses will shed light on other subkaryotypic genomic integrity, and whether reprogramming-associated mutations are present (267). This type of analysis will also give additional information such as reprogramming dynamics i.e. whether certain subclones within the heterogeneous primary tumour are more prone to reprogramming. This could, in turn, inform future approaches to reprogramming primary glioma tissue.

Concerns have emerged regarding residual transgene expression following integrative lentiviral reprogramming approaches (268). This endogenous transgene expression has been shown to reduce the developmental competence of the derived iPSCs both *in vitro* and *in vivo*. Furthermore, profiling of these lines has demonstrated abnormal methylation of the Gtl2 region, which is known to be important in ESC-equivalence transcriptional expression. In order to avoid residual endogenous transgene expression, especially in the context of developing a model aimed at studying the glioma genome and its relationship to the phenotype, a non-integrative approach was used in this study. The non-replicative Sendai virus (SeV) delivery system is specifically designed so that the Yamanaka factors (2) are expressed by only the exogenous genes carried by transduced vectors (185). Since SeV is an RNA virus, it does not enter the nucleus for transcription and so integration of these transgenes into the host cell genome does not occur (184). Accordingly, there should not be an effect on the endogenous expression of these genes in the cell (172).

Since the models developed in the present study are specifically aimed at studying the genotype-phenotype relationship, it was essential that an integration-free method was used. Even with this approach, there appears to have been some changes in CNVs and total number of copies preserved in the derived iPSCs. This most likely represents reprogramming of one of more subclones of the original polyclonal tissue sample. Understanding this better with

clonal evolution analysis will be key to characterising the strengths of this model further. The iPSCs developed in this study are not for use in stem cell therapy approaches, which is where the main concerns for these retained expression signatures arise from (268). Gene expression analysis of the iPSCs shows that the influence of residual factor expression is minimal since the reprogramming process still means that the derived iPSCs cluster with ESCs and iPSCs derived from healthy donor tissue. The use of c-myc as a reprogramming factor has been highlighted as a concern due to reactivation following reprogramming and resultant oncogenic potential (269). An alternative Sendai virus reprogramming kit has therefore been made available which replaces c-myc with L-myc. Again, this is more important for clinical applications of iPSC e.g. stem cell therapy approaches.

Typically, human ESCs contain very few mitochondria (270). It has been shown that somatic mitochondria within human iPSCs acquire human ESC-like features (in terms of morphology, distribution and function) during reprogramming, rather than retaining the phenotype of their parental cells (271,272). This is thought to be due to the negative effects of mitochondrial oxidative stress pathways on senescence and genomic integrity (273). During *in vitro* differentiation, the mitochondria properties of the reprogrammed iPSCs returned to that of their parental cells. The study of the mitochondria in the derived glioma iPSCs (for example with comparative analysis to the primary tumour samples and between HGm/HGb and LGG iPSC lines by extracellular flux readouts) may reveal new insights into the metabolic phenotype of stem-like cells with glioma genotypes.

One criticism of iPSCs is that their parental cell genetic memory might predispose them to a differentiation bias and thus prevent differentiation into certain types of mature cell (244). It could be argued that it is this exact concern about iPSCs in other applications that this study hopes to exploit in the preservation of genes during reprogramming and subsequent identification of drivers that maintain glioma cells in an undifferentiated state. Indeed, Stricker *et al.* (274) reprogrammed cultured GSCs using 2-factor (OCT4 and KLF4) *piggyBac* transposon, a deletion after integration method (275). Despite observing widespread resetting of the DNA methylation signatures, they found that this alone did not alter the tumorigenicity of these cells, with cells remaining highly

infiltrative and proliferative. They postulated that epigenetic changes may occur at the early stages of glioma initiation but that oncogenic mutations accumulate to evolve tumours and promote highly malignant cellular phenotypes (188). The models presented in the present study are complementary to the work of Stricker *et al.* (194) as they build upon reprogramming approaches in glioma (and other cancers (192,193)), and are aimed at studying these genetic changes and their associated phenotypes. There is yet to be a single model that facilitates the study of all aspects of glioma so any new model can potentially add to the range of models available, provided the strengths and weaknesses are characterised (106). Although widespread resetting of the epigenome would be expected in fully reprogrammed iPSCs, as described, this needs confirming in the glioma iPSC models developed herein.

One proposed mechanism for treatment resistance in gliomas has been attributed to efficient DNA repair mechanisms (hence why MGMT hypermethylated gliomas have a better response to the DNA-damaging alkylating agent temozolomide) (276). Human iPSCs have been shown (like human ESCs) to possess highly efficient DNA damage repair mechanisms and express genes that mediate DNA damage signalling and repair pathways (277). This also includes cell cycle arrest in G2/M phase as part of the DNA damage response. If this can be shown to be present in the derived glioma iPSCs described in this study (especially in the context of resetting of methylation signatures as discussed earlier), then they could represent a useful model for studying this aspect of gliomas.

Ways in which these newly derived glioma iPSC models can be used to study gliomas is described in the following chapters.

### **3. Cerebral organoids can incorporate primary brain tumour tissue by co-culturing with mouse embryonic stem cells**

#### **3.1. Results**

##### **3.1.1. mESC organoids demonstrate incorporation of primary low-grade glioma brain tumour tissue**

Cerebral organoid methodology was first published in 2014 (202). In order to become familiar with this relatively new technology, I initially formed normal mouse and human cerebral organoids from mouse embryonic stem cells (mESCs) and H9 human embryonic stem cells (hESCs), respectively. Figure 3.1a shows the formation of an embryoid body (EB) from a starting population of 9000 H9 ESCs. As expected, debris from trituration into single cells prior to plating is present. Not all of the cells have been incorporated into the EB, which is again to be expected (202). Figure 3.1b shows an early organoid after neural induction. A tight rim of neuroepithelial cells is present at the perimeter of the organoid – this is an important indicator of successful progression at this stage (202). Prior to transfer into Matrigel droplets, organoids appear comparable in size (approximately 600-700µm) and morphology (Figure 3.1c and d) to those published in the literature (202). The organoids exhibit features such as outgrowths of neuroepithelial buds (Figure 3.1e and f), which is an encouraging sign of successful neural differentiation, and again is comparable to images published in the protocol (202). Figure 3.1g shows an organoid in a 1000 µm pipette tip prior to transfer into Matrigel on Parafilm indents, which have then subsequently been transferred into a 6cm dish (Figure 3.1h). Matrigel is kept on ice during the transfer process to prevent premature polymerisation, with each droplet containing a single organoid. Figure 3.1i shows organoids formed from mESCs and hESCs in spinner flasks with cerebral differentiation medium (with vitamin A), on low-velocity magnetic stirrer plates. Organoids remained viable in dynamic culture with weekly medium changes. The use of dynamic culture is required at this stage due to the cellular density of the organoids. Spinner flask bioreactors have been shown to improve oxygen and nutrient perfusion (278,279).

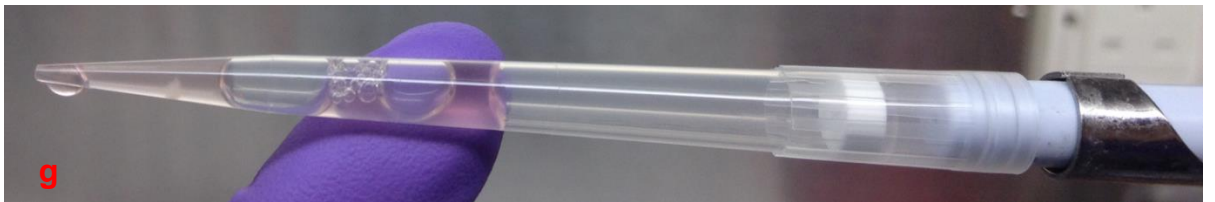
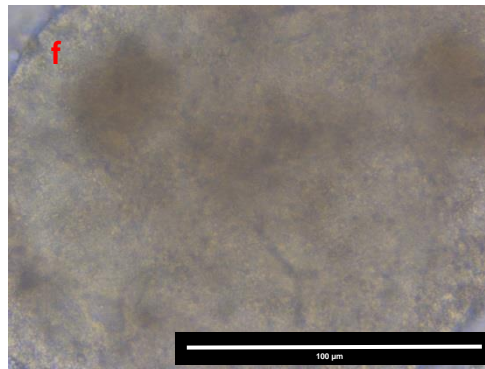
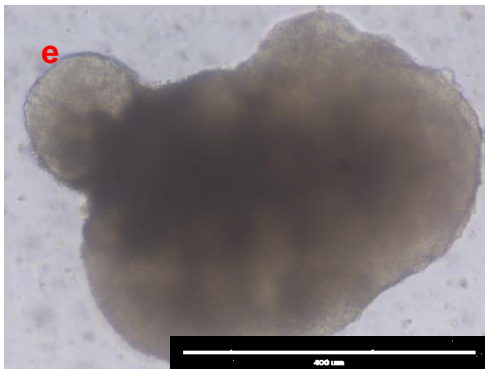
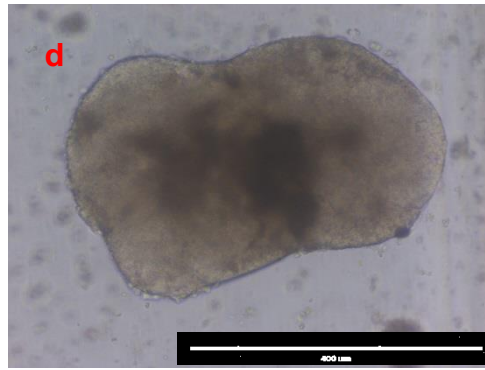
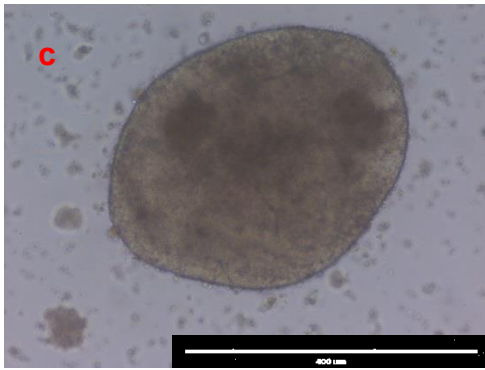
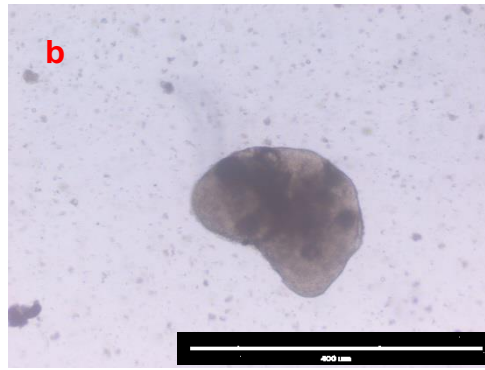
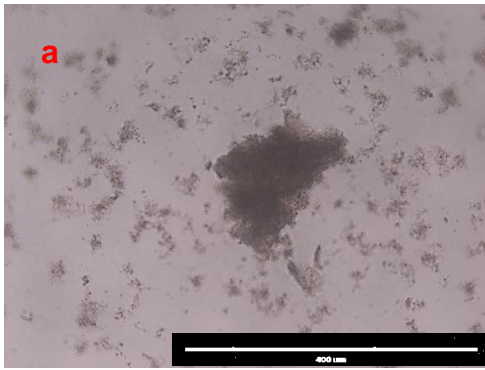


**Figure 3.1:** Cerebral organoids. **(a)** Embryoid body formation in a U-bottom 96-well plate (x10 magnification). **(b)** Early organoid after neural induction (x10 magnification). **(c)** Organoid approximately 600-700  $\mu\text{m}$  formed from mESCs (x10 magnification). **(d)** Organoid approximately 600-700  $\mu\text{m}$  formed from hESCs (x10 magnification). **(e)** Neuroepithelial bud outgrowth from main organoid (x10 magnification). **(f)** High magnification image (x40) of neuroepithelial bud outgrowth region. **(g, h)** Cerebral organoid being transferred in 1000  $\mu\text{m}$  pipette tip into Matrigel droplet. **(i)** Cerebral organoids formed from mESCs and hESCs in spinner flasks with cerebral differentiation medium (with vitamin A).

In order to investigate whether the presence of human primary tissue would still result in the formation of a self-assembling and self-organising cerebral organoid, I co-cultured primary low-grade glioma (LGG) tissue with mESCs, prior to the formation of an EB, as 15% and 30% of the total starting number of cells. All subsequent steps were followed according to the original cerebral organoid methodology (202). No difference was found in either group for the ability to form organoids.

In order to investigate the degree to which the primary tissue will be represented in the co-cultured hybrid, the organoids were formalin-fixed paraffin embedded (FFPE) and microtome sectioned. H&E staining of FFPE organoids sectioned at 20 $\mu\text{m}$  thickness shows distinctly different areas of cells with nuclei of different sizes (Figure 3.2). Cells with large nucleoli and high nuclear/cytoplasm ratio would be expected to be representative of mESCs whilst cells with smaller nuclei would be likely to be human cells.

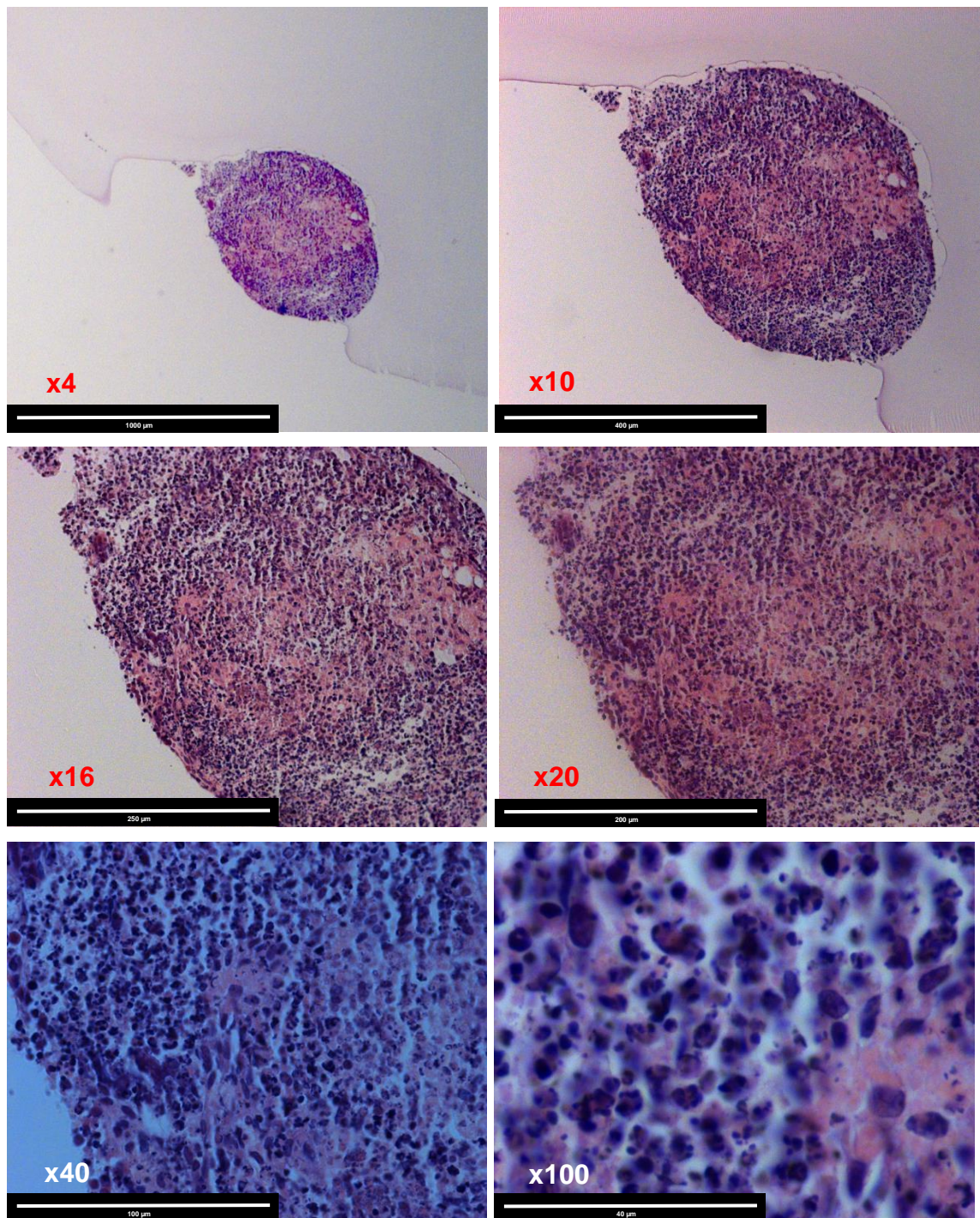


**Figure 3.2:** H&E stains at serial magnifications of cerebral organoids generated from mESCs co-cultured with primary human LGG tissue. Organoids were formalin fixed, embedded in paraffin wax and sectioned at 20 µm slices. Areas of stroma with smaller nuclei potentially represent the primary human tissue. Cells with large nucleoli and high nuclear/cytoplasm ratio are typical of mESCs.

In order to detect the presence of primary human LGG tissue more specifically, immunofluorescence staining was performed on the co-cultured hybrid organoids

using human specific vimentin Ab (AlexaFluor 488 secondary Ab). Positive staining of cells for human specific vimentin on digital fluorescence and confocal microscopy of sectioned and permeabilised whole mouse organoids, respectively, indicates the presence of human tissue (Figures 3.3 and 3.4). Since no other human tissue was used in the formation of these organoids, this can be assumed to originate from the primary LGG tissue. The degree to which the (assumed) human tissue is incorporated, and its distribution appears to be variable in different organoids (Figures 3.3a versus 3.3b, 3.3c and 3.3d). This may indicate that the self-assembly or spatial organisation of the organoid has been disrupted. Neuroepithelial bud outgrowths, a typical feature of organoids and a sign of successful neural differentiation, are seen in immunofluorescence images (Figures 3.3a and 3.3c) and the confocal image (Figure 3.4a, arrow). This provides some evidence that differentiation is still possible despite the presence of primary tissue.

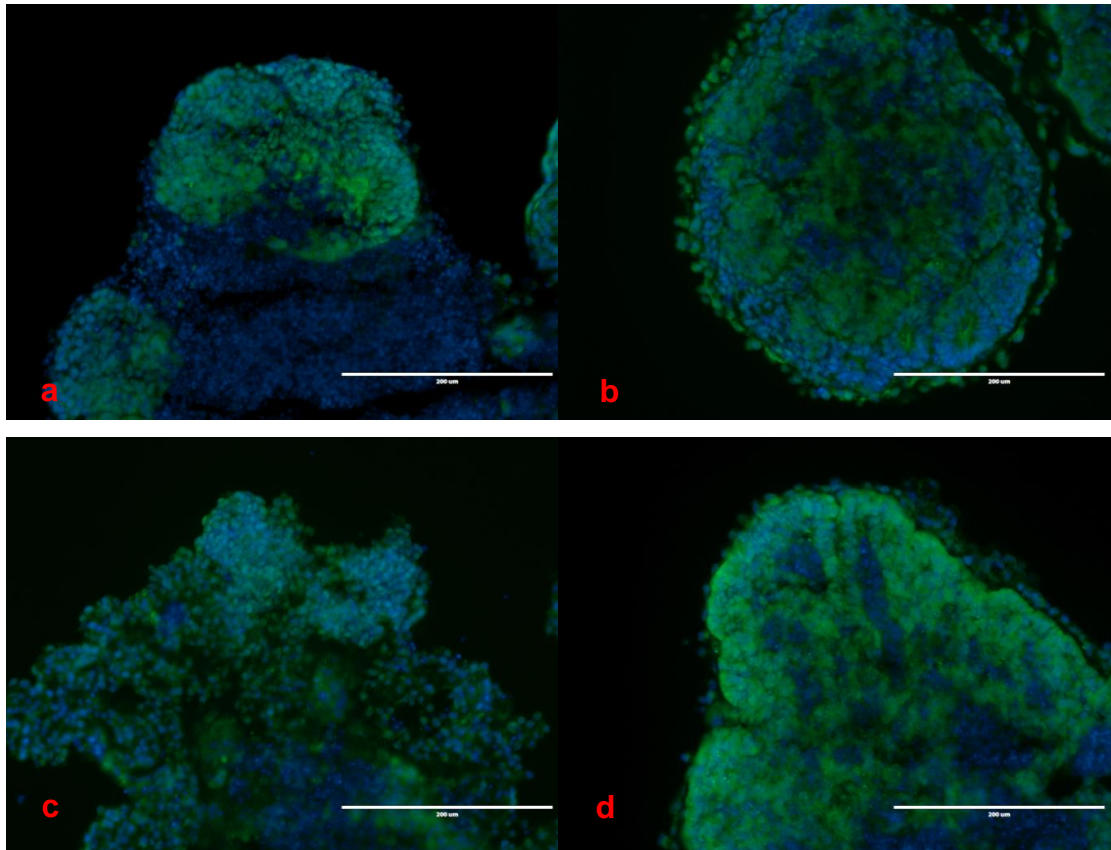


**Figure 3.3:** Digital inverted fluorescence microscope images of organoids formed from mESCs and primary LGG tissue in co-culture. Organoids were embedded in OCT and cryosectioned in 20  $\mu\text{m}$  slices. Cerebral nuclei are stained with DAPI. **(a, c)** Organoids show typical outgrowths of neuroepithelial buds. Areas of green fluorescence represent positive staining for human specific vimentin. Suspected human tissue appears to be arranged variably amongst different organoids: **(a)** staining appears to be very region specific with a distinct central region that does not appear to show any positive staining for vimentin, **(b, c)** staining is very heterogenous and mixed with mESCs, **(d)** tissue staining for vimentin is more positive and occupies more of the area of the organoid than in the other organoids.

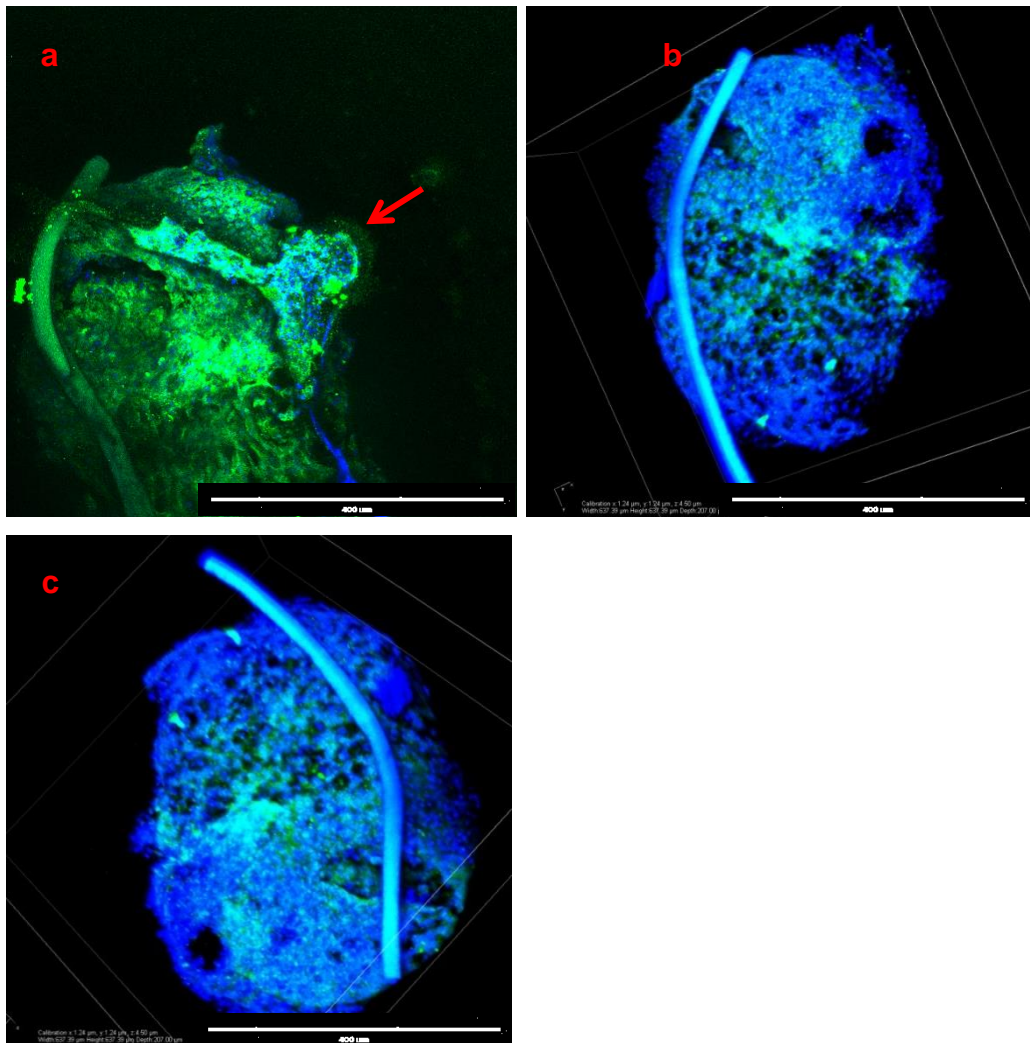


**Figure 3.4:** Z-stack confocal microscope images of a permeabilised whole cerebral organoid formed from mESC co-cultured with primary LGG tissue. Nuclei are stained with DAPI. Fibre artefact is present overlying the organoid. **(a)** A typical neuroepithelial bud outgrowth is indicated by the arrow. Very high levels of staining for human specific vimentin (green) are seen on the surface of the organoid, which may represent high levels of background due to poor penetration of the antibody. **(b, c)** With progressive slices through the organoid, mixed areas of positive staining for human specific vimentin are seen.

### 3.2. Discussion

These results show that it is possible to replicate the published cerebral organoid methodology as originally published (202). The organoids that I formed from both mESCs and hESCs were comparable in size (350-600µm) and morphology (neuroepithelial buds with radial glia) to those published. This forms the basis of method development to create new glioma tumour organoid models.

One new model that I have created is a mouse cerebral organoid that incorporates primary LGG tissue. The results show that cerebral organoid-like structures can be formed with co-culture of LGG tissue, and that this tissue is incorporated into the organoid tissue. It is interesting to note that there is variability in the incorporation of the glioma tissue into organoids. This may represent the batch-to-batch variability seen in cerebral organoids, that has previously been described by other groups (215,280), and that is observed less in the gut organoids from which nearly all organoid methodology has subsequently developed. Further characterisation of this human tissue is required to determine similarity to the original primary LGG tissue, both morphologically and genotypically. It will also be necessary to investigate any disruptive effect the primary tissue has on the structural organisation of these organoids compared to those formed without primary tissue co-culture, and whether this has an impact on the micro-environmental context that using an organoid model aims to provide. This could be done with brain region specific antibodies as per the original protocol (202) and also organoid-specific imaging techniques such as immunolabelling after clearing (e.g. iDISCO (281)) and light-sheet microscopy (282). These, and other current organoid, models lack essential cell types such as a vasculature and immune system. Vasculature is not only important for the presence of a blood-brain barrier (BBB) but also because gliomas have been shown to exhibit a preference for tracking along the peri-vascular spaces (283) and because breakdown of the BBB is one of the clinical imaging signs used to detect malignant transformation in LGGs (63). This co-culture glioma organoid model in its current format therefore limits the study of the natural history of glioma formation and progression (222). It may however reveal other insights into the behaviour of gliomas, such as the interaction of glioma cells with non-cancerous CNS cells.

This work into co-culturing of mESCs and LGG was done in parallel with the iPSC derivation. Once iPSCs were successfully established, it was decided to concentrate on forming human tumour organoids. However, this work was used in the early stages of developing a co-culture model of patient-derived glioma cells with mouse organoids (221). In this more refined model, the key differences were that the glioma cells and mESCs were not in single cell suspension as described here. Rather, the authors pre-formed both the human glioma component (in spheres) and the mouse organoid component, co-culturing them at a relatively early stage of the organoid protocol (day 12). Furthermore, contrary to the model I have described here, the authors avoided the use of Matrigel. This is key to the downstream applications of this model in terms of interference with drug screens (drug washout may not be as complete with Matrigel present (284)), the avoidance of manipulation of the organoid and the reduced overall size – both making it easier to conduct throughput assays.

## **4. Tumour organoid models demonstrating phenotypic and genotypic differences can be derived from patient-derived glioma iPSCs**

### **4.1. Results**

#### **4.1.1. Tumour organoids derived from glioma iPSCs exhibit a 'differentiation block' phenotype**

The glioma iPSCs derived and characterised from primary high-grade glioma (bulk – HGb, and margin – HGm, parts of the tumour) and low-grade glioma previously described were used to form tumour organoids. The methodology was a modification of that described by Lancaster and Knoblich (202) with the starting cell population of each tumour organoid being a glioma iPSC line. Control organoids were formed from human ESCs and a UK Stem Cell Bank gifted human iPSC line derived from reprogramming of fibroblasts donated by a healthy individual.

Through time-point based visual observation and subsequent immunostaining analysis at day 6 (transition to neural induction media), day 11 (transfer to Matrigel droplets) and day 15 (transfer to spinner flask dynamic culture), noticeable differences were observed at day 15 between the organoids formed from the glioma iPSCs, and the control organoids.

Representative stereoscopic microscopy images of day 15 control (Figure 4.1a) and tumour organoids formed from glioma iPSCs (Figures 4.1b-d), embedded in Matrigel and prior to transfer into a spinner flask show marked differences in morphology. The control organoid showed distinct gross regional differences in morphology with neuroepithelial bud outgrowths that are optically clear and surround a visible lumen in some areas (Figure 4.1a, arrow). These observations are consistent with those reported previously for normal cerebral organoids at this stage (202), and thus represent a suitable control for the comparison of tumour organoid formation and morphology. Tumour organoids formed from HGb and HGm iPSCs had less gross regional differences in morphology within the organoids and many more neuroepithelial-like bud outgrowths than the control organoids and LGG tumour organoids, at the same time point (day 15). Many of these bud outgrowths in the tumour organoids were also not optically clear. The

control and LGG tumour organoids are more similar in appearance with evidence of radial glia and neuroepithelial bud outgrowths that are optically clear and surround a visible lumen (Figure 4.1a-b, arrows). although the degree of regional difference within each organoid is less clear in the LGG tumour organoid.



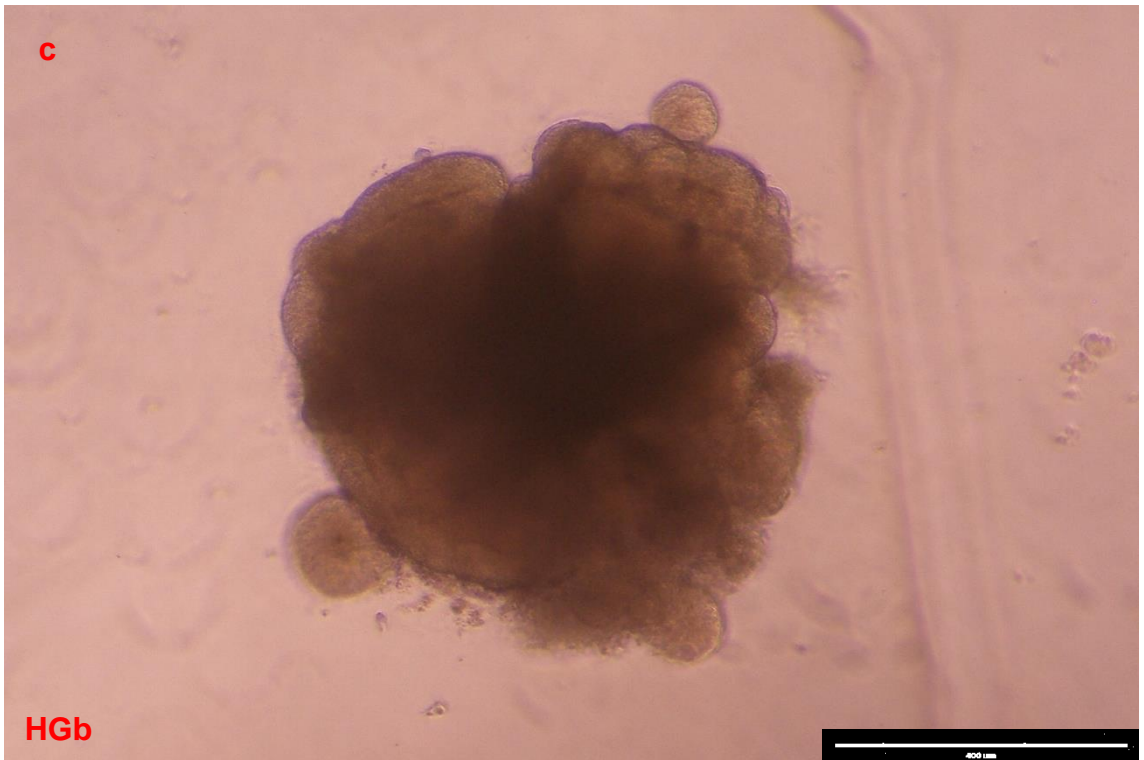




**Figure 4.1:** Representative stereoscopic microscopy images of day 15 organoids, embedded in Matrigel and prior to transfer into spinner flask. Pigmented regions represent retinal pigmented epithelial identity, which is to be expected at this stage (202,285). **(a)** cerebral organoid formed from ESCs shows optically clear neuroepithelial bud outgrowths that in some cases surround a visible lumen (arrow). Gross regional patterning is evident from the morphological differences in different parts of the organoid (star compared with triangle), **(b)** tumour organoids formed from LGG iPSCs show some similarities in gross regional morphology but it is not as clear in the LGG tumour organoid, **(c-d)** tumour organoids formed from HGb and HGm iPSCs show much less gross regional differences in morphology and greater numbers of neuroepithelial bud outgrowths that are not as optically clear and show no evidence of surrounding a lumen.

Histological analysis by haematoxylin and eosin (H&E) (Figure 4.2) showed further evidence of morphological differences between the HGb and HGm tumour organoids, and the control and LGG tumour organoids. The HGb and HGm tumour organoids are grossly more round and predominantly consist of areas of columnar cells arranged in a radial fashion with a central lumen, consistent with neural rosettes (286). The control and LGG organoids in comparison are more elongated and appear to consist of rosettes and other areas of alternative differentiation. Furthermore, there are qualitative similarities in differentiation

between the LGG tumour and the control organoids such as the development of regional cellular morphologies within each organoid.

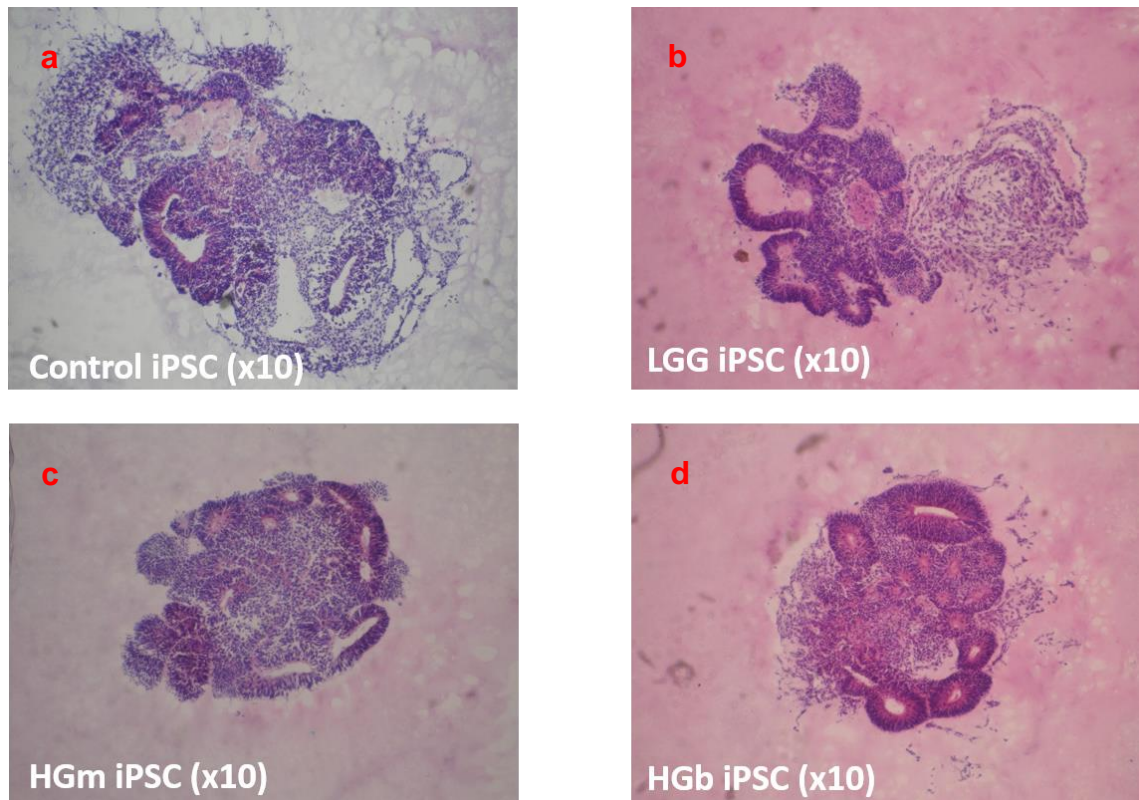


**Figure 4.2:** Representative light microscopy images of fixed, sectioned and haematoxylin and eosin (H&E) stained **(a)** control and **(b-d)** glioma iPSC tumour organoids. The control and LGG tumour organoids are more similar in morphology and show areas within each organoid with different cell types. HGb and HGm tumour organoids show morphological similarities (rounder), that are different to the control and LGG tumour organoid (more elongated), with increased numbers of rosettes.

Further investigation of the organoids with immunocytochemistry using antibodies against SOX2 and TUJ1 at day 15 revealed qualitative differences in morphology and staining (Figures 4.3a-d). HGb and HGm tumour organoids, when compared to control and LGG tumour organoids, showed a distinct phenotype with the organoid consisting predominantly of SOX2 positive radially organised columnar cells, consistent with neural rosettes (287), minimal differences in regional morphology and minimal TUJ1 staining. A representative day 32 control organoid formed from human ESCs, fixed, sectioned and stained for antibodies against SOX2 and TUJ1 is shown in Figure 4.5 as a further point of comparison to the HGG iPSC derived organoids. This organoid, albeit at a later

stage of development, shows a large central area of neuronal differentiation and neuronal outgrowth from its inferior portion. Neuroepithelial cells arranged in a radial fashion persist as expected, particularly in the forebrain area, since this has been postulated (in murine neurodevelopmental models) to drive growth and expansion of the largest part of the adult brain (288,289).

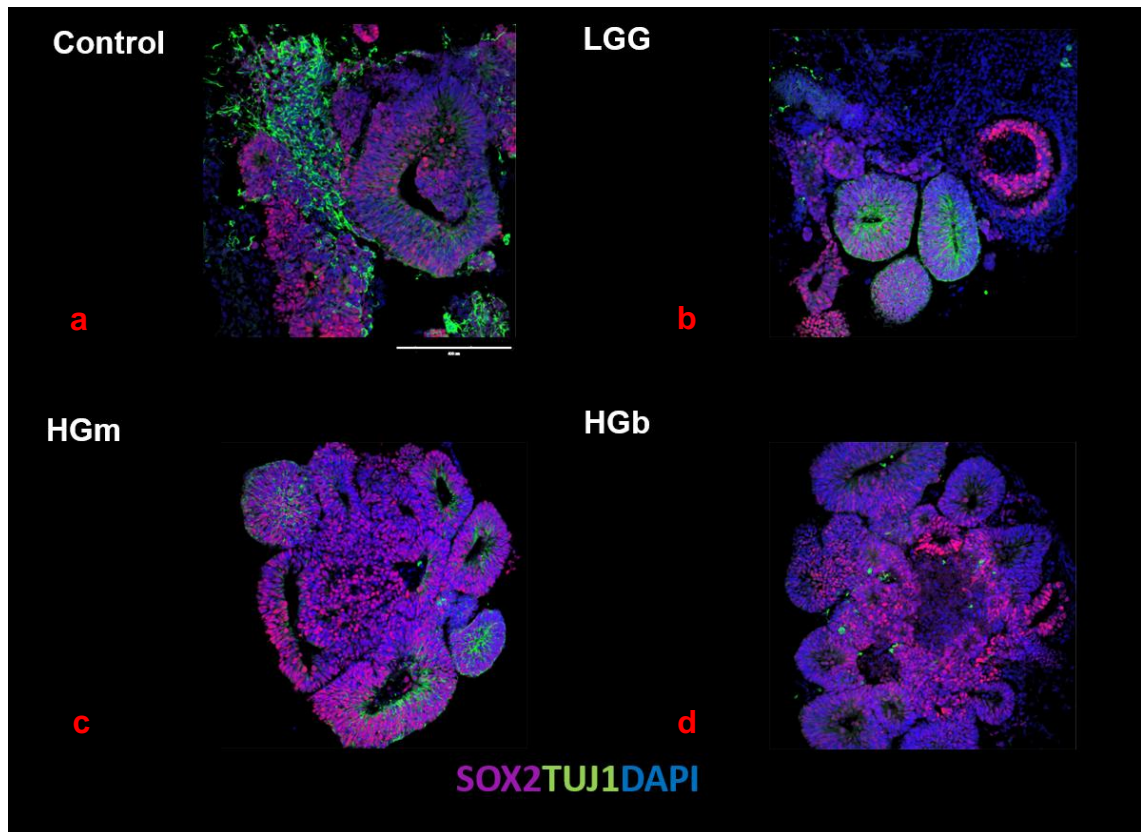


**Figure 4.3:** Representative confocal images of fixed, sectioned day 15 **(a)** control and **(b-d)** tumour organoids immunofluorescence stained with antibodies against SOX2 (a marker for self-renewal and the presence of neural stem cells) and TUJ1 (a marker for post-mitotic differentiated neurons). Qualitative analysis revealed that HGb and HGm tumour organoids exhibited a distinct phenotype with predominant SOX2 positive neural rosettes, relatively little regional differences in morphology and relatively little TUJ1 staining, when compared to control and LGG tumour organoids.

This observation was further characterised by quantification of the numbers of rosettes present within day 15 organoids formed from each of the glioma iPSCs (HGm, HGb, LGG) and control stem cells (human ESCs) (Figure 4.4). This showed a significantly higher mean number of rosettes within each of the organoids formed from the glioma iPSCs, when compared to the control organoid

(control 3.7; LGG 8.7,  $p = 0.0080$ ; HGm 12.7,  $p = 0.0003$ ; HGb 19.3,  $p = 0.0083$ ). There was also a significant difference between the mean number of rosettes within HGm ( $p = 0.0275$ ) and HGb ( $p = 0.0302$ ) organoids when compared to LGG organoids.

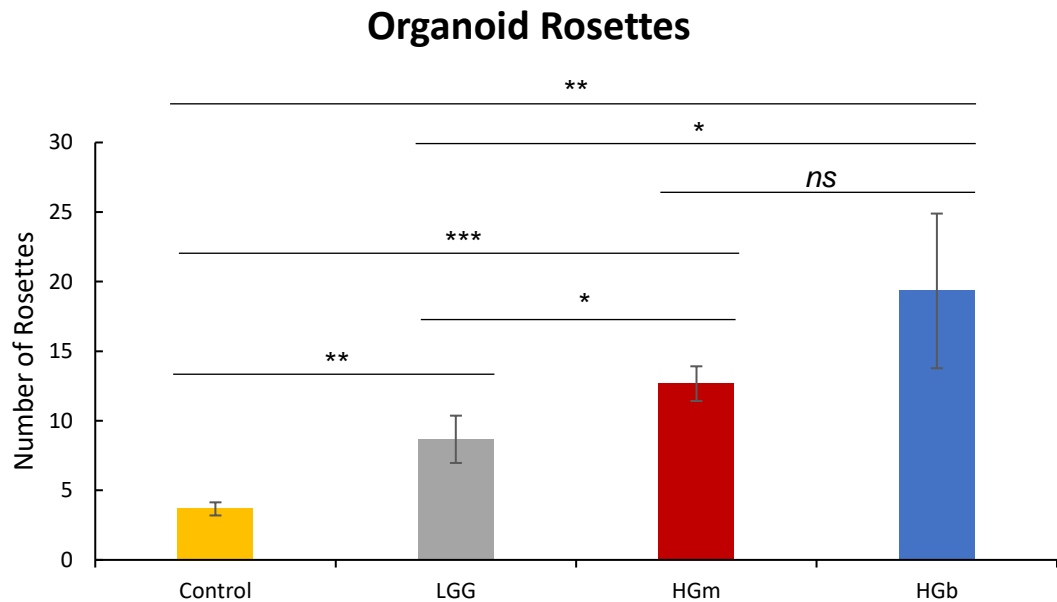


**Figure 4.4:** Quantification of mean number of rosettes within day 15 organoids formed from control and glioma iPSCs showing significant differences between all organoids (LGG 8.7,  $p = 0.0080$ ; HGm 12.7,  $p = 0.0003$ ; HGb 19.3,  $p = 0.0083$ ) versus control organoids (3.7), HGm versus LGG ( $p = 0.0275$ ) and HGb versus LGG ( $p = 0.0302$ ). (3 independent experiments per line; mean  $\pm$  SD; Student's t-test; ns = non-significant,  $P \leq 0.05$  were presented as \*;  $P \leq 0.01$  as \*\*,  $P \leq 0.001$  as \*\*\* and  $P \leq 0.0001$  as \*\*\*\*).

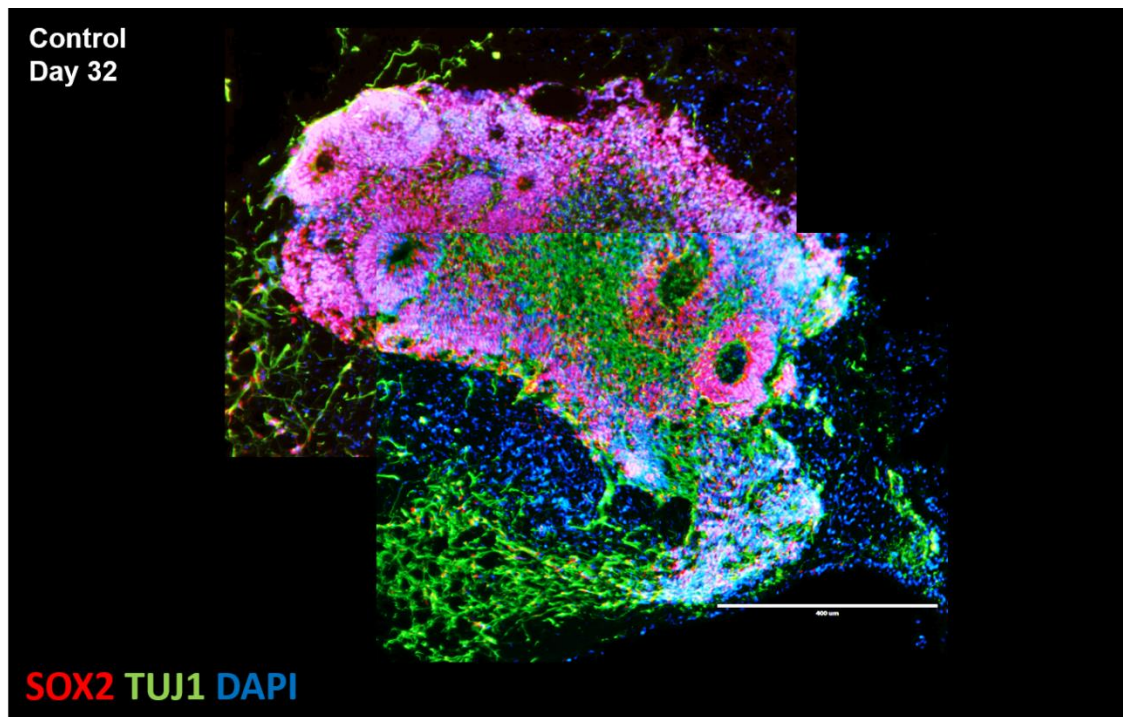


**Figure 4.5:** Representative ‘stitched’ inverted fluorescent microscopy images of fixed and sectioned day 32 control cerebral organoid immunofluorescence stained with antibodies against SOX2 (a marker for self-renewal and the presence of neural stem cells) and TUJ1 (a marker for post-mitotic differentiated neurons). A large area of neuronal differentiation is seen in the central area of the organoid, as well as in the inferior portion where there is neuronal outgrowth. SOX2 positive neuroepithelial cells arranged in a radial fashion persist, particularly at one pole of the organoid, as these cells have been shown to drive expansion of the forebrain region in murine neurodevelopmental models (288,289).

#### **4.1.2. Gene expression analysis of glioma iPSC organoids demonstrates an undifferentiated gene expression signature**

In order to further characterise the ‘differentiation-block’ phenotype observed in the HGb and HGm tumour organoids, bulk qRT-PCR analysis was performed to obtain model-specific gene expression signatures. Fold changes (FC) in gene expression of the analysed genes (*KLF4*, *NANOG*, *POU5F1/OCT4*, *FOXG1*, *NESTIN*, *PAX6*, *SOX1*, *SOX2*, *BCL11B*, *DCX*, *EOMES/TBR2*, *MAP2*, *NEUROD1*, *S100B*, *SATB2*, *TUBB3/TUJ1*, *OLIG2*, *EGFR*, *IDH1*, *MGMT*, *MKI67*, *MYC*, *PDGFRA*, *PTEN*, *TGFB1*, *TP53*, *TRRAP*, *VIM*) in the tumour organoids were calculated relative to gene expression FCs in control organoids that were derived from human H9 ESCs. Genes were targeted based on their cellular function so as to represent the following groups: ‘pluripotency’, ‘neural stem cell

identity', 'neuronal identity' and 'tumour proliferation/suppression.' This was also based on previous work identifying some of these genes and associated groups as relevant in investigating GSC phenotype (50). The analysis yielded a distinctive pattern of gene expression changes, as depicted by the radar plots in Figure 4.6.

The most marked changes in the HGb tumour organoids were the elevated expression of *FOXP1* (FC > 19), *EGFR* (FC > 4), *SOX2* (FC >2) and *PAX6* (FC > 2). HGb tumour organoids also exhibited markedly reduced expression of *DCX* (FC > -11), *EOMES/TBR* (FC > -7), *TUBB3/TUJ1* (FC > -6), *PDGFRA* (FC > -4) and *MGMT* (FC > -5).

A similar pattern was seen with *FOXP1* (FC > 20), *PAX6* (FC > 3), *SOX2* (FC > 2), *DCX* (FC > -7), *TUBB3/TUJ1* (FC > -6), and *PDGFRA* (FC > -6) in HGm tumour organoids. However, *MGMT* (FC > -2) was less markedly reduced in expression and *EGFR* was comparable to control organoids. Expression of *S100B* (FC > -7) and *NEUROD1* (FC > -5) was much more reduced than in HGb tumour organoids (both FC > -2).

In the LGG tumour organoids, expression of *FOXP1* and *PAX6* are elevated (both FC > 4), but to a less extent than in the HGb and HGm organoid. Likewise, there was a modest reduction in expression of *DCX*, *S100B*, *EOMES/TBR*, *NEUROD1*, *TUBB3/TUJ1* and *PDGFRA* (all FC > -2).

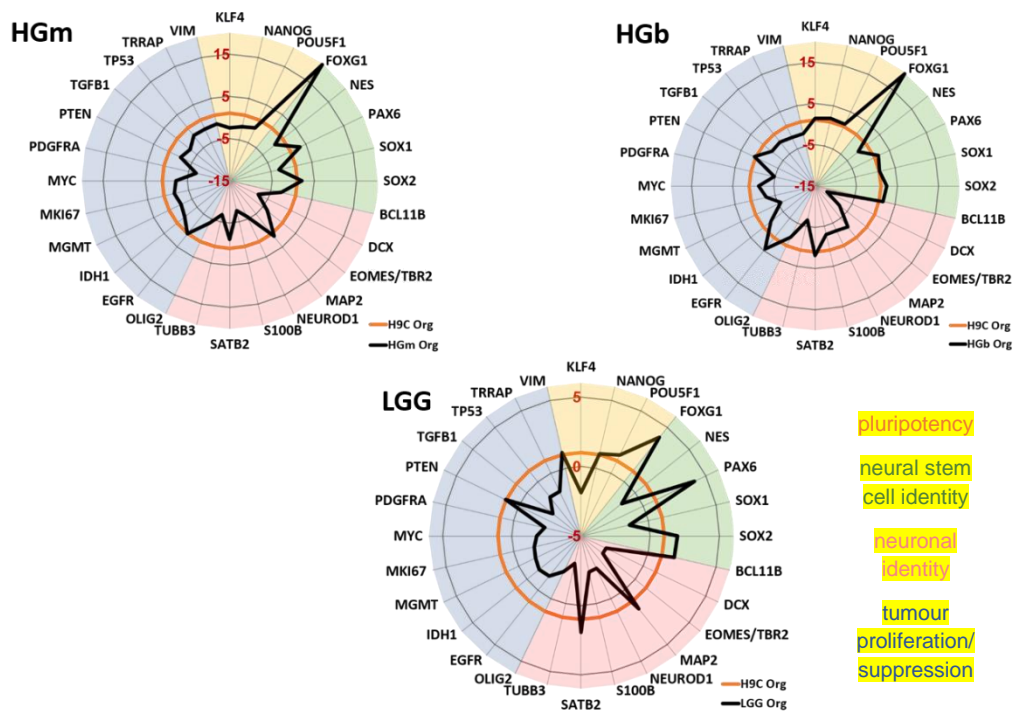


**Figure 4.6:** Radar plots depicting model-specific gene expression signatures obtained by bulk qRT-PCR performed in day 15 tumour and control organoids. Genes are arranged by category (pluripotency, neural stem cell identity, neuronal identity, tumour proliferation/suppression). Expression of *FOXP1* is markedly increased by fold change > 19 and >20, and *DCX* markedly decreased by fold change > -11 and > -7 in HGb and HGm tumour organoids, respectively. These changes were observed to a lesser extent in LGG tumour organoids (*FOXP1* fold change > 4, *DCX* fold change > -2). Fold changes are presented in comparison to day 15 control organoids (3 technical replicates of 3 biological replicates of each organoid).

## 4.2. Discussion

Modelling gliomas using cerebral organoid methodology has been proposed as complementary to current *in vitro* and *in vivo* glioma models (222). Advantages of using organoids are that they are orthotopically more similar to brain tumours than adherent or neurosphere culture, can be grown in bulk, avoid the use of animals, and can be grown from patient-derived iPSCs – the latter providing a human context and potentially enabling personalised approaches (290). Current disadvantages include a lack of a blood-brain barrier, lack of an immune context, length of time and investment of labour required to grow and maintain organoids, and limited evidence of validation and translation that they are suitable for glioma modelling.

The use of Matrigel in organoid culture is worth noting. It undoubtedly adds labour and expense to the process, and might interfere with potential drug screens (212). However, it may make cancer organoid models more physiologically relevant through its laminin-rich and collagen-IV rich properties that may act as a basement membrane substitute (291). In the analysis performed in this study, an organoid recovery step from Matrigel was performed prior to gene expression analysis to minimise contamination during RNA extraction. da Silva *et al.* (221) used so-called ‘early’ cerebral organoids in their glioma invasion assays. These assays are run prior to the stage where the organoid would normally be embedded in Matrigel. More work is required to delineate the effects of Matrigel on glioma organoid models.

The tumour organoids developed in this study represent a potential new model system in glioma with a distinct phenotype. SOX2 is a nuclear marker of NSCs and PSCs that is a key transcription factor in maintaining self-renewal in these cell populations (246). TUJ1 is a neuron-specific class III  $\beta$ -tubulin (TUBB3) present in newly generated immature post-mitotic neurons and differentiated neurons (201). The co-staining of these markers within the same organoid therefore infers the degree of ‘stemness’ versus a more differentiated phenotype. Neural rosettes represent a histological architecture pattern seen within CNS tumours and previous work has established a link between a rosette phenotype and malignancy – medulloblastoma, a childhood posterior fossa brain tumour thought to be of developmental origin (292). The qualitative observation of

organoids formed from the HGG iPSCs (HGm and HGb) consisting predominantly of SOX2 positive neural rosettes, with relatively reduced staining of markers of neuronal differentiation (TUJ1), taken together with the significantly higher number of rosettes within these organoids, relative infers a more stem-like phenotype and may represent a 'differentiation block.' Of note is that the LGG tumour organoids were more similar in morphology and phenotype to the control organoids than the other (higher-grade) HGb and HGm organoids. The targeted gene expression analysis, however, shows that all glioma iPSC-derived tumour organoids exhibited a more undifferentiated phenotype than the control organoids.

*FOXP1* is a member of the forkhead box of family of transcription factors (293). It is consistently one of the most commonly overexpressed genes (transcriptionally rather than through gene amplification) in glioma stem cells (294) and is inversely correlated with patient survival (295). This is perhaps unsurprising given its role in limiting premature differentiation and regulating forebrain expansion through neural progenitor cell proliferation (296,297). The increased expression of *FOXP1* has been previously shown to be important in restricting astrocyte differentiation in glioblastoma stem cells (248) and is thought to be functionally important in driving tumour growth by attenuating the cytostatic effects of TGF- $\beta$  signalling (298). Furthermore, along with elevated SOX2 expression, it has downstream transcriptional targets of epigenetic regulation (Foxo3, Plk1, Mycn, Dnmt1, Dnmt3b and Tet3). Loss of Foxo3 in particular, has been shown to induce astrocyte dedifferentiation and proliferation to a neural stem cell state. Interestingly, it was shown that gene deletion of *FOXP1* (using CRISPR/Cas9) did not impact proliferation *in vitro* but when the edited cells were xenotransplanted, upregulation of Foxo3 and increased astrocyte differentiation was demonstrated. Similar gene editing approaches to *FOXP1* in the HGb and HGm tumour organoids described in the present study may add value and insight into the microenvironmental context required to explain this phenotypic difference.

The concomitant increased expression of *EGFR* in the HGb organoids could be explained by previous work showing that *EGFR* may work in part by triggering a *FOXP1*-dependent transcriptional network (299). *EGFR*, amplified or mutated in

up to 60% of GBMs, persistently activates signalling pathways and reprograms metabolism to promotes tumour growth and tumour cell survival (300). Analysis of clinical samples of GBM in The Cancer Genome Atlas (48) has previously shown that *FOXP1* was the most highly correlated forkhead box transcription factor with *EGFR*, and was significantly elevated in GBMs with *EGFR* mutations (299).

The increased expression of *FOXP1*, *EGFR* (in HGb tumour organoids only) and *SOX2* infers a more aggressive phenotype promoting tumour growth, dedifferentiation and proliferation. This is supported by the relative reduced expression of markers of neuronal identity and maturation in HGb and HGm tumour organoids - *EOMES/TBR*, *TUBB3/TUJ1*, *DCX* and *NEUROD1*. Taken together, it can be argued that these features support the use of these tumour organoids as models of stem-like behaviour and differentiation in glioma.

The *MGMT* gene exerts its effects by coding for a protein that catalyses the transfer of methyl groups from O(6)-alkylguanine and other methylated moieties of the DNA to its own molecule, thus facilitating DNA repair (301). Accordingly, it has been shown that reduced expression of *MGMT* is oncogenic due to the accumulation of unrepaired DNA and resultant mutations (302). Reduced expression of *MGMT* in HGb and HGm organoids is therefore not to be unexpected given the array of mutations that accumulate in GBM. Paradoxically, downregulation of this gene (by hypermethylation of the promoter sequence) has also been associated with an improved response to TMZ, which takes advantage of the diminished DNA repair mechanisms, and a better outcome for patients with GBM (42). Using these tumour organoids in TMZ response assays may provide further validation of their usefulness as glioma models.

*PDGFRA* is a receptor tyrosine kinase that is involved in the PI3K pathway and mutated in 10-15% of primary GBMs (48). This alteration is concurrent with *EGFR* mutations in nearly half of primary GBMs (303). *PDGFRA* is most highly expressed in the proneural subtype of GBM, which itself is most commonly associated with secondary GBM (*IDH1* mutated) (304) and younger patients (the proneural subtype had the greatest number of patients aged < 40 years in the TCGA subtype analysis (305)). Reduced expression of *PDGFRA* in HGb tumour

organoids, in the context of increased expression of *EGFR*, may infer that the HGb tumour organoid is representative of the classical subtype of GBM. However, without further transcriptional analysis of the primary tumour and the HGb iPSCs, it is not possible to fully interpret the reduced expression of *PDGFRA* further in the organoid context.

Given that LGG in humans behaves phenotypically less aggressively and is defined as lower in grade than HGGs, it can be argued that the lower degree of overexpression of *FOXP1* is to be expected in LGG tumour organoids. The representation of lower-grade behaviour in the LGG tumour organoid model is further supported by the greater degree of *PAX6* overexpression, when compared to HGb and HGm tumour organoids. *PAX6* has been shown to suppress the growth of human GBM cells (306) and its expression is inversely correlated to tumour grade (307). On its own, *PAX6* has been shown to suppress cell invasiveness, colony formation and cell proliferation (308). Synergistically with *PTEN*, it acts to suppress *VEGF* expression in GBM (309). Furthermore, TMZ has been shown to increase *PAX6* expression (310), and this may be one of the mechanisms by which it confers a better prognosis. Again, use of these tumour organoids in TMZ assays may reveal further insights into the effects of TMZ on *PAX6* expression, and the relationship to grade. This may consequently inform the use and timing of TMZ treatment in LGG patients, which is subject to debate (311,312).

In order to investigate the 'differentiation block' phenotype observed further and minimise the batch effect (previously discussed) in organoid formation, glioma iPSCs were used to develop a reproducible stem cell differentiation assays in chemically-defined culture conditions. This is addressed in the next chapter.

## 5. Glioma iPSCs can be used to develop reproducible stem cell differentiation assays in chemically-defined culture conditions

### 5.1. Results

#### 5.1.1. Glioma iPSCs fail to differentiate into neurons and provide proof of principle for the development of drug discovery assays

Tumour organoids grown from the glioma iPSCs derived in this study show a distinct 'differentiation block' phenotype characterised qualitatively by differences in morphology and quantitatively by increased numbers of rosettes and gene expression signatures that are different to organoids formed from normal ESCs and iPSCs. To investigate this further, iPSCs ( $3 \times 10^5$  per line) on mouse embryonic feeders (MEFs) were differentiated into neural stem cells (NSCs) with neural induction medium (neurobasal medium and proprietary supplement). NSCs were propagated on a basement membrane matrix (Geltrex) using a neural expansion medium (neurobasal medium, Advanced DMEM/F12 and proprietary supplement). Immunocytochemistry showed differentiated control and glioma iPSCs both stained positively for NSC markers SOX2 and NESTIN (Figure 5.1a). Control, LGG and HGm stained negatively for the pluripotency marker OCT4 (Figure 5.1b). NSCs differentiated from HGb iPSCs were observed qualitatively to have sporadic positive staining for OCT4 (Figure 5.1b).

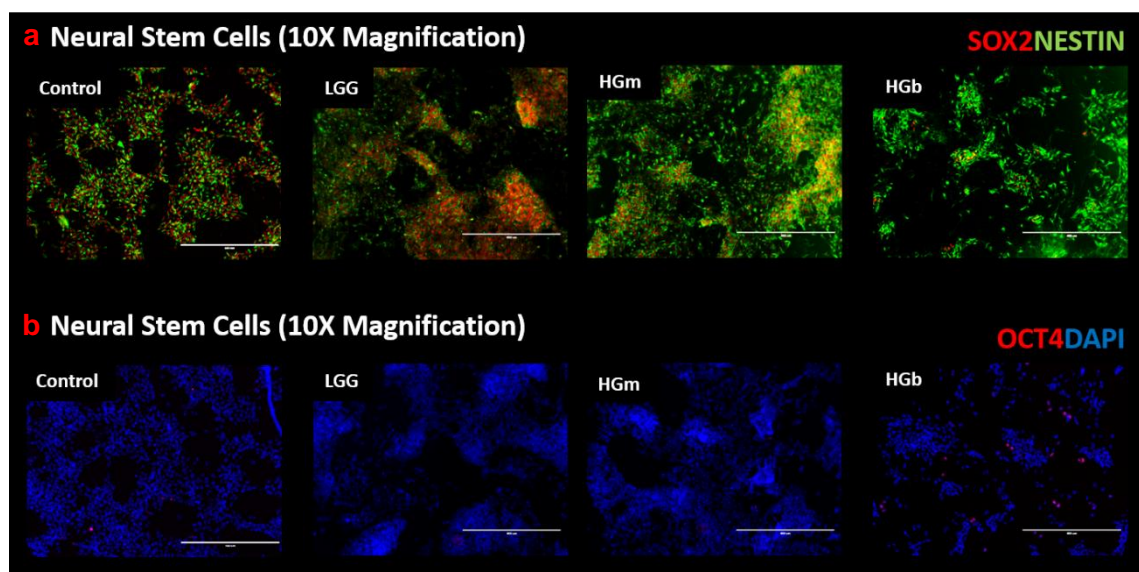


**Figure 5.1:** Immunofluorescence staining of fixed neural stem cells (NSCs) differentiated from control and glioma iPSCs. Starting population for each assay was  $3 \times 10^5$  iPSCs with 3 independent experiments conducted per line. **(a)** Cells stain positively for neural stem

cell markers SOX2 and NESTIN. **(b)** Cells stain negatively for pluripotency marker OCT4 in control, LGG and HGm cultures. There are a few sparse pluripotent stem cells after differentiation of HGb iPSCs to NSCs.

To investigate the terminal differentiation capacity of the control and glioma iPSCs, the derived NSCs ( $5 \times 10^4$  per line) described above were differentiated on poly-L-ornithine/laminin coated plasticware using neuronal differentiation medium (neurobasal medium, B27 and glucose supplements). Immunocytochemistry using antibodies against the neuronal marker TUJ1 was used to confirm the presence of neurons and enable quantification. Counterstaining for the nuclear marker DAPI was used to enable the quantification of total cell area. Qualitatively, results appeared to show highly efficient differentiation of neurons from the control NSCs and formation of neurites to create interconnecting neuronal networks. Neuronal differentiation from NSCs with LGG iPSC lineage appeared qualitatively to be less efficient than the control NSCs. This decrease in efficiency was more pronounced in HGm iPSC lineage NSCs and most pronounced in the HGb iPSC lineage NSCs (Figure 5.2a). Furthermore, brightfield microscopy imaging of the cells that do not stain for TUJ1 (i.e. not neuronally differentiated) in the HGm and HGb cultures appears to show cells with stem cell morphology – large round nuclei with thin surrounding cytoplasm (Figure 5.2b).

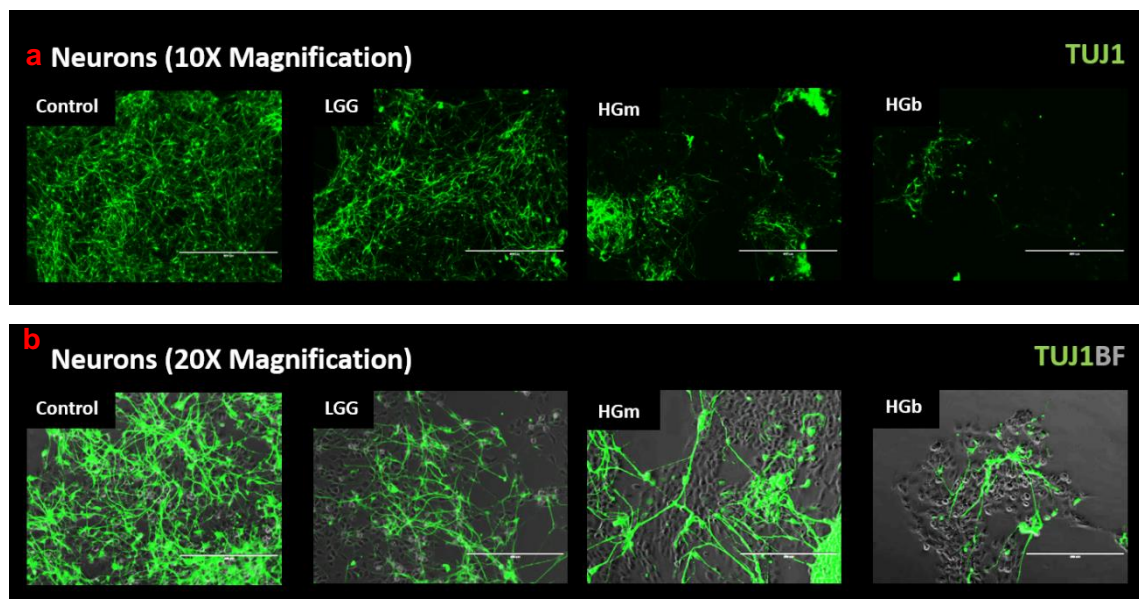


**Figure 5.2:** Immunofluorescence staining of fixed neurons differentiated from control and glioma iPSCs. Starting population for each assay was  $5 \times 10^4$  neural stem cells (NSCs)

with 3 independent experiments conducted per line. **(a)** Cells stain positively for neuronal marker TUJ1. Differentiation efficiency is highest from control iPSCs and appears to decrease with increasing grade. **(c)** Higher magnification images (20X) show that in HGb and HGm cultures, only a few NSCs have differentiated into TUJ1 positive neurons. Background brightfield images show undifferentiated cells with large nuclei and thin cytoplasm, consistent with a stem cell phenotype.

Quantification of the neuronal differentiation assay was conducted by image analysis of fixed cells immunostained for TUJ1 and DAPI. The TUJ1+ neurons generated from each NSC line were expressed as a mean percentage of the total area staining positively for TUJ1 and DAPI (3 independent experiments per line). This analysis showed a decreasing trend in TUJ1+ neurons generated from control NSCs (61.5%), LGG NSCs (53.0%), HGm NSCs (36.9%) and HGb NSCs (14.9%) (Figure 5.3). Statistical analysis between groups showed that this difference was significant between: control versus HGm ( $p=0.0223$ ), control versus HGb ( $p=0.0002$ ), LGG versus HGb ( $p=0.0002$ ) and HGm versus HGb ( $p=0.0214$ ). The difference was not significant between control versus LGG ( $p=0.1281$ ) and LGG versus HGm ( $p=0.0650$ ).

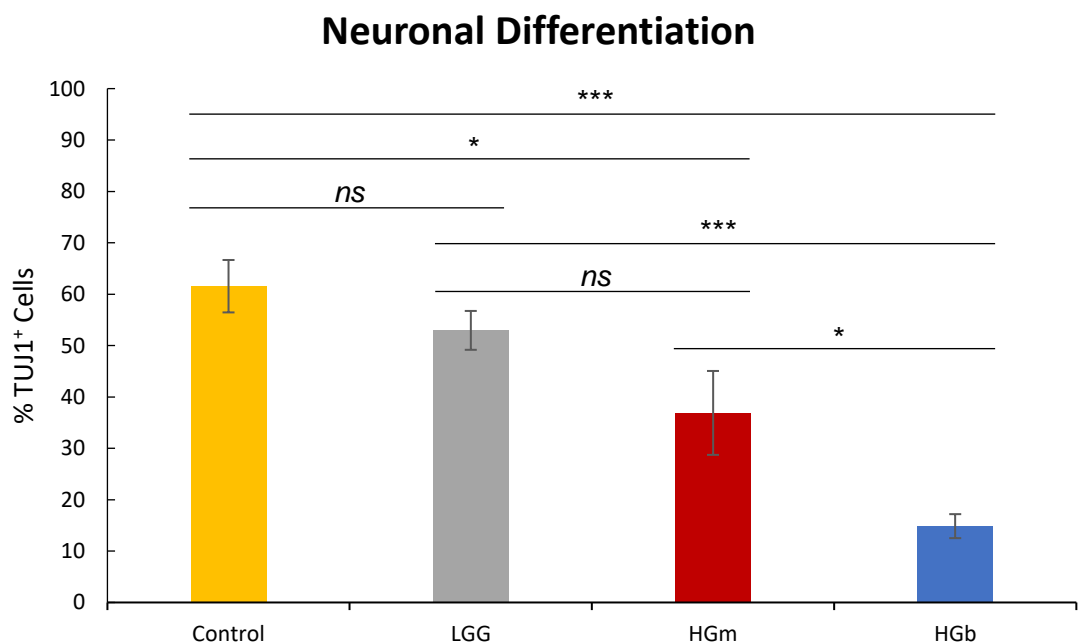


**Figure 5.3:** Quantification of percentage of TUJ1 positive cells showing significant differences in differentiation from NSCs to neurons between control versus HGm, control versus HGb, LGG versus HGb and HGm versus HGb (starting population  $7 \times 10^4$  NSCs;

3 independent experiments per line; mean  $\pm$  SD; Student's t-test; ns = non-significant,  $P \leq 0.05$  were presented as \*,  $P \leq 0.01$  as \*\*,  $P \leq 0.001$  as \*\*\* and  $P \leq 0.0001$  as \*\*\*\*).

### 5.1.2 mRNA-seq analysis of the undifferentiated, partially differentiated and terminally differentiated neurons demonstrate differential gene expression between normal and glioma iPSCs

In order to investigate underlying gene expression differences that might be responsible for the differences qualitatively and quantitatively observed in the neuronal differentiation assay, analysis by mRNAseq was performed at each stage – iPSC, NSC and neuronal. Principal components analysis (Figure 5.4) of the gene expression signatures revealed tight clustering at the iPSC stage of all the lines (control, LGG, HGm and HGb), with minimal divergence. However, at the NSC stage, all iPSC lines exhibited dissimilar gene expression profiles relative to each other, at the same stage of differentiation. This dissimilarity was further pronounced at the neuronal stage but with control and LGG derived gene expression signatures clustering together, and HGm and HGb gene expression signatures clustering together.

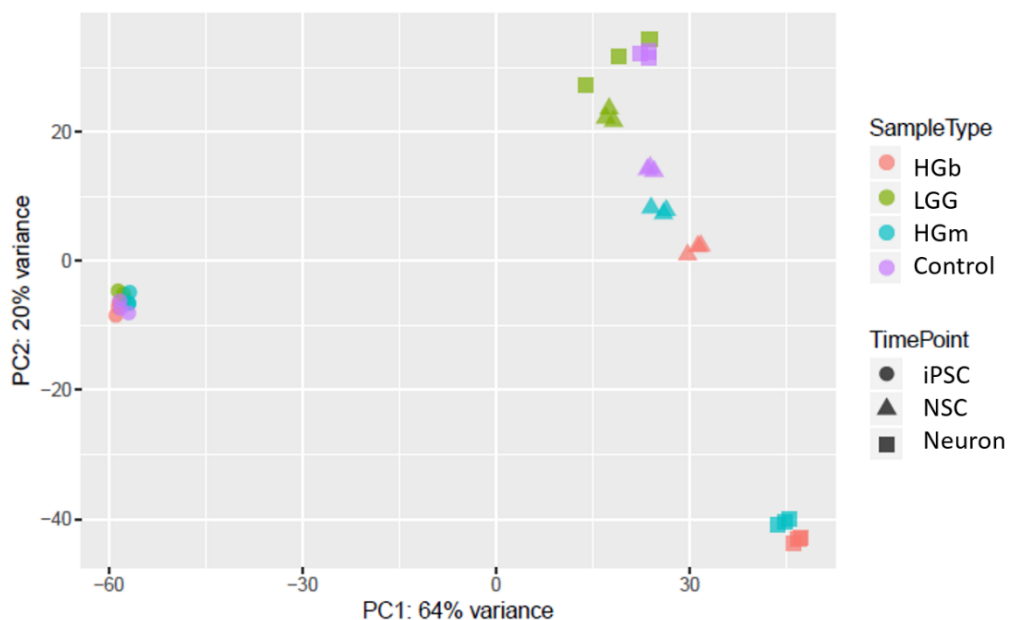


**Figure 5.4:** Principal components analysis of gene expression signatures (by mRNAseq) shows tight clustering at the iPSC stage of all the lines (control, LGG, HGm and HGb). At the neural stem cell stage, all lines exhibit dissimilarity between gene expression profiles. This is further pronounced at the neuronal stage where it appears that control and LGG gene expression signatures appear to cluster, and HGm and HGb gene

expression signatures cluster. *iPSC* = induced pluripotent stem cell, *NSC* = neural stem cell.

In order to further delineate the differential gene expression at each stage of differentiation of the HGG iPSCs (HGm and HGb), individual gene expression fold changes > 1 relative to the control and LGG iPSCs were plotted and identified (Figure 5.5). The most significantly differentially expressed gene at the NSC stage was *hand* and neural crest derivatives expressed 1 (*HAND1*, fold change > -20,  $p < 0.05$ ). The most significantly differentially expressed genes at the neuronal stage were endogenous retrovirus group FRD member 1 (*ERVFRD-1*) and endogenous retrovirus group V member 1 (*ERVV-1*) (both fold change > -20,  $p < 0.05$ ).

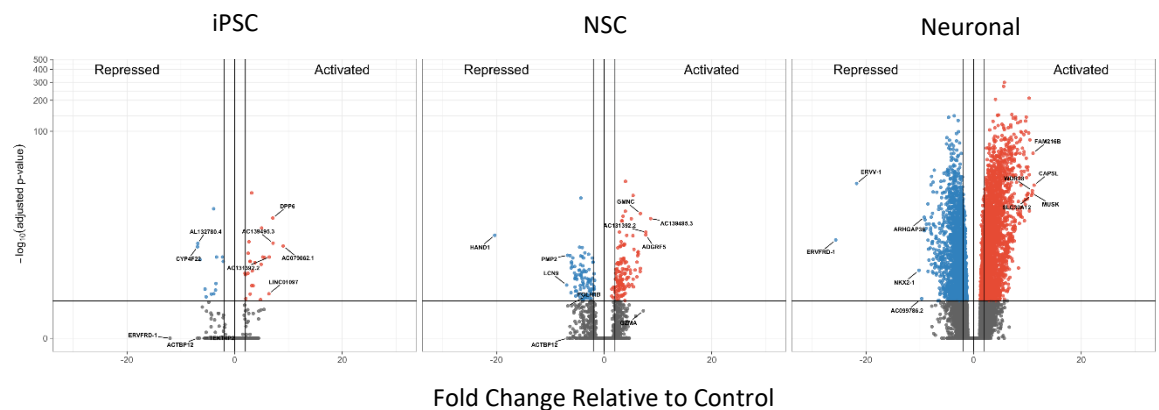


**Figure 5.5:** Volcano plot showing individual gene expression values (by mRNAseq) with fold change > 1 at iPSC, NSC and neuronal stages of differentiation for both contrast-enhancing tumour bulk (HGb) and non-contrast-enhancing tumour margin (HGm) lines. Horizontal line depicts statistically significant results ( $p < 0.05$ ). Interesting candidates for further investigation are *HAND1* (at the NSC stage) as this gene is implicated in neuronal development. *iPSC* = induced pluripotent stem cell, *NSC* = neural stem cell.

Together, these data suggest that the ‘differentiation-block’ phenotype of glioma iPSCs (particularly HGm and HGb) correlates with gene expression profiles that are different to those seen in control iPSCs that have undergone neuronal differentiation. Furthermore, individual genes of interest with highly differential expression at defined stages of differentiation have been identified.

## 5.2. Discussion

Hierarchies of differentiation, with subpopulations of stem-cell-like cells that are capable of self-renewal – as seen in normal tissues – have been previously proposed as an explanation for cellular heterogeneity in cancer (313). This model of cancer has been extended to GBM where it has been proposed that a subset of cells with stem-cell-like characteristics, that fail to differentiate (or dedifferentiate), drive tumour growth and recurrence. Therefore, developing models to study differentiation are important in understanding this subpopulation of cells. This might be in two ways – identifying genes and their transcriptional networks that regulate differentiation/maintain ‘stemness’ and understanding better why previous forced differentiation therapies have failed to be developed into clinical trials or evaluating new forced differentiation therapies.

Reprogramming glioma tissue to pluripotency and then attempting to re-differentiate the derived iPSCs raises interesting questions about the influence of the underlying cancer genome, and at what stage of differentiation it regains dominance over the cell phenotype (60). The results presented here show that iPSCs derived from HGG tissue have a reduced propensity to be directed to terminal (neuronal) differentiation. This infers maintenance of a stem-like phenotype. Previous work has identified the influence of a variety of genes on the maintenance of ‘stemness’ in GSCs – NESTIN, SOX2, ASCL1, FOXP1 and OLIG2 (295,314–316). It has been stated that directed transcriptional programs, involving interactions between so-called ‘master’ transcriptional factors and cis-regulatory elements, dictate developmental fate decisions (314). Genetic aberrations may alter these programs and fates in GBM. Indeed, the transcription factors POU3F2, SOX2, SALL2 and OLIG2 have been shown to alter neurodevelopment and propagate GBM. It may be that in the very same way that over-expression of certain transcription factors can artificially induce pluripotency, they or others can maintain pluripotency and resist differentiation. Characterising the gene expression signatures at the different stages of differentiation may add to our knowledge of transcriptional programs that are responsible for the ‘differentiation block’ phenotype. Indeed, the genes identified in this differential gene expression analysis – HAND1, ERVFRD-1 and ERVV-1 – can be investigated further for their role in glioma biology. HAND1 in particular is very contextual since it is linked to neural-crest development. It remains to be

elucidated whether under-expression of a single gene or wider regulatory networks might be responsible for reduced differentiation capacity. HAND1 is a basic helix-loop-helix (bHLH) transcription factor gene that regulates early trophoblast differentiation (317) and has been associated in humans with cardiac anomalies such as congenital heart defects (318), cleft lips and palates (319) although this latter study showed that under-expression of HAND1 in the distal regions of the neural crest spared the craniofacial anomalies. In mouse brain development, HAND1 has been shown to rely on heterodimerisation with the bHLH E-factor ME2 (317), which in turn is expressed in the cerebral cortex, pyramidal cells of the hippocampal layers of CA1-CA4, Purkinje and granule cell layers of the cerebellum, granular cells of the dentate gyrus and the olfactory neuroepithelium (320). Interrogating the REpository for Molecular BRAin DaTa (REMBRANDT), an US National Institute of Health cancer initiative to provide a large collection of genomic data from brain cancer patients, shows that patients with low expression of HAND1 have a significantly worse overall survival when compared to patients with high expression of HAND1 ( $p = 0.0159$  at 25% threshold) (321,322). Expression of HAND1 in regions of (mouse) brain that are associated with development and neuronal plasticity, in conjunction with the significant under-expression at the neural stem cell stage in the differentiation assay presented in this study, and the clinical link to reduced overall survival in patients with low-expression of HAND1 makes HAND1 a potentially worthwhile target to investigate further.

It has been shown that iPSCs retain a preference to preferentially differentiate into their lineages of origin (323). This has also been shown to extend to iPSCs derived from pancreatic cancer cells (324). When developing human cell models of cancer progression, this preferential differentiation (assuming it extends to iPSCs derived from gliomas) may be considered an advantage as it may be activated during directed differentiation and therefore recapitulate the pathways of differentiation resistance (60). Furthermore, it has been shown previously that some transcription factors can function as oncogenes by hijacking developmental programs to drive tumorigenesis (325). Using iPSC models, as has been done in the differentiation assays described here, could contribute to understanding this dynamic between pluripotency, the cancer genome and the related cell phenotype. Such insights might reveal new therapeutic targets.

Forced differentiation has previously been proposed as a therapeutic strategy in GBM. This builds on the work done in leukaemia where cellular differentiation was shown to override genetic aberrations driving malignant programs (326,327). However, the stability of the induced differentiated state is an important consideration in the efficacy and evaluation of such an approach. One example of this has been the promise shown in using bone morphogenetic protein (BMP) to specifically target glioma stem cells (96), triggering them to exit the cell cycle and differentiate into astrocytes. However, the robustness of the exit from the cell cycle and the ability of all BMP-treated cells to terminally differentiate has been questioned (328). DNA methylation has been found to be incomplete in these cells, with some cells continuing to express high levels of SOX2 and therefore expressing resistance to terminal differentiation (329). Furthermore, some cells retained the capacity to re-enter the cell cycle. Thus, although it appears that GSCs can be engaged in differentiation programs, this failure to achieve differentiation commitment means that more work on BMP-induced differentiation is required. Further refinement of the differentiation assays described in this study using glioma iPSC models may help further delineate the effects of BMP on GSC differentiation and cell cycle dynamics. It may also help evaluate the therapy with respect to the stability of the induced differentiation since glial cells have a much longer life than cells of the haematopoietic system for example and so the possibility of reversion and dedifferentiation must be considered, and studied (329).

An alternative approach towards forcing cells towards a differentiated state may be based on the finding that propagating GSCs in serum culture induced more post-mitotic phenotypic characteristics (102). Again, the differentiation assay described in this study could potentially be used to investigate this in LGGs and HGGs. Furthermore, the chemically defined nature of these assays would lend themselves to the reintroduction of growth factors such as EGF and FGF (aimed at mimicking the hallmark amplifications of EGFR and FGFR signalling pathways in GBM) to investigate their ability to re-enter the cell cycle and reactivate proliferation. In summary, the development of differentiation therapy for gliomas will rely on an improved understanding of why glioma cells evade differentiation commitment (328).

Image quantification of neuronal differentiation assays using patient-derived iPSCs has been shown to be useful in other areas of neuroscience; for functional drug screening and disease modelling (330–332). This approach allows defined readout *in vitro* work to be conducted in a high-throughput (384-well plate) fashion at relatively low cost. Furthermore, the ability to derive the starting population of cells for these screens directly from patients makes them amenable to personalised experimental investigation and precision medicine strategies (333). The differentiation assays described in the present study, particularly the ability to quantify them using image analysis and the ability to interrogate the gene expression signatures at defined stages of the differentiation pathway, potentially make them useful for similar drug screening and disease modelling work in gliomas.

One caveat of using the glioma iPSCs described in the present study in differentiation assays is that it is currently unknown which subclones of the original heterogenous tumour they represent. Thus, any positive findings on forced differentiation observed using this assay must consider that other, differentiation-resistant, clones may be selected after such treatment, that the current model fails to recapitulate.

## 5. Conclusion and Future Work

Despite the significant advances in glioma biology modelling, new models are always desirable. It can be argued that an ideal preclinical glioma model has a few key criteria – genomic similarity to human gliomas (or a defined subset), genetic, epigenetic and intratumoural heterogeneity resembles that of human gliomas, incorporates a micro-environment with regard to presence of BBB, immunocompetence and cell to cell interactions (between glioma cells and with normal brain cells), the model should be stable and reproducible (116).

Despite the significant advances in glioma modelling, treatment for patients has remained largely unchanged over many decades and outcomes remain extremely poor for the highest-grade tumours. Overall survival lags far behind the substantial gains made in other cancers, making glioma very much a cancer of unmet need. The patient journey from rapid onset of symptoms to major neurosurgical intervention followed by adjuvant chemoradiotherapy is life-changing. Worse still, not all patients will respond to this ‘gold standard’ therapy; yet all of them will be exposed to the risk of complications from surgery and suffer the debilitating side effects of the cytotoxic drugs and radiation. Immortalised cell lines grown on adherent tissue culture provide a standardised and well characterised model [66]. However, they suffer from limitations in quantity and quality, exhibit natural senescence (Hayflick limit, [72]) and unpredictable mutational drift in adherent culture with serial passaging [66]. Any downstream translational findings are also not personalised beyond the original donor. New glioma models are therefore urgently needed to offer different insights into the underlying biology of gliomagenesis, treatment resistance and recurrence. Furthermore, models that incorporate personalisation – for example by allowing for the study of an individual patient’s tumour – will enhance the potential to develop precision medicine approaches. Increasingly available, affordable and technically accessible technologies such as reprogramming and cerebral organoid differentiation mean that new *in vitro* glioma models can potentially be developed using these approaches. The ability to use patient primary tissue in these experimental models makes them attractive for future translation.

The existence of a rare fraction of brain tumour initiating cells with stem-like properties that escape anti-tumour therapy has previously been proposed [13].

Previous investigators have shown that glioma cells can be reprogrammed [25]. However, iPSCs that carry genetic drivers of gliomagenesis, derived from primary tissue, with matched controls, would provide a new tool to study glioma stem cells. I have demonstrated that reprogramming well characterised primary tissue that is transferred from the theatre to culture in a timely fashion offers the possibility of investigating the stemness phenotype of brain tumour cells. This is especially valuable in low-grade glioma where there is a paucity of *in vitro* models. Confirming these iPSCs as stable and interrogating them to ensure they faithfully recapitulate enough drivers of the parent glioma to make them worthwhile studying creates a resource that is self-renewing. These iPSCs have been used in well-established neuronal and astrocytic adherent differentiation experiments to study the relationship between the phenotypic stemness characteristics (i.e. terminal differentiation block) and possible responsible underlying genotypic drivers. iPSCs derived from high grade gliomas demonstrate a phenotype resistant to terminal neuronal and astrocytic formation and exhibit a gene expression signature that is significantly different to that of control iPSCs when both undergo differentiation in microenvironmental and chemically controlled conditions. Future work will concentrate on analysing the gene expression signatures at each stage of the differentiation to identify candidate genes possibly responsible for this 'differentiation block' in order to uncover new druggable targets or mechanisms to force differentiate these cells or halt their self-renewal. Orthotopically xenografting partially differentiated iPSCs into NSG mice show that they retain the ability to form tumours in a well-established preclinical model.

Well characterised, truly pluripotent iPSCs derived from primary tissue provide an interesting model in themselves but the potential to differentiate them into a 3-dimensional organoid model is potentially even more useful. Cerebral/tumour organoids formed from iPSCs derived from patient tissue advance current models by offering a human-human context in a 3-dimensional model that is more orthotopic to the parent tumour. Their ability to more faithfully recapitulate human brain development and architecture is in many ways one of their disadvantages too, since the variation in biology observed between humans is also observed *in vitro* between batches of organoids formed from the same iPSCs. However, acknowledging these strengths and caveats makes them complement the wider model systems as no single model system has been shown to be perfect thus far.

I have created tumour organoids from patient-derived iPSCs that demonstrate markedly different phenotypes. Analysing their gene expression demonstrates upregulation of previously established drivers of stemness seen in patient derived cell lines such as *FOXG1* (248). This finding partly validates the tumour organoid model, but other candidate genes are also of potential interest, such as the marked under-expression of *DCX* and *TUBB3*. The LGG tumour organoids show an even more interesting picture where a number of genes are under- (*SOX1*, *DCX*, *NESTIN*) and over-expressed (*FOXG1*, *PAX6*). Investigating these further and potentially manipulating them using gene editing technologies such as CRISPR-Cas9 may provide insights into their role in maintaining the stemness phenotype. Future work will also concentrate on using organoids formed from different combinations of iPSCs e.g. HGb iPSCs with HGm iPSCs, LGG iPSCs with Control iPSCs to study the interaction of potential glioma cells with different invasive and migratory characteristics, and also potential transformation of LGG, respectively.

The interaction of tumour cells with adjacent normal differentiated tissue has been shown to be important in cancer progression (334,335). The environment in which tumours expand and invade would be incorporated in the ideal model (336). Cerebral organoids provide a simplified human brain environment in which to study glioma biology.

Future work comparing the primary tissue samples and the derived iPSCs will need to delineate the genomic mutational signatures, characterise the gain or loss of specific mutations shown to be important in gliomas (48), and elucidate primary cell heterogeneity and its consequences for clonal/subclonal reprogramming dynamics. It will also be important to repeat this analysis and karyotyping at interval passages to determine if there is any genetic mutational drift and/or structural abnormalities that develop after prolonged time in culture. Although reprogramming has been shown to cause widespread resetting of the epigenome (194), it will still be important to characterise the epigenome in the iPSCs derived in this study. Further investigation into the role of *HAND1* in the development of gliomas, through RNA interference (RNAi) for example, may reveal insights into the 'differentiation-block' phenotype. Further interrogating the gene expression signatures at different stages of differentiation may reveal other

gene candidates and/or underlying regulatory transcriptional networks that might be responsible for the 'differentiation block' observed in both the tumour organoid and adherent differentiation cultures. Gene editing approaches, such as CRISPR/Cas9 could then be applied to the iPSCs and/or the tumour organoids directly to evaluate the modulation of targets identified as a result of these analyses.

Ultimately, the iPSC and tumour organoid models that I have developed have significant strengths and limitations. They have the potential to complement the armamentarium of current glioma models and provide further experimental systems to understand the underlying biology of these unrelenting tumours. These model systems also partly address the 3Rs (reduction, replacement, refinement) of *in vivo* testing, provide a human context, could be used in quantifiable throughput drug screening and have the potential to form part of a personalised translational therapy approach. All of these developments and advances are aimed at addressing the very real problems and improving the lives of the ultimate sufferers of this devastating disease – our patients.

## **7. Methods**

### **7.1. Surgical procedure, tissue transfer and cell culture**

Following discussion at the neuro-oncology multi-disciplinary meeting, patients were identified by suitability for surgical debulking of suspected GBM or LGG. Consent for tissue was obtained under the governance of an ethically approved multi-disciplinary regional tissue bank, based at the University of Leeds and compliant with the UK Human Tissue Act 2004. Tumour samples surplus to diagnostic requirements were collected during debulking (High-Grade Bulk = HGb and Low-Grade Glioma = LGG). In addition, non-contrast-enhancing brain tissue peripheral to the mass was collected as part of the routine surgical approach in GBM cases (High-Grade Margin = HGm). It would be anticipated that HGm tissue would exhibit different genotypic and phenotypic properties to the enhancing tumour mass, and thus provide an additional patient-matched model.

Tissue was transported to the lab in PBS and on ice. Following a PBS wash, Dulbecco's modified eagle medium (DMEM)/F-12 medium (Gibco) supplemented with 0.5x B-27 (Invitrogen), 0.5x N-2 (Invitrogen), 40 ng/mL recombinant human basic fibroblast growth factor (bFGF; Gibco), 40 ng/mL epidermal growth factor (rhEGF; R&D Systems), 1x GlutaMAX (Gibco) and 5% (v/v) foetal bovine serum (FBS) (hereafter named 'NP media') based on [24] was added to HGm and LGG samples, and Neurobasal medium (Gibco) supplemented in 0.5x B-27 (Invitrogen), 0.5x N-2 (Invitrogen), 40 ng/mL bFGF (Gibco) and 40 ng/mL rhEGF (R&D systems) (hereafter named 'NB media') based on (88) was added to HGb samples. Mechanical and enzymatic (TrypLE Express, Thermo Fisher Scientific) dissociation into small pieces was undertaken in a 10 cm petri dish (Corning). Contents were transferred to a 50 mL falcon tube (Corning), resuspended in 40 mL of PBS and centrifuged at 300g for 5 minutes. The supernatant was discarded, the pellet resuspended in red cell lysis buffer (BioLegend) 1:10 with dH<sub>2</sub>O and centrifuged at 300g for 5 minutes. The supernatant was discarded, the pellet resuspended in 40 mL PBS and centrifuged at 300g for 5 minutes. The supernatant was discarded, and the pellet resuspended in a quantity of media appropriate to the number of flasks planned for culture. Poly-ornithine/laminin coated 25cm<sup>2</sup> flasks (Corning) were washed with PBS and then 6 mL NP or NB media added (depending on sample). 1 mL of the cell suspension was then pipetted into the flask. Flasks were placed in a humidified 37°C, 5% CO<sub>2</sub>

incubator. Media was changed every 3-4 days and cells passaged at 70-80% confluence. Flasks were washed with PBS prior to enzymatic passaging with TrypLE Express (Thermo Fisher Scientific). The contents of the flask were aspirated and centrifuged in a 50 mL falcon tubes (Corning) at 400g for 5 minutes. The supernatant was discarded, and the pellet resuspended in sample-appropriate media (NB or NP media).

## **7.2. Extracellular flux analysis – quantification of metabolic phenotyping**

Metabolic analysis in real-time was achieved using the XFp extracellular flux analyser (Seahorse Bioscience). Cells were harvested and seeded in triplicate into poly-ornithine/laminin coated microplates (Seahorse Bioscience) at a density of 20,000 live cells per well in sample-appropriate media (NP or NB). Prior to analysis, media was replaced with XF base media (Seahorse Bioscience) supplemented with 25 mM glucose (Sigma) and 0.5 mM sodium pyruvate (Sigma) and adjusted to pH 7.4. Microplates were transferred to a 37°C non-CO<sub>2</sub> humidified incubator and allowed to acclimatise for 30 minutes prior to analysis. Over 60 minutes, 10 measurements were taken for baseline oxygen consumption rate (OCR, pmol/minute) and extracellular acidification rate (ECAR, mpH/minute). Following analysis, a cell count was performed for each well (Countess Automated Cell Counter, Life Technologies) and averaged per cell line to calculate a final rate per 1x10<sup>4</sup> cells.

## **7.3. Sendai virus feasibility in primary cells**

Cells were seeded into poly-ornithine/laminin coated 6-well plates (Corning, 2 wells per cell line) 2 days prior to transduction in sample-appropriate media (NP or NB) and cultured in a humidified 37°C, 5% CO<sub>2</sub> incubator. On the day on transduction, cells were harvested from one well by enzymatic trypsinisation (TrypLE Express, Life Technologies) and used to estimate the cell count in the other well (Countess Automated Cell Counter, Life Technologies). Using the equation below, the volume of virus required was calculated to achieve a multiplicity of infection (MOI) of 5 (Table 4). The titer of virus (Cellular Infectious Units, CIU) was taken from the product Certificate of Analysis (CoA).

$$\text{Volume of virus } (\mu\text{L}) = \frac{\text{MOI (CIU/cell)} \times \text{number of cells}}{\text{Titer of virus (CIU/ml)} \times 10^{-3} (\mu\text{L})}$$

The vector was thawed from -80°C storage by immersing in a 37°C water bath for 5-10 seconds and resting at RT before placing on ice. The calculated volume of virus was added to pre-warmed media and exchanged with the media in the well of seeded cells. Cells were cultured in a humidified 37°C, 5% CO<sub>2</sub> incubator. Media was replaced daily, and images were acquired at 72 hours post-transduction using a digital inverted fluorescence microscope (EVOS, Life Technologies). Cytotoxicity of the cells (up to 50%) was observed to indicate uptake of the virus [40].

**EmGFP Reporter**

<b>LOT LG120001</b>	<b>HGm p3</b>	<b>HGb p3</b>	<b>LGG p0</b>
Cell count total	637000	143850	225750
EmGFP MOI	5	5	5
EmGFP Titer	110000000	110000000	110000000
<b>EmGFP Vol</b>	<b>29.0</b>	<b>6.5</b>	<b>10.3</b>

**Table 4:** EmGFP reporter calculations

**7.4. Reprogramming glioma cells to human induced pluripotent stem cells (hiPSCs)**

The CytoTune-iPS 2.0 Sendai Reprogramming Kit (Life Technologies) was used to transduce each cell line. Cells were seeded, harvested for cell counting and viral volume calculations performed as described above using the following MOIs: KOS = 5, cMyc = 5, Klf4 = 3 (Table 5). Each viral volume was added to appropriate pre-warmed media and exchanged with the media in the well of seeded cells. Workflow was as outlined in Figure 7.1.

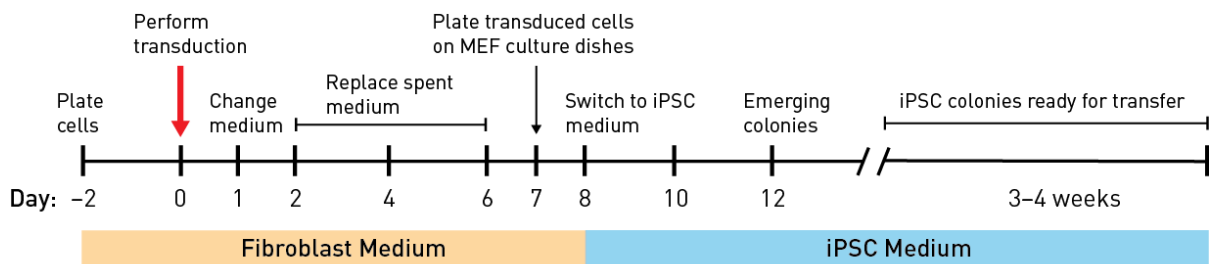


**Figure 7.1:** Workflow for feeder-dependent Sendai iPSC reprogramming (taken from CytoTune®-iPS 2.0 Sendai Reprogramming Kit Manual) [56]

Media was replaced 24 hours after transduction and alternate days thereafter.

### Cytotune 2.0 Sendai

#### LOT

**2120012**

	<b>HGm2 p3</b>	<b>HGb2 p3</b>	<b>LGG p0</b>	<b>HGm p5</b>	<b>HGb p5</b>
Cell count total	637000	143850	1249500	58750	770000
KOS MOI	5	5	3	5	5
KOS Titer	120000000	120000000	120000000	120000000	120000000
<b>KOS Vol</b>	<b>26.5</b>	<b>6.0</b>	<b>31.2</b>	<b>2.4</b>	<b>32.1</b>
Myc MOI	5	5	0.3	5	5
Myc Titer	84000000	84000000	84000000	84000000	84000000
<b>Myc Vol</b>	<b>37.9</b>	<b>8.6</b>	<b>4.5</b>	<b>3.5</b>	<b>45.8</b>
Klf4 MOI	3	3	3	3	3
Klf4 Titer	140000000	140000000	140000000	140000000	140000000
<b>Klf Vol</b>	<b>13.7</b>	<b>3.1</b>	<b>26.8</b>	<b>1.3</b>	<b>16.5</b>

**Table 5:** CytoTune-iPS 2.0 Sendai reprogramming calculations

#### 7.4.1. Plating mouse embryonic feeders (MEFs)

6-well plates (Corning) were coated with 0.1% gelatin solution (Millipore) and allowed to sit at RT for 30 minutes. Commercially irradiated MEFs (Global Stem Cell) containing approximately 2 million MEFs per vial were retrieved from vapour phase liquid nitrogen and placed in a 37°C water bath until defrosted. 1 mL of MEF media consisting of DMEM high glucose (Gibco) supplemented with 10% (v/v) foetal bovine serum (FBS; Gibco), 1% (v/v) minimum essential medium non-essential-amino-acids solution (MEM-NEAA; Gibco) and 55µM β-mercaptoethanol (Sigma) was added drop-wise (to minimise osmotic shock) to the vial and gently mixed. The contents of the vial were pipetted into a 15 mL tube containing 8 mL MEF media. 1 mL of medium from the tube was taken up, used to wash the vial and returned to the tube prior to centrifugation at 300g for 5 minutes. The supernatant was discarded, and the pellet resuspended in fresh MEF media. The gelatin solution was aspirated from the wells and MEFs were plated at a density of  $2.5 \times 10^4$  cells/cm<sup>2</sup>. MEF media was added to each well of a 6-well plate to achieve a final volume of 2 mL/well. Plates were cultured in a humidified 37°C, 5% CO<sub>2</sub> incubator overnight to allow MEFs to adhere. Feeder plates were used within 2-3 days of seeding.

#### 7.4.2. Transfer onto feeder-culture

Transduced cells were transferred onto MEFs at day 7. MEF media was aspirated from feeder plates and replaced with sample-appropriate media (NP or NB).

Wells containing transduced cells were washed with PBS and then enzymatically passaged (0.05% trypsin/EDTA). After rounding up of cells was observed by microscopy, 2 mL media was added to each well and the contents pipetted into a 15 mL falcon tube (Corning) prior to centrifugation at 200g for 4 minutes. The supernatant was discarded, and the pellet resuspended in 5 mL of media. A cell count was performed (Countess Automated Cell Counter) and transduced cells seeded onto MEFs as per Table 6.

Transduced Cell Line	HGm2	HGb2	LGG	HGm	HGb
Cell count/ml	46900	106000	46900	57000	51000
Cells plated onto MEFs	281600	212000	281600	199500	178500

**Table 6:** Numbers of Sendai virus reprogrammed transduced cells seeded onto feeder-culture (mouse embryonic fibroblasts, MEFS)

#### 7.4.3. Picking iPSC colonies

On day 8 after transduction, media was replaced with hESC/hiPSC media consisting of DMEM/F12 (Gibco) supplemented with 20% (v/v) knockout serum (KSR; Gibco), 1% (v/v) MEM-NEAA (Gibco), 1% (v/v) GlutaMAX (Gibco), 55µM β-mercaptoethanol (Sigma) and 10 ng/mL basic fibroblast growth factor (bFGF; Peprotech; added fresh just prior to use) and exchanged daily thereafter. Cells were observed daily under an inverted microscope for the emergence of colonies. Between days 21-28 post-transduction, live cell staining was used to identify colonies that were fully reprogrammed. Colonies for transfer were marked under an inverted light microscope (x10 magnification). Using a sterile 25-gauge needle, the colony was cut into 5-6 pieces in a grid-like pattern and then pipetted using a 200 µL tip into a pre-prepared well of a 12-well plate (Corning) with MEF-feeder layer. Colonies were maintained, passaged and frozen as per protocols described hereafter.

#### 7.4.4. Live stain immunocytochemistry

AlexaFluor 488 conjugated Tra-1-60 mouse anti-human antibody solution (Life Technologies) was retrieved from 4°C storage and centrifuged at 10000g for 30 seconds at RT. A 1:50 volume of the antibody solution was added directly to the cell culture media and mixed by gentle swirling. The plate was incubated at 37°C and 5% CO<sub>2</sub> for 30 minutes. The staining solution was aspirated, and the cells

washed with FluoroBrite DMEM (Life Technologies) 3 times, without aspirating after the last wash. Images were immediately acquired using a digital inverted fluorescence microscope (EVOS, Life Technologies). The FluoroBrite DMEM was replaced with fresh hESC/hiPSC medium and cells returned to culture in a humidified 37°C, 5% CO<sub>2</sub> incubator.

Plates were inspected daily. Differentiated colonies were marked under an inverted light microscope (x10 magnification) and removed in a sterile tissue culture hood using a P200 pipette tip with the aid of magnification loupes. hESC/hiPSC media was replaced daily. iPSCs were passaged when reaching confluence and/or when differentiation within colonies started to appear.

#### **7.4.5. Maintenance, passage and freezing of iPSCs**

Differentiated colonies were removed as described above. Wells were washed with PBS prior to addition of 1mg/mL Collagenase IV (1 mL per well of a 6-well plate Thermo Fisher Scientific). The plate was incubated at 37°C for 10 minutes, or until curling or thickening of the colony edges was visible. The enzyme was aspirated, the well washed with PBS and 1 mL hESC/hiPSC medium added. A cell lifter (Corning) was used to scrape the well and the contents pipetted into a 15 mL falcon tube (Corning). A further 2 mL of hESC/hiPSC media was used to wash the well and added to the tube prior to centrifugation at 200g for 4 minutes. The supernatant was discarded, and the pellet resuspended in 1 mL hESC/hiPSC medium supplemented with 10 ng/mL bFGF 10ng/mL added fresh just prior to use. The pellet was gently triturated to get medium-small fragments prior to seeding into a well of a 6-well plate of MEFs (pre-washed with PBS and containing 1 mL hESC/hiPSC medium supplemented with 10 ng/mL bFGF added fresh just prior to use). Cells were cultured in a humidified 37°C, 5% CO<sub>2</sub> incubator and media replaced daily thereafter.

To freeze iPSCs, cells were passaged up to the point of centrifugation as described above. The supernatant was discarded and 500 µL of hESC/hiPSC medium added. 500 µL of freezing medium consisting of hESC-quality FBS (Gibco) supplemented with 20% (v/v) dimethyl sulfoxide (DMSO; Sigma) was then added and the pellet resuspended in the combined media. The contents were pipetted into a cryovial (Corning), which was then placed inside an

isopropanol-containing freezing container (Mr Frosty, VWR) and stored at -80°C for 24-48 hours prior to transfer into vapour phase liquid nitrogen storage.

The maintenance (on MEF-feeder culture), passaging and freezing of human embryonic cells (hESCs) used the same hESC/hiPSC media and followed the same protocols as those described for hiPSCs.

#### **7.4.6. Mycoplasma testing**

Supernatant was collected from culture media of cells at 70-80% confluence and centrifuged at 400g for 5 minutes to remove debris. 1 mL of the cleared supernatant was transferred to a sterile microcentrifuge tube (Eppendorf). Samples were tested using the MycoAlert Mycoplasma Detection Kit (Lonza). Briefly, the test exploits the activity of mycoplasma enzymes which react with the MycoAlert substrate and catalyse the conversion of ADP to ATP, which is in turn converted to a light signal via the luciferase enzyme in the MycoAlert reagent. A ratio is calculated between the amount of ATP in the sample before and after the addition of the substrate. A result of <0.9 is negative. The MycoAlert Assay Control Set (Lonza) is used alongside to provide a lyophilised positive control (proprietary) and the assay buffer is used as the negative control.

#### **7.4.7. Sendai virus clearance testing**

SeV clearance testing (expected between five and fifteen passages following reprogramming according to the manufacturer's instructions (CytoTune-iPS 2.0 Sendai Reprogramming Kit, Life Technologies) was performed by qRT-PCR (as described later) using the Sendai Virus TaqMan Gene Expression Assay (Applied Biosystem; Mr04269880\_mr; forward primer GGA TCA CTA GGT GAT ATC GAG C; reverse primer ACC AGA CAA GAG TTT AAG AGA TAT GTA TC; 181 bp). As per the manufacturer's instructions, SeV transduced cells saved at day 7 of the reprogramming protocol was used as a positive control.

#### **7.4.8. Transfer onto feeder-free culture**

Complete StemFlex medium (Gibco) was prepared as per the manufacturer's instructions. Plasticware (Corning) was coated with 0.15 mL/cm<sup>2</sup> with Geltrex (Gibco) thawed overnight at 4°C, mixed by gentle inversion and diluted 1:100 in cold DMEM/F12 with Glutamax supplement (Gibco). Once coated, plates were

incubated at 37°C, 5% CO<sub>2</sub> for 1 hour. When iPSCs reached confluency on MEFs, manual clean-up of any differentiated colonies was performed by marking under inverted light microscope and scraping using a 200 µm pipette tip. Then the well containing the iPSCs was rinsed with 0.2 mL/cm<sup>2</sup> of DPBS (no calcium and no magnesium, Gibco), 0.1 mL/cm<sup>2</sup> of 1 mg/mL Collagenase Type IV (Thermo Fisher Scientific) added and the cells incubated at 37°C, 5% CO<sub>2</sub> for approximately 45 minutes. The plate was intermittently inspected, and the incubation stopped when the edges of the colonies curled up. Complete StemFlex medium (Gibco) 0.1 mL/cm<sup>2</sup> was then added and the colonies dislodged using a 1 mL pipette. The suspended colonies were then transferred to a 15 mL conical tube. More complete StemFlex medium (Gibco) 0.1 mL/cm<sup>2</sup> was added to the well previously containing the iPSCs to capture any remaining colonies and this also added to the same 15 mL conical tube. The suspended colonies were gently triturated using a 200 µm pipette. The colony fragments were allowed to sediment to the bottom of the tube by gravity over 5 minutes, the supernatant discarded, and the colony fragments resuspended using 0.2 mL/cm<sup>2</sup> (of the original well surface area) complete StemFlex medium (Gibco) and pipetting up and down twice. The clusters were again allowed to gravity sediment over 5 mins, the supernatant discarded, and the colony fragments resuspended using 0.2 mL/cm<sup>2</sup> (of the original well surface area) complete StemFlex medium (Gibco) and pipetting up and down twice. During this time, the Geltrex (Gibco) matrix was aspirated from the plate into which the iPSCs were planned to be transferred and 0.2 mL/cm<sup>2</sup> complete StemFlex medium (Gibco) added. The resuspended iPSC colony fragments were distributed into wells of the Geltrex (Gibco) coated plates. The plates were moved quickly in several side-to-side motions in both directions in order to disperse the colony fragments evenly in each well. Cells were cultured in a humidified 37°C, 5% CO<sub>2</sub> incubator and complete StemFlex medium (Gibco) 0.2 mL/cm<sup>2</sup> replaced daily thereafter. The first passage after transfer from feeder-to feeder-free culture was performed in the same way as on feeder-culture (described earlier) but with 0.2 mL/cm<sup>2</sup> 500 µm EDTA (Gibco) instead of Collagenase Type IV (Thermo Fisher Scientific) and without the use of ROCKi. From this point onwards, 0.2 mL/cm<sup>2</sup> complete StemFlex medium was replaced on an every-other-day basis. If the cells were to be left for two days without feeding (for example, over a weekend), double the medium was used on the prior feed (i.e. 0.4 mL/cm<sup>2</sup>).

#### **7.4.9. Characterisation of glioma iPSCs**

Flow cytometry for pluripotency markers (SSEA1, SSEA4, EpCam, Tra-1-60) and embryoid body formation for tri-germinal layer differentiation analysis (endoderm – *SOX17, CXCR4, Gata6*; mesoderm – *NCAM, MixL1, vimentin, DCN*; ectoderm – *Pax6, NeuroD1, Hes5*) by qRT-PCR was performed by Orla O’Shea (UK Stem Cell Bank, National Institute for Biological Standards and Control). Karyotyping was performed by the North East Thames Regional Genetics Laboratory (Great Ormond Street Hospital for Children NHS Foundation Trust).

#### **7.5. Maintenance, passage and freezing of R1 mouse embryonic stem cells (mESCs)**

Mouse R1 (ATCC) embryonic stem cells (mESCs) were cultured MEF feeder layer (plated as described above). mESCs were cultured in mESC media consisting of DMEM high glucose (Gibco) supplemented with 10% (v/v) KSR (Gibco), 0.1 mM MEM-NEAA (Gibco), 2mM glutamine (Gibco), 1 mM sodium pyruvate (Gibco), 0.1 mM  $\beta$ -mercaptoethanol (Sigma) and 1000U/mL leukaemia inhibitory factor (LIF; Millipore) in a humidified 37°C, 5% CO<sub>2</sub> incubator and media replaced daily thereafter. Cells were passaged as described above every 2-3 days or when mESC colonies were confluent and in close contact. Stocks were frozen down in vials as described above.

#### **7.6. Cerebral and tumour organoid formation**

The method for cerebral organoid formation is based on the protocol published by Lancaster and Knoblich [57]. Briefly, embryoid bodies (EBs) reaggregate from dissociated single stem cells (mESCs, hESCs or iPSCs). Using media that only supports the growth of ectoderm, EBs were subjected to neural induction and then transferred to Matrigel (Corning) droplets to promote neuroepithelial bud outgrowth. Following expansion and formation of fluid-filled lumens of the buds, the tissues were transferred to spinner flasks to promote growth and development into defined brain regions through improved nutrient and oxygen exchange. As the protocol is faster for organoids formed from mESCs than from hESCs, mouse organoids were generated first to become familiar with the methods and characterisation methods. To investigate tumour incorporation of primary tissue

into organoids, mESCs were co-cultured with dissociated primary LGG cells and then standard organoid protocols followed.

Stem cells (mESCs or hESCs) were expanded on MEF-feeder culture in a 6-well plate as previously described. Cells were harvested using dispase (Life Technologies) and incubated (up to 40 minutes) at 37°C until the colonies were only attached to the plate at their centres. hESC/hiPSC or mESC media as appropriate was added and the dish tapped vigorously to release the colonies (differentiated cells and MEFs remain in the well). The intact colonies and media were transferred to a 15 mL falcon tube and the colonies allowed to settle to the bottom. The supernatant was discarded and further hESC/hiPSC or mESC media added. This was repeated. The colonies were then resuspended in 1 mL of trypsin/EDTA (Gibco) and incubated for 2 minutes at 37°C. 1 mL trypsin inhibitor (Sigma) was added and the mixture triturated until cloudy with single cells. A cell count was then performed (Countess Automated Cell Counter, Life Technologies). hESC/hiPSC or mESC media as appropriate was added to the tube prior to centrifugation at 270g for 5 minutes. The supernatant was discarded, and the pellet resuspended in sufficient hESC/hiPSC or mESC media as appropriate to achieve a final solution of 9000 live hESCs/hiPSCs or 2000 mESCs per 150 µL. This volume was plated in each well of a low-attachment 96-well U-bottom plate (Corning). EBs were fed on alternate days with hESC/hiPSC96 or mESC96 media as appropriate. When EBs reached >350 µm, hESC/hiPSC96 or mESC96 media (without bFGF/ROCKi or SB431542 respectively) was continued on alternate days until EBs reached ~ 500-600 µm in diameter. EBs were then individually transferred to single wells of a low-attachment 24-well plate (Corning) containing 500 µL neural induction medium consisting of DMEM-F12 (Gibco) supplemented with 1% (v/v) N2 (Gibco), 1% (v/v) GlutaMAX (Gibco), 1% (v/v) MEM-NEAA (Gibco) and 1 µg/mL heparin (Sigma). A further 500 µL neural induction medium was added 48 hours later. After EBs began to show radial organisation of a pseudostratified epithelium and appeared brighter on the outside (approximately 4-5 days), they were transferred to Matrigel (Corning) droplets. All steps were performed under a sterile tissue culture hood. Plates were placed in a humidified 37°C, 5% CO<sub>2</sub> incubator with in-between all steps. All steps were followed as per human organoids in the formation of mouse organoids, except faster timings were used – EBs were

transferred to 24-well plates on day 4, into Matrigel droplets on day 6 and into the spinner flask on day 9.

Primary LGG tissue was surgically obtained and made into single cell suspension as described earlier. The average human brain volume is 1130cm<sup>3</sup> in women and 1260cm<sup>3</sup> in men [58] and the range of LGG tumour sizes has been reported in one study as 2.7-231 mL [59]. Taking the largest tumour size in the average of the two brain sizes equates to approximately 20% LGG tumour volume in a full adult brain. Cells were therefore co-cultured in the following ratios (mESCs:LGG cells): 1700:300 (15% LGG) and 1400:600 (30% LGG). The largest tumour size was taken into account in order to maximise the chance of successfully establishing presence of LGG cells in the organoid.

Matrigel was thawed on ice at 4°C. Parafilm was sprayed with 70% ethanol and dimples created by pressing using a gloved finger into a 200 µL pipette tip tray. The aggregates were individually transferred into each dimple, the excess media aspirated, 30 µL Matrigel (Corning) added per aggregate and a 10 µL pipette tip used to centre the aggregate within the droplet. The Parafilm was placed into a 60 mm plate and the droplets allowed to polymerise in a 37°C incubator. 5 mL cerebral organoid differentiation media consisting of DMEM/F12 (Gibco) and NB medium (Gibco) in a 50:50 ratio supplemented with 0.5% (v/v) N2 (Gibco), 0.025% (v/v) insulin (Sigma), 1% (v/v) penicillin-streptomycin (Sigma), 1% (v/v) GlutaMAX (Gibco), 0.5% (v/v) MEM-NEAA (Gibco), 52.2 µM β-mercaptoethanol (Sigma) and 1% (v/v) B27 without vitamin A (Gibco) was added to the dish and the droplets shaken off the Parafilm into the media. The dish was placed in a humidified 37°C, 5% CO<sub>2</sub> incubator for 4 days, with replacement of the cerebral organoid differentiation media on alternate days.

Using a cut 1 mL pipette tip, the droplets were transferred to spinner flasks (Corning) containing spinner flask media (the same as cerebral organoid differentiation media but the B27 supplement has vitamin A). Spinner flasks were sited on magnetic stirrer plates and placed in a humidified 37°C, 5% CO<sub>2</sub> incubator. Spinner flask media was changed weekly.

### **7.6.1. Preparing organoids for immunocytochemistry**

Organoids in Matrigel (Corning) were transferred from the spinner flask into a 24-well plate. Media was aspirated, and a PBS wash performed. 4% (w/v) paraformaldehyde (PFA) was added and the plate chilled at 4°C for 15 minutes. The PFA was replaced with PBS and allowed to stand at RT for 10 minutes. The PBS wash was repeated twice more. On the final wash, 1 mL of 30% (w/v) sucrose solution was replaced and the plate chilled at 4°C overnight. In a fume cupboard, a metal container was filled with isopentane and then placed on dry ice for 5 minutes. Tissue-Tek Optimal Cutting Temperature solution (OCT, Sakura) was poured slowly into a histology cassette until half full and allowed to partially polymerise. Organoids were then transferred from sucrose using a cut 1 mL pipette and embedded into the OCT. More OCT was added and allowed to polymerise until a block was formed around the embedded organoids. 20 µm sections were cut on a cryostat and collected on glass slides.

### **7.7. iPSC differentiation to neural stem cells (NSCs) and neurons**

iPSCs were differentiated to NSCs using a neural stem cell induction kit (Thermo Fisher Scientific) according to the manufacturer's instructions. Briefly,  $3 \times 10^5$  iPSCs were plated into 1 well of a 6-well plate on MEF-feeder culture, as previously described, with hESC/hiPSC media supplemented with 10 µM ROCKi (Sigma) and 10 ng/mL bFGF (Peprotech) (day 0). Media was exchanged for 2.5 mL pluripotent stem cell neural induction medium (PSC NIM) consisting of NB media (Gibco) supplemented with 0.4% (v/v) neural induction supplement (Gibco) on days 1 and 3. Media was exchanged for 5 mL PSC NIM on days 4 and 6. On day 7, cells were harvested by aspirating the media, adding 1 mL StemPro Accutase Cell Dissociation reagent (Gibco), incubating at 37°C for 5-8 minutes and mobilising with a cell lifter (Corning). Cells were transferred to a 15 mL conical tube, triturated with a 5 mL pipette, passed through a 100 µm cell strainer and centrifuged at 300g for 4 minutes. The supernatant was discarded, DPBS (Gibco) added and centrifuged at 300g for 4 minutes. The supernatant was discarded, and pre-warmed (37°C) neural expansion medium (NEM) consisting of 50:50 NB media (Gibco) and DMEM/F12 (Gibco) supplemented with 2% (v/v) neural induction supplement (Gibco) and 5 µM ROCKi (Sigma) was added. A cell count was performed using an automated cell counter (Countess, Thermo Fisher Scientific). Cells were plated at a density of  $1 \times 10^5/\text{cm}^2$  on Geltrex (Gibco) coated

6-well plates (Corning) or 4-chamber slides (Corning). Media was exchanged for 2.5 mL NEM without ROCKi (Sigma) in each well of a 6-well plate on days 8, 10 and 12. Cells were passaged when confluent using StemPro Accutase Cell Dissociation reagent (Gibco), and stocks frozen down in NEM supplemented with 10% DMSO (Sigma) using an isopropanol-containing freezing container (Mr Frosty, VWR) as required. Cryovials (Corning) were stored at -80°C for 24-48 hours prior to transfer into vapour phase liquid nitrogen storage. The cells in the 4-side chambers were fixed on day 8 for immunocytochemistry.

NSCs at passage 2 or beyond were plated at a density of  $5 \times 10^4/\text{cm}^2$  in 4-well slide chambers (Corning) coated with  $5 \mu\text{g}/\text{mL}$  poly-L-ornithine (Sigma) and  $5 \mu\text{g}/\text{mL}$  laminin (Gibco) containing NEM (day 0). Media was exchanged to neuronal media consisting of NB media (Gibco) supplemented with 2% (v/v) B27 (Gibco) and 2 mM GlutaMAX (Gibco) on days 2, 5 and 8. On day 10, cells were washed with PBS (Gibco) three times and fixed with 4% PFA for immunocytochemistry and image analysis.

### **7.8. Immunocytochemistry**

Cells were fixed with 4% (w/v) paraformaldehyde (PFA) at RT for 10 minutes. Cells were permeabilised with PBS containing 0.2% (v/v) Triton X-100 for 20 minutes. Non-specific antibody (Ab) binding was reduced by adding PBS containing 10% (v/v) FBS and 0.03% (v/v) Triton X-100 at RT for 1 hour. Subsequently, cells were incubated with primary Abs in PBS containing 10% (v/v) FBS and 0.03% (v/v) Triton X-100 at 4°C overnight. The following primary Abs were used: anti-human SOX2 (Cell Signaling, 1:200), anti-human Nestin (Millipore, 1:200), anti-TUJ1 (Covance, 1:200), anti-GFAP (Dako 1:200), anti-Ki67 (abcam; 1:200) anti-MAP2 (abcam, 1:1000). Secondary Abs were used at 1:200 dilutions: AlexaFluor- (Molecular Probes) or Cy3-conjugated (Jackson ImmunoResearch). Nuclei were counterstained with DAPI (Sigma, 1:10000) and images were acquired using a digital inverted fluorescence microscope (EVOS, Life Technologies).

Whole organoids and cryosections were permeabilised and staining performed as described above. The primary Ab used was anti-human vimentin (Dako, 1:100). An AlexaFluor 488 (Molecular Probes) conjugated secondary Ab (1:200)

was used. Nuclei were counterstained with DAPI (Sigma, 1:10000). Images were acquired using an EVOS digital inverted fluorescence microscope (Life Technologies) and confocal microscope (Nikon A1).

## 7.9. Illumina gene expression analysis

### 7.9.1. qRT-PCR

Cells were harvested from adherent culture and RNA was extracted using the RNeasy mini kit (Qiagen), according to the manufacturer's instructions for purification of animal cells. Briefly, samples were lysed and homogenized by passing through QIAshredder spin columns prior to the addition of a binding solution and ethanol. Spin-column centrifugation was then used to promote hydrogen-binding of RNA to a hydrophilic silica membrane. RNA was then eluted into water. Buffers that inhibit RNase were used during isolation and purification to minimise RNA degradation. Complementary DNA (cDNA) was synthesised using the SuperScript II Reverse Transcriptase with oligo(dT) (Invitrogen) according to the manufacturer's instructions. This method anneals the single-stranded DNA oligo(dT) to the 3' end of RNA that in turn primes reverse transcriptase (that has been genetically engineered to reduce RNase activity) to synthesise cDNA from the RNA.

For qRT-PCR cDNA was analysed using TaqMan Gene Expression Assays (Applied Biosystems) using an ABI 7500 thermal-cycler. Reaction mixtures were prepared in triplicates as per Figure 7.2. The TaqMan probes used are shown in Table 7.

<b>Component</b>	<b>Volume for 1 reaction</b>
20x TaqMan Gene Expression Assay	0.75 $\mu$ L
2x TaqMan Universal PCR Master Mix II, no	7.5 $\mu$ L
UNG	0.375 $\mu$ L
cDNA	6.375 $\mu$ L
Nuclease-free H <sub>2</sub> O	
Total reaction volume	15 $\mu$ L

<b>Time</b>	<b>Temperature</b>
-------------	--------------------

10 min	95°C	}	40 cycles
15 sec	95°C		
1 min	60°C		

**Figure 7.2:** Reaction mixture compositions and qRT-PCR conditions

Data was analysed using the  $2^{-\Delta\Delta C_t}$  method. *GAPDH* was used as the housekeeping gene.

Gene	Assay ID
<i>KLF4</i>	Hs00358836_m1
<i>NANOG</i>	Hs02387400_g1
<i>POU5F1/OCT4</i>	Hs04260367_gH
<i>FOXG1</i>	Hs04407035_g1
<i>NES</i>	Hs04187831_g1
<i>PAX6</i>	Hs01088114_m1
<i>SOX1</i>	Hs01057642_s1
<i>SOX2</i>	Hs00415716_m1
<i>BCL11B</i>	Hs01102259_m1
<i>DCX</i>	Hs00167057_m1
<i>EOMES/TBR2</i>	Hs00172872_m1
<i>MAP2</i>	Hs00258900_m1
<i>NEUROD1</i>	Hs01922995_s1
<i>S100B</i>	Hs00902901_m1
<i>SATB2</i>	Hs00328182_m1
<i>TUBB3/TUJ1</i>	Hs00801390_s1
<i>OLIG2</i>	Hs00300164_s1
<i>EGFR</i>	Hs01076090_m1
<i>IDH1</i>	Hs01909600_s1
<i>MGMT</i>	Hs01037698_m1
<i>MKI67</i>	Hs04260396_g1
<i>MYC</i>	Hs00153408_m1
<i>PDGFRA</i>	Hs00998018_m1
<i>PTEN</i>	Hs02621230_s1

<i>TGFB1</i>	Hs00998133_m1
<i>TP53</i>	Hs01034249_m1
<i>TRRAP</i>	Hs00268883_m1
<i>VIM</i>	Hs00958111_m1
<i>GFAP</i>	Hs00909233_m1
<i>GAPDH</i>	Hs02758991 g1

**Table 7:** List of TaqMan probes used for qRT-PCR

For organoids at day 15, an additional retrieval step was performed to remove the Matrigel prior to RNA extraction. Briefly, the organoid embedded in 30  $\mu$ L Matrigel was submerged into 300  $\mu$ L of non-enzymatic Cell Recovery Solution (BD) in a microcentrifuge tube which was subsequently gently shaken on a flat shaking platform in a 4°C cold room for 1 hour. PBS washes (1 mL each) were performed 3 times prior to RNA extraction. For organoids, 3 biological replicates were analysed (2 organoids each from 3 separate batches used per biological replicate). Organoids derived from LGG, HGm, and HGb iPSCs were compared to organoids derived from hESCs.

### 7.9.2. Whole genome sequencing

Genomic DNA (gDNA) was extracted from single cell suspensions generated from LGG, HGm and HGb primary tissue and derived iPSCs using the QIAmp DNA mini kit (Qiagen) following the manufacturer's spin column protocol. Extracted gDNA was purified (to eliminate RNA) by using Riboshredder RNase Blend (Epicentre) and cleaned up using gDNA Clean and Concentrator kit (Zymo), following the manufacturer's protocol in both cases. Quantification of extracted and purified gDNA was performed on a microplate reader using PicoGreen dsDNA reagent (Thermo Fisher Scientific). Quality control was performed using agarose gel electrophoresis to detect DNA and RNA bands. Whole genome sequencing was performed at 30X read depth per sample in triplicate (to achieve a final read depth per primary/iPSC line of 90X) by Edinburgh Genomics using the Illumina HiSeq X.

### **7.9.3. mRNA sequencing**

Total RNA was extracted from cells at the iPSC, NSC and neuronal stages of differentiation. Randomisation of plating was calculated by a statistician at the University of Cambridge. Gene expression profiling was done by Cambridge Genomic Services, University of Cambridge using the Illumina HiSeq 4000. The hg19 (GRCh37) homo sapiens genome was used as a reference.

### **7.10. Computational mRNA-seq gene expression analysis**

Raw data at the iPSC stage was analysed by aligning reads to the hg19 (GRCh37) reference using STAR (2.5.2b) on Galaxy. Actual read counts against the GRCh37.75 gene annotation were obtained using the package featurecounts (1.4.6) on Galaxy. Read counts were normalized using variance stabilising transformation (VST) and regularised log transformation (rld) using DeSeq2 in RStudio. VST-normalized expression levels were transformed to Z-scores by subtracting the mean value of each gene and dividing by the standard deviation. Expression levels were compared on 34 genes known to be relevant based on the TaqMan hPSC Scorecard Assay (235). Our lines were compared to the GSE73211 set by hierarchical Euclidean clustering and generating a heatmap using the Pheatmap R and RColorBrewer packages. Principal components analysis (PCA) plots of both the VST and rld expression levels were generated using the prcomp function and the ggplot2 R package in RStudio.

Analysis of the raw data comparing the different stages of differentiation was performed by Stephane Ballereau and Florian Markowitz (both University of Cambridge).

### **7.11. Computational whole genome sequencing analysis**

Analysis of the raw data comparing the primary tissue to the derived iPSCs was performed by Stephane Ballereau and Florian Markowitz (both University of Cambridge).

### **7.12. Animal experiments**

Animal experiments were carried out under UK Home Office project and personal licensing. All *in vivo* work was approved by the University of Leeds Animal Welfare & Ethical Review Committee (AWERC) and in line with the Animal

(Scientific Procedures) Act 1986 and in accordance with the UK National Cancer Research Institute (NCRI) Guidelines for the welfare of animals. Mice were maintained under standard conditions on a 12-hour day/night cycle with food and water ad libitum.

Orthotopic xenotransplantation assays were performed aseptically on 6- to 10-week old mice under general gas anaesthesia by stereotactically injecting  $1 \times 10^5$  NSCs (derived from LGG, HGm and HGb iPSCs as described earlier) suspended in 2  $\mu$ L PBS (Gibco) with 30% Matrigel (Corning) into the right striatum (2.5 mm from the midline, 2.5 mm anterior to the bregma, 3 mm deep) of NSG mice. Mice were monitored daily for signs of sickness, pain or weight loss. After 16 weeks, mice were sacrificed, and tissue fixed by intracardiac perfusion of PBS (Gibco) followed by 4% (w/v) PFA. The brains were removed, transferred into 4% (w/v) PFA and subsequently sectioned for immunocytochemical analysis as described later.

### **7.13. Histology**

This method was derived from Bancroft and Gamble (2008) [60]. Organoids were fixed in 4% (w/v) PFA overnight prior to securing in histology cassettes. Tissues were then dehydrated through graded alcohols and xylene. The cassettes were then incubated in two lots of 100ml liquid paraffin wax for 1 hour each. A small amount of liquid paraffin wax was poured into a wax block mould and partially allowed to set. Organoids were then embedded into the partially set wax and covered in liquid paraffin wax prior to cooling on ice. Upon hardening of the wax, excess wax was trimmed from the blocks before the tissues were sectioned at 5  $\mu$ m on a microtome. Sections were floated on a 40°C water bath, collected onto glass slides and left on a hot plate to dry. Once dry, sections were dewaxed and rehydrated through graded alcohols before finally rinsing in running tap water for 3 minutes.

The slides were dipped in 100ml Modified Mayer's haematoxylin for 1 minute and then washed in running tap water until the slides were clear (5-10 minutes). The slides were then dipped in eosin for 3 minutes before being finally dehydrated through graded alcohols and xylene. Coverslips were mounted using DPX mountant (Sigma). Slides were dried for 30 minutes prior to viewing under a light

microscope (Olympus) and selected slides digitally imaged using a microscope camera (Zeiss AxioCam HR).

#### **7.14. Image analysis**

Quantification of neuronal differentiation was performed by calculating the region of interest (ROI) by defining the area staining positively for DAPI and the area staining positively for TUJ1 (neurons) using colour thresholding in ImageJ (default setting, colour space: HSB). The area staining positively for TUJ1 was then calculated as a percentage of the total area staining positively for TUJ1 and DAPI.

#### **7.15. Statistical analysis**

Differentiation data was analysed by 1-way analysis of variance (ANOVA) and one-tailed paired Student's t-test and expressed as mean  $\pm$  standard deviation (SD). P values of  $\leq 0.05$  were presented as \*;  $P \leq 0.01$  as \*\*,  $P \leq 0.001$  as \*\*\* and  $P \leq 0.0001$  as \*\*\*\*.

## List of Abbreviations

<i>μL</i>	microlitre
<i>μm</i>	micrometre
<i>μM</i>	micromolar
<i>Ab</i>	Antibody
<i>AFP</i>	Alpha Feto Protein
<i>ANOVA</i>	Analysis Of Variance
<i>AWERC</i>	Animal Welfare & Ethical Review Committee
<i>bFGF</i>	basic Fibroblast Growth Factor
<i>bHLH</i>	basic Helix-Loop-Helix
<i>BMP</i>	Bone Morphogenetic Protein
<i>BTIC</i>	Brain Tumour Initiating Cell
<i>BTSC</i>	Brain Tumour Stem Cell
<i>cDNA</i>	complementary DNA
<i>CE</i>	Contrast Enhancement
<i>CGH</i>	Comparative Genomic Hybridisation
<i>CIU</i>	Cellular Infectious Units
<i>cm</i>	centimetre
<i>CM</i>	Confocal Microscopy
<i>CNV</i>	Copy Number Variation
<i>CNS</i>	Central Nervous System
<i>CoA</i>	Certificate of Analysis
<i>CSC</i>	Cancer Stem Cell
<i>DAPI</i>	4',6-diamidino-2-phenylindole
<i>DMEM</i>	Dulbecco's Modified Eagle Medium
<i>DMSO</i>	Dimethylsulfoxide
<i>DNA</i>	Deoxyribonucleic Acid
<i>DWI</i>	Diffusion Weighted Imaging
<i>EB</i>	Embryoid Body
<i>ECAR</i>	Extracellular Acidification Rate
<i>eCO</i>	Early Cerebral Organoid
<i>EDTA</i>	Ethylenediaminetetraacetic acid
<i>e.g.</i>	exempli gratia
<i>EGF</i>	Epidermal Growth Factor

<i>EGFR</i>	Epidermal Growth Factor Receptor
<i>EmGFP</i>	Emerald Green Fluorescent Protein
<i>ERVFRD-1</i>	Endogenous Retrovirus FRD Member 1
<i>ERVV-1</i>	Endogenous Retrovirus Group V Member 1
<i>ESC</i>	Embryonic Stem Cell
<i>EM</i>	Electron Microscopy
<i>ENU</i>	N-ethyl-nitrosourea
<i>FACS</i>	Fluorescence Activated Cell Sorting
<i>FBS</i>	Foetal Bovine Serum
<i>FC</i>	Fold Change
<i>FFPE</i>	Formalin Fixed Paraffin Embedded
<i>FGF</i>	Fibroblast Growth Factor
<i>FGFR</i>	Fibroblast Growth Factor Receptor
<i>FISH</i>	Fluorescent In-Situ Hybridisation
<i>FOXP1</i>	Forkhead box G1
<i>GAPDH</i>	Glyceraldehyde 3-phosphate dehydrogenase
<i>GBM</i>	Glioblastoma Multiforme
<i>GEMM</i>	Genetically Engineered Mouse Model
<i>GFAP</i>	Glial Fibrillary Astrocytic Protein
<i>GFP</i>	Green Fluorescent Protein
<i>GMEM</i>	Glasgow Minimum Essential Medium
<i>GSC</i>	Glioma Stem Cell
<i>GSEA</i>	Gene Set Enrichment Analysis
<i>HAND1</i>	Heart and Neural Crest Derivatives Expressed 1
<i>H&amp;E</i>	Haematoxylin and Eosin
<i>hESC</i>	human Embryonic Stem Cell
<i>HGb</i>	High Grade Glioma bulk
<i>HGm</i>	High Grade Glioma migratory
<i>HLA</i>	Human Leukocyte Antigen
<i>ICC</i>	Immunocytochemistry
<i>IDH1</i>	Isocitrate Dehydrogenase 1
<i>IDH2</i>	Isocitrate Dehydrogenase 2
<i>i.e.</i>	id est
<i>IF</i>	Immunofluorescence

<i>IHC</i>	Immunohistochemistry
<i>iPSC</i>	Induced Pluripotent Stem Cell
<i>LGG</i>	Low Grade Glioma
<i>MAP2</i>	Microtubule Associated Protein 2
<i>MEF</i>	Mouse Embryonic Fibroblast
<i>mESC</i>	mouse Embryonic Stem Cell
<i>mg</i>	milligram
<i>miRNA</i>	micro Ribose Nucleic Acid
<i>MGMT</i>	O <sup>6</sup> -methylguanine-DNA methyltransferase
<i>mm</i>	millimetre
<i>MOI</i>	Multiplicity of Infection
<i>MRI</i>	Magnetic Resonance Imaging
<i>mRNA</i>	messenger Ribose Nucleic Acid
<i>N/A</i>	Not Applicable
<i>NB</i>	Neural Basal
<i>NCRI</i>	National Cancer Research Institute
<i>NEBT</i>	Non-Enhancing Brain Tissue
<i>NESTIN</i>	Neuroectodermal Stem Cell Marker
<i>NGS</i>	Next Generation Sequencing
<i>nm</i>	nanometre
<i>nM</i>	nanomolar
<i>NOD</i>	Non-Obese Diabetic
<i>NOS</i>	Not Otherwise Specified
<i>NP</i>	Neural Progenitor
<i>NF1</i>	Neurofibromatosis Type 1
<i>NSC</i>	Neural Stem Cell
<i>NSG</i>	NOD SCID Gamma
<i>OCR</i>	Oxygen Consumption Rate
<i>OCT</i>	Optimal Cutting Temperature
<i>OCT4</i>	Octamer-binding Transcription Factor 4
<i>OLIG2</i>	Oligodendrocyte Transcription Factor 2
<i>OS</i>	Overall Survival
<i>PBS</i>	Phosphate Buffered Saline
<i>PCA</i>	Principal Components Analysis

<i>PCR</i>	Polymerase Chain Reaction
<i>PDGFRA</i>	Platelet-Derived Growth Factor Receptor A
<i>PDX</i>	Patient-Derived Xenograft
<i>PFA</i>	Paraformaldehyde
<i>PFS</i>	Progression Free Survival
<i>PI3K</i>	Phosphoinositide-3-Kinase
<i>POU3F1</i>	POU Class 3 Homeobox 1
<i>PTEN</i>	Phosphatase and Tensin homolog
<i>PWI</i>	Perfusion Weighted Imaging
<i>qRT-PCR</i>	quantitative Real-Time Polymerase Chain Reaction
<i>RA</i>	Retinoic Acid
<i>rld</i>	Regularised Log Transformation
<i>RNA</i>	Ribonucleic Acid
<i>ROCKi</i>	Rho-associated Protein Kinase inhibitor
<i>RT</i>	Room Temperature
<i>RTK</i>	Receptor Tyrosine Kinase
<i>SCID</i>	Severe Combined Immunodeficient
<i>SD</i>	Standard Deviation
<i>seq</i>	Sequencing
<i>SeV</i>	Sendai Virus
<i>SKY</i>	Spectral Karyotyping
<i>SMA</i>	Smooth Muscle Actin
<i>SNP</i>	Single Nucleotide Polymorphism
<i>SOX2</i>	Sry(sex determining region Y)-Box 2
<i>SSEA4</i>	Stage-specific Embryonic Antigen-4
<i>STR</i>	Short Tandem Repeat
<i>TCGA</i>	The Cancer Genome Atlas
<i>TMZ</i>	Temozolomide
<i>TP53</i>	Tumour Protein p53
<i>Tra-1-60</i>	Terato-related-antigen-1-60
<i>TUJ1</i>	Beta-III Tubulin
<i>VEGF</i>	Vascular Endothelial Growth Factor
<i>VST</i>	Variance Stabilising Transformation

<i>WGS</i>	Whole Genome Sequencing
<i>WHO</i>	World Health Organisation
<i>v/v</i>	volume per volume
<i>w/v</i>	weight per volume

## References

1. Yaffe MP, Noggle SA, Solomon SL. Raising the standards of stem cell line quality. *Nat Cell Biol* [Internet]. 2016;18(3):236–7. Available from: <http://dx.doi.org/10.1038/ncb3313>
2. Yamanaka S, Takahashi K. [Induction of pluripotent stem cells from mouse fibroblast cultures]. *Tanpakushitsu Kakusan Koso* [Internet]. 2006;51(15):2346–51. Available from: <http://www.ncbi.nlm.nih.gov/pubmed/17154061>
3. Lancaster MA, Renner M, Martin C-A, Wenzel D, Bicknell LS, Hurles ME, et al. Cerebral organoids model human brain development and microcephaly. *Nature* [Internet]. 2013 Sep;501(7467):373–9. Available from: <http://www.nature.com/articles/nature12517>
4. Lenting K, Verhaak R, Mark Ter Laan -, Wesseling P, Leenders W. Glioma: experimental models and reality. *Acta Neuropathol* [Internet]. 2017 [cited 2018 Sep 8];133:263–82. Available from: [https://www.ncbi.nlm.nih.gov/pmc/articles/PMC5250671/pdf/401\\_2017\\_Article\\_1671.pdf](https://www.ncbi.nlm.nih.gov/pmc/articles/PMC5250671/pdf/401_2017_Article_1671.pdf)
5. National Institute for Health and Care Excellence. Brain tumours (primary) and brain metastases in adults. NICE Guidel [NG99] [Internet]. 2018;July. Available from: <https://www.nice.org.uk/guidance/NG99/resources>
6. Ostrom QT, Bauchet L, Davis FG, Deltour I, Fisher JL, Langer CE, et al. The epidemiology of glioma in adults: a “state of the science” review. *Neuro Oncol* [Internet]. 2014 Jul;16(7):896–913. Available from: <https://academic.oup.com/neuro-oncology/article-lookup/doi/10.1093/neuonc/nou087>
7. Messali A, Villacorta R, Hay JW. A review of the economic burden of glioblastoma and the cost effectiveness of pharmacologic treatments. *Pharmacoeconomics* [Internet]. 2014 Dec;32(12):1201–12. Available from: <http://www.ncbi.nlm.nih.gov/pubmed/25085219>
8. Louis DN, Perry A, Reifenberger G, von Deimling A, Figarella-Branger D, Cavenee WK, et al. The 2016 World Health Organization Classification of Tumors of the Central Nervous System: a summary. *Acta Neuropathol*. 2016;131(6):803–20.
9. Ostrom QT, Gittleman H, De Blank PM, Finlay JL, Gurney JG, McKean-Cowdin R, et al. American Brain Tumor Association Adolescent and

## Young Adult Primary Brain and Central Nervous System Tumors

Diagnosed in the United States in 2008-2012. *Neuro Oncol.* 2015;18:i1–50.

10. Claus EB, Walsh KM, Wiencke JK, Molinaro AM, Wiemels JL, Schildkraut JM, et al. Survival and low-grade glioma: the emergence of genetic information. *Neurosurg Focus* [Internet]. 2015 Jan;38(1):E6. Available from: <http://www.ncbi.nlm.nih.gov/pubmed/25552286>
11. Cancer Genome Atlas Research N, Brat DJ, Verhaak RG, Aldape KD, Yung WK, Salama SR, et al. Comprehensive, Integrative Genomic Analysis of Diffuse Lower-Grade Gliomas. *N Engl J Med* [Internet]. 2015;372(26):2481–98. Available from: <http://www.ncbi.nlm.nih.gov/pubmed/26061751>
12. Ohgaki H, Kleihues P. The definition of primary and secondary glioblastoma. *Clin Cancer Res* [Internet]. 2013 Feb 15;19(4):764–72. Available from: <http://www.ncbi.nlm.nih.gov/pubmed/23209033>
13. Ohgaki H, Kleihues P. Genetic pathways to primary and secondary glioblastoma. *Am J Pathol* [Internet]. 2007 May;170(5):1445–53. Available from: <http://www.ncbi.nlm.nih.gov/pubmed/17456751>
14. Cancer IA for R on. World Health Organization Histological Classification of Tumours of the Central Nervous System. Revised 4t. Louis DN, Ohgaki H, Wiestler OD, Cavenee WK, editors. Lyon: World Health Organization; 2016.
15. Bates A, Gonzalez-Viana E, Cruickshank G, Roques T, Guideline Committee. Primary and metastatic brain tumours in adults: summary of NICE guidance. *BMJ* [Internet]. 2018 Jul 17;362:k2924. Available from: <http://www.ncbi.nlm.nih.gov/pubmed/30018066>
16. Brodbelt A, Greenberg D, Winters T, Williams M, Vernon S, Collins VP. Glioblastoma in England: 2007–2011. *Eur J Cancer* [Internet]. 2015 Mar;51(4):533–42. Available from: <http://linkinghub.elsevier.com/retrieve/pii/S0959804915000039>
17. Nørøxe DS, Poulsen HS, Lassen U. Hallmarks of glioblastoma: a systematic review. *ESMO Open* [Internet]. 2016;1(6):e000144. Available from: <http://esmoopen.bmj.com/lookup/doi/10.1136/esmoopen-2016-000144>
18. Hanif F, Muzaffar K, Perveen K, Malhi SM, Simjee SU. Glioblastoma

- Multiforme: A Review of its Epidemiology and Pathogenesis through Clinical Presentation and Treatment. *Asian Pac J Cancer Prev* [Internet]. 2017;18(1):3–9. Available from: <http://www.ncbi.nlm.nih.gov/pubmed/28239999>
19. Ohgaki H, Kleihues P. Epidemiology and etiology of gliomas. *Acta Neuropathol* [Internet]. 2005 Jan;109(1):93–108. Available from: <http://www.ncbi.nlm.nih.gov/pubmed/15685439>
  20. Omuro A, DeAngelis LM. Glioblastoma and other malignant gliomas: A clinical review. *JAMA - J Am Med Assoc*. 2013;310(17):1842–50.
  21. Sanai N, Chang S, Berger MS. Low-grade gliomas in adults. *J Neurosurg* [Internet]. 2011;115(5):948–65. Available from: <http://www.ncbi.nlm.nih.gov/pubmed/22043865>
  22. De WE, Satoer D, Colle H, Robert E, Visch-Brink E, Marien P. Subcortical language and non-language mapping in awake brain surgery: the use of multimodal tests. *Acta Neurochir (Wien)* [Internet]. 2015;157(4):577–88. Available from: <http://www.ncbi.nlm.nih.gov/pubmed/25585834>
  23. Bourne TD, Schiff D. Update on molecular findings, management and outcome in low-grade gliomas. *Nat Rev Neurol* [Internet]. 2010;6(12):695–701. Available from: <http://www.ncbi.nlm.nih.gov/pubmed/21045797>
  24. Clarke J, Butowski N, Chang S. Recent advances in therapy for glioblastoma. *Arch Neurol* [Internet]. 2010;67(3):279–83. Available from: <http://www.ncbi.nlm.nih.gov/pubmed/20212224>
  25. Grossman SA, Batara JF. Current management of glioblastoma multiforme. *Semin Oncol* [Internet]. 2004 Oct;31(5):635–44. Available from: <http://linkinghub.elsevier.com/retrieve/pii/S0093775404003276>
  26. Dhermain F. Radiotherapy of high-grade gliomas: current standards and new concepts, innovations in imaging and radiotherapy, and new therapeutic approaches. *Chin J Cancer* [Internet]. 2014;33(1):16–24. Available from: <http://www.ncbi.nlm.nih.gov/pubmed/24384237>
  27. Stupp R, Mason WP, van den Bent MJ, Weller M, Fisher B, Taphoorn MJB, et al. Radiotherapy plus Concomitant and Adjuvant Temozolomide for Glioblastoma. *N Engl J Med* [Internet]. 2005 Mar;352(10):987–96. Available from: <http://www.nejm.org/doi/abs/10.1056/NEJMoa043330>
  28. Gilbert MR, Wang M, Aldape KD, Stupp R, Hegi M, Jaeckle KA, et al.

- RTOG 0525: A randomized phase III trial comparing standard adjuvant temozolomide (TMZ) with a dose-dense (dd) schedule in newly diagnosed glioblastoma (GBM). *J Clin Oncol* [Internet]. 2011 May;29(15\_suppl):2006. Available from: [http://ascopubs.org/doi/10.1200/jco.2011.29.15\\_suppl.2006](http://ascopubs.org/doi/10.1200/jco.2011.29.15_suppl.2006)
29. Bobek-Billewicz B, Stasik-Pres G, Hebda A, Majchrzak K, Kaspera W, Jurkowski M. Original article Anaplastic transformation of low-grade gliomas (WHO II) on magnetic resonance imaging. *Folia Neuropathol* [Internet]. 2014;2(Who li):128–40. Available from: <http://www.termedia.pl/doi/10.5114/fn.2014.43784>
30. Karim AB, Maat B, Hatlevoll R, Menten J, Rutten EH, Thomas DG, et al. A randomized trial on dose-response in radiation therapy of low-grade cerebral glioma: European Organization for Research and Treatment of Cancer (EORTC) Study 22844. *Int J Radiat Oncol Biol Phys* [Internet]. 1996 Oct 1;36(3):549–56. Available from: <http://www.ncbi.nlm.nih.gov/pubmed/8948338>
31. van den Bent MJ, Afra D, de Witte O, Ben Hassel M, Schraub S, Hoang-Xuan K, et al. Long-term efficacy of early versus delayed radiotherapy for low-grade astrocytoma and oligodendroglioma in adults: the EORTC 22845 randomised trial. *Lancet* (London, England) [Internet]. 366(9490):985–90. Available from: <http://www.ncbi.nlm.nih.gov/pubmed/16168780>
32. Shaw E, Arusell R, Scheithauer B, O’Fallon J, O’Neill B, Dinapoli R, et al. Prospective randomized trial of low- versus high-dose radiation therapy in adults with supratentorial low-grade glioma: initial report of a North Central Cancer Treatment Group/Radiation Therapy Oncology Group/Eastern Cooperative Oncology Group study. *J Clin Oncol* [Internet]. 2002 May 1;20(9):2267–76. Available from: <http://www.ncbi.nlm.nih.gov/pubmed/11980997>
33. Kiebert GM, Curran D, Aaronson NK, Bolla M, Menten J, Rutten EH, et al. Quality of life after radiation therapy of cerebral low-grade gliomas of the adult: results of a randomised phase III trial on dose response (EORTC trial 22844). EORTC Radiotherapy Co-operative Group. *Eur J Cancer* [Internet]. 1998 Nov;34(12):1902–9. Available from: <http://www.ncbi.nlm.nih.gov/pubmed/10023313>

34. Kesari S, Schiff D, Drappatz J, LaFrankie D, Doherty L, Macklin EA, et al. Phase II study of protracted daily temozolomide for low-grade gliomas in adults. *Clin Cancer Res* [Internet]. 2009 Jan 1;15(1):330–7. Available from: <http://www.ncbi.nlm.nih.gov/pubmed/19118062>
35. Quinn JA, Reardon DA, Friedman AH, Rich JN, Sampson JH, Provenzale JM, et al. Phase II trial of temozolomide in patients with progressive low-grade glioma. *J Clin Oncol* [Internet]. 2003 Feb 15;21(4):646–51. Available from: <http://www.ncbi.nlm.nih.gov/pubmed/12586801>
36. Brada M, Viviers L, Abson C, Hines F, Britton J, Ashley S, et al. Phase II study of primary temozolomide chemotherapy in patients with WHO grade II gliomas. *Ann Oncol Off J Eur Soc Med Oncol* [Internet]. 2003 Dec;14(12):1715–21. Available from: <http://www.ncbi.nlm.nih.gov/pubmed/14630674>
37. Tosoni A, Franceschi E, Ermani M, Bertorelle R, Bonaldi L, Blatt V, et al. Temozolomide three weeks on and one week off as first line therapy for patients with recurrent or progressive low grade gliomas. *J Neurooncol* [Internet]. 2008 Sep;89(2):179–85. Available from: <http://www.ncbi.nlm.nih.gov/pubmed/18431544>
38. McLendon R, Friedman A, Bigner D, Van Meir EG, Brat DJ, M. Mastrogiannakis G, et al. Comprehensive genomic characterization defines human glioblastoma genes and core pathways. *Nature* [Internet]. 2008 Oct;455(7216):1061–8. Available from: <http://www.nature.com/doi/10.1038/nature07385>
39. Marusyk A, Polyak K. Tumor heterogeneity: causes and consequences. *Biochim Biophys Acta* [Internet]. 2010 Jan;1805(1):105–17. Available from: <http://www.ncbi.nlm.nih.gov/pubmed/19931353>
40. Soeda A, Hara A, Kunisada T, Yoshimura S, Iwama T, Park DM. The evidence of glioblastoma heterogeneity. *Sci Rep* [Internet]. 2015 Jan 27;5:7979. Available from: <http://www.ncbi.nlm.nih.gov/pubmed/25623281>
41. Patel AP, Tirosh I, Trombetta JJ, Shalek AK, Gillespie SM, Wakimoto H, et al. Single-cell RNA-seq highlights intratumoral heterogeneity in primary glioblastoma. *Science* [Internet]. 2014;344 VN-(6190):1396–401. Available from: /Users/yurikoharigaya/Documents/ReadCube Media/Science 2014 Patel AP.pdf%5Cn<http://dx.doi.org/10.1126/science.1254257>

42. Hegi ME, Diserens A-C, Gorlia T, Hamou M-F, de Tribolet N, Weller M, et al. MGMT Gene Silencing and Benefit from Temozolomide in Glioblastoma. *N Engl J Med* [Internet]. 2005 Mar;352(10):997–1003. Available from: <http://www.nejm.org/doi/abs/10.1056/NEJMoa043331>
43. Hanahan D, Weinberg RA. The hallmarks of cancer. *Cell* [Internet]. 2000;100(1):57–70. Available from: <http://www.ncbi.nlm.nih.gov/pubmed/10647931>
44. Hanahan D, Weinberg RA. Hallmarks of Cancer: The Next Generation. *Cell* [Internet]. 2011 Mar;144(5):646–74. Available from: <http://linkinghub.elsevier.com/retrieve/pii/S0092867411001279>
45. Mischel PS, Shai R, Shi T, Horvath S, Lu K V, Choe G, et al. Identification of molecular subtypes of glioblastoma by gene expression profiling. *Oncogene* [Internet]. 2003 Apr;22(15):2361–73. Available from: <http://www.nature.com/articles/1206344>
46. Brennan C, Momota H, Hambardzumyan D, Ozawa T, Tandon A, Pedraza A, et al. Glioblastoma Subclasses Can Be Defined by Activity among Signal Transduction Pathways and Associated Genomic Alterations. Creighton C, editor. *PLoS One* [Internet]. 2009 Nov;4(11):e7752–e7752. Available from: <http://dx.plos.org/10.1371/journal.pone.0007752>
47. Wilson T, Karajannis M, Harter D. Glioblastoma multiforme: State of the art and future therapeutics. *Surg Neurol Int* [Internet]. 2014;5(1):64. Available from: <http://surgicalneurologyint.com/surgicalint-articles/glioblastoma-multiforme-state-of-the-art-and-future-therapeutics/>
48. Brennan CW, Verhaak RGW, McKenna A, Campos B, Noushmehr H, Salama SR, et al. The somatic genomic landscape of glioblastoma. *Cell*. 2013;155(2):462–77.
49. Verhaak RGW, Hoadley KA, Purdom E, Wang V, Qi Y, Wilkerson MD, et al. Integrated Genomic Analysis Identifies Clinically Relevant Subtypes of Glioblastoma Characterized by Abnormalities in PDGFRA, IDH1, EGFR, and NF1. *Cancer Cell* [Internet]. 2010 Jan;17(1):98–110. Available from: <http://linkinghub.elsevier.com/retrieve/pii/S1535610809004322>
50. Polson ES, Kuchler VB, Abbosh C, Ross EM, Mathew RK, Beard HA, et al. KHS101 disrupts energy metabolism in human glioblastoma cells and reduces tumor growth in mice. *Sci Transl Med* [Internet]. 2018 Aug

- 15;10(454). Available from:  
<http://www.ncbi.nlm.nih.gov/pubmed/30111643>
51. Patel AP, Tirosh I, Trombetta JJ, Shalek AK, Gillespie SM, Wakimoto H, et al. Single-cell RNA-seq highlights intratumoral heterogeneity in primary glioblastoma. *Science* (80- ) [Internet]. 2014 Jun;344(6190):1396–401. Available from:  
<http://www.sciencemag.org/cgi/doi/10.1126/science.1254257>
52. Roy S, Lahiri D, Maji T, Biswas J. Recurrent Glioblastoma: Where we stand. *South Asian J cancer* [Internet]. 4(4):163–73. Available from:  
<http://www.ncbi.nlm.nih.gov/pubmed/26981507>
53. Karnofsky DA, Abelmann WH, Craver LF, Burchenal JH. The use of the nitrogen mustards in the palliative treatment of carcinoma. With particular reference to bronchogenic carcinoma. *Cancer* [Internet]. 1948 Nov;1(4):634–56. Available from: <http://doi.wiley.com/10.1002/1097-0142%28194811%291%3A4%3C634%3A%3AAID-CNCR2820010410%3E3.0.CO%3B2-L>
54. Gallego O. Nonsurgical treatment of recurrent glioblastoma. *Curr Oncol* [Internet]. 2015 Aug;22(4):e273-81. Available from:  
<http://www.ncbi.nlm.nih.gov/pubmed/26300678>
55. Torok JA, Wegner RE, Mintz AH, Heron DE, Burton SA. Re-irradiation with radiosurgery for recurrent glioblastoma multiforme. *Technol Cancer Res Treat* [Internet]. 2011 Jun;10(3):253–8. Available from:  
<http://www.ncbi.nlm.nih.gov/pubmed/21517131>
56. Gaspar LE, Fisher BJ, Macdonald DR, Leber D V, Halperin EC, Schold SC, et al. Supratentorial malignant glioma: Patterns of recurrence and implications for external beam local treatment. *Int J Radiat Oncol* [Internet]. 1992 Jan;24(1):55–7. Available from:  
<http://linkinghub.elsevier.com/retrieve/pii/036030169291021E>
57. Kim J, Lee IH, Cho HJ, Park CK, Jung YS, Kim Y, et al. Spatiotemporal Evolution of the Primary Glioblastoma Genome. *Cancer Cell* [Internet]. 2015;28(3):318–28. Available from:  
<http://www.ncbi.nlm.nih.gov/pubmed/26373279>
58. Ogura K, Mizowaki T, Arakawa Y, Ogura M, Sakanaka K, Miyamoto S, et al. Initial and cumulative recurrence patterns of glioblastoma after temozolomide-based chemoradiotherapy and salvage treatment: a

- retrospective cohort study in a single institution. *Radiat Oncol* [Internet]. 2013;8(1):97. Available from: <http://ro-journal.biomedcentral.com/articles/10.1186/1748-717X-8-97>
59. Brandes AA, Tosoni A, Franceschi E, Sotti G, Frezza G, Amistà P, et al. Recurrence pattern after temozolomide concomitant with and adjuvant to radiotherapy in newly diagnosed patients with glioblastoma: correlation With MGMT promoter methylation status. *J Clin Oncol* [Internet]. 2009 Mar 10;27(8):1275–9. Available from: <http://www.ncbi.nlm.nih.gov/pubmed/19188675>
  60. Kim J, Zaret KS. Reprogramming of human cancer cells to pluripotency for models of cancer progression. *EMBO J* [Internet]. 2015;34(6):739–47. Available from: <http://www.ncbi.nlm.nih.gov/pubmed/25712212>
  61. Louis DN, Ohgaki H, Wiestler OD, Cavenee WK, Burger PC, Jouvet A, et al. The 2007 WHO Classification of Tumours of the Central Nervous System. *Acta Neuropathol* [Internet]. 2007 Jul 12;114(2):97–109. Available from: <http://link.springer.com/10.1007/s00401-007-0243-4>
  62. Tonn J-C, Grossman SA, Rutka JT, Westphal M, editors. *Neuro-Oncology of CNS Tumors* [Internet]. Berlin, Heidelberg: Springer Berlin Heidelberg; 2006. Available from: <http://link.springer.com/10.1007/3-540-31260-9>
  63. Freitag MT, Maier-Hein KH, Binczyk F, Laun FB, Weber C, Bonekamp D, et al. Early detection of malignant transformation in resected WHO II low-grade glioma using diffusion tensor-derived quantitative measures. *PLoS One*. 2016;11(10):1–19.
  64. Smirniotopoulos JG, Murphy FM, Rushing EJ, Rees JH, Schroeder JW. Patterns of Contrast Enhancement in the Brain and Meninges. *RadioGraphics* [Internet]. 2007 Mar;27(2):525–51. Available from: <http://pubs.rsna.org/doi/10.1148/rg.272065155>
  65. Sage MR, Wilson AJ, Scroop R. Contrast media and the brain. The basis of CT and MR imaging enhancement. *Neuroimaging Clin N Am* [Internet]. 1998 Aug;8(3):695–707. Available from: <http://www.ncbi.nlm.nih.gov/pubmed/9673320>
  66. Pallud J, Capelle L, Taillandier L, Fontaine D, Mandonnet E, Guillemin R, et al. Prognostic significance of imaging contrast enhancement for WHO grade II gliomas. *Neuro Oncol* [Internet]. 2009 Apr;11(2):176–82. Available from: <http://www.ncbi.nlm.nih.gov/pubmed/18697954>

67. Ginsberg LE, Fuller GN, Hashmi M, Leeds NE, Schomer DF. The significance of lack of MR contrast enhancement of supratentorial brain tumors in adults: histopathological evaluation of a series. *Surg Neurol* [Internet]. 1998 Apr;49(4):436–40. Available from: <http://www.ncbi.nlm.nih.gov/pubmed/9537664>
68. Scott JN, Brasher PMA, Sevick RJ, Rewcastle NB, Forsyth PA. How often are nonenhancing supratentorial gliomas malignant? A population study. *Neurology* [Internet]. 2002 Sep 24;59(6):947–9. Available from: <http://www.ncbi.nlm.nih.gov/pubmed/12297589>
69. Stupp R, Brada M, van den Bent MJ, Tonn J-C, Pentheroudakis G. High-grade glioma: ESMO Clinical Practice Guidelines for diagnosis, treatment and follow-up. *Ann Oncol* [Internet]. 2014 Sep 1;25(suppl 3):iii93-iii101. Available from: <https://academic.oup.com/annonc/article-lookup/doi/10.1093/annonc/mdu050>
70. White ML, Zhang Y, Kirby P, Ryken TC. Can tumor contrast enhancement be used as a criterion for differentiating tumor grades of oligodendrogliomas? *AJNR Am J Neuroradiol* [Internet]. 2005 Apr;26(4):784–90. Available from: <http://www.ncbi.nlm.nih.gov/pubmed/15814921>
71. Ward RJ, Dirks PB. Cancer stem cells: at the headwaters of tumor development. *Annu Rev Pathol* [Internet]. 2007;2:175–89. Available from: <http://www.ncbi.nlm.nih.gov/pubmed/18039097>
72. Vescovi AL, Galli R, Reynolds BA. Brain tumour stem cells. *Nat Rev Cancer* [Internet]. 2006;6(6):425–36. Available from: <http://www.ncbi.nlm.nih.gov/pubmed/16723989>
73. Tan BT, Park CY, Ailles LE, Weissman IL. The cancer stem cell hypothesis: a work in progress. *Lab Invest* [Internet]. 2006;86(12):1203–7. Available from: <http://www.ncbi.nlm.nih.gov/pubmed/17075578>
74. Dirks PB. Brain tumor stem cells: the cancer stem cell hypothesis writ large. *Mol Oncol* [Internet]. 2010;4(5):420–30. Available from: <http://www.ncbi.nlm.nih.gov/pubmed/20801091>
75. Rheinbay E, Suva ML, Gillespie SM, Wakimoto H, Patel AP, Shahid M, et al. An aberrant transcription factor network essential for Wnt signaling and stem cell maintenance in glioblastoma. *Cell Rep* [Internet]. 2013;3(5):1567–79. Available from:

<http://www.ncbi.nlm.nih.gov/pubmed/23707066>

76. Parada LF, Dirks PB, Wechsler-Reya RJ. Brain Tumor Stem Cells Remain in Play. *Vol. 35*. 2017. p. 2428–31.
77. Suva ML, Rheinbay E, Gillespie SM, Patel AP, Wakimoto H, Rabkin SD, et al. Reconstructing and reprogramming the tumor-propagating potential of glioblastoma stem-like cells. *Cell [Internet]*. 2014;157(3):580–94. Available from: <http://www.ncbi.nlm.nih.gov/pubmed/24726434>
78. Singh SK, Hawkins C, Clarke ID, Squire JA, Bayani J, Hide T, et al. Identification of human brain tumour initiating cells. *Nature [Internet]*. 2004 Nov;432(7015):396–401. Available from: <http://www.nature.com/articles/nature03128>
79. Read T-A, Fogarty MP, Markant SL, McLendon RE, Wei Z, Ellison DW, et al. Identification of CD15 as a marker for tumor-propagating cells in a mouse model of medulloblastoma. *Cancer Cell [Internet]*. 2009 Feb 3;15(2):135–47. Available from: <http://www.ncbi.nlm.nih.gov/pubmed/19185848>
80. Ward RJ, Lee L, Graham K, Satkunendran T, Yoshikawa K, Ling E, et al. Multipotent CD15+ cancer stem cells in patched-1-deficient mouse medulloblastoma. *Cancer Res [Internet]*. 2009 Jun 1;69(11):4682–90. Available from: <http://www.ncbi.nlm.nih.gov/pubmed/19487286>
81. Vanner RJ, Remke M, Gallo M, Selvadurai HJ, Coutinho F, Lee L, et al. Quiescent sox2(+) cells drive hierarchical growth and relapse in sonic hedgehog subgroup medulloblastoma. *Cancer Cell [Internet]*. 2014 Jul 14;26(1):33–47. Available from: <http://www.ncbi.nlm.nih.gov/pubmed/24954133>
82. Li P, Du F, Yuelling LW, Lin T, Muradimova RE, Tricarico R, et al. A population of Nestin-expressing progenitors in the cerebellum exhibits increased tumorigenicity. *Nat Neurosci [Internet]*. 2013 Dec;16(12):1737–44. Available from: <http://www.ncbi.nlm.nih.gov/pubmed/24141309>
83. Chen J, Li Y, Yu T-S, McKay RM, Burns DK, Kernie SG, et al. A restricted cell population propagates glioblastoma growth after chemotherapy. *Nature [Internet]*. 2012 Aug 23;488(7412):522–6. Available from: <http://www.ncbi.nlm.nih.gov/pubmed/22854781>
84. Chen J, McKay RM, Parada LF. Malignant glioma: Lessons from genomics, mouse models, and stem cells. *Cell*. 2012;149(1):36–47.

85. Lan X, Jörg DJ, Cavalli FMG, Richards LM, Nguyen L V, Vanner RJ, et al. Fate mapping of human glioblastoma reveals an invariant stem cell hierarchy. *Nature* [Internet]. 2017 Aug;549(7671):227–32. Available from: <http://www.nature.com/doi/10.1038/nature23666>
86. Meyer M, Reimand J, Lan X, Head R, Zhu X, Kushida M, et al. Single cell-derived clonal analysis of human glioblastoma links functional and genomic heterogeneity. *Proc Natl Acad Sci* [Internet]. 2015;112(3):851–6. Available from: <http://www.pnas.org/lookup/doi/10.1073/pnas.1320611111>
87. Galli R. The neurosphere assay applied to neural stem cells and cancer stem cells. *Methods Mol Biol* [Internet]. 2013;986:267–77. Available from: <http://www.ncbi.nlm.nih.gov/pubmed/23436418>
88. Pollard SM, Yoshikawa K, Clarke ID, Danovi D, Stricker S, Russell R, et al. Glioma Stem Cell Lines Expanded in Adherent Culture Have Tumor-Specific Phenotypes and Are Suitable for Chemical and Genetic Screens. *Cell Stem Cell* [Internet]. 2009;4(6):568–80. Available from: <http://dx.doi.org/10.1016/j.stem.2009.03.014>
89. Venteicher AS, Tirosh I, Hebert C, Yizhak K, Neftel C, Filbin MG, et al. Decoupling genetics, lineages, and microenvironment in IDH-mutant gliomas by single-cell RNA-seq. *Science* (80- ) [Internet]. 2017 Mar 31 [cited 2018 Sep 8];355(6332):eaai8478. Available from: <http://www.ncbi.nlm.nih.gov/pubmed/28360267>
90. Tirosh I, Venteicher AS, Hebert C, Escalante LE, Patel AP, Yizhak K, et al. Single-cell RNA-seq supports a developmental hierarchy in human oligodendroglioma. *Nature* [Internet]. 2016 Nov 2 [cited 2018 Sep 8];539(7628):309–13. Available from: <http://www.ncbi.nlm.nih.gov/pubmed/27806376>
91. Galli R, Binda E, Orfanelli U, Cipelletti B, Gritti A, De Vitis S, et al. Isolation and Characterization of Tumorigenic, Stem-like Neural Precursors from Human Glioblastoma. *Cancer Res* [Internet]. 2004 Oct;64(19):7011–21. Available from: <http://cancerres.aacrjournals.org/lookup/doi/10.1158/0008-5472.CAN-04-1364>
92. Lee JH, Lee JE, Kahng JY, Kim SH, Park JS, Yoon SJ, et al. Human glioblastoma arises from subventricular zone cells with low-level driver mutations. *Nature* [Internet]. 2018 Aug 1;560(7717):243–7. Available

from: <http://www.nature.com/articles/s41586-018-0389-3>

93. Stupp R, Hegi ME. Targeting brain-tumor stem cells. *Nat Biotechnol* [Internet]. 2007;25(2):193–4. Available from: <http://www.ncbi.nlm.nih.gov/pubmed/17287755>
94. Bao S, Wu Q, McLendon RE, Hao Y, Shi Q, Hjelmeland AB, et al. Glioma stem cells promote radioresistance by preferential activation of the DNA damage response. *Nature* [Internet]. 2006 Dec;444(7120):756–60. Available from: <http://www.nature.com/articles/nature05236>
95. Dean M, Fojo T, Bates S. Tumour stem cells and drug resistance. *Nat Rev Cancer* [Internet]. 2005 Apr 1 [cited 2018 Sep 8];5(4):275–84. Available from: <http://www.ncbi.nlm.nih.gov/pubmed/15803154>
96. Piccirillo SGM, Reynolds BA, Zanetti N, Lamorte G, Binda E, Broggi G, et al. Bone morphogenetic proteins inhibit the tumorigenic potential of human brain tumour-initiating cells. *Nature* [Internet]. 2006 Dec;444(7120):761–5. Available from: <http://www.nature.com/articles/nature05349>
97. Persano L, Pistollato F, Rampazzo E, Della Puppa A, Abbadi S, Frasson C, et al. BMP2 sensitizes glioblastoma stem-like cells to Temozolomide by affecting HIF-1 $\alpha$  stability and MGMT expression. *Cell Death Dis* [Internet]. 2012 Oct 18 [cited 2018 Sep 8];3(10):e412. Available from: <http://www.ncbi.nlm.nih.gov/pubmed/23076220>
98. Teres S, Llado V, Higuera M, Barcelo-Coblijn G, Martin ML, Noguera-Salva MA, et al. 2-Hydroxyoleate, a nontoxic membrane binding anticancer drug, induces glioma cell differentiation and autophagy. *Proc Natl Acad Sci* [Internet]. 2012 May 29 [cited 2018 Sep 8];109(22):8489–94. Available from: <http://www.ncbi.nlm.nih.gov/pubmed/22586083>
99. Stockhausen M-T, Kristoffersen K, Stobbe L, Poulsen HS. Differentiation of glioblastoma multiforme stem-like cells leads to downregulation of EGFR and EGFRvIII and decreased tumorigenic and stem-like cell potential. *Cancer Biol Ther* [Internet]. 2014 Feb [cited 2018 Sep 8];15(2):216–24. Available from: <http://www.tandfonline.com/doi/abs/10.4161/cbt.26736>
100. Zhuang W, Long L, Zheng B, Ji W, Yang N, Zhang Q, et al. Curcumin promotes differentiation of glioma-initiating cells by inducing autophagy. *Cancer Sci* [Internet]. 2012 Apr [cited 2018 Sep 8];103(4):684–90.

Available from: <http://www.ncbi.nlm.nih.gov/pubmed/22192169>

101. Niu CS, Li MW, Ni YF, Chen JM, Mei JM, Li J, et al. Effect of all-trans retinoic acid on the proliferation and differentiation of brain tumor stem cells. *J Exp Clin Cancer Res* [Internet]. 2010 Aug 17 [cited 2018 Sep 8];29(1):113. Available from: <http://www.ncbi.nlm.nih.gov/pubmed/20716331>
102. Lee J, Kotliarova S, Kotliarov Y, Li A, Su Q, Donin NM, et al. Tumor stem cells derived from glioblastomas cultured in bFGF and EGF more closely mirror the phenotype and genotype of primary tumors than do serum-cultured cell lines. *Cancer Cell* [Internet]. 2006 May;9(5):391–403. Available from: <http://linkinghub.elsevier.com/retrieve/pii/S1535610806001176>
103. Joo KM, Kim SY, Jin X, Song SY, Kong D-S, Lee J-I, et al. Clinical and biological implications of CD133-positive and CD133-negative cells in glioblastomas. *Lab Invest* [Internet]. 2008 Aug 16 [cited 2018 Sep 8];88(8):808–15. Available from: <http://www.ncbi.nlm.nih.gov/pubmed/18560366>
104. Beier D, Hau P, Proescholdt M, Lohmeier A, Wischhusen J, Oefner PJ, et al. CD133+ and CD133- Glioblastoma-Derived Cancer Stem Cells Show Differential Growth Characteristics and Molecular Profiles. *Cancer Res* [Internet]. 2007 Apr 24 [cited 2018 Sep 8];67(9):4010–5. Available from: <http://www.ncbi.nlm.nih.gov/pubmed/17483311>
105. Wang J, Sakariassen PØ, Tsinkalovsky O, Immervoll H, Bøe SO, Svendsen A, et al. CD133 negative glioma cells form tumors in nude rats and give rise to CD133 positive cells. *Int J Cancer* [Internet]. 2008 Feb 15 [cited 2018 Sep 8];122(4):761–8. Available from: <http://www.ncbi.nlm.nih.gov/pubmed/17955491>
106. Appolloni PMFCI. Experimental Models of Glioma. In: Sedo A, Mentlein R, editors. *Glioma Cell Biology*. 1st ed. Springer-Verlag Wien; 2014. p. 399–432.
107. Ponten J, Macintyre EH. Long term culture of normal and neoplastic human glia. *Acta Pathol Microbiol Scand* [Internet]. 1968;74(4):465–86. Available from: <http://www.ncbi.nlm.nih.gov/pubmed/4313504>
108. Westermark B, Pontén J, Hugosson R. Determinants for the establishment of permanent tissue culture lines from human gliomas. *Acta*

- Pathol Microbiol Scand A [Internet]. 1973 Nov [cited 2018 Sep 10];81(6):791–805. Available from:  
<http://www.ncbi.nlm.nih.gov/pubmed/4359449>
109. Wurdak H, Zhu S, Romero A, Loriger M, Watson J, Chiang C yuan, et al. An RNAi Screen Identifies TRRAP as a Regulator of Brain Tumor-Initiating Cell Differentiation. *Cell Stem Cell* [Internet]. 2010;6(1):37–47. Available from: <http://dx.doi.org/10.1016/j.stem.2009.11.002>
110. Allen M, Bjerke M, Edlund H, Nelander S, Westermark B. Origin of the U87MG glioma cell line: Good news and bad news. *Sci Transl Med* [Internet]. 2016;8(354):354re3-354re3. Available from:  
<http://stm.sciencemag.org/cgi/doi/10.1126/scitranslmed.aaf6853>
111. Torsvik A, Stieber D, Enger PO, Golebiewska A, Molven A, Svendsen A, et al. U-251 revisited: Genetic drift and phenotypic consequences of long-term cultures of glioblastoma cells. *Cancer Med*. 2014;3(4):812–24.
112. Ernst A, Hofmann S, Ahmadi R, Becker N, Korshunov A, Engel F, et al. Genomic and Expression Profiling of Glioblastoma Stem Cell-Like Spheroid Cultures Identifies Novel Tumor-Relevant Genes Associated with Survival. *Clin Cancer Res* [Internet]. 2009 Nov 1 [cited 2018 Sep 10];15(21):6541–50. Available from:  
<http://www.ncbi.nlm.nih.gov/pubmed/19861460>
113. Huszthy PC, Daphu I, Niclou SP, Stieber D, Nigro JM, Sakariassen PØ, et al. In vivo models of primary brain tumors: pitfalls and perspectives. *Neuro Oncol* [Internet]. 2012 Aug [cited 2018 Sep 10];14(8):979–93. Available from: <http://www.ncbi.nlm.nih.gov/pubmed/22679124>
114. Clark MJ, Homer N, O'Connor BD, Chen Z, Eskin A, Lee H, et al. U87MG decoded: the genomic sequence of a cytogenetically aberrant human cancer cell line. *PLoS Genet* [Internet]. 2010 Jan 29 [cited 2018 Sep 10];6(1):e1000832. Available from:  
<http://www.ncbi.nlm.nih.gov/pubmed/20126413>
115. Freedman LP, Gibson MC, Ethier SP, Soule HR, Neve RM, Reid YA. Reproducibility: changing the policies and culture of cell line authentication. *Nat Methods* [Internet]. 2015 Jun 1 [cited 2018 Sep 10];12(6):493–7. Available from:  
<http://www.ncbi.nlm.nih.gov/pubmed/26020501>
116. Lenting K, Verhaak R, ter Laan M, Wesseling P, Leenders W. Glioma:

- experimental models and reality. *Acta Neuropathol.* 2017;133(2):263–82.
117. Reynolds BA, Weiss S. Generation of neurons and astrocytes from isolated cells of the adult mammalian central nervous system. *Science* (80- ) [Internet]. 1992;255(5052):1707–10. Available from: <http://www.ncbi.nlm.nih.gov/pubmed/1553558>
118. Son MJ, Woolard K, Nam D-H, Lee J, Fine HA. SSEA-1 Is an Enrichment Marker for Tumor-Initiating Cells in Human Glioblastoma. *Cell Stem Cell* [Internet]. 2009 May;4(5):440–52. Available from: <http://linkinghub.elsevier.com/retrieve/pii/S1934590909001040>
119. Claes A, Schuurin J, Boots-Sprenger S, Hendriks-Cornelissen S, Dekkers M, van der Kogel AJ, et al. Phenotypic and Genotypic Characterization of Orthotopic Human Glioma Models and Its Relevance for the Study of Anti-glioma Therapy. *Brain Pathol* [Internet]. 2008 Jul;18(3):423–33. Available from: <http://doi.wiley.com/10.1111/j.1750-3639.2008.00141.x>
120. Jin G, Reitman ZJ, Duncan CG, Spasojevic I, Gooden DM, Rasheed BA, et al. Disruption of Wild-Type IDH1 Suppresses D-2-Hydroxyglutarate Production in IDH1-Mutated Gliomas. *Cancer Res* [Internet]. 2013 Jan 15;73(2):496–501. Available from: <http://cancerres.aacrjournals.org/cgi/doi/10.1158/0008-5472.CAN-12-2852>
121. Kim W, Liau LM. IDH mutations in human glioma. *Neurosurg Clin N Am* [Internet]. 2012 Jul;23(3):471–80. Available from: <http://www.ncbi.nlm.nih.gov/pubmed/22748659>
122. Cairns RA, Mak TW. Oncogenic isocitrate dehydrogenase mutations: Mechanisms, models, and clinical opportunities. *Cancer Discov.* 2013;3(7):730–41.
123. Rohle D, Popovici-Muller J, Palaskas N, Turcan S, Grommes C, Campos C, et al. An Inhibitor of Mutant IDH1 Delays Growth and Promotes Differentiation of Glioma Cells. *Science* (80- ) [Internet]. 2013 May 3;340(6132):626–30. Available from: <http://www.sciencemag.org/cgi/doi/10.1126/science.1236062>
124. Xie Y, Bergström T, Jiang Y, Johansson P, Marinescu VD, Lindberg N, et al. The Human Glioblastoma Cell Culture Resource: Validated Cell Models Representing All Molecular Subtypes. *EBioMedicine.*

- 2015;2(10):1351–63.
125. García-Romero N, González-Tejedo C, Carrión-Navarro J, Esteban-Rubio S, Rackov G, Rodríguez-Fanjul V, et al. Cancer stem cells from human glioblastoma resemble but do not mimic original tumors after in vitro passaging in serum-free media. *Oncotarget* [Internet]. 2016 [cited 2018 Sep 12];7(40):65888–901. Available from: <http://www.ncbi.nlm.nih.gov/pubmed/27589567>
  126. Baskaran S, Mayrhofer M, Kultima HG, Bergström T, Elfineh L, Cavelier L, et al. Primary glioblastoma cells for precision medicine: A quantitative portrait of genomic (in)stability during the first 30 passages. *Neuro Oncol*. 2018;20(8):1080–91.
  127. Haley EM, Kim Y. The role of basic fibroblast growth factor in glioblastoma multiforme and glioblastoma stem cells and in their in vitro culture. *Cancer Lett* [Internet]. 2014;346(1):1–5. Available from: <http://dx.doi.org/10.1016/j.canlet.2013.12.003>
  128. Lathia JD, Hitomi M, Gallagher J, Gadani SP, Adkins J, VasANJI A, et al. Distribution of CD133 reveals glioma stem cells self-renew through symmetric and asymmetric cell divisions. *Cell Death Dis* [Internet]. 2011 Sep 1 [cited 2018 Sep 12];2(9):e200–e200. Available from: <http://www.ncbi.nlm.nih.gov/pubmed/21881602>
  129. Li G, Chen Z, Hu Y-D, Wei H, Li D, Ji H, et al. Autocrine factors sustain glioblastoma stem cell self-renewal. *Oncol Rep* [Internet]. 2009 Feb [cited 2018 Sep 12];21(2):419–24. Available from: <http://www.ncbi.nlm.nih.gov/pubmed/19148517>
  130. Kelly JJP, Stechishin O, Chojnacki A, Lun X, Sun B, Senger DL, et al. Proliferation of Human Glioblastoma Stem Cells Occurs Independently of Exogenous Mitogens. *Stem Cells* [Internet]. 2009;27(8):1722–33. Available from: <http://doi.wiley.com/10.1002/stem.98>
  131. Roberts WG, Delaat J, Nagane M, Huang S, Cavenee WK, Palade GE. Host Microvasculature Influence on Tumor Vascular Morphology and Endothelial Gene Expression. *Am J Pathol* [Internet]. 1998 Oct;153(4):1239–48. Available from: <http://linkinghub.elsevier.com/retrieve/pii/S0002944010656684>
  132. Wachsberger PR, Burd R, Cardi C, Thakur M, Daskalakis C, Holash J, et al. VEGF Trap in Combination With Radiotherapy Improves Tumor

- Control in U87 Glioblastoma. *Int J Radiat Oncol* [Internet]. 2007 Apr;67(5):1526–37. Available from: <http://linkinghub.elsevier.com/retrieve/pii/S0360301606033943>
133. Klink B, Miletic H, Stieber D, Huszthy PC, Valenzuela J. A Novel, Diffusely Infiltrative Xenograft Model of Human Anaplastic Oligodendroglioma with Mutations in FUBP1, CIC, and IDH1. *PLoS One* [Internet]. 2013 [cited 2018 Sep 12];8(3):59773. Available from: [www.plosone.org](http://www.plosone.org)
134. Luchman HA, Stechishin OD, Dang NH, Blough MD, Chesnelong C, Kelly JJ, et al. endogenous IDH1-mutant glioma. 2012;14(2):184–91.
135. Rankin SL, Zhu G, Baker SJ. Review: insights gained from modelling high-grade glioma in the mouse. *Neuropathol Appl Neurobiol* [Internet]. 2012;38(3):254–70. Available from: <http://www.ncbi.nlm.nih.gov/pubmed/22035336>
136. Navis AC, Niclou SP, Fack F, Stieber D, van Lith S, Verrijp K, et al. Increased mitochondrial activity in a novel IDH1-R132H mutant human oligodendroglioma xenograft model: in situ detection of 2-HG and  $\alpha$ -KG. *Acta Neuropathol Commun* [Internet]. 2013 May 29 [cited 2018 Sep 13];1(1):18. Available from: <http://actaneurocomms.biomedcentral.com/articles/10.1186/2051-5960-1-18>
137. Ben-David U, Ha G, Tseng Y-Y, Greenwald NF, Oh C, Shih J, et al. Patient-derived xenografts undergo mouse-specific tumor evolution. *Nat Genet* [Internet]. 2017 Nov;49(11):1567–75. Available from: <http://www.ncbi.nlm.nih.gov/pubmed/28991255>
138. Hawkins-Daarud A, Rockne RC, Anderson ARA, Swanson KR. Modeling Tumor-Associated Edema in Gliomas during Anti-Angiogenic Therapy and Its Impact on Imageable Tumor. *Front Oncol* [Internet]. 2013;3:66. Available from: <http://www.ncbi.nlm.nih.gov/pubmed/23577324>
139. Morton JJ, Bird G, Refaeli Y, Jimeno A. Humanized Mouse Xenograft Models: Narrowing the Tumor–Microenvironment Gap. *Cancer Res* [Internet]. 2016 Nov 1;76(21):6153–8. Available from: <http://cancerres.aacrjournals.org/lookup/doi/10.1158/0008-5472.CAN-16-1260>
140. Zitvogel L, Pitt JM, Daillère R, Smyth MJ, Kroemer G. Mouse models in

- oncoimmunology. *Nat Rev Cancer* [Internet]. 2016 Dec 30 [cited 2018 Sep 13];16(12):759–73. Available from:  
<http://www.nature.com/articles/nrc.2016.91>
141. Russell WL, Kelly EM, Hunsicker PR, Bangham JW, Maddux SC, Phipps EL. Specific-locus test shows ethylnitrosourea to be the most potent mutagen in the mouse. *Proc Natl Acad Sci U S A* [Internet]. 1979 Nov;76(11):5818–9. Available from:  
<http://www.ncbi.nlm.nih.gov/pubmed/293686>
142. Slikker W. N-Ethyl-N-nitrosourea (ENU) Increased Brain Mutations in Prenatal and Neonatal Mice but Not in the Adults. *Toxicol Sci* [Internet]. 2004 May 24;81(1):112–20. Available from:  
<https://academic.oup.com/toxsci/article-lookup/doi/10.1093/toxsci/kfh177>
143. Zook BC, Simmens SJ, Jones R V. Evaluation of ENU-induced gliomas in rats: nomenclature, immunochemistry, and malignancy. *Toxicol Pathol* [Internet]. 28(1):193–201. Available from:  
<http://www.ncbi.nlm.nih.gov/pubmed/10669007>
144. Wang Q, Satomi K, Oh JE, Hutter B, Brors B, Diessl N, et al. Braf Mutations Initiate the Development of Rat Gliomas Induced by Postnatal Exposure to N-Ethyl-N-Nitrosourea. *Am J Pathol* [Internet]. 2016 Oct;186(10):2569–76. Available from:  
<https://linkinghub.elsevier.com/retrieve/pii/S0002944016302310>
145. Reifenberger G, Bilzer T, Seitz RJ, Wechsler W. Expression of vimentin and glial fibrillary acidic protein in ethylnitrosourea-induced rat gliomas and glioma cell lines. *Acta Neuropathol* [Internet]. 1989;78(3):270–82. Available from: <http://www.ncbi.nlm.nih.gov/pubmed/2475009>
146. Barth RF, Kaur B. Rat brain tumor models in experimental neuro-oncology: the C6, 9L, T9, RG2, F98, BT4C, RT-2 and CNS-1 gliomas. *J Neurooncol* [Internet]. 2009 Sep 21;94(3):299–312. Available from:  
<http://link.springer.com/10.1007/s11060-009-9875-7>
147. Ausman JI, Shapiro WR, Rall DP. Studies on the chemotherapy of experimental brain tumors: development of an experimental model. *Cancer Res* [Internet]. 1970 Sep 1 [cited 2018 Sep 13];30(9):2394–400. Available from: <http://www.ncbi.nlm.nih.gov/pubmed/5475483>
148. Szatmari T, Lumniczky K, Desaknai S, Trajcevski S, Hidvegi EJ, Hamada H, et al. Detailed characterization of the mouse glioma 261 tumor model

- for experimental glioblastoma therapy. *Cancer Sci* [Internet]. 2006 Jun;97(6):546–53. Available from: <http://doi.wiley.com/10.1111/j.1349-7006.2006.00208.x>
149. Zhou X, Liao Y, Li H, Zhao Z, Liu Q. Dendritic cell vaccination enhances antiangiogenesis induced by endostatin in rat glioma. *J Cancer Res Ther* [Internet]. 2016;12(1):198. Available from: <http://www.cancerjournal.net/text.asp?2016/12/1/198/151430>
150. Federspiel MJ, Bates P, Young JA, Varmus HE, Hughes SH. A system for tissue-specific gene targeting: transgenic mice susceptible to subgroup A avian leukosis virus-based retroviral vectors. *Proc Natl Acad Sci U S A* [Internet]. 1994 Nov 8 [cited 2018 Sep 13];91(23):11241–5. Available from: <http://www.ncbi.nlm.nih.gov/pubmed/7972042>
151. Greenhouse JJ, Petropoulos CJ, Crittenden LB, Hughes SH. Helper-independent retrovirus vectors with Rous-associated virus type O long terminal repeats. *J Virol* [Internet]. 1988 Dec [cited 2018 Sep 13];62(12):4809–12. Available from: <http://www.ncbi.nlm.nih.gov/pubmed/2460645>
152. Holland EC, Celestino J, Dai C, Schaefer L, Sawaya RE, Fuller GN. Combined activation of Ras and Akt in neural progenitors induces glioblastoma formation in mice. *Nat Genet* [Internet]. 2000 May [cited 2018 Sep 13];25(1):55–7. Available from: <http://www.ncbi.nlm.nih.gov/pubmed/10802656>
153. Guha A. Ras activation in astrocytomas and neurofibromas. *Can J Neurol Sci* [Internet]. 1998 Nov [cited 2018 Sep 13];25(4):267–81. Available from: <http://www.ncbi.nlm.nih.gov/pubmed/9827227>
154. Henson JW, Schnitker BL, Correa KM, von Deimling A, Fassbender F, Xu H-J, et al. The retinoblastoma gene is involved in malignant progression of astrocytomas. *Ann Neurol* [Internet]. 1994 Nov [cited 2018 Sep 13];36(5):714–21. Available from: <http://www.ncbi.nlm.nih.gov/pubmed/7979217>
155. de Vries NA, Bruggeman SW, Hulsman D, de Vries HI, Zevenhoven J, Buckle T, et al. Rapid and Robust Transgenic High-Grade Glioma Mouse Models for Therapy Intervention Studies. *Clin Cancer Res* [Internet]. 2010 Jul 1;16(13):3431–41. Available from: <http://clincancerres.aacrjournals.org/cgi/doi/10.1158/1078-0432.CCR-09->

156. Bardella C, Al-Dalahmah O, Krell D, Brazauskas P, Al-Qahtani K, Tomkova M, et al. Expression of Idh1R132Hin the Murine Subventricular Zone Stem Cell Niche Recapitulates Features of Early Gliomagenesis. *Cancer Cell*. 2016;30(4):578–94.
157. Lin F, de Gooijer MC, Roig EM, Buil LCM, Christner SM, Beumer JH, et al. ABCB1, ABCG2, and PTEN Determine the Response of Glioblastoma to Temozolomide and ABT-888 Therapy. *Clin Cancer Res [Internet]*. 2014 May 15;20(10):2703–13. Available from: <http://clincancerres.aacrjournals.org/cgi/doi/10.1158/1078-0432.CCR-14-0084>
158. Lin F, de Gooijer MC, Hanekamp D, Chandrasekaran G, Buil LCM, Thota N, et al. PI3K–mTOR Pathway Inhibition Exhibits Efficacy Against High-grade Glioma in Clinically Relevant Mouse Models. *Clin Cancer Res [Internet]*. 2017 Mar 1;23(5):1286–98. Available from: <http://clincancerres.aacrjournals.org/lookup/doi/10.1158/1078-0432.CCR-16-1276>
159. Welker AM, Jaros BD, Puduvalli VK, Imitola J, Kaur B, Beattie CE. Standardized orthotopic xenografts in zebrafish reveal glioma cell-line-specific characteristics and tumor cell heterogeneity. *Dis Model Mech [Internet]*. 2016 Feb 1;9(2):199–210. Available from: <http://dmm.biologists.org/lookup/doi/10.1242/dmm.022921>
160. Vittori M, Motaln H, Turnšek TL. The study of glioma by xenotransplantation in zebrafish early life stages. *J Histochem Cytochem [Internet]*. 2015;63(10):749–61. Available from: <http://www.ncbi.nlm.nih.gov/pubmed/26109632>
161. Lam SH, Chua HL, Gong Z, Lam TJ, Sin YM. Development and maturation of the immune system in zebrafish, *Danio rerio*: a gene expression profiling, in situ hybridization and immunological study. *Dev Comp Immunol [Internet]*. 2004 Jan;28(1):9–28. Available from: <http://www.ncbi.nlm.nih.gov/pubmed/12962979>
162. Xie J, Farage E, Sugimoto M, Anand-Apte B. A novel transgenic zebrafish model for blood-brain and blood-retinal barrier development. *BMC Dev Biol [Internet]*. 2010;10(1):76. Available from: <http://bmcdevbiol.biomedcentral.com/articles/10.1186/1471-213X-10-76>

163. Pandey UB, Nichols CD. Human disease models in *Drosophila melanogaster* and the role of the fly in therapeutic drug discovery. *Pharmacol Rev* [Internet]. 2011 Jun;63(2):411–36. Available from: <http://www.ncbi.nlm.nih.gov/pubmed/21415126>
164. Witte HT, Jeibmann A, Klämbt C, Paulus W. Modeling glioma growth and invasion in *Drosophila melanogaster*. *Neoplasia* [Internet]. 2009 Sep;11(9):882–8. Available from: <http://www.ncbi.nlm.nih.gov/pubmed/19724682>
165. Bier E, Reiter LT. Using *Drosophila melanogaster* to uncover human disease gene function and potential drug target proteins. *Expert Opin Ther Targets* [Internet]. 2002 Jun 25;6(3):387–99. Available from: <http://www.tandfonline.com/doi/full/10.1517/14728222.6.3.387>
166. Read RD, Cavenee WK, Furnari FB, Thomas JB. A *Drosophila* Model for EGFR-Ras and PI3K-Dependent Human Glioma. Rulifson E, editor. *PLoS Genet* [Internet]. 2009 Feb 13;5(2):e1000374. Available from: <http://dx.plos.org/10.1371/journal.pgen.1000374>
167. Chan EM, Ratanasirintrawoot S, Park IH, Manos PD, Loh YH, Huo H, et al. Live cell imaging distinguishes bona fide human iPS cells from partially reprogrammed cells. *Nat Biotechnol*. 2009;27(11):1033–7.
168. Evans MJ, Kaufman MH. Establishment in culture of pluripotential cells from mouse embryos. *Nature* [Internet]. 1981;292(5819):154–6. Available from: <http://www.ncbi.nlm.nih.gov/pubmed/7242681>
169. Martin GR. Isolation of a pluripotent cell line from early mouse embryos cultured in medium conditioned by teratocarcinoma stem cells. *Proc Natl Acad Sci U S A* [Internet]. 1981;78(12):7634–8. Available from: <http://www.ncbi.nlm.nih.gov/pubmed/6950406>
170. Thomson JA, Itskovitz-Eldor J, Shapiro SS, Waknitz MA, Swiergiel JJ, Marshall VS, et al. Embryonic stem cell lines derived from human blastocysts. *Science* (80- ) [Internet]. 1998;282(5391):1145–7. Available from: <http://www.ncbi.nlm.nih.gov/pubmed/9804556>
171. Malik N, Rao MS. A review of the methods for human iPSC derivation. *Methods Mol Biol* [Internet]. 2013;997:23–33. Available from: <http://www.ncbi.nlm.nih.gov/pubmed/23546745>
172. Macarthur CC, Fontes A, Ravinder N, Kuninger D, Kaur J, Bailey M, et al. Generation of human-induced pluripotent stem cells by a nonintegrating

- RNA Sendai virus vector in feeder-free or xeno-free conditions. *Stem Cells Int* [Internet]. 2012;2012:564612. Available from: <http://www.ncbi.nlm.nih.gov/pubmed/22550511>
173. Cyranoski D. Next-generation stem cells cleared for human trial [Internet]. *Nature*; 2014. Available from: <http://www.nature.com/news/next-generation-stem-cells-cleared-for-human-trial-1.15897>
174. Waddington CH. *The Strategy of the Genes; a Discussion of Some Aspects of Theoretical Biology*. London: Allen & Unwin; 1957.
175. Gurdon JB. Adult frogs derived from the nuclei of single somatic cells. *Dev Biol* [Internet]. 1962;4:256–73. Available from: <http://www.ncbi.nlm.nih.gov/pubmed/13903027>
176. Wernig M, Meissner A, Foreman R, Brambrink T, Ku M, Hochedlinger K, et al. In vitro reprogramming of fibroblasts into a pluripotent ES-cell-like state. *Nature* [Internet]. 2007;448(7151):318–24. Available from: <http://www.ncbi.nlm.nih.gov/pubmed/17554336>
177. Yu J, Vodyanik MA, Smuga-Otto K, Antosiewicz-Bourget J, Frane JL, Tian S, et al. Induced pluripotent stem cell lines derived from human somatic cells. *Science* (80- ) [Internet]. 2007;318(5858):1917–20. Available from: <http://www.ncbi.nlm.nih.gov/pubmed/18029452>
178. Takahashi K, Tanabe K, Ohnuki M, Narita M, Ichisaka T, Tomoda K, et al. Induction of pluripotent stem cells from adult human fibroblasts by defined factors. *Cell* [Internet]. 2007;131(5):861–72. Available from: <http://www.ncbi.nlm.nih.gov/pubmed/18035408>
179. Tanabe K, Takahashi K, Yamanaka S. Induction of pluripotency by defined factors. *Proc Jpn Acad Ser B Phys Biol Sci* [Internet]. 2014;90(3):83–96. Available from: <http://www.ncbi.nlm.nih.gov/pubmed/24621955>
180. Tanabe K, Nakamura M, Narita M, Takahashi K, Yamanaka S. Maturation, not initiation, is the major roadblock during reprogramming toward pluripotency from human fibroblasts. *Proc Natl Acad Sci U S A* [Internet]. 2013;110(30):12172–9. Available from: <http://www.ncbi.nlm.nih.gov/pubmed/23812749>
181. Fusaki N, Ban H, Nishiyama A, Saeki K, Hasegawa M. Efficient induction of transgene-free human pluripotent stem cells using a vector based on Sendai virus, an RNA virus that does not integrate into the host genome.

- Proc Jpn Acad Ser B Phys Biol Sci [Internet]. 2009;85(8):348–62.  
Available from: <http://www.ncbi.nlm.nih.gov/pubmed/19838014>
182. Warren L, Manos PD, Ahfeldt T, Loh YH, Li H, Lau F, et al. Highly efficient reprogramming to pluripotency and directed differentiation of human cells with synthetic modified mRNA. *Cell Stem Cell* [Internet]. 2010;7(5):618–30. Available from: <http://www.ncbi.nlm.nih.gov/pubmed/20888316>
183. Schopperle WM, Dewolf WC. The TRA-1-60 and TRA-1-81 human pluripotent stem cell markers are expressed on podocalyxin in embryonal carcinoma. *Stem Cells* [Internet]. 2007;25(3):723–30. Available from: <http://www.ncbi.nlm.nih.gov/pubmed/17124010>
184. Schlaeger TM, Daheron L, Brickler TR, Entwisle S, Chan K, Cianci A, et al. A comparison of non-integrating reprogramming methods. *Nat Biotechnol* [Internet]. 2015;33(1):58–63. Available from: <http://dx.doi.org/10.1038/nbt.3070>
185. Lieu PT, Fontes A, Vemuri MC, Macarthur CC. Generation of induced pluripotent stem cells with CytoTune, a non-integrating Sendai virus. *Methods Mol Biol* [Internet]. 2013;997:45–56. Available from: <http://www.ncbi.nlm.nih.gov/pubmed/23546747>
186. Li HO, Zhu YF, Asakawa M, Kuma H, Hirata T, Ueda Y, et al. A cytoplasmic RNA vector derived from nontransmissible Sendai virus with efficient gene transfer and expression. *J Virol* [Internet]. 2000;74(14):6564–9. Available from: <http://www.ncbi.nlm.nih.gov/pubmed/10864670>
187. Papapetrou EP. Induced pluripotent stem cells, past and future. *Science* (80- ) [Internet]. 2016;353(6303):991–2. Available from: <http://dx.doi.org/10.1016/j.stem.2012.05.005>  
<http://linkinghub.elsevier.com/retrieve/pii/S1934590912002378>  
<http://www.sciencemag.org/cgi/doi/10.1126/science.aai7626>
188. Stricker S, Pollard S. Reprogramming cancer cells to pluripotency: an experimental tool for exploring cancer epigenetics. *Epigenetics* [Internet]. 2014;9(6):798–802. Available from: <http://www.ncbi.nlm.nih.gov/pubmed/24686321>
189. Sandoval J, Esteller M. Cancer epigenomics: Beyond genomics. *Curr Opin Genet Dev* [Internet]. 2012;22(1):50–5. Available from:

<http://dx.doi.org/10.1016/j.gde.2012.02.008>

190. Kumano K, Arai S, Hosoi M, Taoka K, Takayama N, Otsu M, et al. Generation of induced pluripotent stem cells from primary chronic myelogenous leukemia patient samples. *Blood* [Internet]. 2012 Jun 28;119(26):6234–42. Available from: <http://www.ncbi.nlm.nih.gov/pubmed/22592606>
191. Carette JE, Pruszk J, Varadarajan M, Blomen VA, Gokhale S, Camargo FD, et al. Generation of iPSCs from cultured human malignant cells. *Blood* [Internet]. 2010 May 20;115(20):4039–42. Available from: <http://www.ncbi.nlm.nih.gov/pubmed/20233975>
192. Miyoshi N, Ishii H, Nagai K, Hoshino H, Mimori K, Tanaka F, et al. Defined factors induce reprogramming of gastrointestinal cancer cells. *Proc Natl Acad Sci U S A* [Internet]. 2010 Jan 5;107(1):40–5. Available from: <http://www.ncbi.nlm.nih.gov/pubmed/20018687>
193. Kim J, Hoffman JP, Alpaugh RK, Rhimm AD, Reichert M, Stanger BZ, et al. An iPSC Line from Human Pancreatic Ductal Adenocarcinoma Undergoes Early to Invasive Stages of Pancreatic Cancer Progression. *Cell Rep* [Internet]. 2013;3(6):2088–99. Available from: <http://dx.doi.org/10.1016/j.celrep.2013.05.036>
194. Stricker SH, Feber A, Engstrom PG, Caren H, Kurian KM, Takashima Y, et al. Widespread resetting of DNA methylation in glioblastoma-initiating cells suppresses malignant cellular behavior in a lineage-dependent manner. *Genes Dev* [Internet]. 2013;27(6):654–69. Available from: <http://www.ncbi.nlm.nih.gov/pubmed/23512659>
195. Ishii K. Reconstruction of dissociated chick brain cells in rotation-mediated culture. *Cytol* [Internet]. 1966;31(1):89–98. Available from: <http://www.ncbi.nlm.nih.gov/pubmed/5959228>
196. S.F. G, S.F G. *Developmental Biology*. 6th ed. Sunderland, MA: Sinauer Associates; 2000.
197. Sato T, Vries RG, Snippert HJ, van de Wetering M, Barker N, Stange DE, et al. Single Lgr5 stem cells build crypt-villus structures in vitro without a mesenchymal niche. *Nature* [Internet]. 2009;459(7244):262–5. Available from: <http://www.ncbi.nlm.nih.gov/pubmed/19329995>
198. Cyranoski D. Tissue engineering: The brainmaker. *Nature* [Internet]. 2012;488(7412):444–6. Available from:

- <http://www.ncbi.nlm.nih.gov/pubmed/22914148>
199. Conti L, Cattaneo E, Papadimou E. Novel neural stem cell systems. *Expert Opin Biol Ther* [Internet]. 2008;8(2):153–60. Available from: <http://www.ncbi.nlm.nih.gov/pubmed/18194072>
  200. Elkabetz Y, Panagiotakos G, G. A, Socci ND, Tabar V, Studer L. Human ES cell-derived neural rosettes reveal a functionally distinct early neural stem cell stage. *Genes Dev*. 2008;22(2):152–65.
  201. Zhang SC, Wernig M, Duncan ID, Brustle O, Thomson JA. In vitro differentiation of transplantable neural precursors from human embryonic stem cells. *Nat Biotechnol* [Internet]. 2001;19(12):1129–33. Available from: <http://www.ncbi.nlm.nih.gov/pubmed/11731781>
  202. Lancaster MA, Knoblich JA. Generation of cerebral organoids from human pluripotent stem cells. *Nat Protoc* [Internet]. 2014 Sep;9(10):2329–40. Available from: <http://www.nature.com/doi/10.1038/nprot.2014.158>
  203. Lancaster MA, Knoblich JA. Organogenesis in a dish: modeling development and disease using organoid technologies. *Science* (80- ) [Internet]. 2014;345(6194):1247125. Available from: <http://www.ncbi.nlm.nih.gov/pubmed/25035496>
  204. Mahe MM, Aihara E, Schumacher MA, Zavros Y, Montrose MH, Helmroth MA, et al. Establishment of Gastrointestinal Epithelial Organoids [Internet]. *Current Protocols in Mouse Biology*. 2013. 217-240 p. Available from: <http://doi.wiley.com/10.1002/9780470942390.mo130179>
  205. Leite SB, Roosens T, El Taghdouini A, Mannaerts I, Smout AJ, Najimi M, et al. Novel human hepatic organoid model enables testing of drug-induced liver fibrosis in vitro. *Biomaterials*. 2016;78:1–10.
  206. Yin X, Mead BE, Safaee H, Langer R, Karp JM, Levy O. Engineering Stem Cell Organoids. *Cell Stem Cell* [Internet]. 2016;18(1):25–38. Available from: <http://dx.doi.org/10.1016/j.stem.2015.12.005>
  207. DeJonge RE, Liu X-P, Deig CR, Heller S, Koehler KR, Hashino E. Modulation of Wnt Signaling Enhances Inner Ear Organoid Development in 3D Culture. *PLoS One* [Internet]. 2016;11(9):e0162508. Available from: <http://dx.plos.org/10.1371/journal.pone.0162508>
  208. Ramachandran SD, Schirmer K, Müntz B, Heinz S, Ghafoory S, Wölfel S, et al. In vitro generation of functional liver organoid-like structures using

- adult human cells. *PLoS One*. 2015;10(10):1–14.
209. Boj SF, Hwang C II, Baker LA, Chio IIC, Engle DD, Corbo V, et al. Organoid models of human and mouse ductal pancreatic cancer. *Cell*. 2015;160(1–2):324–38.
210. Gao D, Vela I, Sboner A, Iaquinta PJ, Karthaus WR, Gopalan A, et al. Organoid cultures derived from patients with advanced prostate cancer. *Cell* [Internet]. 2014;159(1):176–87. Available from: <http://dx.doi.org/10.1016/j.cell.2014.08.016>
211. W.M. R, R.I. B, C.w. H. *Principles of Humane Experimental Technique*. London: Universities Federation for Animal Welfare; 1959.
212. Sachs N, Clevers H. Organoid cultures for the analysis of cancer phenotypes. *Curr Opin Genet Dev* [Internet]. 2014;24(1):68–73. Available from: <http://dx.doi.org/10.1016/j.gde.2013.11.012>
213. Guenot D, Guérin E, Aguilon-Romain S, Pencreach E, Schneider A, Neuville A, et al. Primary tumour genetic alterations and intra-tumoral heterogeneity are maintained in xenografts of human colon cancers showing chromosome instability. *J Pathol* [Internet]. 2006 Apr;208(5):643–52. Available from: <http://www.ncbi.nlm.nih.gov/pubmed/16450341>
214. Emmink BL, Van Houdt WJ, Vries RG, Hoogwater FJH, Govaert KM, Verheem A, et al. Differentiated human colorectal cancer cells protect tumor-initiating cells from irinotecan. *Gastroenterology* [Internet]. 2011 Jul;141(1):269–78. Available from: <http://www.ncbi.nlm.nih.gov/pubmed/21459094>
215. Quadrato G, Nguyen T, Macosko EZ, Sherwood JL, Yang SM, Berger DR, et al. Cell diversity and network dynamics in photosensitive human brain organoids. *Nature*. 2017;545(7652):48–53.
216. Xiang Y, Tanaka Y, Patterson B, Kang YJ, Govindaiah G, Roselaar N, et al. Fusion of Regionally Specified hPSC-Derived Organoids Models Human Brain Development and Interneuron Migration. *Cell Stem Cell* [Internet]. 2017;21(3):383–398.e7. Available from: <http://dx.doi.org/10.1016/j.stem.2017.07.007>
217. Jo J, Xiao Y, Sun AX, Cukuroglu E, Tran HD, Göke J, et al. Midbrain-like Organoids from Human Pluripotent Stem Cells Contain Functional Dopaminergic and Neuromelanin-Producing Neurons. *Cell Stem Cell*.

- 2016;19(2):248–57.
218. Qian X, Nguyen HN, Song MM, Hadiono C, Ogden SC, Hammack C, et al. Brain-Region-Specific Organoids Using Mini-bioreactors for Modeling ZIKV Exposure. *Cell* [Internet]. 2016 May;165(5):1238–54. Available from: <http://linkinghub.elsevier.com/retrieve/pii/S0092867416304676>
219. Bhatia SN, Ingber DE. Microfluidic organs-on-chips. *Nat Biotechnol* [Internet]. 2014;32(8):760–72. Available from: <http://dx.doi.org/10.1038/nbt.2989>
220. Hubert CG, Rivera M, Spangler LC, Wu Q, Mack SC, Prager BC, et al. A Three-Dimensional Organoid Culture System Derived from Human Glioblastomas Recapitulates the Hypoxic Gradients and Cancer Stem Cell Heterogeneity of Tumors Found In Vivo. *Cancer Res* [Internet]. 2016 Apr;76(8):2465–77. Available from: <http://cancerres.aacrjournals.org/lookup/doi/10.1158/0008-5472.CAN-15-2402>
221. da Silva B, Mathew RK, Polson ES, Williams J, Wurdak H. Spontaneous Glioblastoma Spheroid Infiltration of Early-Stage Cerebral Organoids Models Brain Tumor Invasion. *SLAS Discov Adv Life Sci R&D* [Internet]. 2018 Sep 15;23(8):862–8. Available from: <http://journals.sagepub.com/doi/10.1177/2472555218764623>
222. Ogawa J, Pao GM, Shokhirev MN, Verma IM. Glioblastoma Model Using Human Cerebral Organoids. *Cell Rep* [Internet]. 2018 Apr;23(4):1220–9. Available from: <http://linkinghub.elsevier.com/retrieve/pii/S2211124718304819>
223. Sun T, Warrington NM, Luo J, Brooks MD, Dahiya S, Snyder SC, et al. Sexually dimorphic RB inactivation underlies mesenchymal glioblastoma prevalence in males. *J Clin Invest* [Internet]. 2014;124(9):4123–33. Available from: <http://www.ncbi.nlm.nih.gov/pubmed/25083989>
224. Eckel-Passow JE, Lachance DH, Molinaro AM, Walsh KM, Decker PA, Sicotte H, et al. Glioma Groups Based on 1p/19q, IDH, and TERT Promoter Mutations in Tumors. *N Engl J Med* [Internet]. 2015;372(26):2499–508. Available from: <http://www.ncbi.nlm.nih.gov/pubmed/26061753>
225. Ohgaki H, Kleihues P. Epidemiology and etiology of gliomas. *Acta Neuropathol* [Internet]. 2005 Jan;109(1):93–108. Available from:

<http://link.springer.com/10.1007/s00401-005-0991-y>

226. Cairncross JG, Ueki K, Zlatescu MC, Lisle DK, Finkelstein DM, Hammond RR, et al. Specific genetic predictors of chemotherapeutic response and survival in patients with anaplastic oligodendrogliomas. *J Natl Cancer Inst* [Internet]. 1998;90(19):1473–9. Available from: <http://www.ncbi.nlm.nih.gov/pubmed/9776413>
227. Rong Y, Durden DL, Van Meir EG, Brat DJ. ‘Pseudopalisading’ Necrosis in Glioblastoma: A Familiar Morphologic Feature That Links Vascular Pathology, Hypoxia, and Angiogenesis. *J Neuropathol Exp Neurol* [Internet]. 2006 Jun 1;65(6):529–39. Available from: <https://academic.oup.com/jnen/article-lookup/doi/10.1097/00005072-200606000-00001>
228. Vogel TW, Zhuang Z, Li J, Okamoto H, Furuta M, Lee YS, et al. Proteins and protein pattern differences between glioma cell lines and glioblastoma multiforme. *Clin Cancer Res* [Internet]. 2005;11(10):3624–32. Available from: <http://www.ncbi.nlm.nih.gov/pubmed/15897557>
229. FUSAKI N, BAN H, NISHIYAMA A, SAEKI K, HASEGAWA M. Efficient induction of transgene-free human pluripotent stem cells using a vector based on Sendai virus, an RNA virus that does not integrate into the host genome. *Proc Japan Acad Ser B* [Internet]. 2009;85(8):348–62. Available from: <http://joi.jlc.jst.go.jp/JST.JSTAGE/pjab/85.348?from=CrossRef>
230. Kurtz A, Seltmann S, Bairoch A, Bittner MS, Bruce K, Capes-Davis A, et al. A Standard Nomenclature for Referencing and Authentication of Pluripotent Stem Cells. *Stem Cell Reports*. 2018;10(1):300–13.
231. International Stem Cell Initiative, Adewumi O, Aflatoonian B, Ahrlund-Richter L, Amit M, Andrews PW, et al. Characterization of human embryonic stem cell lines by the International Stem Cell Initiative. *Nat Biotechnol* [Internet]. 2007 Jul;25(7):803–16. Available from: <http://www.ncbi.nlm.nih.gov/pubmed/17572666>
232. Chan EM, Ratanasirintrawoot S, Park IH, Manos PD, Loh YH, Huo H, et al. Live cell imaging distinguishes bona fide human iPS cells from partially reprogrammed cells. *Nat Biotechnol* [Internet]. 2009;27(11):1033–7. Available from: <http://www.ncbi.nlm.nih.gov/pubmed/19826408>
233. Quintanilla RH. Cellular characterization of human pluripotent stem cells. *Methods Mol Biol* [Internet]. 2013;997:179–90. Available from:

<http://www.ncbi.nlm.nih.gov/pubmed/23546756>

234. Lotz S, Goderie S, Tokas N, Hirsch SE, Ahmad F, Corneo B, et al. Sustained levels of FGF2 maintain undifferentiated stem cell cultures with biweekly feeding. *PLoS One* [Internet]. 2013;8(2):e56289. Available from: <http://www.ncbi.nlm.nih.gov/pubmed/23437109>
235. Choi J, Lee S, Mallard W, Clement K, Tagliazucchi GM, Lim H, et al. A comparison of genetically matched cell lines reveals the equivalence of human iPSCs and ESCs. *Nat Biotechnol* [Internet]. 2015 Nov 26;33(11):1173–81. Available from: <http://www.nature.com/articles/nbt.3388>
236. Panopoulos AD, D'Antonio M, Benaglio P, Williams R, Hashem SI, Schuldt BM, et al. iPSCORE: A Resource of 222 iPSC Lines Enabling Functional Characterization of Genetic Variation across a Variety of Cell Types. *Stem Cell Reports*. 2017;8(4):1086–100.
237. Burridge PW, Matsa E, Shukla P, Lin ZC, Churko JM, Ebert AD, et al. Chemically defined generation of human cardiomyocytes. *Nat Methods* [Internet]. 2014 Aug 15;11(8):855–60. Available from: <http://www.nature.com/articles/nmeth.2999>
238. Dubois NC, Craft AM, Sharma P, Elliott DA, Stanley EG, Elefanty AG, et al. SIRPA is a specific cell-surface marker for isolating cardiomyocytes derived from human pluripotent stem cells. *Nat Biotechnol* [Internet]. 2011 Nov 23;29(11):1011–8. Available from: <http://www.nature.com/articles/nbt.2005>
239. Vidarsson H, Hyllner J, Sartipy P. Differentiation of Human Embryonic Stem Cells to Cardiomyocytes for In Vitro and In Vivo Applications. *Stem Cell Rev Reports* [Internet]. 2010 Mar 21;6(1):108–20. Available from: <http://link.springer.com/10.1007/s12015-010-9113-x>
240. Tsankov AM, Akopian V, Pop R, Chetty S, Gifford CA, Daheron L, et al. A qPCR ScoreCard quantifies the differentiation potential of human pluripotent stem cells. *Nat Biotechnol* [Internet]. 2015 Nov;33(11):1182–92. Available from: <http://www.ncbi.nlm.nih.gov/pubmed/26501952>
241. Choi J, Lee S, Mallard W, Clement K, Tagliazucchi GM, Lim H, et al. A comparison of genetically matched cell lines reveals the equivalence of human iPSCs and ESCs. *Nat Biotechnol* [Internet]. 2015;33(11):1173–81. Available from: <http://dx.doi.org/10.1038/nbt.3388>

242. Lee DS, Yi TG, Lee HJ, Kim SN, Park S, Jeon MS, et al. Mesenchymal stem cells infected with *Mycoplasma arginini* secrete complement C3 to regulate immunoglobulin production in B lymphocytes. *Cell Death Dis* [Internet]. 2014;5:e1192. Available from: <http://www.ncbi.nlm.nih.gov/pubmed/24763049>
243. Singh SK, Clarke ID, Terasaki M, Bonn VE, Hawkins C, Squire J, et al. Identification of a cancer stem cell in human brain tumors. *Cancer Res* [Internet]. 2003;63(18):5821–8. Available from: <http://www.ncbi.nlm.nih.gov/pubmed/14522905>
244. Martins-Taylor K, Xu R-H. Concise review: Genomic stability of human induced pluripotent stem cells. *Stem Cells* [Internet]. 2012 Jan;30(1):22–7. Available from: <http://www.ncbi.nlm.nih.gov/pubmed/21823210>
245. Omuro A, DeAngelis LM. Glioblastoma and other malignant gliomas: a clinical review. *JAMA* [Internet]. 2013;310(17):1842–50. Available from: <http://www.ncbi.nlm.nih.gov/pubmed/24193082>
246. Zhang S, Cui W. Sox2, a key factor in the regulation of pluripotency and neural differentiation. *World J Stem Cells* [Internet]. 2014 Jul 26;6(3):305–11. Available from: <http://www.ncbi.nlm.nih.gov/pubmed/25126380>
247. Jin X, Jin X, Jung J-E, Beck S, Kim H. Cell surface Nestin is a biomarker for glioma stem cells. *Biochem Biophys Res Commun* [Internet]. 2013 Apr 19;433(4):496–501. Available from: <http://www.ncbi.nlm.nih.gov/pubmed/23524267>
248. Bulstrode H, Johnstone E, Marques-Torrejon MA, Ferguson KM, Bressan RB, Blin C, et al. Elevated FOXP1 and SOX2 in glioblastoma enforces neural stem cell identity through transcriptional control of cell cycle and epigenetic regulators. *Genes Dev*. 2017;31(8):757–73.
249. Lendahl U, Zimmerman LB, McKay RD. CNS stem cells express a new class of intermediate filament protein. *Cell* [Internet]. 1990 Feb 23;60(4):585–95. Available from: <http://www.ncbi.nlm.nih.gov/pubmed/1689217>
250. Scholzen T, Gerdes J. The Ki-67 protein: From the known and the unknown. *J Cell Physiol* [Internet]. 2000 Mar;182(3):311–22. Available from: <http://doi.wiley.com/10.1002/%28SICI%291097-4652%28200003%29182%3A3%3C311%3A%3AAID-JCP1%3E3.0.CO%3B2-9>

251. Daheron L. Induction of pluripotency : State of the art Human induced pluripotent stem cells. *Cell*. 2010;
252. Brivanlou AH. STEM CELLS: Enhanced: Setting Standards for Human Embryonic Stem Cells. *Science* (80- ) [Internet]. 2003 May 9;300(5621):913–6. Available from: <http://www.sciencemag.org/cgi/doi/10.1126/science.1082940>
253. Nelakanti R V, Kooreman NG, Wu JC. Teratoma formation: a tool for monitoring pluripotency in stem cell research. *Curr Protoc Stem Cell Biol* [Internet]. 2015 Feb 2;32:4A.8.1-17. Available from: <http://www.ncbi.nlm.nih.gov/pubmed/25640819>
254. Buta C, David R, Dressel R, Emgård M, Fuchs C, Gross U, et al. Reconsidering pluripotency tests: Do we still need teratoma assays? *Stem Cell Res* [Internet]. 2013 Jul;11(1):552–62. Available from: <http://linkinghub.elsevier.com/retrieve/pii/S1873506113000275>
255. HipSci. Human Induced Pluripotent Stem Cells Initiative (HipSci) [Internet]. Human Induced Pluripotent Stem Cells Initiative (HipSci). 2018. Available from: <http://www.hipsci.org/>
256. Swaiman's Pediatric Neurology [Internet]. Elsevier; 2017 [cited 2018 Sep 18]. Available from: <https://linkinghub.elsevier.com/retrieve/pii/C20131000790>
257. Tautz D. Hypervariability of simple sequences as a general source for polymorphic DNA markers. *Nucleic Acids Res* [Internet]. 1989 Aug 25;17(16):6463–71. Available from: <http://academic.oup.com/nar/article/17/16/6463/1074659/Hypervariability-of-simple-sequences-as-a-general>
258. Morrison M, Bell J, George C, Harmon S, Munsie M, Kaye J. The European General Data Protection Regulation: challenges and considerations for iPSC researchers and biobanks. *Regen Med* [Internet]. 2017 Sep;12(6):693–703. Available from: <https://www.futuremedicine.com/doi/10.2217/rme-2017-0068>
259. Isasi R, Andrews PW, Baltz JM, Bredenoord AL, Burton P, Chiu I-M, et al. Identifiability and Privacy in Pluripotent Stem Cell Research. *Cell Stem Cell* [Internet]. 2014 Apr;14(4):427–30. Available from: <http://linkinghub.elsevier.com/retrieve/pii/S1934590914001088>
260. Mayshar Y, Ben-David U, Lavon N, Biancotti J-C, Yakir B, Clark AT, et al.

- Identification and Classification of Chromosomal Aberrations in Human Induced Pluripotent Stem Cells. *Cell Stem Cell* [Internet]. 2010 Oct;7(4):521–31. Available from:  
<http://linkinghub.elsevier.com/retrieve/pii/S1934590910004418>
261. Lund RJ, Nikula T, Rahkonen N, Närvä E, Baker D, Harrison N, et al. High-throughput karyotyping of human pluripotent stem cells. *Stem Cell Res* [Internet]. 2012;9(3):192–5. Available from:  
<http://dx.doi.org/10.1016/j.scr.2012.06.008>
262. Draper JS, Smith K, Gokhale P, Moore HD, Maltby E, Johnson J, et al. Recurrent gain of chromosomes 17q and 12 in cultured human embryonic stem cells. *Nat Biotechnol* [Internet]. 2004 Jan;22(1):53–4. Available from:  
<http://www.ncbi.nlm.nih.gov/pubmed/14661028>
263. Taapken SM, Nisler BS, Newton MA, Sampsell-Barron TL, Leonhard KA, McIntire EM, et al. Karyotypic abnormalities in human induced pluripotent stem cells and embryonic stem cells. *Nat Biotechnol* [Internet]. 2011 Apr;29(4):313–4. Available from:  
<http://www.ncbi.nlm.nih.gov/pubmed/21478842>
264. Laurent LC, Ulitsky I, Slavin I, Tran H, Schork A, Morey R, et al. Dynamic changes in the copy number of pluripotency and cell proliferation genes in human ESCs and iPSCs during reprogramming and time in culture. *Cell Stem Cell* [Internet]. 2011 Jan 7;8(1):106–18. Available from:  
<http://www.ncbi.nlm.nih.gov/pubmed/21211785>
265. Gore A, Li Z, Fung H-L, Young JE, Agarwal S, Antosiewicz-Bourget J, et al. Somatic coding mutations in human induced pluripotent stem cells. *Nature* [Internet]. 2011 Mar 3;471(7336):63–7. Available from:  
<http://www.ncbi.nlm.nih.gov/pubmed/21368825>
266. Lund RJ, Närvä E, Lahesmaa R. Genetic and epigenetic stability of human pluripotent stem cells. *Nat Rev Genet* [Internet]. 2012 Oct;13(10):732–44. Available from:  
<http://www.ncbi.nlm.nih.gov/pubmed/22965355>
267. Roth A, Khattra J, Yap D, Wan A, Laks E, Biele J, et al. PyClone: statistical inference of clonal population structure in cancer. *Nat Methods* [Internet]. 2014 Apr 16;11(4):396–8. Available from:  
<http://www.nature.com/articles/nmeth.2883>
268. Sommer CA, Christodoulou C, Gianotti-Sommer A, Shen SS, Sailaja BS,

- Hezroni H, et al. Residual Expression of Reprogramming Factors Affects the Transcriptional Program and Epigenetic Signatures of Induced Pluripotent Stem Cells. Asakura A, editor. PLoS One [Internet]. 2012 Dec 14;7(12):e51711. Available from:  
<http://dx.plos.org/10.1371/journal.pone.0051711>
269. Hu K. All Roads Lead to Induced Pluripotent Stem Cells: The Technologies of iPSC Generation. *Stem Cells Dev* [Internet]. 2014;23(12):1285–300. Available from:  
<http://online.liebertpub.com/doi/abs/10.1089/scd.2013.0620>
270. Bukowiecki R, Adjaye J, Prigione A. Mitochondrial function in pluripotent stem cells and cellular reprogramming. *Gerontology* [Internet]. 2014;60(2):174–82. Available from:  
<http://www.ncbi.nlm.nih.gov/pubmed/24281332>
271. Suhr ST, Chang EA, Tjong J, Alcasid N, Perkins GA, Goissis MD, et al. Mitochondrial Rejuvenation After Induced Pluripotency. Klymkowsky M, editor. PLoS One [Internet]. 2010 Nov 23;5(11):e14095. Available from:  
<http://dx.plos.org/10.1371/journal.pone.0014095>
272. Armstrong L, Tilgner K, Saretzki G, Atkinson SP, Stojkovic M, Moreno R, et al. Human induced pluripotent stem cell lines show stress defense mechanisms and mitochondrial regulation similar to those of human embryonic stem cells. *Stem Cells* [Internet]. 2010 Apr;28(4):661–73. Available from: <http://www.ncbi.nlm.nih.gov/pubmed/20073085>
273. Prigione A, Fauler B, Lurz R, Lehrach H, Adjaye J. The senescence-related mitochondrial/oxidative stress pathway is repressed in human induced pluripotent stem cells. *Stem Cells* [Internet]. 2010 Apr;28(4):721–33. Available from: <http://www.ncbi.nlm.nih.gov/pubmed/20201066>
274. Stricker SH, Feber A, Engström PG, Carén H, Kurian KM, Takashima Y, et al. Widespread resetting of DNA methylation in glioblastoma-initiating cells suppresses malignant cellular behavior in a lineage-dependent manner. *Genes Dev*. 2013;27(6):654–69.
275. Zhou Y ye, Zeng F. Integration-free Methods for Generating Induced Pluripotent Stem Cells. *Genomics, Proteomics Bioinforma* [Internet]. 2013;11(5):284–7. Available from:  
<http://dx.doi.org/10.1016/j.gpb.2013.09.008>
276. Annovazzi L, Caldera V, Mellai M, Riganti C, Battaglia L, Chirio D, et al.

- The DNA damage/repair cascade in glioblastoma cell lines after chemotherapeutic agent treatment. *Int J Oncol* [Internet]. 2015;46(6):2299–308. Available from: <http://www.ncbi.nlm.nih.gov/pubmed/25892134>
277. Momcilovic O, Knobloch L, Fornsgaglio J, Varum S, Easley C, Schatten G. DNA Damage Responses in Human Induced Pluripotent Stem Cells and Embryonic Stem Cells. Capogrossi MC, editor. *PLoS One* [Internet]. 2010 Oct 15;5(10):e13410. Available from: <http://dx.plos.org/10.1371/journal.pone.0013410>
278. Pagliuca FW, Millman JR, Gürtler M, Segel M, Van Dervort A, Ryu JH, et al. Generation of functional human pancreatic  $\beta$  cells in vitro. *Cell* [Internet]. 2014 Oct 9;159(2):428–39. Available from: <http://www.ncbi.nlm.nih.gov/pubmed/25303535>
279. Martin Y, Vermette P. Bioreactors for tissue mass culture: design, characterization, and recent advances. *Biomaterials* [Internet]. 2005 Dec;26(35):7481–503. Available from: <http://www.ncbi.nlm.nih.gov/pubmed/16023202>
280. Camp JG, Badsha F, Florio M, Kanton S, Gerber T, Wilsch-Bräuninger M, et al. Human cerebral organoids recapitulate gene expression programs of fetal neocortex development. *Proc Natl Acad Sci* [Internet]. 2015;112(51):201520760. Available from: <http://www.pnas.org/lookup/doi/10.1073/pnas.1520760112>
281. Renier N, Wu Z, Simon DJ, Yang J, Ariel P, Tessier-Lavigne M. iDISCO: A Simple, Rapid Method to Immunolabel Large Tissue Samples for Volume Imaging. *Cell* [Internet]. 2014 Nov;159(4):896–910. Available from: <https://linkinghub.elsevier.com/retrieve/pii/S0092867414012975>
282. Rios AC, Clevers H. Imaging organoids: a bright future ahead. *Nat Methods* [Internet]. 2018 Jan 3;15(1):24–6. Available from: <http://www.nature.com/doi/10.1038/nmeth.4537>
283. Scherer HJ. Structural development in gliomas. *Am J Cancer*. 1938;34:333–51.
284. Jabs J, Zickgraf FM, Park J, Wagner S, Jiang X, Jechow K, et al. Screening drug effects in patient-derived cancer cells links organoid responses to genome alterations. *Mol Syst Biol* [Internet]. 2017;13(11):955. Available from:

<http://www.ncbi.nlm.nih.gov/pubmed/29180611>

285. Eiraku M, Takata N, Ishibashi H, Kawada M, Sakakura E, Okuda S, et al. Self-organizing optic-cup morphogenesis in three-dimensional culture. *Nature* [Internet]. 2011;472(7341):51–8. Available from: <http://dx.doi.org/10.1038/nature09941>
286. Wilson PG, Stice SS. Development and differentiation of neural rosettes derived from human embryonic stem cells. *Stem Cell Rev* [Internet]. 2006 Mar;2(1):67–77. Available from: <http://link.springer.com/10.1007/s12015-006-0011-1>
287. Elkabetz Y, Panagiotakos G, Al SG, Socci ND, Tabar V, Studer L. Human ES cell-derived neural rosettes reveal a functionally distinct early neural stem cell stage. *Genes Dev* [Internet]. 2008;22(2):152–65. Available from: <http://www.ncbi.nlm.nih.gov/pubmed/18198334>
288. Elkabetz Y, Panagiotakos G, Al Shamy G, Socci ND, Tabar V, Studer L. Human ES cell-derived neural rosettes reveal a functionally distinct early neural stem cell stage. *Genes Dev* [Internet]. 2008 Jan 15;22(2):152–65. Available from: <http://www.genesdev.org/cgi/doi/10.1101/gad.1616208>
289. Dennis D, Picketts D, Slack RS, Schuurmans C. Forebrain neurogenesis: From embryo to adult. *Trends Dev Biol* [Internet]. 2016 Jan 1;9(1):77–90. Available from: <http://www.ncbi.nlm.nih.gov/pubmed/28367004>
290. Lancaster MA, Knoblich JA. Organogenesis in a dish: Modeling development and disease using organoid technologies. *Science* (80- ). 2014;345(6194).
291. Kleinman HK, McGarvey ML, Liotta LA, Robey PG, Tryggvason K, Martin GR. Isolation and characterization of type IV procollagen, laminin, and heparan sulfate proteoglycan from the EHS sarcoma. *Biochemistry* [Internet]. 1982 Nov;21(24):6188–93. Available from: <http://pubs.acs.org/doi/abs/10.1021/bi00267a025>
292. Wippold FJ, Perry A. Neuropathology for the neuroradiologist: rosettes and pseudorosettes. *AJNR Am J Neuroradiol* [Internet]. 2006 Mar;27(3):488–92. Available from: <http://www.ncbi.nlm.nih.gov/pubmed/16551982>
293. Mariani J, Coppola G, Zhang P, Abyzov A, Provini L, Tomasini L, et al. FOXP1-Dependent Dysregulation of GABA/Glutamate Neuron Differentiation in Autism Spectrum Disorders. *Cell* [Internet]. 2015

- Jul;162(2):375–90. Available from:  
<http://linkinghub.elsevier.com/retrieve/pii/S009286741500759X>
294. Engström PG, Tommei D, Stricker SH, Ender C, Pollard SM, Bertone P. Digital transcriptome profiling of normal and glioblastoma-derived neural stem cells identifies genes associated with patient survival. *Genome Med* [Internet]. 2012;4(10):76. Available from:  
<http://www.ncbi.nlm.nih.gov/pubmed/23046790>
295. Verginelli F, Perin A, Dali R, Fung KH, Lo R, Longatti P, et al. Transcription factors FOXP1 and Groucho/TLE promote glioblastoma growth. *Nat Commun* [Internet]. 2013 Dec 20;4(1):2956. Available from:  
<http://www.nature.com/articles/ncomms3956>
296. Xuan S, Baptista CA, Balas G, Tao W, Soares VC, Lai E. Winged helix transcription factor BF-1 is essential for the development of the cerebral hemispheres. *Neuron* [Internet]. 1995 Jun;14(6):1141–52. Available from:  
<http://www.ncbi.nlm.nih.gov/pubmed/7605629>
297. Martynoga B, Morrison H, Price DJ, Mason JO. Foxg1 is required for specification of ventral telencephalon and region-specific regulation of dorsal telencephalic precursor proliferation and apoptosis. *Dev Biol* [Internet]. 2005 Jul 1;283(1):113–27. Available from:  
<http://www.ncbi.nlm.nih.gov/pubmed/15893304>
298. Seoane J, Le H-V, Shen L, Anderson SA, Massagué J. Integration of Smad and Forkhead Pathways in the Control of Neuroepithelial and Glioblastoma Cell Proliferation. *Cell* [Internet]. 2004 Apr;117(2):211–23. Available from:  
<http://linkinghub.elsevier.com/retrieve/pii/S0092867404002983>
299. Liu F, Hon GC, Villa GR, Turner KM, Ikegami S, Yang H, et al. EGFR Mutation Promotes Glioblastoma through Epigenome and Transcription Factor Network Remodeling. *Mol Cell* [Internet]. 2015 Oct 15;60(2):307–18. Available from: <http://www.ncbi.nlm.nih.gov/pubmed/26455392>
300. Furnari FB, Cloughesy TF, Cavenee WK, Mischel PS. Heterogeneity of epidermal growth factor receptor signalling networks in glioblastoma. *Nat Rev Cancer* [Internet]. 2015 May;15(5):302–10. Available from:  
<http://www.ncbi.nlm.nih.gov/pubmed/25855404>
301. Hegi ME, Liu L, Herman JG, Stupp R, Wick W, Weller M, et al. Correlation of O<sup>6</sup>-Methylguanine Methyltransferase (MGMT) Promoter Methylation

- With Clinical Outcomes in Glioblastoma and Clinical Strategies to Modulate MGMT Activity. *J Clin Oncol* [Internet]. 2008 Sep;26(25):4189–99. Available from: <http://ascopubs.org/doi/10.1200/JCO.2007.11.5964>
302. Yarosh DB. The role of O6-methylguanine-DNA methyltransferase in cell survival, mutagenesis and carcinogenesis. *Mutat Res Repair Reports* [Internet]. 1985 Jan;145(1–2):1–16. Available from: <http://linkinghub.elsevier.com/retrieve/pii/0167881785900343>
303. Szerlip NJ, Pedraza A, Chakravarty D, Azim M, McGuire J, Fang Y, et al. Intratumoral heterogeneity of receptor tyrosine kinases EGFR and PDGFRA amplification in glioblastoma defines subpopulations with distinct growth factor response. *Proc Natl Acad Sci* [Internet]. 2012 Feb;109(8):3041–6. Available from: <http://www.pnas.org/cgi/doi/10.1073/pnas.1114033109>
304. Nørøxe DS, Poulsen HS, Lassen U. Hallmarks of glioblastoma: a systematic review. *ESMO open*. 2016;1(6):e000144–e000144.
305. Verhaak RGW, Hoadley KA, Purdom E, Wang V, Qi Y, Wilkerson MD, et al. Integrated Genomic Analysis Identifies Clinically Relevant Subtypes of Glioblastoma Characterized by Abnormalities in PDGFRA, IDH1, EGFR, and NF1. *Cancer Cell* [Internet]. 2010;17(1):98–110. Available from: <http://dx.doi.org/10.1016/j.ccr.2009.12.020>
306. Zhou Y-H, Wu X, Tan F, Shi Y-X, Glass T, Liu TJ, et al. PAX6 suppresses growth of human glioblastoma cells. *J Neurooncol* [Internet]. 2005 Feb;71(3):223–9. Available from: <http://www.ncbi.nlm.nih.gov/pubmed/15735909>
307. Zhou Y-H, Tan F, Hess KR, Yung WKA. The expression of PAX6, PTEN, vascular endothelial growth factor, and epidermal growth factor receptor in gliomas: relationship to tumor grade and survival. *Clin Cancer Res* [Internet]. 2003 Aug 15;9(9):3369–75. Available from: <http://www.ncbi.nlm.nih.gov/pubmed/12960124>
308. Muratovska A, Zhou C, He S, Goodyer P, Eccles MR. Paired-Box genes are frequently expressed in cancer and often required for cancer cell survival. *Oncogene* [Internet]. 2003 Sep 11;22(39):7989–97. Available from: <http://www.nature.com/articles/1206766>
309. Hegge B, Sjøttem E, Mikkola I. Generation of a PAX6 knockout glioblastoma cell line with changes in cell cycle distribution and sensitivity

- to oxidative stress. *BMC Cancer* [Internet]. 2018 Dec 2;18(1):496.  
Available from:  
<https://bmccancer.biomedcentral.com/articles/10.1186/s12885-018-4394-6>
310. Cheng Q, Ma X, Cao H, Chen Z, Wan X, Chen R, et al. Role of miR-223/paired box 6 signaling in temozolomide chemoresistance in glioblastoma multiforme cells. *Mol Med Rep* [Internet]. 2017 Feb;15(2):597–604. Available from:  
<http://www.ncbi.nlm.nih.gov/pubmed/28035389>
311. Baumert BG, Hegi ME, van den Bent MJ, von Deimling A, Gorlia T, Hoang-Xuan K, et al. Temozolomide chemotherapy versus radiotherapy in high-risk low-grade glioma (EORTC 22033-26033): a randomised, open-label, phase 3 intergroup study. *Lancet Oncol* [Internet]. 2016 Nov;17(11):1521–32. Available from:  
<https://linkinghub.elsevier.com/retrieve/pii/S1470204516303138>
312. Roxas RC De, Fernandez MLL. *iMedPub Journals Temozolomide as Treatment in Low-grade Glioma : A Systematic Review Abstract*. 2016;1–7.
313. Shackleton M, Quintana E, Fearon ER, Morrison SJ. Heterogeneity in Cancer: Cancer Stem Cells versus Clonal Evolution. *Cell* [Internet]. 2009 Sep;138(5):822–9. Available from:  
<http://linkinghub.elsevier.com/retrieve/pii/S0092867409010307>
314. Suvà ML, Rheinbay E, Gillespie SM, Patel AP, Wakimoto H, Rabkin SD, et al. Reconstructing and reprogramming the tumor-propagating potential of glioblastoma stem-like cells. *Cell*. 2014;157(3):580–94.
315. Dahlstrand J, Collins VP, Lendahl U. Expression of the class VI intermediate filament nestin in human central nervous system tumors. *Cancer Res* [Internet]. 1992 Oct 1;52(19):5334–41. Available from:  
<http://www.ncbi.nlm.nih.gov/pubmed/1382841>
316. Climate B, Dyck V, Phylogenies TF, Compare EP, Singh SK, Hawkins C, et al. Identification of human brain tumour initiating cells. *Nature* [Internet]. 2004;432(November):396–401. Available from:  
<http://dx.doi.org/10.1038/nature03128>
317. Scott IC, Anson-Cartwright L, Riley P, Reda D, Cross JC. The HAND1 basic helix-loop-helix transcription factor regulates trophoblast

- differentiation via multiple mechanisms. *Mol Cell Biol* [Internet]. 2000 Jan;20(2):530–41. Available from: <http://www.ncbi.nlm.nih.gov/pubmed/10611232>
318. Reamon-Buettner SM, Ciribilli Y, Traverso I, Kuhls B, Inga A, Borlak J. A functional genetic study identifies HAND1 mutations in septation defects of the human heart. *Hum Mol Genet* [Internet]. 2009 Oct 1;18(19):3567–78. Available from: <https://academic.oup.com/hmg/article-lookup/doi/10.1093/hmg/ddp305>
319. Firulli BA, Fuchs RK, Vincentz JW, Clouthier DE, Firulli AB. Hand1 phosphoregulation within the distal arch neural crest is essential for craniofacial morphogenesis. *Development* [Internet]. 2014 Aug 1;141(15):3050–61. Available from: <http://dev.biologists.org/cgi/doi/10.1242/dev.107680>
320. Soosaar A, Chiaramello A, Zuber MX, Neuman T. Expression of basic-helix-loop-helix transcription factor ME2 during brain development and in the regions of neuronal plasticity in the adult brain. *Brain Res Mol Brain Res* [Internet]. 1994 Aug;25(1–2):176–80. Available from: <http://www.ncbi.nlm.nih.gov/pubmed/7984047>
321. Madhavan S, Zenklusen J-C, Kotliarov Y, Sahni H, Fine HA, Buetow K. Rembrandt: Helping Personalized Medicine Become a Reality through Integrative Translational Research. *Mol Cancer Res* [Internet]. 2009 Feb 1;7(2):157–67. Available from: <http://mcr.aacrjournals.org/cgi/doi/10.1158/1541-7786.MCR-08-0435>
322. Gusev Y, Bhuvaneshwar K, Song L, Zenklusen J-C, Fine H, Madhavan S. The REMBRANDT study, a large collection of genomic data from brain cancer patients. *Sci Data* [Internet]. 2018 Aug 14;5:180158. Available from: <http://www.nature.com/articles/sdata2018158>
323. Kim K, Zhao R, Doi A, Ng K, Unternaehrer J, Cahan P, et al. Donor cell type can influence the epigenome and differentiation potential of human induced pluripotent stem cells. *Nat Biotechnol* [Internet]. 2011 Nov 27 [cited 2018 Sep 14];29(12):1117–9. Available from: <http://www.ncbi.nlm.nih.gov/pubmed/22119740>
324. Bar-Nur O, Russ HA, Efrat S, Benvenisty N. Epigenetic memory and preferential lineage-specific differentiation in induced pluripotent stem cells derived from human pancreatic islet beta cells. *Cell Stem Cell*

- [Internet]. 2011 Jul 8;9(1):17–23. Available from:  
<http://www.ncbi.nlm.nih.gov/pubmed/21726830>
325. Suva ML, Riggi N, Bernstein BE. Epigenetic Reprogramming in Cancer. *Science* (80- ) [Internet]. 2013 Mar 29;339(6127):1567–70. Available from: <http://www.sciencemag.org/cgi/doi/10.1126/science.1230184>
326. Ito K, Bernardi R, Morotti A, Matsuoka S, Saglio G, Ikeda Y, et al. PML targeting eradicates quiescent leukaemia-initiating cells. *Nature* [Internet]. 2008 Jun 19;453(7198):1072–8. Available from:  
<http://www.ncbi.nlm.nih.gov/pubmed/18469801>
327. Wang JCY, Dick JE. Cancer stem cells: lessons from leukemia. *Trends Cell Biol* [Internet]. 2005 Sep;15(9):494–501. Available from:  
<http://www.ncbi.nlm.nih.gov/pubmed/16084092>
328. Carén H, Beck S, Pollard SM. Differentiation therapy for glioblastoma - too many obstacles? *Mol Cell Oncol* [Internet]. 2016 Mar;3(2):e1124174. Available from: <http://www.ncbi.nlm.nih.gov/pubmed/27308621>
329. Carén H, Stricker SH, Bulstrode H, Gargra S, Johnstone E, Bartlett TE, et al. Glioblastoma Stem Cells Respond to Differentiation Cues but Fail to Undergo Commitment and Terminal Cell-Cycle Arrest. *Stem Cell Reports* [Internet]. 2015 Nov;5(5):829–42. Available from:  
<http://linkinghub.elsevier.com/retrieve/pii/S2213671115002763>
330. Niedringhaus M, Dumitru R, Mabb AM, Wang Y, Philpot BD, Allbritton NL, et al. Transferable neuronal mini-cultures to accelerate screening in primary and induced pluripotent stem cell-derived neurons. *Sci Rep* [Internet]. 2015 Jul 10;5(1):8353. Available from:  
<http://www.nature.com/articles/srep08353>
331. Boissart C, Poulet A, Georges P, Darville H, Julita E, Delorme R, et al. Differentiation from human pluripotent stem cells of cortical neurons of the superficial layers amenable to psychiatric disease modeling and high-throughput drug screening. *Transl Psychiatry* [Internet]. 2013 Aug 20;3(8):e294–e294. Available from:  
<http://www.nature.com/articles/tp201371>
332. Efthymiou A, Shaltouki A, Steiner JP, Jha B, Heman-Ackah SM, Swistowski A, et al. Functional Screening Assays with Neurons Generated from Pluripotent Stem Cell–Derived Neural Stem Cells. *J Biomol Screen* [Internet]. 2014 Jan;19(1):32–43. Available from:

<http://journals.sagepub.com/doi/10.1177/1087057113501869>

333. Rubin LL. Stem Cells and Drug Discovery: The Beginning of a New Era? *Cell* [Internet]. 2008 Feb;132(4):549–52. Available from:  
<http://linkinghub.elsevier.com/retrieve/pii/S0092867408002183>
334. Hanahan D, Weinberg RA. The hallmarks of cancer. *Cell* [Internet]. 2000;100(1):57–70. Available from:  
<http://www.ncbi.nlm.nih.gov/pubmed/10647931>
335. Bissell MJ, Radisky D. Putting tumours in context. *Nat Rev Cancer* [Internet]. 2001;1(1):46–54. Available from:  
<http://www.ncbi.nlm.nih.gov/pubmed/11900251>
336. Tzukerman M, Rosenberg T, Ravel Y, Reiter I, Coleman R, Skorecki K. An experimental platform for studying growth and invasiveness of tumor cells within teratomas derived from human embryonic stem cells. *Proc Natl Acad Sci U S A* [Internet]. 2003;100(23):13507–12. Available from:  
<http://www.ncbi.nlm.nih.gov/pubmed/14573705>